Ex vivo experimental investigations and modelling of the layer-dependent, anisotropic, visco-hyperelastic behaviour of the human oesophagus

CIARA BRIGIT DURCAN

Zienkiewicz Institute (ZI) for Modelling, Data and Artificial Intelligence

Swansea University

&

Laboratoire Recherche Translationnelle et Innovation en Médecine et Complexité (TIMC)

Université Grenoble Alpes

Submitted to Swansea University and Université Grenoble Alpes in fulfilment of the requirements for the Degree of

Doctor of Philosophy

2023

Abstract

As a mechanical organ, the material properties of the oesophagus are integral to its function. The quantification of these properties is necessary to investigate the organ's pathophysiology and is required for a range of applications including medical device design, surgical simulations and tissue engineering. However, according to a systematic review of mechanical experimentation conducted on the gastrointestinal organs, the discrete layer-dependent properties of the oesophagus have not been investigated using human tissue, especially regarding its viscoelastic and stress-softening behaviour. Therefore, extensive experimentation was conducted to determine the time, layer and direction-dependent material response of the oesophagus using cadaveric human tissue. The residual strains of the organ were also considered via opening angle experiments. Overall, the results showed distinct properties in each layer, highlighting the importance of treating the oesophagus as a multi-layered composite material. Furthermore, a strong anisotropy was exhibited across both layers, where the longitudinal directions were much stiffer than the circumferential directions. Due to the COVID-19 pandemic, fresh human cadavers were not available from the anatomy laboratory for a considerable amount of time. Therefore, mechanical testing was first completed on embalmed human tissue and then, once available, on fresh human tissue. This unforeseen circumstance, through comparison of the two preservation states, allowed for an interesting discussion on the role of the tissue's constituents on its complex material behaviour. In addition, histological analysis was carried out to determine the density of the oesophagus' most mechanically relevant fibres: collagen and elastin. This knowledge was then used to inform constitutive modelling of the soft tissue's behaviour, the outcome of which was able to capture the anisotropy, visco-hyperelasticity and stress-softening observed in the experimental data.

Declarations

This work has not previously been accepted in substance for any degree and is not being concurrently submitted in candidature for any degree.

Signed.....[redacted].....

Date.....10/02/2024.....

This thesis is the result of my own investigations, except where otherwise stated. Other sources are acknowledged by footnotes giving explicit references. A bibliography is appended.

Signed..[redacted].....

Date.....10/02/2024.....

I hereby give consent for my thesis, if accepted, to be available for electronic sharing

Signed...[redacted].....

Date.....10/02/2024.....

The University's ethical procedures have been followed and, where appropriate, that ethical approval has been granted.

Signed.....[redacted].....

Date.....10/02/2024.....

Contents

List of Figures VIII

List of Tables XV

Abbreviations XVIII

1 MOTIVATION 2

1.1 Aims, objectives and thesis structure . . . 7

2 LITERATURE REVIEW 11

2.1 Introduction . . . 11

2.2 Review strategy . . . 16

2.3 Experimental techniques . . . 17

2.3.1 *Ex vivo* . . . 18

2.3.2 *In vivo* . . . 28

2.4 Review findings . . . 29

2.4.1 Oesophagus . . . 31

2.4.2 Stomach . . . 32

2.4.3 Small intestine . . . 34

2.4.4 Large intestine . . . 37

2.4.5 Rectum . . . 39

2.4.6 Experimental particulars . . . 42

2.5 Discussion . . . 47

2.5.1 *In vivo* vs. *ex vivo* . . . 47

2.5.2 Organs tested . . . 49

2.5.3 Species tested . . . 49

2.5.4 Sample size . . . 50

2.5.5 Anisotropy . . . 51

2.5.6 Layer-dependency . . . 51

2.5.7 Preconditioning . . . 52

2.5.8 Limitations of the review . . . 52

2.6 Conclusion . . . 53

3 EXPERIMENTAL METHODS **56**
3.1 Anatomy of the human oesophagus . . . 56
3.2 Specimen extraction . . . 57
3.3 Histology . . . 59
3.4 Uniaxial tensile testing . . . 59
3.4.1 Sample preparation . . . 59
3.4.2 Experimental setup . . . 61
3.4.3 Cyclic tests . . . 61
3.4.4 Stress-relaxation tests . . . 62
3.4.5 Mechanical characterisations . . . 63
3.5 Zero-stress state . . . 64
3.5.1 Sample preparation . . . 64
3.5.2 Experimental setup and protocol . . . 65
3.5.3 Measurement of circumferential residual strains . . . 65
3.6 Statistical analysis . . . 65
3.7 Conclusion . . . 66

4 EXPERIMENTAL RESULTS **69**
4.1 Histology of the human oesophagus . . . 69
4.1.1 Qualitative analysis . . . 69
4.1.2 Quantitive analysis . . . 71
4.2 Demographics and specimen details . . . 71
4.3 Cyclic results . . . 72
4.3.1 Variations in experimental samples . . . 72
4.3.2 Statistical analysis . . . 75
4.3.3 Presentation of cyclic results . . . 81
4.3.4 Cyclic stress-strain behaviour . . . 81
4.4 Stress-relaxation results . . . 87
4.4.1 Variations in experimental samples and statistical analysis . . . 87
4.4.2 Stress-relaxation behaviour . . . 88
4.5 Opening angle and residual strains . . . 89
4.6 Conclusion . . . 90

5 CONSTITUTIVE MODELLING **94**
5.1 Introduction . . . 94

5.2 Anisotropic matrix-fibre model with damage . . . 97
5.3 One-dimensional formulation of the model . . . 104
5.4 Parameter identification and model validation . . . 106
5.4.1 Embalmed tissue . . . 106
5.4.2 Fresh tissue . . . 109
5.5 Local sensitivity analysis . . . 111
5.6 Conclusion . . . 115

6 COMPARISON OF FRESH AND EMBALMED TISSUE 118
6.1 Experimental findings . . . 118
6.2 Constitutive modelling . . . 120
6.3 Conclusion . . . 121

7 DISCUSSION 125
7.1 Experimentation . . . 125
7.1.1 Oesophageal mechanical behaviour and physiological perspectives . . . 125
7.1.2 Comparison with other experimental studies . . . 126
7.1.3 Variation in experimental results and statistical analysis . . . 129
7.2 Modelling . . . 130
7.3 Comparison of fresh and embalmed tissue . . . 133
7.3.1 Experimentation . . . 133
7.3.2 Modelling . . . 134

8 SUMMARY AND OUTLOOK 138
8.1 Contributions to the field . . . 140

References 142

Appendix 182

Dedication

To Vukadin

Acknowledgements

I would like to thank my supervisors, Dr. Mokarram Hossain and Prof. Grégory Chagnon, for their time and effort in supervising me, for believing in me and for pushing me - this would not have been possible without you. I would also like to thank Dr. Edouard Girard MD for his medical consultation and for his work in performing and organising the dissections for this PhD project – this thesis would also not have been possible without you. Furthermore, I would like to thank my secondary supervisor, Prof. Djordje Perić, for his useful discussions and support from afar.

To my parents, Michael and Lynda, for supporting my education and for inspiring me to be part of the field I am currently in. To my sister, Berna, who has shared in this PhD journey with me and been a special part of the process. To the rest of my family, Rosie, Riz, Fran, Robin, Dom and Nanny, thank you for listening to me, encouraging me, loving me and for being on call whenever I needed; to Lizzie and Max, for being the best niece and nephew ever and for bringing their joy into my life. Finally, I would like to thank most of all my partner, Vukadin, for being there through it all and for shining a light when there has been darkness.

List of Figures

1 The various organs of the gastrointestinal tract situated in the human body. Figure adapted from [1]. 12

2 Haematoxylin and eosin histological staining of the oesophagus of diabetic Wistar rats (realised through the Goto-Kakizaki rat model for type-2 diabetes [2]) compared to non-diabetic (normal) Wistar rats, showing the difference between muscle layer thicknesses. The thickness of the longitudinal and circular muscle layers were significantly greater in the diabetic rats compared to the normal rats ($p<0.01$). The figure has been modified from the review by Zhao and Gregersen [3] and was originally from a study by Zhao et al. [4]. 13

3 A uniaxial tensile test experimental setup used to investigate the small intestine of pigs. The bottom clamp (grip) is fixed while the upper clamp is moved in a displacement-controlled way **(a)**. Sample preparation of strips of small intestinal tissue for uniaxial tensile testing; to investigate anisotropy (direction-dependent behaviour) of the tissue, specimens can be cut in the longitudinal and circumferential directions, as well as at various angles **(b)** [5]. 19

4 A biaxial tensile test experimental setup used to investigate the small intestine of pigs. Deformation is applied to a square sample (10 mm $\times$ 10 mm) through hooks attached to each side. Four graphite markers were placed on the surface of the sample to optically track its displacement during testing [6]. 21

5 Schematic diagram of pure shear (planar tension) sample preparation and experimental setup. Figure modified from the work of Marsi et al. [7] on the human male urethra. Although the urethra is not part of the GI tract, it has similar anatomical characteristics and physiological roles as the GI organs in that it is tubular and enacts peristalsis to excrete a waste product (urine). The hashed lines depict a fixed lower grip, while the arrow shows the direction the upper grip moves to apply tension to the sample. Note that Masri et al. [7] studied the anisotropic properties of the human urethra under planar tension by testing samples in both the longitudinal and circumferential directions. 23

6 Schematic diagram of a simple shear test being conducted on the rectum from pigs. The arrows indicate the direction the plates move during testing [8]. 23

7 **a)** Schematic diagram of a compression test being conducted on the rectum from pigs. The arrow indicates the direction the top plate moves during testing [8]. **b)** Semi-spherical indenter used to investigate the large intestine from rats. The indenter is rigid and has a 3 mm-diameter which comes into contact with the tissue during testing. Figure **(b)** modified from [9]. 24
8 **a)** Schematic diagram of both *in vitro*, i.e. *ex vivo*, and *in situ* experimental setups for distension testing. Distension and contractility were studied in regard to the small and large intestines of mice [10]. **b)** A distension test experimental setup used to investigate the stomach of diabetic and non-diabetic rats. A range of luminal pressures were applied to the organ specimen and the displacements were measured through three-dimensional ultrasound imaging. Figure **(b)** modified from [11]. 25
9 Schematic diagram of an inflation-extension experimental setup **(a)** and a close-up of a segment of rodent (Wistar rat) large intestine held in the grips prior to testing **(b)** [12]. 26
10 Schematic diagram showing the no-load state (**a**) and the zero-stress state (**b**) of a ring segment, including the definition of the opening angle, θ. 27
11 Experimental results showing the no-load and zero-stress state of circumferential ring specimens from the oesophagus of pigs, investigating the residual strains of the intact wall as well as the separated layers (mucosa-submucosa, circular muscle and longitudinal muscle). Figure modified from [13]. 28
12 Number of articles published per year per GI organ according to this review. 30
13 The number of *ex vivo* and *in vivo* studies collected per organ. 31
14 Pie charts indicating the species used in the *ex vivo* experimentation (n=107) **(a)** and *in vivo* experimentation (n=30) **(b)** on the oesophagus, highlighting, in particular, the proportion of experiments conducted on human tissue. 32
15 Pie charts indicating the species used in the *ex vivo* experimentation (n=40) **(a)** and *in vivo* experimentation (n=3) **(b)** on the stomach, highlighting, in particular, the proportion of experiments conducted on human tissue. 36
16 Pie charts indicating the species used in the *ex vivo* experimentation (n=103) **(a)** and *in vivo* experimentation (n=12) **(b)** on the small intestine, highlighting, in particular, the proportion of experiments conducted on human tissue. 37

17 Pie charts indicating the species used in the *ex vivo* experimentation (n=55) **(a)** and *in vivo* experimentation (n=6) **(b)** on the large intestine, highlighting, in particular, the proportion of experiments conducted on human tissue. 41
18 Pie charts indicating the species used in the *ex vivo* experimentation (n=18) **(a)** and *in vivo* experimentation (n=9) **(b)** on the rectum, highlighting, in particular, the proportion of experiments conducted on human tissue. 42
19 Proportion of studies for each organ, specified according to *ex vivo* and *in vivo* experimentation, that investigated the time-dependent properties of the tissue. . . . 43
20 Proportion of studies for each organ, specified according to *ex vivo* and *in vivo* experimentation, that preconditioned the tissue. 45
21 Proportion of *ex vivo* studies for each organ that conducted the experiments within a salt solution bath. 46
22 Proportion of studies for each organ, specified according to *ex vivo* and *in vivo* experimentation, that investigated the histological composition of the tissue alongside their mechanical tests. 47
23 Diagram showing the regions of the oesophagus in relation to the rest of the body (modified from [14]) (**a**) and a segment of the organ showing its histological layers (**b**). 57
24 During dissection of the human oesophagus, showing the chest cavity opened up (**a**) and the oesophagus *in situ* in the body before being sectioned below the pharynx (**b**). 58
25 **a**) Separation of a fresh oesophagus into its three main regions (cervical, thoracic and abdominal). **b**) Dissection of the two main oesophageal layers. **c**) Fully separated layers of the human oesophagus showing the unravelled muscularis propria on the left and the tubular mucosa-submucosa on the right. 60
26 Sample positioned on the support ready to be secured within the grips. 62
27 Machine setup (**a**) and a sample loaded within the machine (**b**). 62
28 Stretch-time schematic of the mechanical test protocol for the cyclic tests for both the longitudinal and circumferential samples (**a**) and for the stress-relaxation tests for the longitudinal samples (**b**). 63
29 Drawing illustrating the location of the zero-stress state analysis samples. 64

30 Sirius Red staining in the longitudinal plane (**a**) and Haematoxylin Eosin Saffron staining in the transversal plane (**b**) showing the mucosa (**1**), submucosa (**2**), the circular muscle fibres of the muscularis propria (**3**), the longitudinal muscle fibres of the muscularis propria (**4**) and the adventitia (**5**). 70
31 Comparison of the collagen (**a**) and elastin (**b**) in the different layers and planes of the human oesophagus determined by histological image analysis. 72
32 Rupture points of each test conducted at $10\%s^{-1}$ on embalmed tissue, highlighting the dispersion between cadavers and the longitudinal and circumferential directions for the muscular (**a**) and mucosa-submucosa layers (**b**). The circled points show the rupture stress-stretch of the curves selected for analysis via statistical means. 75
33 The combined histogram and probability distribution graph showing the dispersion of Young's modulus for the $10\%s^{-1}$ circumferential experimental results across three cadavers for the embalmed muscular layer (**a**) and the embalmed mucosa-submucosa layer (**b**), displaying a significant Fréchet distribution at $\alpha = 0.05$ with a mode (range) of 18.5 (5.2–62.9) for the muscularis propria (**a**) and 34.4 (14.4–67.4) for the mucosa-submucosa (**b**). The vertical red and green lines show the mode of the probability distribution for the muscular and mucosal layers, respectively, while the horizontal bars depict the range. 76
34 Schematic diagram showing the different characteristics extracted from the two 1.1 cycles, where E_1 = Young's modulus of the loading curve of the first cycle, E_2 = Young's modulus of the loading curve of the second cycle, A_{H1} = hysteresis area of the first cycle, A_{H2} = hysteresis area of the second cycle, ΔA_H = difference in hysteresis area between the two cycles, A_{L1} = area under loading curve of the first cycle, A_{U1} = area under unloading curve of the first cycle, A_{L2} = area under loading curve of the second cycle, and A_{U2} = area under unloading curve of the second cycle. 79
35 Effects of loading direction on the results at $1\%s^{-1}$ (**a**) and $10\%s^{-1}$ (**b**) and effects of loading rate on the results in the longitudinal direction (**c**) and the circumferential direction (**d**) of the embalmed muscularis propria layer. 82
36 Effects of loading direction on the results at $1\%s^{-1}$ (**a**) and $10\%s^{-1}$ (**b**) and effects of loading rate on the results in the longitudinal direction (**c**) and the circumferential direction (**d**) of the embalmed mucosa-submucosa layer. 83

37 Markers showing the permanent set of the $1\%s^{-1}$ circumferential results for the embalmed mucosa-submucosa layer for each stretch level and cycle. 84
38 Permanent set in each loading direction with respect to the maximum stretch of the previous cycle for the embalmed muscular layer (**a**) and mucosa-submucosa layer (**b**) for both the first and second cycles at both strain rates ($1\%s^{-1}$ and $10\%s^{-1}$). 84
39 Effects of loading direction on the results at $1\%s^{-1}$ (**a**) and $10\%s^{-1}$ (**b**) and effects of loading rate on the results in the longitudinal direction (**c**) and the circumferential direction (**d**) of the fresh muscularis propria. 85
40 Effects of loading direction on the results at $1\%s^{-1}$ (**a**) and $10\%s^{-1}$ (**b**) and effects of loading rate on the results in the longitudinal direction (**c**) and the circumferential direction (**d**) of the fresh mucosa-submucosa layer. 86
41 Fresh cyclic results showing the difference between the the two fresh layers at $1\%s^{-1}$ (**a**) and $10\%s^{-1}$ (**b**). 87
42 Stress-time example of the fresh mucosa-submucosa layer in the longitudinal direction from the multi-step stress-relaxation experiments. 89
43 Mean equilibrium stress-stretch obtained from multi-step stress-relaxation tests for the fresh muscular layer (**a**) and the mucosa-submucosa layer (**b**) including shaded areas showing the sample standard deviations. 90
44 **a**) Opening angle as a function of axial length along the oesophagus, where $x/L = 0$ is the proximal end and $x/L = 1$ is the distal end. **b**) Circumferential residual stretch of the thoracic region of the human oesophagus throughout the tissue wall, where the dashed $(- - -)$ green and red lines represent the residual strains of the mucosa-submucosa layer and muscularis propria, respectively, calculated by considering their inner and outer surfaces within the inact wall samples. 91
45 Drawing to illustrate the fibre orientations in the layers of the human oesophagus based on the histological observations outlined in Section 4.1. 99
46 Rheological representation of the viscoelastic model. 101
47 A decomposition of the deformation gradient tensor $\boldsymbol{F}$, where κ_0 is the undeformed configuration, κ_i is the intermediate configuration and κ is the final configuration. 101
48 Identification of the hyperelastic parameters in the longitudinal and circumferential directions for the embalmed muscularis propria (**a**) and mucosa-submucosa (**b**) layers from the $1\%s^{-1}$ cyclic experimental results using the loading path of the second cycle of the final full stretch level. 106

49 Parameter identification and modelling of the $1\%s^{-1}$ cyclic behaviour of the embalmed muscularis propria layer in the longitudinal (**a**) and circumferential (**b**) directions, and the embalmed mucosa-submucosa layer in the longitudinal (**c**) and circumferential (**d**) directions. 108
50 Parameter validation and modelling of the $10\%s^{-1}$ cyclic behaviour of the embalmed muscularis propria layer in the longitudinal (**a**) and circumferential (**b**) directions, and the embalmed mucosa-submucosa layer in the longitudinal (**c**) and circumferential (**d**) directions. 110
51 Parameter identification for the hyperelastic behaviour of the fresh muscularis propria layer (**a**) and mucosa-submucosa layer (**b**) in the longitudinal and circumferential directions using the equilibrium stress-stretch response as determined by stress-relaxation experiments. 111
52 Parameter identification and modelling of the $1\%s^{-1}$ cyclic behaviour of the fresh muscularis propria layer in the longitudinal (**a**) and circumferential (**b**) directions, and the mucosa-submucosa in the longitudinal (**c**) and circumferential (**d**) directions. 112
53 Parameter validation and modelling of the $10\%s^{-1}$ cyclic behaviour of the fresh muscularis propria layer in the longitudinal (**a**) and circumferential (**b**) directions, and the mucosa-submucosa in the longitudinal (**c**) and circumferential (**d**) directions. 113
54 Local sensitivity analysis results for each parameter for the fresh muscularis propria layer in the longitudinal (**a**) and circumferential (**b**) directions, and the mucosa-submucosa in the longitudinal (**c**) and circumferential (**d**) directions. . . . 114
55 Comparing the fresh (**a**) and embalmed (**b**) $1\%s^{-1}$ cyclic results of the muscular layer, and the fresh (**c**) and embalmed (**d**) $1\%s^{-1}$ cyclic results of the mucosa-submucosa layer. 120
56 Permanent set of the fresh and embalmed muscularis propria (**a**) and mucosa-submucosa (**b**) at $1\%s^{-1}$, including the differences between the first and second cycles. 121
57 Change in k_1 and k_2 material parameters from the fresh to embalmed tissue for each direction and layer. 121

58 Effects of the two most sensitive parameters on the model for the $1\%s^{-1}$ cyclic behaviour of the fresh muscularis propria layer in the longitudinal (**a**) and circumferential (**b**) directions, and the mucosa-submucosa in the longitudinal (**c**) and circumferential (**d**) directions. 182

List of Tables

1 Search terms specific to each organ of the GI tract, including the Boolean operators used in the systematic search. . . . 17
2 The number of search results for each organ, screened articles from the search, articles added by the author and the total number of articles considered per organ. Altogether, the total number of articles collected was 245. . . . 30
3 Summary of *ex vivo* studies on the oesophagus. . . . 33
4 Summary of *in vivo* studies on the oesophagus. . . . 34
5 Summary of *ex vivo* studies on the stomach. . . . 35
6 Summary of *in vivo* studies on the stomach. . . . 35
7 Summary of *ex vivo* studies on the small intestine. . . . 38
8 Summary of *in vivo* studies on the small intestine. . . . 38
9 Summary of *ex vivo* studies on the large intestine. . . . 40
10 Summary of *in vivo* studies on the large intestine. It should be noted that all the studies referenced here studied the behaviour of the large intestine in just one direction (isotropic). . . . 40
11 Summary of *ex vivo* studies on the rectum. . . . 42
12 Summary of *in vivo* studies on the rectum. . . . 43
13 Summary of studies that considered the time-dependent behaviour of the GI tissues. 44
14 Distribution of collagen and elastin in the muscularis propria; +, low density; +++++, high density. . . . 71
15 Distribution of collagen and elastin in the mucosa-submucosa; +, low density; +++++, high density. . . . 71
16 Patient demographics, length of oesophagus extracted, which layers were tested and the type of tests conducted for each cadaver. . . . 72
17 Number of cyclic tests performed on embalmed tissue per layer, per direction, per strain rate, per cadaver. . . . 73
18 Number of cyclic tests performed on fresh tissue per layer, per direction, per strain rate, per cadaver. . . . 74
19 Mean $\pm$ population standard deviation of sample dimensions for the cyclic experiments across both strain rates. . . . 74
20 p-values for the Young's moduli of the embalmed tissue cyclic results following a Fréchet distribution, where $p > 0.05$ indicates a significant distribution. . . . 77

21 Statistical differences in characteristics between the layers (muscularis propria and mucosa-submucosa) for both the fresh and embalmed tisssue. Blank cells indicate no statistical significance between the two groups, "−" mean that a statistical test is not relevant, and filled cells indicate the layer for which the characteristic is statistically higher than for the other layer, including the respective p-value. 79
22 Statistical differences in characteristics between the strain rates ($1\%s^{-1}$ and $10\%s^{-1}$) for both the fresh and embalmed tisssue. Blank cells indicate no statistical significance between the two groups, "−" mean that a statistical test is not relevant, and filled cells indicate the strain rate for which the characteristic is statistically higher than for the other strain rate, including the respective p-value. 80
23 Statistical differences in characteristics between the directions (longitudinal and circumferential) for both the fresh and embalmed tisssue. Blank cells indicate no statistical significance between the two groups , "−" mean that a statistical test is not relevant, and filled cells indicate the direction for which the characteristic is statistically higher than for the other direction, including the respective p-value. . . 80
24 Spearman's correlation coefficient, r_s, and p-values between days since dissection that the sample was tested and the maximum stress of the sample, where $p < 0.05$ indicates a statistically significant correlation and $|r_s|$ close to 1 shows a strong correlation, for which a positive r_s is a positive correlation. 81
25 Number of stress-relaxation tests performed on fresh tissue per layer, per direction, per cadaver. 88
26 Mean ± population standard deviation of sample dimensions for the stress-relaxation experiments performed on fresh tissue. 88
27 A complete set of material parameter values for the visco-anisotropic damage model identified in a modularised way for the layers of the embalmed human oesophagus. 107
28 Effect of a one parameter Kaliske [15] SEF on the coefficient of determination, R^2, when modelling the fresh $1\%s^{-1}$ cyclic results for each layer and direction. . . 114
29 A complete set of material parameter values for the visco-anisotropic damage model identified in a modularised way for the layers of the fresh human oesophagus. 115

30 Statistical differences in characteristics between the preservation states (fresh and embalmed) for both the muscularis propria and the mucosa-submucosa. Blank cells indicate no statistical significance between the two groups, and filled cells indicate the preservation state for which the characteristic is statistically higher than for the other preservation state, including the respective p-value. 118
31 Fresh and embalmed tissue's mode and range of Young's modulus, E_1, for each layer and direction from the first loading path of the $1\%s^{-1}$ cyclic results, and p-values for testing if the distribution of Young's moduli followed a Fréchet distribution. The circumferential muscularis propria for the fresh tissue did not follow a Fréchet distribution and was normally distributed, therefore, for this layer, direction and preservation state, the mean, standard deviation and p-value for the Shapiro-Wilk test are presented. 119
32 Publications from the research outlined in this thesis. 140

Abbreviations

CIM	*Convolution Integral Model*
CSA	*Cross-sectional area*
DIC	*Digital image correlation*
EGF	*Epidermal growth factor*
FE	*Finite Element*
GI	*Gastrointestinal*
HES	*Haematoxylin Eosin Saffron*
IBS	*Irritable bowel syndrome*
IVM	*Internal Variable Model*
KCl	*Potassium chloride*
NaCl	*Sodium chloride*
OCE	*Optical coherence elastography*
OCT	*Optical coherence tomography*
PBS	*Phosphate-buffered saline*
PK	*Piola-Kirchhoff*
SEF	*Strain energy function*
SHG	*Second-harmonic generation*

CHAPTER

ONE

1 MOTIVATION

The oesophagus is the organ of the upper digestive tract that transports food and drink, collectively known as the fluid bolus, from the pharynx to the stomach via a relatively simple but highly effective mechanical process. This process, called peristalsis, is responsible for the transport of various matters throughout the body [16–20] and consists of wave-like contractions of the hollow organs' muscular wall. For the oesophagus, its primary role of bolus transport is a result of a combination of the passive and active properties of the tissue wall [21,22], as well as the interaction of the forces generated with the hydrodynamic fluid bolus [23]. Therefore, it is crucial to understand each of these aspects to assess how they contribute to the function of the oesophagus in both health and disease. Out of these aspects, the passive properties may be viewed as the most fundamental, providing the baseline properties that allow transport to take place [22]. There have been a number of *in vivo* studies performed on the human oesophagus [24–38, 38–44], including those that looked at its passive properties by administrating muscle relaxants, such as atropine and butylscopolamine, to the volunteers in the study [41, 44]. The results of these investigations showed that the stiffness of the oesophageal wall in the circumferential direction increases as luminal pressure and cross-sectional area increase [24]; that the stress-stretch relation of the human oesophagus is non-linear in the circumferential direction [26, 41, 44]; and that stretch, rather than tension, is the main factor involved with oesophageal pain [42]. The oesophagus is made of two main composite layers, the muscularis propria (muscular layer) and the mucosa-submucosa (mucosal layer), which are thought to individually contribute to the organ's passive material response [45]. To the best of the author's knowledge, Frøkjær et al. [43, 44] were the only ones to study the direction-dependent and layer-dependent behaviour of the human oesophagus. They found, through their *in vivo* tests on human subjects, that distension resulted in tension in the circumferential direction, shortening in the longitudinal direction and compression in the radial direction [44]. Furthermore, they found that the stiffness was lowest at the mucosal (inner) surface and increased throughout the oesophageal wall, while circumferential stress and strain decreased throughout the wall and were lowest at the outer (muscular) surface [44]. However, as the mucosal layer is folded *in vivo*, Frøkjær et al. [43, 44] were not able to quantify the discrete behaviour of this layer, rather its properties in relation to the outer, muscular layer. Additionally, none of the referenced *in vivo* studies considered the time or history-dependent behaviour of the human oesophagus.

The layer-dependent properties of the oesophagus can be established *ex vivo* due to it being the only visceral organ which can be relatively easily separated into its two main layers (the mucosa-

submucosa and the muscularis propria) after explantation through careful cutting to the loose connective tissue binding the layers together [46]. However, as of yet, the passive mechanical properties of the discrete layers of the oesophagus have not been investigated using human tissue [47–49], apart from by Tottrup et al. [50] who tested the behaviour of only isolated longitudinal and circular smooth muscle from the human oesophagus over three decades ago. There have been many studies investigating the mechanical properties of different animal oesophagi, including rat [51–55], guinea pig [56–58], porcine [59–66], rabbit [67–69] and ovine [70, 71], with most conducting a layer-dependent analysis [51, 52, 55, 57, 59, 60, 62–70]. Animal studies are highly valuable for assessing the direct influence of diseases, e.g. diabetes [4, 72–77], oesophageal varices [78–80] and IBS [81], through the use of animal models, and interventions, e.g. surgical approaches [82–84] and medicinal compounds [76, 85, 86], as they allow for a very controlled environment and, often, a larger sample size compared to human studies. However, in terms of mechanical behaviour, it has been found that animal soft tissues, including the gastrointestinal tract, can differ significantly from their human counterparts [87–89]. Therefore, as they may not accurately represent the material response of human tissue, experimental findings from animal studies should not ideally be used quantitatively for modelling the human oesophagus for applications within medicine [87]. For instance, layer-dependent computational models of the human oesophagus provide a means to investigate how a medical device would interact with the different oesophageal layers. However, currently, models developed for devices, such as oesophageal stents [90], utilise material parameters determined from animal experimental data [91, 92]. Furthermore, tissue engineered oesophagi are a promising treatment for diseases such as atresia [93, 94]. For this, the establishment of the passive mechanical properties of the native human oesophagus can be used to cross-reference the properties of the grown tissue, ensuring the material behaviour is sufficiently close to that of the native [71]. Moreover, quantification of the viscoelastic properties of human organs can be used to increase the realism of surgical simulations, by providing a training technique that is both time-dependent and stress-strain-dependent [95, 96].

As previously stated, the vast majority of mechanical experimentation on the oesophagus has been carried out *ex vivo* on animal tissue, most likely due to its wider availability and reduced ethical constraints compared to human tissue. For instance, Sommer et al. [70] investigated the layer-dependent properties of ovine oesophageal tissue using a series of uniaxial tension, biaxial tension, and extension-inflation tests. The tissue exhibited heterogeneous and anisotropic behaviour, with different mechanical properties within the individual layers. The rupture strength of the muscularis propria was found to be much lower than that of the mucosa-submucosa layer. Stavropoulou

et al. [63] found similar results for porcine oesophagi, where the muscularis propria was less stiff than the mucosa-submucosa layer, associating these findings with the lower collagen content of the muscular layer. Furthermore, Yang et al. [53] investigated the properties of rat oesophagi and tested the tissue with the layers intact. In terms of anisotropy, they found the longitudinal direction to be significantly stiffer than the circumferential direction. This is in line with the anisotropic properties established by Sommer et al. [70] and Stavropoulou et al. [63].

In terms of *ex vivo* human experimentation, Egorov et al. [47] conducted a series of experiments on the human GI tract, including the oesophagus. They experimented on fresh human cadavers, tested within 24 hours after death. The tissues were stored in a Euro-Collins solution at 4°C prior to testing and their samples were preconditioned. They studied only the distal third of the oesophagus with the layers intact, and tested only in the longitudinal direction. Their main conclusions included that the longitudinal direction of the wall was found to have a high stressibility and exert a maximal stress of 1200kPa. Note that Egorov and co-workers [47] did not consider the layer-dependent properties of the human oesophagus and only explored its behaviour in one direction. Furthermore, Vanags et al. [48] investigated the effect of pathology and ageing on the mechanical properties of different regions of the human oesophagus, comparing the results to healthy tissue. The fresh oesophagi, which were studied with their layers intact, were cut into rectangular specimens in both the circumferential and longitudinal directions and subjected to uniaxial tension until rupture. They found that all oesophagi displayed anisotropic behaviour, with higher resistance in the longitudinal direction than the circumferential direction. With age, the Young's modulus of the tissue wall was found to increase. In addition, the cervical part of the oesophagus displayed the highest ultimate stress and strain when compared with the other two regions (thoracic and abdominal). Note that Vanags and co-workers [48] investigated both directions of loading, but did not consider the layer-dependent properties of the organ. They also conducted distension tests of oesophagi with their layers intact to explore the organ's mechanism of rupture, however they did not present any stress-strain plots of these results [48]. Very recently, Wang et al. [97] investigated the viability of optical coherence tomography (OCT) and vibrational optical coherence elastography (OCE) for determining the mechanical and structural properties of the human oesophagus using samples extracted from cadavers embalmed in Thiel. They found the mucosa-submucosa layer of the human oesophagus to have a Young's modulus in the range of 60–205 kPa, however they did not consider the properties of the muscular layer of the organ.

Investigations into the cyclic behaviour of a wide range of soft tissues, from skin to the aorta

to the brain, have been conducted on both animal tissues [98–103], including the oesophagus [59, 71, 104], and human tissues [7, 105–110]. Currently, studies exploring the softening of the oesophagus have only been carried out using animal tissue [54, 55, 58, 77]. For instance, Liao et al. [58] used guinea pig oesophagi to investigate the predominant mode of softening, whether either through stress-softening, in which the previous maximum strain affects the loss of stiffness, or softening due to the viscoelastic behaviour, wherein the time-dependent properties contribute to the loss of stiffness seen. It was concluded that both modes had an influence, however stress-softening was the predominant mode, attributing to 90% of the stiffness loss. This is supported by the earlier findings of Gregersen et al. [99] who conducted similar studies on the guinea pig small intestine. Liao et al. [58] also determined the softening behaviour to be anisotropic, with greater softening effects seen in the circumferential direction than the longitudinal direction for the intact oesophageal wall. Further to this, Jiang et al. [54] performed experimentation on rat oesophagi, looking at the effect of stress-softening on its passive stiffness, and investigating whether active muscle contraction had any effect on this. They found that the softening of the oesophageal wall could be reversed through muscular contractions induced by potassium chloride (KCl). This finding is very interesting in terms of the oesophagus' physiological function wherein the organ passively distends due to the entering of the bolus [111], for which the stiffness of the oesophageal wall would be reduced if the tissue were to be distended by the same amount again. This distension triggers peristalsis through the mechano-sensory response and then, via the peristaltic muscular contractions, the stress-softening is reversed and the stiffness of the wall returns to the degree at which it was before the bolus passed. This was proposed by Jiang et al. [54] to be some form of 'self-protection' for the oesophagus. The authors then went on to study this phenomenon in each of the two main layers of the rat oesophagus [55], and found that the passive stiffness and energy loss were reversible in both layers upon KCl activation.

Research into the oesophagus is becoming increasingly popular with advancements in tissue engineering providing a promising solution to the undesired consquences associated with the current treatments for long-gap oesophageal atresia [71, 94, 112–114]. Although the oesophagus is one of the most frequently examined gastrointestinal (GI) organs (as revealed through the literature review presented in Chapter 2), there exists no studies investigating the mechanical properties of its discrete layers using human tissue. In addition, there are no studies which use human tissue to evaluate the time-dependent material behaviour of the organ. Therefore, to more fully understand the behaviour and function of the different oesophageal layers, to provide experimental data for modelling the human oesophagus with respect to its individual layers, as well as to allow for

comparison between the native and tissue engineered oesophagus, this thesis focuses on exploring the direction, layer, time and history-dependent mechanical behaviour of the human oesophagus. Further to this, a constitutive formulation is employed to model the more complex aspects of the tissue layers' material response.

For a considerable amount of time, instead of live patients in the operating theatre, corpses have been used for the training of medical students on anatomy and surgical techniques [115]. Although the benefit of using surgical simulations for this purpose is great, reducing the need for any human cadavers to be used and providing the opportunity to repeat a procedure an infinite number of times, surgical simulation systems are currently not developed enough in terms of initial system acquisition cost, force-feedback experience and overall realism to be widely used within the medical population [116, 117]. Therefore, cadaveric surgical training is still prominent. An important consideration when using cadavers for this purpose is how they are preserved. There are a number of ways in which this is possible, including fresh-frozen, Thiel's method [118–120] and through formalin fixation; each with their own advantages and disadvantages. Formalin is the traditional solution used for embalming, while Thiel's method is a more recently developed technique that provides organs with a softer appearance and more realistic colours [121]. It is of value to establish how the cadaver preservation method affects the organ's mechanical behaviour, providing insight into the experience the medical student will have and the differences they might expect between training and surgery on living organs [122]. In regard to current preservation process studies, some have looked into the effect of just Thiel on the mechanical properties of soft tissues [123–125], however formalin preserved cadavers are still used for medical students' anatomical and surgical training due to its wider availability, lower cost, simpler embalming technique, and the little effect it has on the functional anatomical knowledge of students when compared to Thiel [115, 122]. The current findings on the effects of formalin on the material properties of human tissues are contradictory [126, 127]. The understanding of Hohmann et al. [126] is that the cross-links formed between the collagen molecules caused by formalin solution increases the stiffness of tissues. However, Girard et al. [127] believes there is a balance between partial denaturing of collagen and the formation of collagen cross-links, with the partial denaturing of the fibres explaining why they found a decrease in the stiffness caused by formalin preservation. Restrictions caused by the COVID-19 pandemic meant that initially only embalmed oesophageal tissue was allowed for testing. However, the overall lack of preservation studies on formalin embalming means that there was not a surplus of experimental data to provide a concrete understanding of how embalmed oesophageal tissue would differ from fresh oesophageal tissue in terms their mechanical properties. Therefore,

once restrictions were lifted, experimentation was carried out on oesophagi retrieved from recently deceased cadavers which had not been preserved. These results were then compared to the embalmed tissue findings to study the effects of formalin on the mechanical properties of the human oesophagus, and soft tissues in general.

1.1 Aims, objectives and thesis structure

The mechanical properties of the human oesophagus were studied in this thesis, in which the specific aims and objectives were as follows:

- To explore the layer, direction and time-dependent mechanical behaviour of the human oesophagus through a series of increasing stretch level cyclic tests and stress-relaxation experiments.
- To investigate the histological composition of the human oesophagus and how it relates to the observed behaviour of the layers.
- To assess the residuals strains of the organ via zero-stress state analysis using the opening angle method.
- To constitutively model the stress-strain response of the oesophageal layers using a matrix-fibre visco-hyperelastic model.
- To compare the mechanical behaviour and constitutive modelling of oesophagi retrieved from embalmed and fresh cadavers.

Following this chapter, a review is presented outlining the different experimental techniques currently found in literature to characterise the GI tissues. The review also highlights the experimentation that has been performed on each of the five GI organs, and includes an overview of what characterisation is still required to enhance biomechanical understanding of these tissues. In Chapter 3, the experimental methods used to investigate the passive biomechanical behaviour and histological composition of the human oesophagus are stated. After this, Chapter 4 presents the main results from the mechanical tests and histological analysis. Subsequently, a constitutive model to simulate the experimental data is detailed in Chapter 5, in which material parameters for the human oesophageal layers are also identified and verified. A comparison is then carried out regarding the similarities and differences in experimental behaviour and model parameters between the fresh and embalmed oesophageal layers in Chapter 6. Finally, Chapter 7 provides an

extensive discussion on the overall findings of the thesis, and in Chapter 8, the main conclusions are summarised and a selection of objectives for future work are proposed.

CHAPTER

TWO

2 LITERATURE REVIEW

Within the field of biomechanics, there has been seemingly less mechanical investigation into the GI organs, despite them being predominantly mechanical in function, compared to other soft tissues such as brain [128, 129] or those from the cardiovascular system [130, 131]. Therefore, the second chapter of this thesis consists of a systematic review of the mechanical experimentation carried out on the GI organs, to outline which areas are lacking and highlight which organs still require investigation to more fully understand their mechanical behaviour. This was used to inform the selection of the oesophagus as the organ studied in this thesis, and the design of experiments that will be presented in subsequent chapters. This chapter also includes an overview of the most common experimental techniques used to characterise the soft tissues of the GI tract, as well as a critical discussion on popular experimental practises[1].

2.1 Introduction

The GI tract is a muscular tube which extends from the mouth all the way to the anus [132], as can be seen in Figure 1. The tube is hollow and allows for the passage of food and drink through the body with the aim of extracting its nutrients and expelling the waste products. The oesophagus, the first organ of the GI tract, is responsible for moving the food from the mouth to the stomach. The stomach is responsible for temporarily storing the food, breaking it down both mechanically and chemically and passing it onto the small intestine. The small intestine is the site where 90% of the absorption of nutrients from the food takes place, after which the remaining material is passed onto the large intestine. The large intestine absorbs water and electrolytes from the remaining materials. The rectum then stores the solid waste product before expelling it through the anus [132]. Each tissue has a slightly different microstructural composition, evolved for the specific function of each organ, for example villi in the small intestine greatly increases its internal surface area for increased efficiency of nutrient absorption and digestive secretion [133]. However, all the GI organs have an innermost mucosal layer, an adjacent submucosal layer, then a muscular layer, named the muscularis propria, and, finally, an outermost adventitial (for the oesophagus) or serosal (for the stomach, small intestine, large intestine and rectum) layer. The mucosal layer also contains a thin, muscular layer called the muscularis mucosae [134]. Most collagen and elastin of the GI organs are situated in the mucosal, submucosal and outer layers [135–137]. For a more

[1] This chapter is mainly based on "Mechanical experimentation of the gastrointestinal tract: a systematic review", a paper accepted by Biomechanics and Modeling in Mechanobiology and currently in print, as outlined in Chapter 8.

comprehensive outline of the anatomy of the GI organs, readers are referred to Van de Graaff [135].

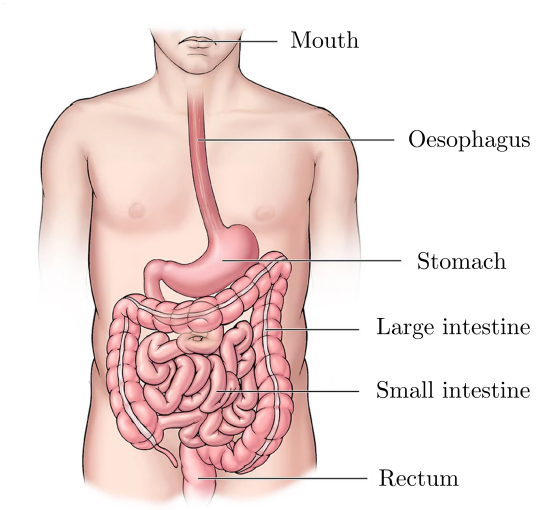

Figure 1. The various organs of the gastrointestinal tract situated in the human body. Figure adapted from [1].

Mechanics are innate to the GI tract's function. The transportation of food and drink through the tract is brought about by peristalsis: a mechanical process which propels the ingested material, named "bolus" when in the oesophagus and "chyme" when in the other GI organs, through sequential contractions of the muscular wall [135]. Peristalsis is also responsible for churning in the stomach which is a form of physical digestion where the food is mechanically broken down rather than chemically such as with enzymes or stomach acid. The passive mechanical, i.e. material, properties of the wall are also important. They provide the stiffness (degree of force exerted by a material when it is loaded) needed along with the active force of the muscle fibres to move the bolus/chyme during peristalsis. Such passive properties are organ-specific, depending on their function. For example, the material properties of the rectal wall must possess a certain compliance (opposite of stiffness) to be able to accommodate the changing amount of faecal waste product that is temporarily stored there, while the oesophagus requires a different level of compliance to be able to adjust to various bolus sizes that enter it while not being too great as to hinder its primary goal of transporting the bolus to the stomach. However, diseases can affect the passive and active properties of the GI tract, disrupting the role of each organ and leading to complications within a patient's digestive system. For instance, type-2 diabetes has been found to significantly increase the circumferential stiffness of the oesophageal wall in rats [4].

From the histological images in Figure 2, one can see that the onset of diabetes in this oesophageal

animal model has greatly influenced the thickness of the muscularis propria layer, and, as reported by Zhao et al. [4], has significantly increased the amount of collagen in the mucosa-submucosa layer. These changes in morphology and fraction of microstructural components may allude to the origin of mechanical disorders of the GI tract commonly found in diabetic patients [138]; due to the disease, the tissue wall is remodelled and the careful balance of forces that exist in the GI tract between the bolus/chyme and the passive and active properties of the wall, that keep the digestive system of so many humans running smoothly, has been disrupted [43]. Similar biomechanical changes caused by type-1 and type-2 diabetes have been found for other organs of the GI tract including the stomach [11], small intestine [139, 140] and large intestine [141]. Experimentation allows for the investigation into the origin of these disruptions to the tract's mechanical function, providing the information needed to devise creative ways to treat them. As is known within the scientific method, controls, or study of the healthy tissue's properties, are required to understand the normal function of the GI tissues, thus allowing the effects of the diseases, and potential ways to remedy them, to be properly established.

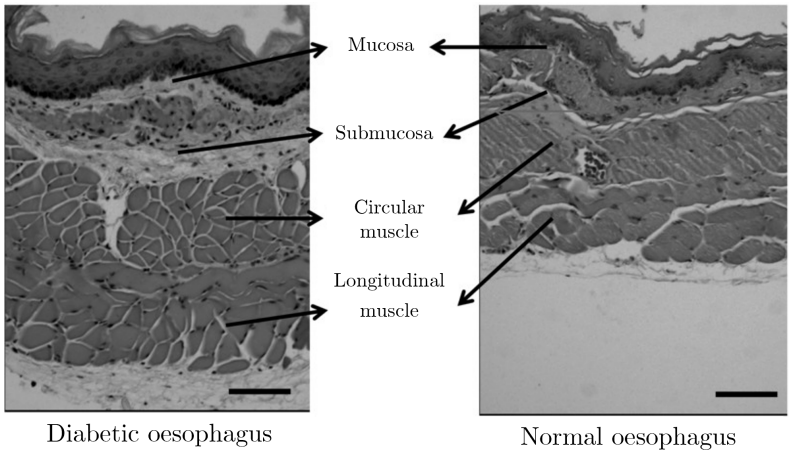

Figure 2. Haematoxylin and eosin histological staining of the oesophagus of diabetic Wistar rats (realised through the Goto-Kakizaki rat model for type-2 diabetes [2]) compared to non-diabetic (normal) Wistar rats, showing the difference between muscle layer thicknesses. The thickness of the longitudinal and circular muscle layers were significantly greater in the diabetic rats compared to the normal rats ($p<0.01$). The figure has been modified from the review by Zhao and Gregersen [3] and was originally from a study by Zhao et al. [4].

Another way that allows for the investigation into the mechanisms of how a healthy GI tract functions, and the effect of the changes that occur under pathophysiological conditions, is through the use of *in silico* (computational) models. These models, within the field of biomechanics, are based on the finite element (FE) method and provide a numerical approximation of how the tissue

mechanically behaves with consideration of its unique geometry and boundary conditions. They have the ability to deliver understanding of the organs' stress-strain relations not always possible through experimentation alone [142]. For instance, using a two-layered FE model, Yang et al. [143] established why, in a mechanical context, mucosal folds arise within the oesophagus, presenting what would happen to the active tension required of the muscle layer to maintain normal function if these folds were not present. Physiological processes such as peristalsis [144] and the mechanical breakdown of food in the stomach [145] can be studied using FE models to provide insight into which circumstances (e.g., certain wall thickness, amount of collagen, etc.) lead to inoptimial function [146]. In addition, computational models can be used to establish how the organ responds when medical devices are introduced, either to assess the mechanical effects of traditional devices such as endoscopes [92], or to aid with the design of novel medical devices such as stents [91,147], capsule endoscopes [148,149], capsule biopsy devices [150] and surgical staples [151,152]. Used in this way, FE models can help save time, biological test specimens and other resources needed during the design process. Further to this, FE models can be used to investigate the effects of surgical interventions, such as bariatric surgery used in the treatment of patients with obesity (e.g. reduction in the size of the stomach through a partial gastrectomy), on the biomechanics of the GI organs [153], with one aim being to have patient-specific pre- and post-operative computational models of the organ prior to the procedure to provide a means to assess the best surgical intervention and predict potential post-procedural complications. Moreover, surgical simulations are a growing technology which utilise FE models to allow surgeons to practise and hone their skills before conducting surgery on a patient [154]. They may also be used to examine the competency of a surgeon before they are allowed to practise [117]. In essence, FE models allow us to predict and numerically assess the complex mechanical behaviour of the GI organs under a wide variety of conditions, and thus have valuable applications throughout engineering and medicine.

The equations underpinning the type of FE models mentioned above are conservation and constitutive laws, which describe the mechanical behaviour of the tissue according to Newton's principles and the individual composition of the material, respectively [131]. Constitutive laws, originating in this case from the domain of continuum solid mechanics, provide a mathematical representation of the tissue's behaviour and are based on the well-informed theory that each component (constituent) of the material contributes to its overall behaviour, and thus its material response can be modelled through a summation of the behaviour of each part. This type of modelling, specifically using (micro)structural-based constitutive models, allows for the investigation of the effect of different constituents on the material behaviour of the tissue [155]. Due to the different types of fibres in

each of the GI organs, and the differing fractions of mechanically-influential fibres such as collagen and elastin, the individual layers tend to present distinct material behaviour, bearing different loads when forces are applied to the whole tissue structure [156]. Due to the soft nature of the GI tissues, which allow easily for large deformations of the organs, the stress-strain response is typically linear at very small strains but quickly becomes non-linear when deformed further [47, 62, 87, 157, 158]. Therefore, hyperelastic laws, rather than purely elastic (which are used for traditional engineering materials such as metals and concrete), are often used to describe the behaviour of such tissues (and more modern engineering materials such as polymers) [159, 160]. Additionally, the arrangement of the microstructural components of the tissue, such as collagen, elastin and muscle fibres, normally result in the GI organs exhibiting an anisotropic material response [161], i.e. they present different stress-strain relations depending on the direction in which the tissue is loaded. For this reason, anisotropic constitutive models are often employed when representing the behaviour of the GI tissues. Other, more complex behaviour can also be considered in the constitutive model, such as the time or history-dependent response of the tissue. In this regard, constitutive laws can be used to simulate their passive and active behaviour. For a comprehensive review on the constitutive laws used to model the GI tract, readers are referred to Patel et al. [131].

The parameters, i.e. constants, of the constitutive model are specific to the material in question. This, along with the formulation of the model based on knowledge of the material's microstructure and the observed experimental behaviour, distinguishes one material from another for, for example, use in multi-material FE simulations. The parameters can also allow for a quantitative comparison between different materials, particularly if the same constitutive law is used. To determine these parameters, the model must be compared with experimental data of the tissue [162]. Then, the parameters that provide a mathematical simulation closest to that of the experimental data are determined through an optimisation method [131]. Different types of experiments are required to establish the various aspects of the material's behaviour, e.g. active or passive, anisotropic, hyperelastic, viscoelastic, stress-softening. Therefore, to be able to determine the effects of disease on the function of the GI organs (experimentally and *in silico*), to model their constitutive behaviour and further understand the contribution of each component, and to be able to model using the FE method the behaviour of the organ as a function of its geometry and boundary conditions, experimental data is required.

This chapter considers this topic, providing a comprehensive, systematic review of the experimental studies currently available in literature on the biomechanical behaviour of the GI organs. The

articles found in the search are presented for each GI organ in terms of their test condition (*ex vivo* or *in vivo*), the origin of tissue tested (human, rodent, porcine, etc.), type of experiment conducted (uniaxial tension, distension (pressure-diameter), zero-stress state, etc.), and in terms of whether the direction-dependent and layer-dependent behaviour of the organ was studied. Furthermore, the articles investigating the time-dependent properties of the GI organs are shown, and those studying the active or diseased state are mentioned. The proportion of experiments conducted on different species for each GI organ are also illustrated, highlighting, in particular, which organs are lacking experimental data on human tissue. Additionally, the most common experimental techniques to characterise the GI organs are outlined, and the prominence within literature of certain experimental practices, such as preconditioning and the use of a solution bath, are displayed. This review aims to bring awareness to the experimental data that exists in regard to the mechanical characterisation of the GI organs and highlight what is currently absent as a call for further experimentation in this area. The information presented in this chapter can also be used to direct readers to studies in their particular area of interest, for instance, to provide further understanding or experimental data for their own constitutive and FE modelling.

2.2 Review strategy

The systematic search for this review was carried out using the PubMed database. The search was conducted using key terms associated with biomechanical experimentation, such as "biomechanical", "mechanical", "properties", "behaviour", "response", "stress", "strain", that could be found in the title or abstract of an article in combination with terms for each of the organs studied: oesophagus, stomach, small intestine, large intestine and rectum. The terms used for each organ can be found in Table 1. Even though the rectum is part of the large intestine, it has been treated as a separate organ here due to its unique function in comparison to the remaining large intestine; the rectum is responsible for the storage and excretion of faeces, whereas the other regions of the large intestine absorb water and electrolytes from the consumed material. The results of the search for each organ were then screened according to certain criteria; these included articles published in peer-reviewed journals, i.e. no pre-prints or conference proceedings, that provided novel (original) experimental data on the macrostructural mechanical properties of the organs in question, in particular experimental data that presented/allowed for the establishment of the stress-strain relations of the tissue or provided the pressure-volume relationship of the organ structure. Experimental studies on the sphincters of the GI tract were not included. There was no lower date limit for the articles, however studies available online after 15th October 2022 were not included. Any articles

Table 1: Search terms specific to each organ of the GI tract, including the Boolean operators used in the systematic search.

Organ	Search terms
Oesophagus	oesophagus OR oesophageal OR esophagus OR esophageal
Stomach	stomach OR (gastric AND tissue)
Small intestine	small intestine OR duodenum OR jejunum OR ileum
Large intestine	large intestine OR colon OR sigmoid OR cecum
Rectum	rectum OR rectal

not retrieved from the search but known by the author were added to the pool of articles included in this review. Additionally, the papers formed from the experimentation conducted for this thesis work were not included, a summary of which will be given later in Chapter 8.

2.3 Experimental techniques

A variety of techniques are used to mechanically characterise the GI tissues. The type of test chosen should be in line with the proposed research question, e.g. are physiological or supraphysiological loading conditions more suitable to quantify the material properties of the GI tissues in the setting/application that we are interested in? In this section, we will outline some of the most common experimental techniques used to quantify the biomechanical behaviour of the GI tract.

For the interpretation of data obtained from such experimental techniques, it is commonly assumed that tissues of the GI tract are incompressible. That is to say that during experimental loading, the volume of the tissue does not change [163]. While this, physically, is not completely true, the high water content of soft tissues means that they often exhibit properties close to incompressibility [164], therefore the assumption is sufficient in producing meaningful results and is valuable in that it provides a simplification that reduces computational cost.

Mechanical experimentation of human or animal soft tissues can be separated into three categories; *in vivo*, *in situ* and *ex vivo*. *In vivo* experimentation is carried out in the natural environment of the organ while the human/animal is still living. For organs such as the skin, these experiments can be conducted on the surface of the body. However, for the GI organs, as they are inside the body, a device must be inserted into the body to obtain biomechanical measurements. *In situ* tests are those conducted whilst the tissue is still connected to the body but is not in its completely natural state, such as experiments conducted on an organ accessed via a surgical opening to the chest. *In*

situ experiments can be carried out both while the human/animal is alive or post-mortem. *Ex vivo* experimentation (sometimes called "*in vitro*", although "*ex vivo*" is technically more accurate in regard to the macromechanical characterisations of soft tissues) is when the organ is removed via dissection from its natural environment and, thus, is no longer alive during the mechanical tests. Tissue can be taken from either alive or deceased subjects, however when the tissue is tested, it is always deceased. Firstly, we will describe the *ex vivo* experimental techniques commonly used to characterise the GI tissues, and secondly, we will summarise the *in vivo* techniques. *In situ* tests are the same as those used for either *ex vivo* or *in vivo* experimentation, and therefore have not been given their own section.

2.3.1 *Ex vivo*

Ex vivo experiments are those performed on naturally grown tissues taken outside of their physiological environment i.e. excised via dissection from alive or deceased subjects. When the experiments are conducted, the tissue is deceased, therefore measures should be taken to test the tissue as soon as possible to reduce the time-dependent effects of death, such as ischemia, on the mechanical properties of the tissue [84]. In addition, measures are also taken within the test setup to simulate a more physiological environment in terms of moisture, temperature and, sometimes, carbon dioxide and oxygen concentrations [12, 165]; reducing these factors as ones that can cause a discrepancy between *in vivo* and *ex vivo* material behaviour (as *in vivo* is often the environment of interest).

2.3.1.1 Uniaxial tension

Uniaxial tensile tests are the most basic tension test in which a specimen of a planar material is loaded along its length, often until failure. For a uniaxial tensile test, the specimen must have a length-to-width ratio of at least 4:1 [166] (which can be an issue when working with small organs such as the rabbit oesophagus [78]), and the specimens can either be dogbone shaped [59, 70] or rectangular, as seen in Figure 3. Dogbone samples are more ideal as they ensure that rupture takes place in the middle of the specimen and not at the grip, however it can be difficult to punch consistent dogbone specimens from soft tissues and so in the field of soft tissue biomechanics, it is common to use rectangular shaped specimens [47, 87, 167–170].

Uniaxial tensile tests are commonly employed for isotropic materials, such as some metals and

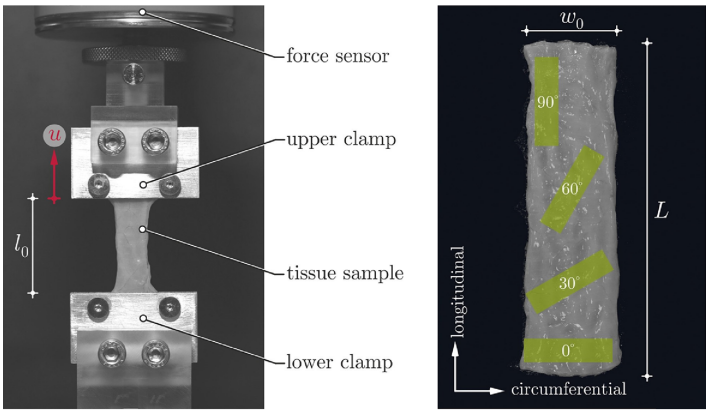

(a) (b)

Figure 3. A uniaxial tensile test experimental setup used to investigate the small intestine of pigs. The bottom clamp (grip) is fixed while the upper clamp is moved in a displacement-controlled way **(a)**. Sample preparation of strips of small intestinal tissue for uniaxial tensile testing; to investigate anisotropy (direction-dependent behaviour) of the tissue, specimens can be cut in the longitudinal and circumferential directions, as well as at various angles **(b)** [5].

polymers [171, 172], however they can be used to study the anisotropy of a GI tissue by testing strips from the longitudinal (axial) and circumferential directions, and also from various angles in-between these two directions, as seen in Figure 3b. They cannot, however, be used to determine the radial stress-strain relation of the tissue. Often the grips used to secure the tissue for uniaxial tensile testing have serrated edges or sand-paper attached to their inner surfaces to prevent the sample from slipping during testing [5, 173]. Sometimes the grips are tightened to a pre-established torque level to find the optimal balance between preventing slippage during testing and not causing the sample to rupture at the grip because they are too tightly secured. Furthermore, tightening the grips to a specific torque provides consistency and reduces the influence of a factor that could affect the repeatability of the results [173, 174].

The time-independent (elastic) behaviour of a tissue can be established under uniaxial tension by loading a sample at a quasi-static strain rate; that is, a strain rate slow enough to allow, theoretically, the viscous relaxation to take place during loading, thus the material is close to its equilibrium state (material properties once all viscous effects have disappeared). Some experimental studies that perform tests like these precondition their sample first (which will be discussed later in Section 2.4.6.2), removing some of the history- and time-dependent effects that occur during initial loading of a soft biological tissue. Moreover, experiments such as stress-relaxation tests may be carried out to determine the equilibrium stress-strain of the sample [175]. Sometimes also called

ramp and hold tests, stress-relaxation tests consist of very quickly stretching a sample to a certain strain and holding it there for a considerable amount of time. For soft tissues, it is expected that the stress within the tissue will decrease when held. The length of time that the material is held depends on its relaxation time: for some soft tissues it can take as little as 5 minutes for the stress to plateau during relaxation [175–177], while for some polymers it can take around 30 minutes [178]. When carried out over various stretch levels, the stress after the relaxation period plotted against the strain at which the sample was stretched provides the equilibrium stress-strain relation of the material and, in the context of large strain, can be used to model its hyperelastic behaviour. Creep tests are similar to stress-relaxation tests in that the equilibrium stress-strain relation of the material can be established, however creep tests are load-controlled rather than strain-controlled. For creep tests, a certain stress is applied to the material and the stress is held at that level while the strain of the sample changes due to viscous effects [176, 177]. For soft tissues, it can normally be expected that the strain will increase as the sample is held at a certain stress. The maximum deformation after the creep period can then be plotted against the stress level the sample was held at, which, when carried out for several stress levels, presents the equilibrium stress-strain relationship of the material.

In order to provide a complete picture of the viscoelasticity of a tissue, the time-dependent properties of the material should be investigated alongside the time-independent properties. The time-dependent behaviour can be studied by conducting uniaxial tensile tests at several different strain rates, including those within and above the quasi-static range and ideally an order of magnitude apart, e.g. 0.1 mms^{-1}, 1.0 mms^{-1} and 10 mms^{-1} (due to the variable nature of soft tissues and thus their mechanical response, an order of magnitude between the strain rates provides a big enough range to be able to experimentally observe the strain rate effects). Tensile tests can also be carried out at dynamic strain rates to establish the behaviour of the tissue under impact. Additionally, cyclic tests can be performed to investigate the differences between the loading and unloading curves. If the sample has been preconditioned, the difference between the loading-unloading curve that remains is thought to be mainly due to the time-dependent relaxation of the specimen.

Uniaxial tensile tests are popular in determining the active properties of soft tissues. In this case, the sample is held at a certain strain, zero or otherwise, and is either activated using a compound which activates muscle contraction, such as potassium chloride, or via electrical stimulation [55, 179]. The measured force and change in length of the sample are then used to establish the stress-strain relation under active conditions.

2.3.1.2 Biaxial tension

Biaxial tensile tests are similar to uniaxial tension tests in that they are performed on planar materials under tension, however biaxial tests consist of stretching a square sample of a material along two orthogonal directions simultaneously, as seen in Figure 4: hence, with each individual tissue sample, biaxial tests allow the direction-dependent properties of the tissue to be studied. On this note, biaxial tensile tests are often preferred to uniaxial tensile tests in the domain of hollow soft tissue mechanics as, by stretching the tissue in two directions at the same time rather than testing isolated strips in only one direction, biaxial tension is closer to the *in vivo* loading environment of the organ wall. The stretching in two directions can either be to the same degree, which is called equibiaxial tension, or by different amounts per direction. The choice of this will depend on the application, e.g. during physiological loading conditions, the tissue may undergo differing amounts of stretch in the circumferential and longitudinal directions, thus it may be of value to prescribe different amounts of loading to the circumferential and longitudinal directions to match those typically experienced *in vivo*.

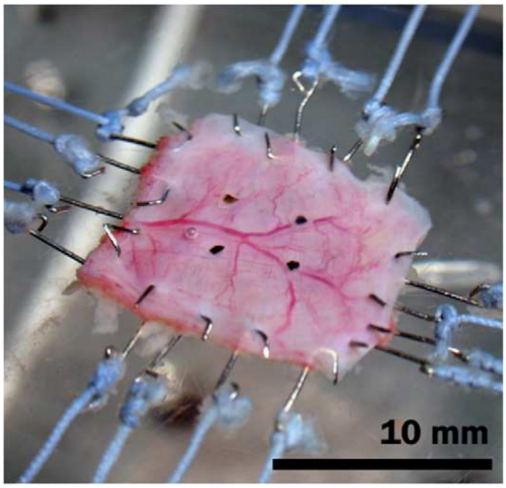

Figure 4. A biaxial tensile test experimental setup used to investigate the small intestine of pigs. Deformation is applied to a square sample (10 mm $\times$ 10 mm) through hooks attached to each side. Four graphite markers were placed on the surface of the sample to optically track its displacement during testing [6].

For biaxial tension, the samples must be square but the size is not critical as long as it is well supported by the testing machine [6, 70]. This freedom with size can be useful in particular for soft tissue specimens where the number of samples available is either often severely limited, e.g.

with human testing, or should be kept to a minimum due to ethical considerations, e.g. with animal testing. The square sample size can be adjusted to allow for as many test samples as possible from a single excised organ. As shown in Figure 4, the gripping mechanism for biaxial tensile tests is different to that for a uniaxial tension system. Here, several hooks placed equidistantly along each side of the square sample are used to secure and then stretch the specimen. When the specimen is setup, the time-independent and time-dependent properties of the tissue can be studied using similar methods for uniaxial tension, e.g. cyclic testing, varying strain rates, stress-relaxation etc., as outlined in Section 2.3.1.1.

2.3.1.3 Pure shear

Pure shear tests, sometimes called planar tensile tests, are similar to uniaxial tensile tests in that rectangular samples are stretched in only one direction. With pure shear tests, however, the width of the sample is much larger than its length, as can be seen in Figure 5, for which the length-to-width ratio must be at least 1:2 [180]. This ensures that no significant contraction can take place along the width of the sample during loading, making it that the tension in one direction is equal to the orthogonal direction's compression, producing no rigid body rotation and thus only shear strains within the specimen. Furthermore, pure shear tests are similar to uniaxial tensile tests in that the grips are often serrated or have sand-paper attached to them to reduce slippage of the sample during testing [173], and similar tests can be conducted to establish the time-independent and time-dependent properties (Section 2.3.1.1).

2.3.1.4 Simple shear

A typical simple shear test setup is like that which can be seen in Figure 6, where the sample's bottom and top surfaces are translated relative to each other. In the domain of small deformation, simple shear is similar to pure shear but differs in the sense that rotation can occur; this was found to not be fully the case for large deformations however [181]. Simple shear tests provide the opportunity to determine the behaviour of the tissue under non-normal forces (those applied parallelly to the tissue surface), as well as the material's shear modulus, which is useful when considering the types of deformations that exist during normal function of the GI tract [182].

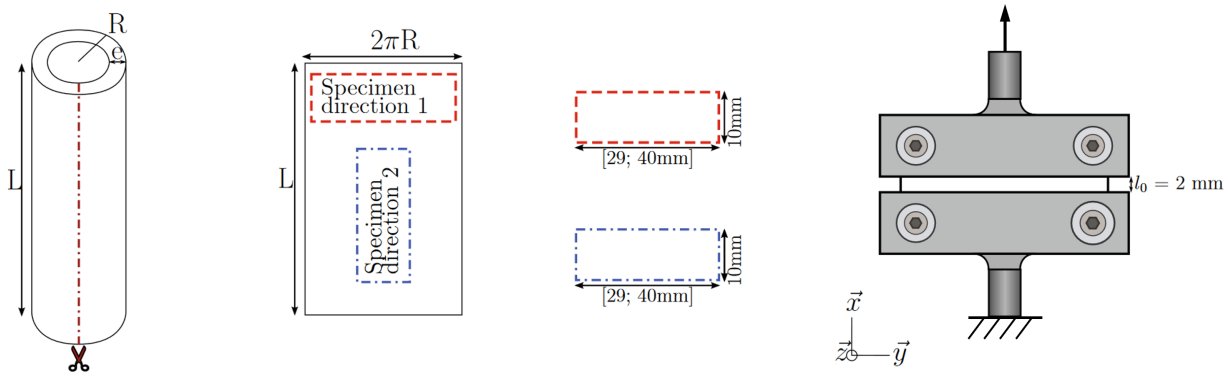

Figure 5. Schematic diagram of pure shear (planar tension) sample preparation and experimental setup. Figure modified from the work of Marsi et al. [7] on the human male urethra. Although the urethra is not part of the GI tract, it has similar anatomical characteristics and physiological roles as the GI organs in that it is tubular and enacts peristalsis to excrete a waste product (urine). The hashed lines depict a fixed lower grip, while the arrow shows the direction the upper grip moves to apply tension to the sample. Note that Masri et al. [7] studied the anisotropic properties of the human urethra under planar tension by testing samples in both the longitudinal and circumferential directions.

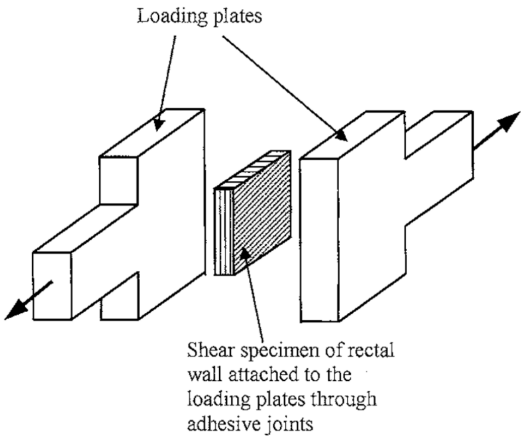

Figure 6. Schematic diagram of a simple shear test being conducted on the rectum from pigs. The arrows indicate the direction the plates move during testing [8].

2.3.1.5 Uniaxial compression

Uniaxial compression tests are carried out by pressing a sample of tissue between two plates, as seen in Figure 7a. These tests involve subjecting a uniform sample, either a square or a short cylinder, to compressive deformation in order to study the behaviour of the tissue and its ability to bear load under compressive strains. The tests used to establish the time-independent and time-dependent properties of a soft tissue outlined in Section 2.3.1.1, such as creep, stress-relaxation and cyclic tests, can also be applied to compression tests, however instead of stretching the mate-

rial, the applied load will be a compression.

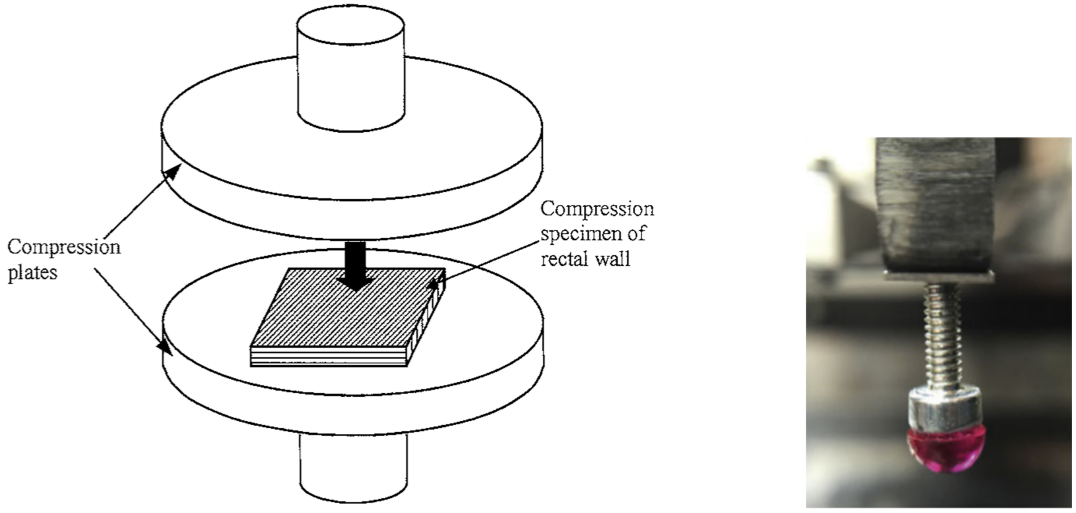

(a) (b)

Figure 7. **a)** Schematic diagram of a compression test being conducted on the rectum from pigs. The arrow indicates the direction the top plate moves during testing [8]. **b)** Semi-spherical indenter used to investigate the large intestine from rats. The indenter is rigid and has a 3 mm-diameter which comes into contact with the tissue during testing. Figure **(b)** modified from [9].

2.3.1.6 Indentation

Similarly to compression tests, indentation tests also prescribe compressive strains to a material, however the indenter causing the displacement is not a plate covering the entirety of the sample, rather a probe with a compression area that is much smaller than the surface of the sample where the compression is taking place. The shape of the indenter attached the probe can be a more unusual shape compared to the flat plate used for traditional compression testing, for instance a semi-sphere as seen in Figure 7b, allowing for more nuanced loading regimes [142]. As the only constraints are that the surface where the test takes place is much larger than the size of the indenter and is relatively flat, the tissue specimens for indentation testing can be almost any shape. This is useful for tissues where it can be difficult to cut uniform specimens.

2.3.1.7 Distension

Distension tests, also called inflation tests, for the GI organs, or other hollow organs, involve the stretching of the organ from its inside. A schematic diagram of a distension test conducted both *ex vivo* and *in situ* on the small and large intestines is shown in Figure 8a [10], and an example of an experimental setup for a distension test on the stomach can be seen in Figure 8b [11]. Note that in Figure 8a, the fluid being injected into one end of the oesophagus flows out the other end of the organ [10]. In this study, Lu et al. [10] recorded the pressure exerted by the fluid on the wall of the organ and measured the intestinal diameter. Contrarily, the fluid injected into the stomach seen in Figure 8b is not able to pass out of the other side [11]; for this study, Liao et al. [11] measured the circumferential and longitudinal deformations using three-dimensional ultrasound imaging. These studies show just two examples of how a distension test can be carried out, in which there are many variations. The essence of the test is the same, however, in that a fluid (liquid or gas) is injected into the hollow organ creating a pressure on the organ wall. The pressure is recorded along with a strain measure (diameter, cross-sectional area (CSA), wall thickness, arc length, three-dimensional imaging) and/or the volume of fluid. Usually *ex vivo* distension tests are performed on passive tissue, however it is possible to quantify the contractility of the specimen, and thus calculate the contribution of the passive and active stress on the organ's mechanical behaviour.

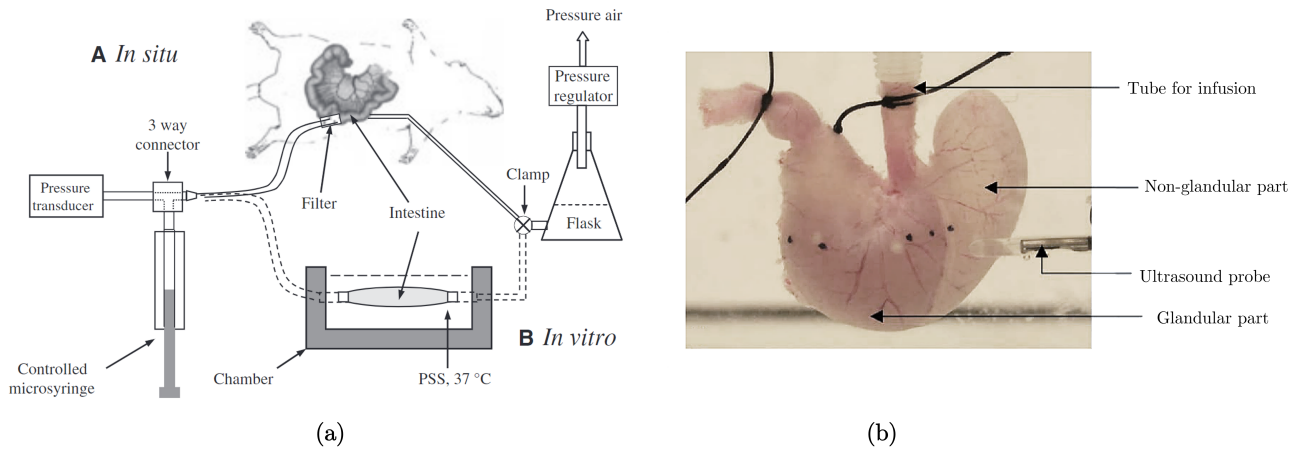

(a) (b)

Figure 8. **a)** Schematic diagram of both *in vitro*, i.e. *ex vivo*, and *in situ* experimental setups for distension testing. Distension and contractility were studied in regard to the small and large intestines of mice [10]. **b)** A distension test experimental setup used to investigate the stomach of diabetic and non-diabetic rats. A range of luminal pressures were applied to the organ specimen and the displacements were measured through three-dimensional ultrasound imaging. Figure **(b)** modified from [11].

2.3.1.8 Inflation-extension

While distension tests measure the stress-strain relation of an organ in one loading direction, inflation-extension tests measure it in two directions. Inflation-extension tests, as the name suggests, involve both distension of the tissue in the circumferential direction and stretch in the axial/-longitudinal direction, allowing for characterisation of the tissue's anisotropic properties in a state closer to *in vivo* conditions compared to uniaxial or biaxial tensile testing, i.e., with the luminal structure intact. An example of the experimental setup for an inflation-extension test can be seen in Figure 9.

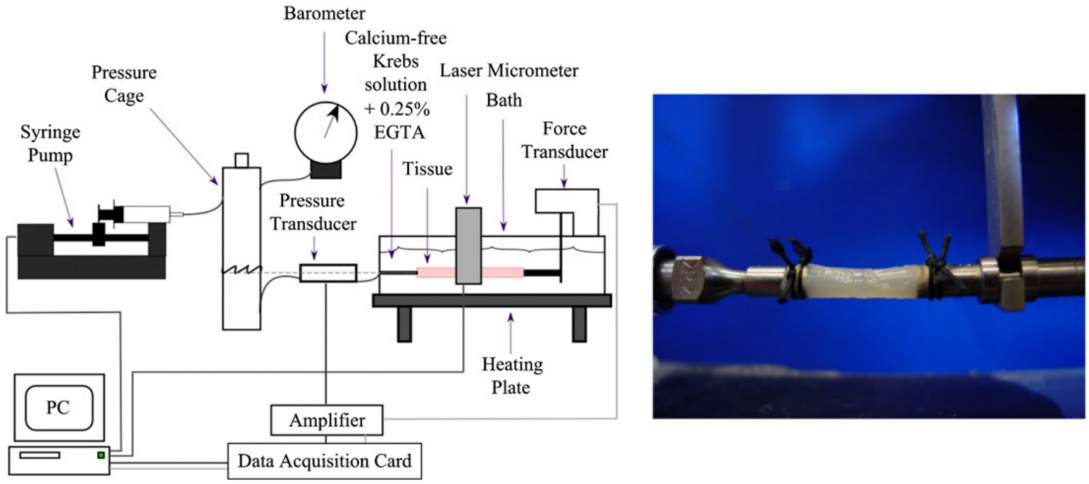

Figure 9. Schematic diagram of an inflation-extension experimental setup **(a)** and a close-up of a segment of rodent (Wistar rat) large intestine held in the grips prior to testing **(b)** [12].

2.3.1.9 Zero-stress state

It can be the case that a tissue in its no-load state is not necessarily also in its zero-stress state. In 1983, both Vaishnav and Vossoughi [183] and Fung [184] demonstrated this to be the case with arteries, and since then it has been determined that other soft biological tissues also possess residual stresses and strains in their no-load configuration [185], including the GI tract [186]. Figure 10 shows a schematic diagram of how a ring segment of a residually-stressed tubular tissue deforms between its no-load state (Figure 10a), i.e. no external loads, such as luminal pressures, are exerted on the wall, and its zero-stress state (Figure 10b), i.e. when all internal, residual stresses of the material have been released. The ring specimen deforms into a sector when, in its no-load state, it

is cut radially, producing a parameter by which the degree of residual strains within a tubular tissue can be evaluated: the opening angle, θ. The greater the opening angle, the greater the residual strains in the tissue specimen. Therefore, the opening angle can be used to compare the varying degree of residual strains throughout an organ (e.g. along its axial length) or between organs. To determine the residual stresses, however, the residual strains must be quantified, then the residual stresses can be calculated via a constitutive law.

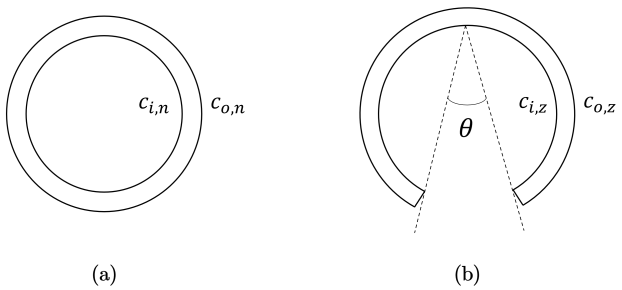

Figure 10. Schematic diagram showing the no-load state (**a**) and the zero-stress state (**b**) of a ring segment, including the definition of the opening angle, θ.

To determine the circumferential residual strains of a tubular tissue, the usual protocol is that described in Fung and Liu [187] where ring-like specimens of the tissue, 1-2 mm in length, are cut. The cross-section of these specimens are photographed, as seen in the pictures on the left and in the centre of Figure 11, then a radial cut is made to the wall of the ring. Usually this causes the specimens to open into an sector, as seen in Figure 10b and on the right in Figure 11. The specimens are given time to equilibrate, allowing any viscous effects to dissipate, and are then photographed again. The difference in lengths of the inner and outer circumferences of the specimens from the closed ring to the open sector are used to calculate the residual strains of the tissue. This method is based on some assumptions such as that the ring specimen is a perfect circle, though in reality this is not often the case. Recently, in 2019 and 2021, respectively, Sigaeva et al. [188] and Lefloch et al. [189] developed novel ways of assessing residual strains without this perfect circle assumption to make the measurement of tissue rings more accurate, particularly when the tissue being investigated is diseased (as these specimens are often more irregular compared to healthy tissue). However, within literature, currently most zero-stress state studies still use the method outlined in Fung and Liu [187] which is reasonably accurate when the samples keep their mainly circular geometric formation. As can be seen in Figure 11, this technique can be carried out on intact wall specimens or on ring-like specimens separated into their different layers [13]. It is also possible to study how the ring segments open over time, thus including the viscous effects (i.e.

time-dependent effects) in the residual stress/strain analysis.

Longitudinal prestretch can be determined by measuring the difference between the length of the tissue *in situ* and comparing this to its length *ex vivo*. In addition, longitudinal strips can be cut free from the wall and allowed to equilibrate. Similarly to the circumferential samples, the deformations of these longitudinal strips can be used to determine the residual strains in the longitudinal direction [190].

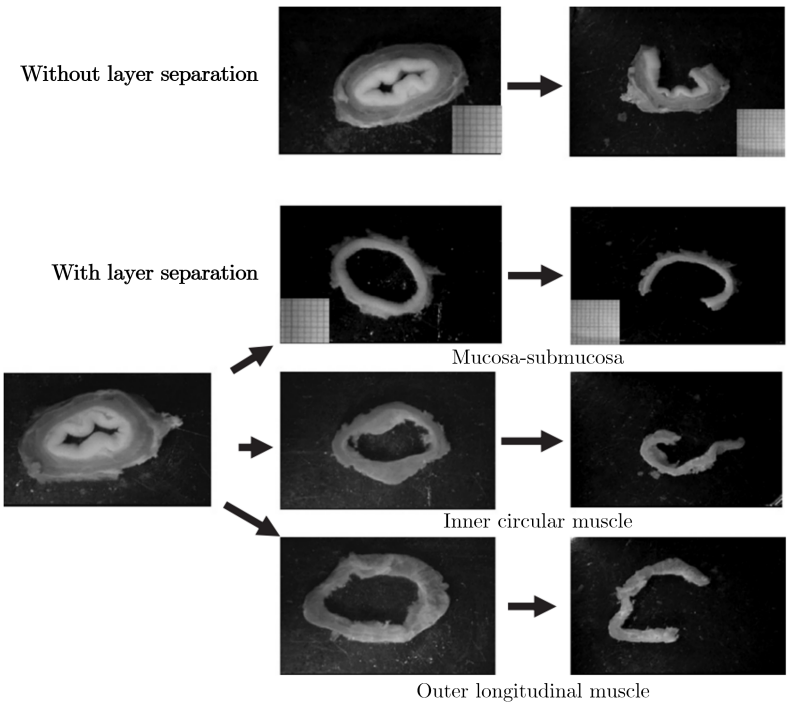

Figure 11. Experimental results showing the no-load and zero-stress state of circumferential ring specimens from the oesophagus of pigs, investigating the residual strains of the intact wall as well as the separated layers (mucosa-submucosa, circular muscle and longitudinal muscle). Figure modified from [13].

2.3.2 *In vivo*

In vivo experimentation is that carried out in the organ's natural environment on a subject which is alive. While *ex vivo* experimentation is often very similar to standard engineering material characterisation tests, *in vivo* tests on the GI organs pose an added complication of needing to measure the deformations of a material which cannot be seen with the naked eye [191].

2.3.2.1 Distension

Distension tests conducted *in vivo* are similar to those carried out *ex vivo* (Section 2.3.1.7), however, while a balloon is sometimes used when testing *ex vivo*, it is always used *in vivo* in order to keep the fluid contained. Unlike *ex vivo* distension testing, the outer diameter cannot be simply measured using a camera to determine the strain of the sample. Therefore, modalities such as impedance planimetry and ultrasound must be employed to determine the strain of the wall in relation to the pressure exerted by the volume of fluid injected into the organ's lumen [30,41,192,193].

2.3.2.2 Elastography

Elastography refers to a technique that uses imaging to non-destructively determine the stiffness of soft tissues *in vivo*, and thus can be used to quantify their material behaviour in their physiological environment [194]. Furthermore, elastography can be used clinically to identify the health state of soft tissues [195–197]. There are many different types of elastography and their type depends on how the strains are measured; however, in essence, firstly a stimulus is applied to the tissue, for instance a vibration [195] or a compression [156], the deformation is then tracked via an imaging modality such as ultrasound, magnetic resonance or optics, and, finally, the tissue's mechanical properties are determined computationally through inverse analysis [194]. For a comprehensive understanding of ultrasound, optical and magnetic resonance elastography, readers are referred to the reviews by Li and Cao [194], Kennedy et al. [198] and Low et al. [199], respectively.

2.4 Review findings

The number of search results, articles screened from the search and articles added by the author for each organ can be found in Table 2. Out of all the articles, the proportion of studies collected for the oesophagus was 33%, for the small intestine 29%, for the large intestine 18%, for the stomach 11% and for the rectum 9%. Figure 12 shows the number of publications for each organ as a function of year in which they were published. The results for each organ were organised into whether the experimentation was conducted *ex vivo* or *in vivo*, for which the number of articles for each state can be seen in Figure 13.

It should be noted that in this review, experiments conducted *in situ* on alive subjects have been considered as *in vivo*, and *in situ* experiments conducted on deceased subjects have been regarded as *ex vivo*. There were so few *in situ* experiments that they did not warrant a results table of their own. This explains how an "indentation test" may be conducted *in vivo* (Table 4); in actuality it

was conducted *in situ* while the subject was still alive.

In some studies, different types of experiments were conducted, either using various techniques, e.g. *ex vivo* inflation-extension and *ex vivo* zero-stress state analysis, and/or different organs, e.g. large intestine and rectum, and/or different species, e.g. pig and human. From this point forward, each test situation (i.e. species, organ and experimental technique) will be treated as separate even if they are presented within the same article, and will, therefore, be referred to as individual "experiments".

Table 2: The number of search results for each organ, screened articles from the search, articles added by the author and the total number of articles considered per organ. Altogether, the total number of articles collected was 245.

	Oesophagus	Stomach	Small intestine	Large intestine/colon	Rectum
PubMed search results	732	464	556	653	311
Screened articles from search	59	22	61	36	13
Articles added by author	21	6	11	7	8
Total number of articles	80	28	72	44	21

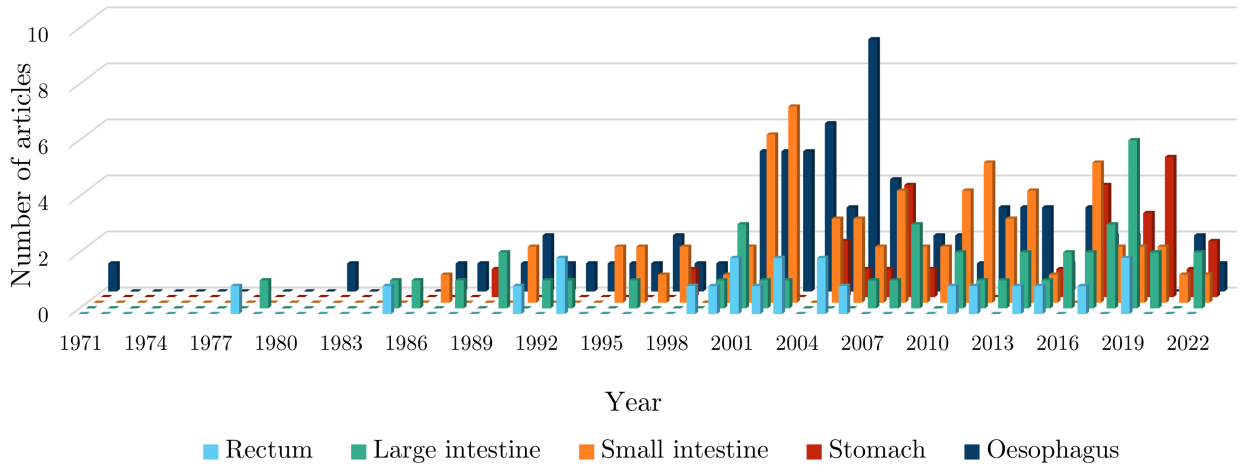

Figure 12. Number of articles published per year per GI organ according to this review.

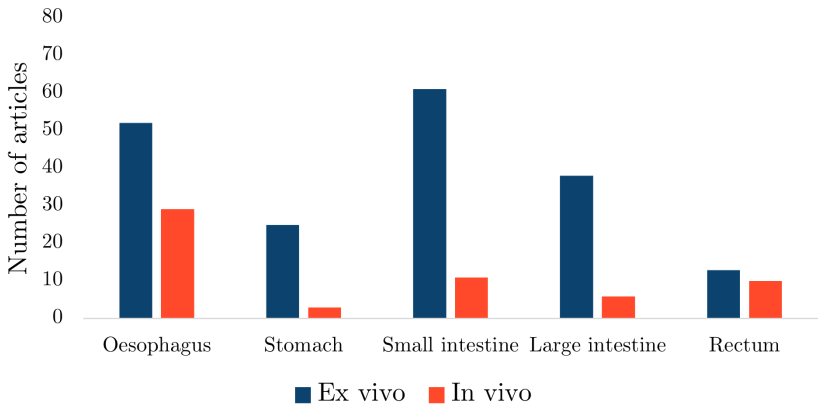

Figure 13. The number of *ex vivo* and *in vivo* studies collected per organ.

2.4.1 Oesophagus

The oesophagus had the greatest number of experimental studies out of all the GI organs (Table 2). The experiments conducted on the oesophagus *ex vivo* have been summarised in Table 3. Of these studies, several looked into the effects of pathological conditions on the organ's mechanical properties, including oesophageal varices in rabbits [78, 79], osteogenesis imperfecta in mice [200], oesophagitis in humans [48], diabetes in rats [4, 72–77] and cancer in pigs [201]. Zeng et al. [74] looked at how diabetes affects the material behaviour of rodent oesophagi over time. As a treatment for diabetic GI disorder, Liu et al. [76] studied the effect of Tangweian Jianji (a Chinese medicinal compound) on the mechanical properties of the oesophagus in diabetic rats. Others looked at the effects of epidermal growth factor (EGF) to investigate how abnormal growth may affect the function of the oesophagus in rats [140], while some investigated the effect of ageing on the mechanical properties of the oesophagus in humans [48] and Wistar rats [202, 203].

Most *ex vivo* studies of the oesophagus investigated its passive material properties, however some studied its active properties: Tøttrup et al. [50] looked at the active properties of human oesophageal muscle, and Wareham and Whitmore [204] investigated the active mechanical properties of the muscularis propria of guinea pig oesophagi. As can be seen in Figure 14a, *ex vivo* experimentation on the oesophagus was conducted using a wide variety of animals. Experiments conducted on oesophagi from rats were the most prevalent, while *ex vivo* experimentation conducted on human tissue accounted for only 4%.

The oesophagus had the most *in vivo* studies of all the organs considered (Figure 13), a summary of which can be found in Table 4. Several conditions were studied in regard to their effect on the

mechanical properties of the oesophagus *in vivo*, including oesophageal varices in rabbits [79, 80], nutcracker oesophagus (i.e. abnormal peristalsis) in humans [27], chest pain of oesophageal origin (sometimes referred to as functional chest pain) in humans [28, 32, 35, 36], systemic sclerosis in humans [25, 29, 37] and type-1 diabetes in humans [43]. Gregersen et al. [205] studied the mechanical changes that occur in the oesophagi of opossums that have been obstructed. Juhl et al. [206] investigated the effect of damage caused by endoscopic sclerotherapy on the mechanical properties of minipig oesophagi, while Vinter et al. [85] studied the potential viability of EGF as a treatment (therapeutic potential) for this damage, also using oesophagi from minipigs. Drewes et al. [31, 33, 34] conducted several studies on pain perception in relation to distension of the oesophagus in humans. Takeda et al. [41] studied the active and passive properties of the human oesophagus *in vivo* through the use of a muscle relaxant, atropine. As can be seen in Figure 14b, the majority of *in vivo* experimentation of the oesophagus was carried out on humans.

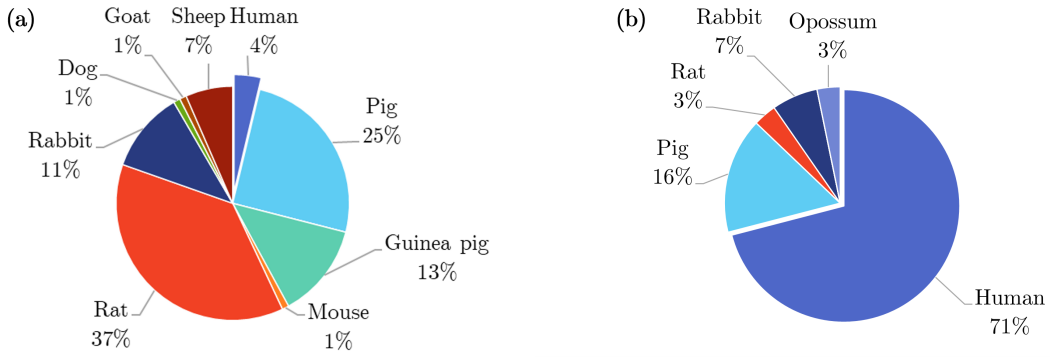

Figure 14. Pie charts indicating the species used in the *ex vivo* experimentation (n=107) **(a)** and *in vivo* experimentation (n=30) **(b)** on the oesophagus, highlighting, in particular, the proportion of experiments conducted on human tissue.

2.4.2 Stomach

Only 11% of all the articles collected in this review investigated the mechanical properties of the stomach (Table 2). A summary of the experiments conducted *ex vivo* on the stomach can be found in Table 5. Of these studies, Liao et al. [11] looked into the effects of disease on the stomach's material behaviour, in particular the impact of type-2 diabetes on the mechanical properties of stomach tissue from rats. Notably, Carniel et al. [175] and Toniolo et al. [142] studied stomach tissue removed from patients (humans) suffering with morbid obesity who had undergone a laparoscopic sleeve gastrectomy, while Marie et al. [84] investigated how sleeve gastrectomies affect the biomechanical behaviour of the stomach using specimens from pigs for which the surgical pro-

Table 3: Summary of *ex vivo* studies on the oesophagus.

	Species family	Tissue characterisation	Type of test	References
Isotropic	Human	Intact wall	Uniaxial tension	[47]
		Layer-dependent	Uniaxial tension	[50]
	Porcine	Intact wall	Uniaxial tension	[64]
			Pure shear	[64]
			Indentation (dynamic)	[207]
			Distension (pressure-CSA-wall thickness)	[61]
			Inflation-extension	[66]
			Tribological test	[208]
			Shear wave vibrometry	[201]
			Zero-stress state	[13, 66]
		Layer-dependent	Uniaxial tension	[64]
			Pure shear	[64]
			Inflation-extension	[66]
			Tribological test	[208]
			Shear wave vibrometry	[201]
			Zero-stress state	[13, 66, 209]
	Ovine	Intact wall	Axial tension of tubular specimens	[71]
	Caprine	Layer-dependent	Tension test of ring specimens	[210]
	Canine	Intact wall	Distension (pressure-diameter)	[211]
	Lagomorph	Intact wall	Uniaxial tension	[78]
			Axial tension of tubular specimens	[212]
			Distension (pressure-CSA)	[79, 213]
			Zero-stress state	[68, 212]
		Layer-dependent	Zero-stress state	[67, 68, 212]
	Rodent	Intact wall	Distension (pressure-diameter)	[4, 52, 54, 58, 77, 140, 214]
			Distension (pressure-CSA)	[56]
			Inflation-extension	[56, 57]
			Axial tension of tubular specimens	[58]
			Acoustic microsopy	[215]
			Zero-stress state	[4, 52–54, 57, 58, 72, 73, 75–77, 140, 200, 202, 203, 214, 216, 217]
		Layer-dependent	Uniaxial tension	[204]
			Distension (pressure-diameter)	[52, 55, 77, 214]
			Acoustic microsopy	[215]
			Zero-stress state	[52, 55, 77, 214, 216, 217]
Anisotropic	Human	Intact wall	Uniaxial tension	[48]
			Distension (pressure-diameter-length)	[48]
	Porcine	Intact wall	Uniaxial tension	[218]
			Indentation	[207]
			Sonometry	[65]
		Layer-dependent	Uniaxial tension	[59, 60, 63, 104, 208]
			Inflation-extension	[209]
			Tribological test	[218]
			Sonometry	[65]
	Ovine	Intact wall	Biaxial tension	[219]
			Inflation-extension	[70]
			Zero-stress state	[70]
		Layer-dependent	Uniaxial tension	[70]
			Biaxial tension	[70]
			Zero-stress state	[70]
	Lagomorph	Intact wall	Inflation-extension	[68, 69]
		Layer-dependent	Inflation-extension	[67]
	Rodent	Intact wall	Torsion	[74]
			Distension (pressure-diameter-length)	[76, 202, 203]
			Distension (pressure-CSA)	[56]
			Inflation-extension	[56]
			Inflation-extension-torsion	[53, 72, 73, 75]
		Layer-dependent	Inflation-extension-torsion	[73, 75]

Table 4: Summary of *in vivo* studies on the oesophagus.

	Species family	Tissue characterisation	Type of test	References
Isotropic	Human	Intact wall	Distension (pressure-CSA)	[24–39]
			Distension (pressure-volume)	[38, 40]
			Distension (pressure-CSA-wall thickness)	[41]
			Distension (pressure-CSA-volume)	[42]
	Porcine	Intact wall	Indentation (dynamic)	[207]
			Distension (pressure-CSA)	[85, 206, 220]
	Lagomorph	Intact wall	Distension (pressure-CSA)	[79, 80]
	Marsupial	Intact wall	Distension (pressure-CSA)	[205]
	Rodent	Intact wall	Distension (pressure-diameter)	[51]
Anisotropic	Human	Layer-dependent	Distension (pressure-CSA)	[43]
			Distension (pressure-CSA-volume)	[44]
	Porcine	Intact wall	Indentation	[207]

cedure had been performed *ex vivo*. In terms of the active behaviour of the stomach, Merlo and Cohen [221] evaluated the active mechanical properties of its muscle layers with tissue excised from cats, and Tomalka et al. [179] electrically stimulated the smooth muscle of pig stomachs to assess their behaviour. Furthermore, Klemm et al. [222] studied both the intact wall of the stomach from pigs (mucosal and muscular layers) and just its muscle layer to determine the contribution of each layer in the tissue's active behaviour, while Borsdorf et al. [158] investigated the active response of the combined muscle layer (oblique, longitudinal and circular muscle) and just the circular gastric smooth muscle layer to compare their influence on the mechanical behaviour of the stomach from domestic pigs.

In vivo experimentation on the stomach was the least common compared to the other GI organs (Figure 13), for which only the healthy, passive properties were investigated. A summary of the experiments carried out *in vivo* on the stomach can be found in Table 6. Stomach tissue originating from porcine was the overwhelming choice for studying the organ both *in vivo* and *ex vivo*, as can be seen in Figure 15, with one author stating that this decision originated from "the similarities between the porcine and the human digestive systems" [223]. Only 22% of the *ex vivo* experimentation was performed on human tissue (Figure 15a), while no human tissue was studied *in vivo* (Figure 15b).

2.4.3 Small intestine

Of all the GI organs, the majority of *ex vivo* experimentation was conducted on the small intestine (Figure 13). The summary of *ex vivo* experiments on the small intestine can be found in Table

Table 5: Summary of *ex vivo* studies on the stomach.

	Species family	Tissue characterisation	Type of test	References
Isotropic	Human	Intact wall	Simple shear (dynamic)	[224]
			Indentation	[142, 225]
			Confined compression (dynamic)	[224]
			Distension (pressure-volume)	[142, 175]
	Porcine	Intact wall	Indentation	[157]
			Distension (pressure-volume)	[84, 223, 226]
		Layer-dependent	Uniaxial tension	[158, 170, 179]
			Indentation	[227]
			Compressive elastography	[191]
			T-peel	[170]
	Feline	Layer-dependent	Uniaxial tension	[221]
	Rodent	Intact wall	Distension (pressure-CSA)	[228]
Anisotropic	Human	Intact wall	Uniaxial tension	[47, 142, 175]
	Porcine	Intact wall	Uniaxial tension	[84, 168, 177, 222, 229]
			Uniaxial tension (dynamic)	[230]
			Biaxial tension	[231, 232]
		Layer-dependent	Uniaxial tension	[177, 222, 229]
			Biaxial tension	[232]
			Pure shear	[173]
	Lagomorph	Intact wall	Uniaxial tension	[167]
			Zero-stress state	[167]
	Rodent	Intact wall	Uniaxial tension	[167]
			Distension (pressure-volume)	[11, 167]
			Zero-stress state	[167]

Table 6: Summary of *in vivo* studies on the stomach.

	Species family	Tissue characterisation	Type of test	References
Isotropic	Porcine	Intact wall	Indentation	[157]
	Canine	Intact wall	Distension (pressure-volume)	[233]
Anisotropic	Porcine	Layer-dependent	Compressive elastography	[156]

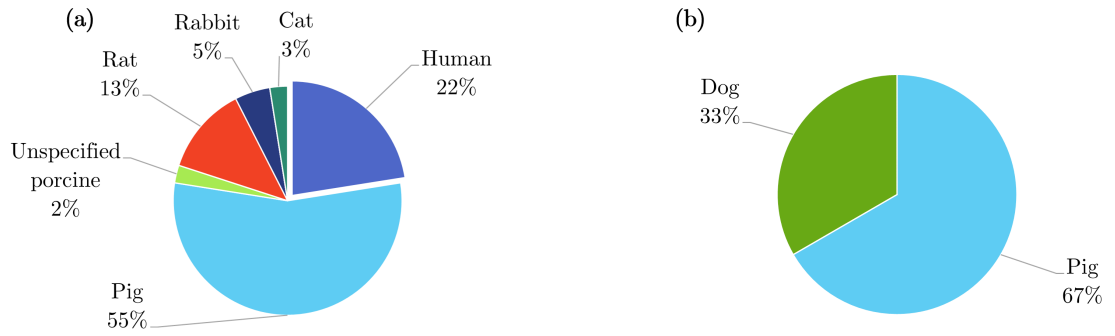

Figure 15. Pie charts indicating the species used in the *ex vivo* experimentation (n=40) **(a)** and *in vivo* experimentation (n=3) **(b)** on the stomach, highlighting, in particular, the proportion of experiments conducted on human tissue.

7. Conditions affecting the small intestine were studied, including diabetes in rats [139, 140, 176, 234–236], intestinal oedema in rats [237, 238], and Chinese medicines, namely Kaiyu Qingwei Jianji [86] and Tangweian Jianji [76], were investigated in rats regarding to their ability to treat the GI symptoms associated with diabetes. In addition, Zhao et al. [81, 239] investigated the active mechanical properties of the small intestine from rats with diabetes [239] and rats with a condition that mimics human irritable bowl syndrome (IBS) [81]. The effects of clinical interventions on the properties of the small intestine were also studied, including irradiation as a treatment for jejunal fibrosis in mice [240], chronic coeliac ganglionectomy in rats [82], small intestinal resection in rats [83] and distraction enterogenesis in pigs [241].

The influence of growth on the material behaviour of the small intestine was evaluated naturally, i.e. during physiological growth, in rats [242] and using EGF [243–246]. In addition, the effects of partial obstruction of the organ on its mechanical properties were studied in rodents [247, 248], and how these properties changed as a function of obstruction time was also investigated [249, 250]. The effect of partial obstruction on the active behaviour of the small intestine was studied in guinea pigs [251, 252], while Zhao et al. [253] studied the effect of ageing on the passive material response of the organ in rats.

Several studies investigated the effects of diet on the small intestine: how starvation [254] and re-feeding affects the mechanical properties of the small intestine was evaluated in rats by Dou et al. [255], how varying amounts of dietary protein affects minks by Chen et al. [256], the effects of a low-residue [257] and low-fibre [165] diet in rabbits, and the influence of a low-fibre diet on the active mechanical properties of the small intestine was studied in rabbits [258]. The active prop-

erties of the small intestine were considered *ex vivo* in rabbits [258, 259], rats [81, 82, 239, 260], guinea pigs [251, 252], mice [10] and pigs [261], while no active studies were conducted using human tissue *ex vivo*.

There were a number of studies that looked at the properties of the small intestine *in vivo*, a summary of which can be found in Table 8. Of these, Pedersen et al. [262], Gregersen et al. [263] and Gao et al. [264] evaluated the effect (disease compared to healthy controls) of systemic sclerosis on both the passive and active mechanical properties of the small intestine in humans, and Frøkjær et al. [43] investigated the active response of the small intestine in patients with type-1 diabetes and compared the observed behaviour to that of healthy controls. Moreover, the active properties of healthy humans and mice were studied *in vivo* by Gao et al. [265] and Lu et al. [10], respectively. Figure 16 shows the proportion of each type of tissue used for both the *ex vivo* experimentation (Figure 16a) and the *in vivo* experimentation (Figure 16b). The majority of *ex vivo* experiments were conducted using rats, with only 4% on human tissue, while the main proportion of *in vivo* experiments were carried out on humans (42%) closely followed by pigs (34%).

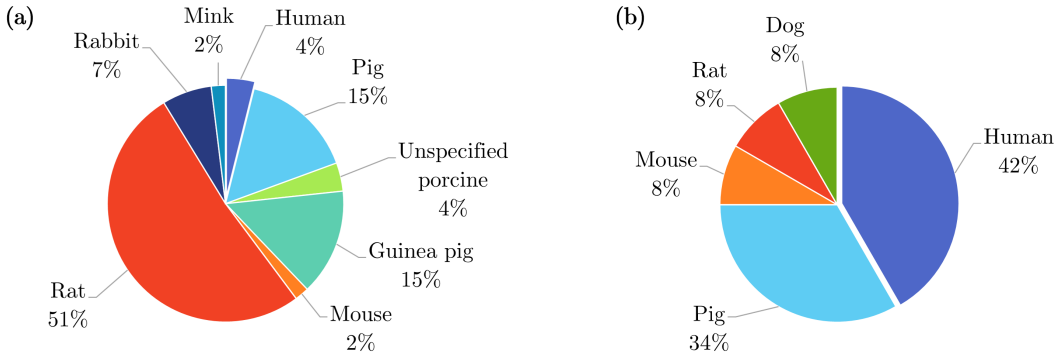

Figure 16. Pie charts indicating the species used in the *ex vivo* experimentation (n=103) **(a)** and *in vivo* experimentation (n=12) **(b)** on the small intestine, highlighting, in particular, the proportion of experiments conducted on human tissue.

2.4.4 Large intestine

Approximately 20% of all *ex vivo* articles collected in the review conducted experimentation on the large intestine (Figure 13); a summary of these experiments can be found in Table 9. Notably, the effects of a number of diseases on the mechanical behaviour of the large intestine were investigated, including chronic obstruction of the colon in mice which mimics human Hirschsprung's disease [285], colitis in rodents [286–289] and human growth hormone as a potential treatment

Table 7: Summary of *ex vivo* studies on the small intestine.

	Species family	Tissue characterisation	Type of test	References
Isotropic	Human	Intact wall	Uniaxial tension	[241, 266]
			Uniaxial tension (dynamic)	[267]
	Porcine	Intact wall	Uniaxial tension	[241, 266, 268]
			Simple shear (dynamic)	[269, 270]
			Indentation	[157]
			Distension (pressure-CSA)	[271]
			Tribological test	[269]
			Extrusion test	[272]
			Zero-stress state	[273]
		Layer-dependent	Uniaxial tension	[241]
			Tribological test	[261]
	Lagomorph	Intact wall	Distension (pressure-diameter)	[165, 257, 258]
			Zero-stress state	[165, 257, 258]
	Weasel	Intact wall	Zero-stress state	[256]
	Rodent	Intact wall	Distension (pressure-diameter)	[76, 81, 235, 236, 239, 274, 275]
			Distension (pressure-length)	[190]
			Distension (pressure-CSA)	[139, 243, 276]
			Distension (pressure-volume)	[99, 277]
			Inflation-extension	[249, 251, 252, 260]
			Tension of ring specimens	[240]
			Axial tension of tubular specimens	[176, 237, 238]
			Zero-stress state	[83, 140, 190, 234, 237, 238, 242, 244–246, 254, 255, 278–281] [76, 81, 86, 235, 239, 247–249, 251–253, 260, 274, 282, 283]
		Layer-dependent	Uniaxial tension	[82]
			Distension (pressure-diameter)	[274]
			Zero-stress state	[274]
Anistoropic	Human	Intact wall	Uniaxial tension	[47]
	Porcine	Intact wall	Uniaxial tension	[5, 18]
			Biaxial tension	[6, 261, 268]
			Pure shear	[173]
			Distension (pressure-diameter-length)	[273]
		Layer-dependent	Uniaxial tension	[259]
	Weasel	Intact wall	Distension (pressure-diameter-length)	[256]
	Rodent	Intact wall	Distension (pressure-diameter-length)	[76, 83, 140, 242, 244, 253–255, 280]
			Inflation-extension	[245–247, 283]
			Inflation-extension-torsion	[248]
			Zero-stress state	[250]

Table 8: Summary of *in vivo* studies on the small intestine.

	Species family	Tissue characterisation	Type of test	References
Isotropic	Human	Intact wall	Distension (pressure-CSA)	[262–265]
			Distension (pressure-volume)	[265]
	Porcine	Intact wall	Indentation	[157]
			Distension (pressure-CSA)	[284]
			Contact force test	[261]
		Layer-dependent	Tribological test	[261]
	Canine	Intact wall	Distension (pressure-volume)	[233]
Anisotropic	Human	Layer-dependent	Distension (pressure-CSA)	[43]

for this in rats [290], ulcerative colitis in mice [291], diabetes in rats [141], Crohn's disease in humans [286], IBS in rats [81], and cancer in humans [292]. Conditions such as hypertension were also studied in rats [9], and the active response of large intestinal muscle to inflammatory mediators was investigated in both humans and rabbits [293]. Additionally, the effect of coeliac ganglionectomy on the mechanical properties of the large intestine was evaluated in rats [82]. Yang et al. [294] looked at the result of EGF treatment over varying periods of time on the mechanical properties of the rat large intestine. Watters et al. [295] and Massalou et al. [296] considered the effects of age and sex on the material behaviour of the large intestine in rats and humans, respectively, and in another study, Watters et al. [297] looked at the influence of ethnic origin in humans. In terms of the effect of food-intake on the mechanical properties of the intestines, Liu et al. [165] investigated the consequence of a long-term low-fibre diet in rabbits.

As can be seen in Figure 17a, experiments on rodents, specifically mice and rats, accounted for 51% of the *ex vivo* experimentation on the large intestine, with only 18% conducted using human tissue. Contrarily, half of all *in vivo* experimentation regarding the large intestine was carried out on humans, as shown in Figure 17b. A summary of the *in vivo* experiments conducted on the colon can be found in Table 10. Of these experiments, Petersen et al. [298] assessed the relationship between pain during distension of the large intestine and its stress-strain response in healthy human subjects, while Drewes et al. [192] studied the difference in pain during large intestinal distension, and its associated biomechanical parameters, between patients with IBS and healthy human controls.

In terms of the active properties of the large intestine, *ex vivo* experimentation was carried out on rabbit [293, 299], human [293, 300], cat [301] and rat [81, 82] tissue, and *in vivo* experimentation was conducted on humans [302]. For further understanding of the active behaviour of the large intestine from a mechanical perspective, readers are referred to the literature review of Bhattarai et al. [303].

2.4.5 Rectum

The rectum had the least amount of *ex vivo* mechanical experimentation compared to the other GI organs (Figure 13), a summary of which can be found in Table 11. Notable studies included those by Watters et al. [295] who looked at the influence of sex and age on the material behaviour of the rectum in rats; Glavind et al. [318] who conducted experimentation in regard to the active prop-

Table 9: Summary of *ex vivo* studies on the large intestine.

	Species family	Tissue characterisation	Type of test	References
Isotropic	Human	Intact wall	Uniaxial tension (dynamic)	[296]
			Shear rheometry	[292]
			Tension of ring specimens	[297]
			Elastography	[286]
		Layer-dependent	Uniaxial tension	[300]
	Porcine	Intact wall	Zero-stress state	[304]
	Caprine	Intact wall	Uniaxial compression	[305]
	Feline	Layer-dependent	Uniaxial tension	[301]
	Lagomorph	Intact wall	Distension (pressure-diameter)	[165]
			Zero-stress state	[165]
	Rodent	Intact wall	Uniaxial tension	[287]
			Indentation	[9]
			Distension (pressure-diameter)	[10, 81, 306]
			Tension of ring specimens	[285, 295]
			Elastography	[286, 288, 289]
			Zero-stress state	[12, 81, 141, 291, 294, 307, 308]
		Layer-dependent	Uniaxial tension	[82]
			Distension (pressure-diameter)	[306]
Anisotropic	Human	Intact wall	Uniaxial tension	[47, 87]
			Uniaxial tension (dynamic)	[309, 310]
		Layer-dependent	Uniaxial tension	[293]
	Porcine	Intact wall	Uniaxial tension	[87, 169, 311, 312]
			Biaxial tension	[303, 313, 314]
			Pure shear	[173]
			Simple shear	[311]
			Inflation-extension	[304]
		Layer-dependent	Uniaxial tension	[312]
	Lagomorph	Intact wall	Uniaxial tension	[299]
		Layer-dependent	Uniaxial tension	[293]
	Rodent	Intact wall	Biaxial tension	[308]
			Distension (pressure-diameter-length)	[141, 291, 307]
			Inflation-extension	[12, 315]
		Layer-dependent	Biaxial tension	[316]
			Zero-stress state	[316]

Table 10: Summary of *in vivo* studies on the large intestine. It should be noted that all the studies referenced here studied the behaviour of the large intestine in just one direction (isotropic).

Species family	Tissue characterisation	Type of test	References
Human	Intact wall	Distension (pressure-CSA)	[192, 298]
		Distension (pressure-volume)	[302]
Porcine	Intact wall	Indentation	[157]
Caprine	Intact wall	Uniaxial compression	[317]
Rodent	Intact wall	Distension (pressure-diameter)	[10]

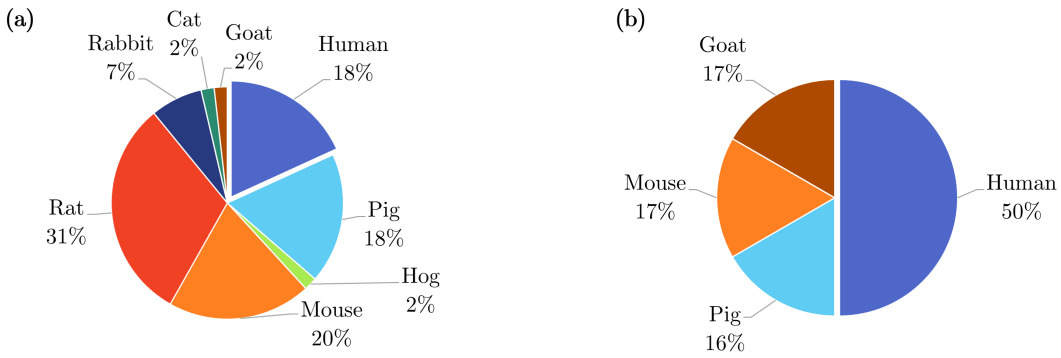

Figure 17. Pie charts indicating the species used in the *ex vivo* experimentation (n=55) **(a)** and *in vivo* experimentation (n=6) **(b)** on the large intestine, highlighting, in particular, the proportion of experiments conducted on human tissue.

erties of the human rectum's muscle layer; Gregersen et al. [319] who studied how the rectum of mice was affected by irradiation; Yang et al. [294] who evaluated the change in mechanical properties experienced when growth of the rat rectum was induced by EGF; and Brunenieks et al. [320] who investigated the effect of obstructed defecation syndrome on the biomechanical properties of the human rectal wall, comparing the abnormal tissue extracted from surgical resection to tissue excised from healthy humans post-mortem. Figure 18a shows that most *ex vivo* experimentation on the rectum was carried out using rodent tissue (mice and rats), comprising 61% of the total number of experiments conducted.

It can be seen in Figure 18b that the vast majority of *in vivo* experimentation of the rectum was conducted on humans. Of these *in vivo* experiments, of which a summary can be found in Table 12, a few investigated the effects of different conditions. For instance, Arhan et al. [321] studied the difference in viscoelastic behaviour of the rectal wall between patients with Hirschsprung's disease and healthy, age-matched controls; Lundby et al. [322] looked at the effect of age on the mechanical properties of the rectum in mice; and Petersen et al. [298] conducted experimentation to assess the biomechanical behaviour of the human rectum, studying how the pain felt by the volunteer during distension was associated with the tissue's stress-strain response. The same group then went on to look at how the mechanical response and pain differed during distension before and after smooth muscle relaxation [193]. Furthermore, Drewes et al. [192] investigated the difference in rectal mechanical parameters and levels of pain between patients with IBS and healthy human controls, and in another study evaluated again the relation between pain and biomechanical properties of the rectum but this time in patients with ulcerative colitis [323], comparing their results against healthy controls.

Table 11: Summary of *ex vivo* studies on the rectum.

	Species family	Tissue characterisation	Type of test	References
Isotropic	Human	Intact wall	Uniaxial tension	[320]
		Layer-dependent	Uniaxial tension	[318]
	Porcine	Intact wall	Uniaxial tension	[324]
			Simple shear	[8]
			Uniaxial compression	[8]
	Rodent	Intact wall	Tension test of ring specimens	[295]
			Zero-stress state	[12, 294, 307, 308, 319]
Anisotropic	Human	Intact wall	Uniaxial tension	[87, 106]
	Porcine	Intact wall	Uniaxial tension	[8, 87]
	Rodent	Intact wall	Biaxial tension	[308]
			Distension (pressure-diameter-length)	[307]
			Inflation-extension	[12]
		Layer-dependent	Biaxial tension	[316]
			Zero-stress state	[316]

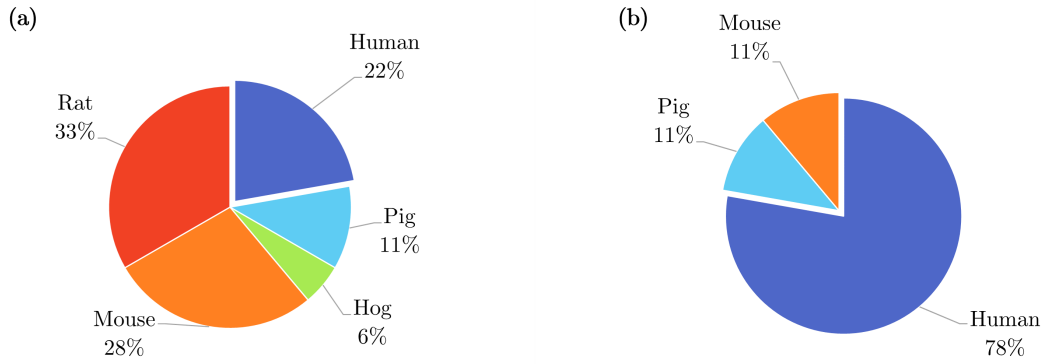

Figure 18. Pie charts indicating the species used in the *ex vivo* experimentation (n=18) **(a)** and *in vivo* experimentation (n=9) **(b)** on the rectum, highlighting, in particular, the proportion of experiments conducted on human tissue.

2.4.6 Experimental particulars

In this section of the review findings, we will focus on the particulars of the experiments, including which experiments involved investigation of the tissue's time-dependent properties (Section 2.4.6.1), whether preconditioning of the sample was performed prior to data collection (Section 2.4.6.2), if, for the *ex vivo* experimentation, the tests were carried out in a saline solution bath (Section 2.4.6.3), and whether the studies conducted histological analysis alongside their mechanical experimentation to provide information on the microstructural components of the tissue and how they might influence its stress-strain behaviour (Section 2.4.6.4).

Table 12: Summary of *in vivo* studies on the rectum.

	Species family	Tissue characterisation	Type of test	References
Isotropic	Human	Intact wall	Distension (pressure-diameter) Distension (pressure-CSA)	[321] [192, 193, 298, 323, 325]
	Porcine	Intact wall	Distension (pressure-CSA)	[326]
	Rodent	Intact wall	Distension (pressure-CSA)	[322]
Anisotropic	Human	Intact wall	Distension (pressure-CSA-arc length)	[327]

2.4.6.1 Time-dependent behaviour

Soft tissues often present as viscoelastic materials [328]; this means that relaxation and creep can be seen in their material response, and, thus, that their mechanical behaviour is time-dependent. Some of the studies included in this review investigated the time-dependent behaviour of the GI organs, a summary of which can be found in Table 13. The proportion of experiments for each organ in which their material properties were considered as a function of time are illustrated in Figure 19.

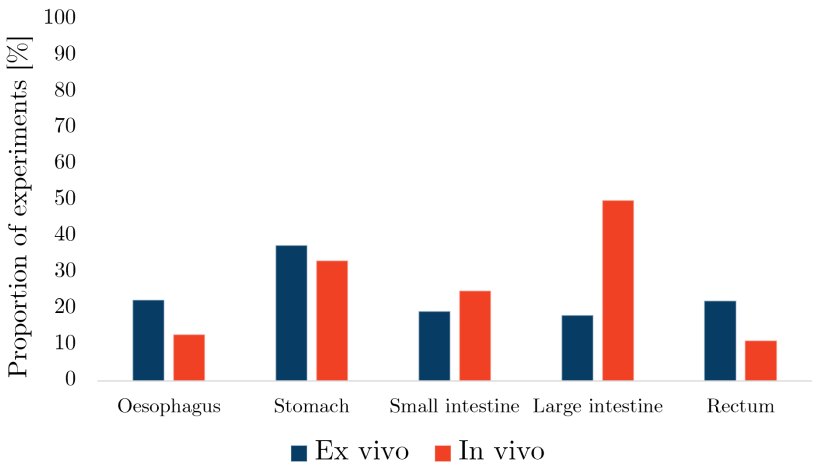

Figure 19. Proportion of studies for each organ, specified according to *ex vivo* and *in vivo* experimentation, that investigated the time-dependent properties of the tissue.

2.4.6.2 Preconditioning

Preconditioning is the process of "conditioning" a sample before collecting data in regard to its material response, and involves loading and unloading the sample successively for a pre-determined number of cycles. The process came about through the study of polymers, which behave in a similar way to soft tissues in that they are highly elastic, usually possess viscous qualities and can exhibit history-dependent behaviour. Preconditioning of polymers is to remove the Mullins effect:

Table 13: Summary of studies that considered the time-dependent behaviour of the GI tissues.

Tissue	**Species family**	**References**	
		Ex vivo	*In vivo*
Oesophagus	Porcine	[59, 65, 104, 201, 207, 208]	[207]
	Caprine	[210]	
	Lagomorph		[80]
	Rodent	[53–55, 58, 77, 204, 216]	[51]
Stomach	Human	[142, 175, 225]	
	Porcine	[158, 177, 179, 223, 230]	[157]
Small intestine	Human	[47, 266]	[263, 265]
	Porcine	[157, 266, 269–272]	[157]
	Lagomorph	[165]	
	Rodent	[99, 176, 236, 260, 275–277, 281]	[329]
Large intestine	Human	[292, 297, 310]	[302]
	Porcine	[311]	[157]
	Caprine	[305]	[317]
	Lagomorph	[165]	
	Rodent	[9, 295, 308, 316]	
Rectum	Human		[321]
	Rodent	[295, 308, 316]	

a purely history-dependent softening of the material that depends on the previous maximum strain that it has been subjected to [330]. With soft tissues, the equivalent term is stress-softening. It was once thought that preconditioning reduced the influence of soft tissues' time-dependent, i.e. viscous, properties, however, through research of the myocardium by Emery et al. [98], it was established that it has mainly an effect on their history-dependent properties. This was confirmed as well for the guinea pig small intestine by Gregersen et al. [99]. Therefore, the preconditioning process for soft tissues results in reducing history-dependent effects on their behaviour, as well as some time-dependent effects, which tend to plateau after a minimum of three repeated cycles. Figure 20 shows the proportion of studies evaluated in this review that preconditioned the tissue before collecting their results, for both *in vivo* and *ex vivo* experiments.

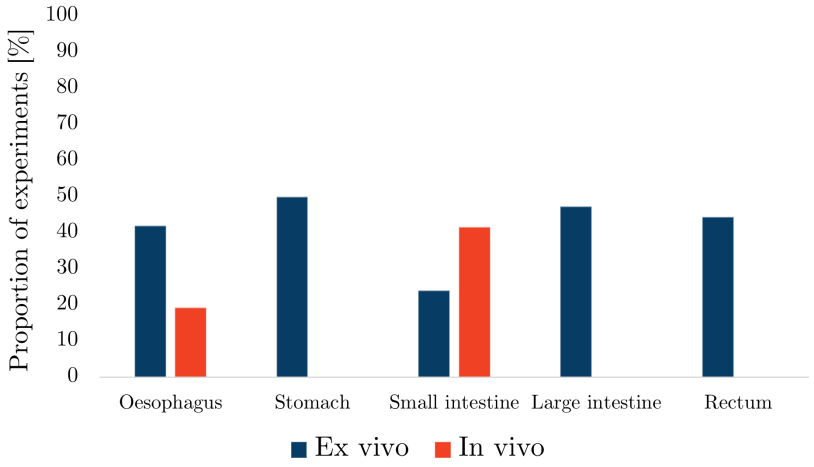

Figure 20. Proportion of studies for each organ, specified according to *ex vivo* and *in vivo* experimentation, that preconditioned the tissue.

2.4.6.3 Saline solution bath

As previously mentioned in Section 2.3.1, for *ex vivo* mechanical experimentation, measures are often taken to simulate a physiological environment. The main method for achieving this is by conducting experiments on samples immersed in a chamber (or bath) filled with a salt solution. This is done to prevent dehydration of the soft tissue, which has been found to cause alteration to their mechanical properties [331]. Sometimes these chambers are thermo-regulated so that the temperature of the tissue can be maintained at internal body temperature (37°C) throughout testing. As can be seen in Figure 21, the majority of *ex vivo* experiments considered in this review were performed using a saline solution bath, the organ with the highest proportion being the oesophagus

with 78%. Almost all *ex vivo* studies stored their tissue specimens in some variety of salt solution between tests, however Figure 21 only shows the percentage of those which performed their tests in a bath of it. The other studies, e.g. the remaining 28% of the oesophageal experiments, often kept the samples moist by alternative means such as spraying the samples with saline during testing [331]. The types of salt solutions that were used in the experimental studies on the GI tissues included physiological saline (0.9% NaCl) [65, 169, 287, 304], phosphate-buffered saline (PBS) [70, 71, 173, 209] and Krebs solution [61, 82, 140, 165, 294, 316], which were sometimes aerated with oxygen and carbon dioxide [61, 82, 165, 294].

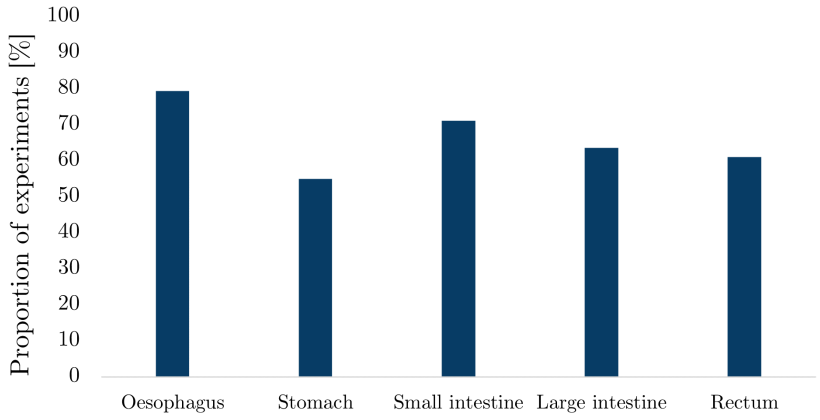

Figure 21. Proportion of *ex vivo* studies for each organ that conducted the experiments within a salt solution bath.

2.4.6.4 Histology

As previously briefly discussed in Section 2.1, the microstructural components of soft tissues influence their macrostructural behaviour. Histological analysis provides a well-established means to investigate the various microstrutural features of tissues, the images from which can be used to establish the prevalence (fraction) and orientation of their collagen, elastin and muscle fibres [217]. The analysis is carried out by removing a very thin slice of a tissue sample, putting the slices on a slide and then using different stains to highlight different microstructural features [127, 137]. Finally, images are taken which can then be post-processed and analysed to establish the fraction and orientation of the aforementioned fibres. This information can help to discuss reasons for the experimentally observed behaviour and potentially deduce their more specific affect (for example, by artificially increasing or decreasing the fraction of fibres and using the histological images to quantify the change), and inform (micro)structural constitutive modelling [7]. Figure 22 shows

the proportion of experiments that conducted histological inspection alongside their biomechanical investigation. Histological analysis was considered here because it is the most prevalent and traditional means of assessing the microstructure of soft tissues, however for an outline of more modern techniques such as second-harmonic generation (SHG) microscopy and optical-based analysis, readers are referred to Siri et al. [161] and Goth et al. [332], respectively.

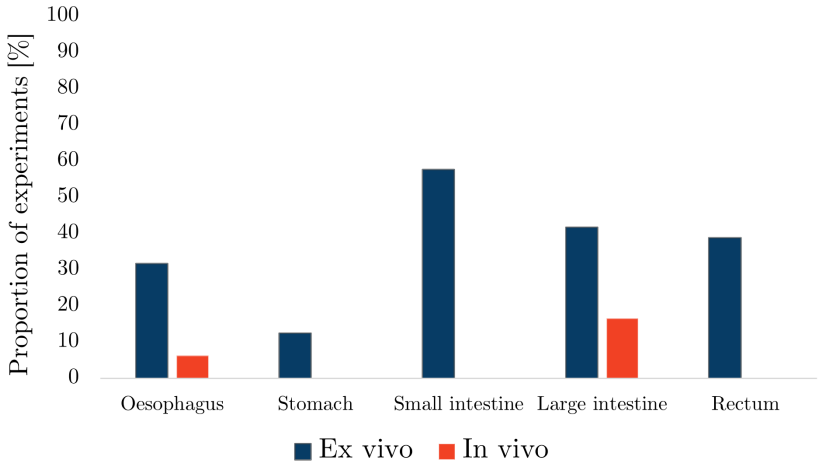

Figure 22. Proportion of studies for each organ, specified according to *ex vivo* and *in vivo* experimentation, that investigated the histological composition of the tissue alongside their mechanical tests.

2.5 Discussion

The review findings showed that the GI tissues of a number of different species were tested using an array of experimental approaches. Here, some of the experimental aspects will be discussed in more detail.

2.5.1 *In vivo* vs. *ex vivo*

The main drive of mechanically testing human soft tissues is to establish their material behaviour in the context of their natural environment, i.e. as digestive organs inside the body for the GI tract, for which *in vivo* studies provide the most accurate behaviour being that the tissue is still alive and perfused with blood [225]. Other aspects such as the internal temperature, moisture levels and structural integrity of the organ are also maintained during *in vivo* testing [191]. The use of a thermo-regulated saline bath can be used for *ex vivo* experimentation in an attempt to control the

temperature and moisture variables, however the tissue is still deceased and will not have exactly the same mechanical properties as it would *in vivo* due to phenomena such as rigor mortis and the relaxation of residual stresses [191]. The structural integrity can be maintained during *ex vivo* experiments such as distension and inflation-extension tests, however, the organ being tested has still been detached from its natural position and the connective tissue holding the organ in place has been cut, therefore aspects such as its interaction with surrounding organs or structures are not included in its characterisation [84]. Despite this, the *in vivo* experimentation carried out on the GI organs were mostly distension tests where the behaviour was characterised in only one direction and a homogeneous tissue wall was assumed, while testing *ex vivo* allows for a wider variety of experimental tests and the more complex behaviour of the organ to be investigated.

In addition, the deformation of the tissue in supraphysiological loading domains, such as is the case in surgery [225] or road traffic accidents [309], cannot be carried out *in vivo* as this may cause irreversible damage to a subject that is still living, whereas *ex vivo* experimentations allows for the rupture points and dynamic properties of the tissues to be established because the organ is no longer required [174, 310]. The ethical constraints associated with *in vivo* testing for both animals and humans are much greater than for *ex vivo* experimentation due to the pain, discomfort and damage the tests might cause to a living subject. Furthermore, data that is collected from a living subject often has more noise associated with it compared to *ex vivo* testing due to the movement caused by the beating heart and respiration [157]. In terms of layer-dependent properties of a GI tissue, these are usually more easily established *ex vivo* by separating the layers and testing them individually. In addition, this allows for the discrete properties of the layers to be established, which is not the case with *in vivo* or *in situ* layer-dependent analysis [44, 156]. Moreover, residual strains within the GI organs are traditionally established *ex vivo*. However, methods to quantify them *in vivo* are being developed for arterial tissue [333], which can be applied to the GI organs due to their similar anatomical structure.

There are benefits and limitations to both *in vivo* and *ex vivo* experimentation, however *in vivo* testing provides a more realistic understanding of the behaviour of soft tissues in the conditions we are interested in. Therefore, effort should be made to further develop *in vivo* mechanical characterisation techniques that establish the organ's direction-dependent behaviour, as well as the internal residual stresses and strains. *Ex vivo* experimental characterisation should still be carried out for the higher end of large strain deformations, i.e. supraphysiological loading, and to establish the properties of the discrete layers of the tract.

2.5.2 Organs tested

Out of all the experimental articles, the oesophagus was the organ investigated the most, with a total of 80 articles collected in this review (Table 2). The tissue studied the least was the rectum for which 21 articles were found in regard to its biomechanical characterisation, closely followed by the stomach with 28 articles. While the small intestine had a greater number of *ex vivo* articles than the oesophagus, the oesophagus had, overwhelmingly, the highest number of *in vivo* articles which contributed towards the organ having the most experimental articles overall. The high number of *in vivo* tests compared with the other organs could be due to the anatomical position of the oesophagus in that it is easily accessible for biomechanical measurements using a probe inserted through the mouth. Something similar can be said for the rectum, where the number of *in vivo* articles is almost the same as the *ex vivo* articles, a relationship not seen for any of the other organs, for which the number of *ex vivo* articles is much higher than the *in vivo* studies, particularly for the stomach, small intestine and large intestine. This is also thought be due to the more accessible position of the rectum where in which a probe can be simply positioned through the anus.

2.5.3 Species tested

The findings show that animal tissue was used far more prevalently than human tissue for mechanical testing of the GI tissues: out of the articles considered, human tissue was investigated in 19% of the studies on the oesophagus, 21% of the studies on the stomach, 8% of the studies on the small intestine, 21% of the studies on the large intestine and in 41% of the studies on the rectum. This could be due to the fact that animals/animal tissues are a lot more accessible and are associated with fewer ethical constraints compared to testing with humans/human tissues. As mentioned in Section 2.5.2, the greater proportion of human studies on the rectum is thought to be due to it being a more easily accessible GI organ (along with the oesophagus) when conducting studies on live humans (*in vivo*).

For applications within medicine where the material properties of the tissue will be used quantitatively, such as in thoracic surgical simulations, biomechanical data from human tissue should be used. However, there are benefits to using animal tissue, particularly for the investigation of diseased states, and discussing this data qualitatively in regard to the human organ. The greatest benefit may be demonstrated through the use of mice or rat models. These animals are able to

be grown in a very controlled environment, where their age, diet, living conditions, etc., can be decided and closely monitored. This allows for the environmental factors that influence the mechanical behaviour of the tissue, and which contribute to variability in the data, to be controlled and recorded, producing more reproducible data than between different humans/human specimens. Additionally, there are many rat and mice models that exist to simulate different human diseases, such as type-1 and type-2 diabetes, IBS, and Hirschsprung's disease. Therefore, testing of these animals allows for a highly controlled investigation of the effects of disease on the mechanical properties of the organs. However, quantitatively, the mechanical results of experiments conducted on animals tissues will not be the same as for human tissues as aspects such as size, tissue structure and digestive demands differ, and so these results should not be used to determine the material parameters for models that will be used in medicine unless no human experimental data is available. Porcine tissue is often chosen due to porcine having a digestive system close to that of humans [223], however when comparing between human and porcine data, there are still significant differences between their mechanical properties and so, ideally, data from porcine tissue should not be used directly for applications within medicine [87].

2.5.4 Sample size

In addition to providing a better control of experimental design than with human specimens, animal specimens often offer the possibility to test a larger sample size, making the final results more robust. Either it is difficult to obtain human volunteers for *in vivo* tests, especially for the GI tract which can bring, compared to testing organs such as the skin, more discomfort, or there is a limited availability of human cadavers or specimens for *ex vivo* testing. For both *in vivo* and *ex vivo* testing with humans, there are ethical constraints which must be considered. For *in vivo* mechanical testing, informed consent must be given and the study protocol must ensure that no unnecessary harm is caused to the patient or volunteer. For *ex vivo* experimentation, the tissue obtained from the human cadavers must not be wasted and should only be completed when a clear experimental methodology is established; knowing the purpose of each test and its aims. With animals, these ethical constraints are still present but are more relaxed than with humans. High quality *in silico* models could reduce the need for animal and human experimentation, which is always preferable from an ethical perspective.

2.5.5 Anisotropy

Approximately half of the *ex vivo* experiments and almost all of the *in vivo* experiments referenced in this review studied the mechanical properties of their respective tissues in only one direction, usually the circumferential direction. However, from the work of Brasseur et al. [334], it can be seen how the behaviour in the longitudinal direction affects the efficiency of peristalsis within the GI tract, and thus the function of the organs. In addition, many studies have found a discrepancy between the longitudinal and circumferential directions in terms of material response, commonly attributed to the arrangement of fibres such as collagen and elastin in the tissue walls [161]. Therefore, direction-dependent behaviour should be considered in future experimental investigations, particularly for *in vivo* studies for which anisotropic studies are lacking (Tables 4, 6, 8, 10, 12).

2.5.6 Layer-dependency

Those who studied the intact wall of the GI organs assumed the mechanical properties in the radial direction to be homogeneous. However, layer-dependent studies show this not to be the case, with the varying amount of microstructural components, namely collagen and elastin, being the main hypothesis as to why the material behaviour of the layers differ [161]. It can be seen that the oesophagus has a higher proportion of layer-dependent studies compared to the other tissues. This is due to the fact that the oesophagus, as mentioned in Chapter 1, can be relatively easily separated into its two main layers after explantation [335]. For the small intestine, it was found in the study by Sokolis [283] that "preliminary attempts to dissect the layers were not successful". Some have been successful using micro-dissection, however, since the layers of the GI organs apart from the oesophagus are tightly bound, it may be hard to ensure that no damage has been incurred to any of the layers during separation.

Whether the layer-dependent properties of the organ are considered depends on the application of the experimental work. For instance, for FE modelling of the interaction of a GI organ and a stent, a layer-dependent model will help to understand how the pressure exerted by the stent is supported by each of the layers. However, if the aim is to study the properties of the organ wall under dynamic loading for use in FE models that investigate the impact of blunt trauma, for instance during road traffic collisions, the layer-dependent properties may provide too much detail for the application [296, 309, 310, 336]. Nevertheless, many studies show large differences between mechanical behaviour of the different layers, and their influence on the overall function of the organ should be considered to provide a more complete biomechanical understanding of the GI tract [143].

2.5.7 Preconditioning

Preconditioning is a technique employed to reduce the influence of history-dependent, and some time-dependent, effects on the recorded behaviour of a material, making the results more stable and repeatable [99, 157]. Within biomechanics, preconditioning is used both *in vivo* and *ex vivo*. Its use, though, is controversial. On one hand, it makes the behaviour of soft tissues more consistent so the observed material response between different samples and subjects is less variable, however, on the other hand, in many of the applications in which the biomechanics of soft tissues are of interest, their behaviour during the first cycle is the one of most importance, for instance, during normal physiological loading [232], surgery [157], blunt trauma [266] and endoscopy [312]. In these situations, for example, the tissue is not preconditioned before the stomach wall is passively stretched by its contents, or surgical tools manipulate and cut the large intestine. It has even been found that with the rat oesophagus, the material properties of the wall return to what they were before stretching once muscle activation has occurred, i.e. the stress-softening of the wall is reversed during peristalsis [54, 55, 77], therefore suggesting that the first-cycle behaviour is the one most often of main interest. In future experimentation, it may be best to quantify both the initial material response and the behaviour after preconditioning as this provides experimental data to be used in the aforementioned applications, as well as information on the history and time-dependent properties of the GI organs [162].

2.5.8 Limitations of the review

In this review, sphincters of the GI tract have not be included. For comprehensive characterisation of the GI tract, these sphincters would have to be considered and also modelled *in silico* if the application requires. Additionally, an experimental aspect that has not been extensively discussed here are the different methods for strain measurement used in the characterisation of the GI tissues. These can include digital image correlation (DIC) [337], image analysis [338], and extensometers within the testing machine [174]. Moreover, only one database was used, and although particular care was taken to add any articles known by the authors not found in the PubMed search, some experimental studies may have been missed and therefore may not be included in this review.

2.6 Conclusion

This literature review was carried out with the aim to consolidate the mechanical experimentation that has been conducted on the GI tract, and to highlight what is missing in literature regarding the characterisation of the GI organs. In terms of *ex vivo* experimentation, there is little data regarding the human oesophagus and small intestine, with no *ex vivo* active studies being conducted on the small intestine from humans, and no anisotropic, layer-dependent studies or viscoelastic investigation being carried out on the human oesophagus. For *in vivo* mechanical characterisation, no studies included in this review involved experimentation on the human stomach, with only three studies being carried out in total on the stomach *in vivo*. Furthermore, very few *in vivo* characterisations involved determination of the layer-dependent properties of the GI tract. Overall, there is a lack of time-dependent studies on the GI organs, particularly for human tissue with only 4% of all the *ex vivo* articles considering the tissues' viscoelastic properties and 2% investigating the time-dependent behaviour of human tissue *in vivo*. Moreover, very few studies investigated the shear properties of the tissues and there were no studies that considered the GI tract's residual stresses and strains *in vivo*. Therefore, a focus should be applied to characterising the more complex aspects of the GI organs' mechanical behaviour using human tissue, including their layer-dependent, anisotropic, viscoelastic, shear and active properties, as well as their residual stresses and strains.

CHAPTER

THREE

3 EXPERIMENTAL METHODS

This chapter focuses on the experimental methods used to characterise the biomechanical behaviour of the human oesophagus, following the aims and objectives of this thesis as outlined in Section 1.1. Firstly, a more detailed anatomy of the oesophagus will be given. Then, the process of histological analysis will be conveyed. Next, the methology used to investigate the layer-dependent mechanical properties of the oeosphagus will be stated, along with the statistical tests used to analyse the results.

3.1 Anatomy of the human oesophagus

The oesophagus is part of the human digestive system and is an organ of the GI tract. Located in the thoracic cavity, as shown in Figure 23a, it is the only visceral organ that can be relatively straightforwardly separated into distinct layers, the muscularis propria and the mucosa-submucosa layer, post explantation without causing damage to either layer [335]. The mucosa-submucosa layer includes both the innermost mucosa layer and the layer adjacent to that, the submucosa, as seen in Figure 23b. The mucosa is best described divided into a further separate three layers: the epithelium, the lamina propria, and a thin layer of longitudinal muscle fibres called the lamina muscularis mucosae [339]. The submucosa is a collagen and elastin-rich layer made up of irregular connective tissue, lymphatics, veins and the submucosal pluxus. The muscularis propria layer contains the majority of muscle fibres in the oesophageal wall, with a layer of circularly oriented muscle fibres closest to the lumen, and a layer of longitudinally oriented muscle fibres towards the periphery (Figure 23b) [339]. The muscle of the oesophagus is striated at the top of the organ (proximal 6 cm) and is smooth at the bottom (distal 11 cm): the muscle between these two sections is a mix of both striated and smooth muscle [340]. Finally, the adventitia is the outermost layer of the oesophageal wall and is made up of connective tissue whose role is to support the position of the oesophagus within the thoracic cavity.

As well as its individual layers, the oesophagus has regions in which it is characterised, as seen in Figure 23a. These include the cervical region located at the proximal end of the organ which is approximately 5 - 6 cm long, the thoracic region located in the middle of the organ which is approximately 17 cm in length, and the abdominal region at the distal end of the oesophagus which is approximately 1 - 2.5 cm long [339]. The abdominal region contains the oesophageal sphincter which controls the direction of flow through the distal end of the oesophagus into the stomach. The total length of an adult oesophagus depends on the person and is usually 18 - 26 cm

in length [341].

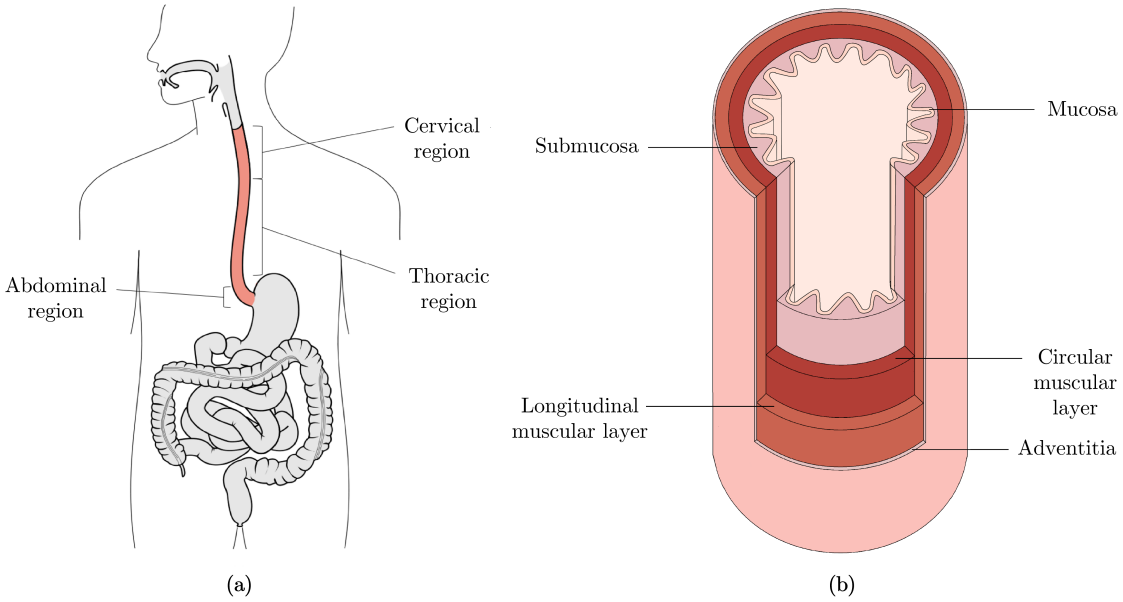

Figure 23. Diagram showing the regions of the oesophagus in relation to the rest of the body (modified from [14]) (**a**) and a segment of the organ showing its histological layers (**b**).

3.2 Specimen extraction

Whole human oesophagi were extracted by means of dissection at the Laboratoire d'Anatomie Des Alpes Françaises, Grenoble, France. Restrictions due to the COVID-19 pandemic meant that during this time all cadavers were required to present a negative COVID-19 test before being allowed for dissection. This could up to take several weeks, and thus, in the meantime, the cadavers had to be preserved. Therefore, initially, four oesophagi were retrieved from embalmed cadavers (Cadavers 1-4). The cadavers were embalmed with a formalin solution (ARTHYL) injected into the carotid artery and drained from the jugular vein, and then preserved in a 4°C refrigerated room. Once the restrictions were lifted, three oesophagi were excised from fresh cadavers all within 24 hrs after death (Cadavers 5-7). The following dissection procedure was used for the explantation of each oesophagus.

A median phreno-laparotomy was performed up to the umbilicus, as well as a left cervical approach following the edge of the sterno-cleido-mastoid muscle, as shown in Figure 24a. Starting from the stomach, the abdominal part of oesophagus was individualised from the hiatus in the diaphragm. The left triangular ligament, which connects the diaphragm and the posterior surface of

the left lobe, was freed, allowing the liver to be reclined. The small omentum was then sectioned off so that the stomach could be freed and hooked up to locate the abdominal oesophagus. The visceral peritoneum in front of the oesophagus was dissected, then a phrenotomy was performed. Dissection of the oesophagus continued in a cranial direction until the pulmonary hilum with its triangular ligament was severed. A right thoracic approach was chosen for the rest of the dissection, allowing the oesophagus to be individualised without being obstructed by the aorta and the heart in the left part of the mediastinum. The right lung was then redirected to the front, and the pulmonary hilum was above the oesophagus. The great azygos vein was also dissected on the right edge of the oesophagus. The abdominal oesophagus was sectioned by making an incision in the fundus of the stomach. The trachea was then sectioned in front of the oesophagus due to it preventing access to the cervical part of the organ. Finally, the cervical oesophagus was sectioned below the pharynx, as seen in Figure 24b, and the whole oesophagus extracted.

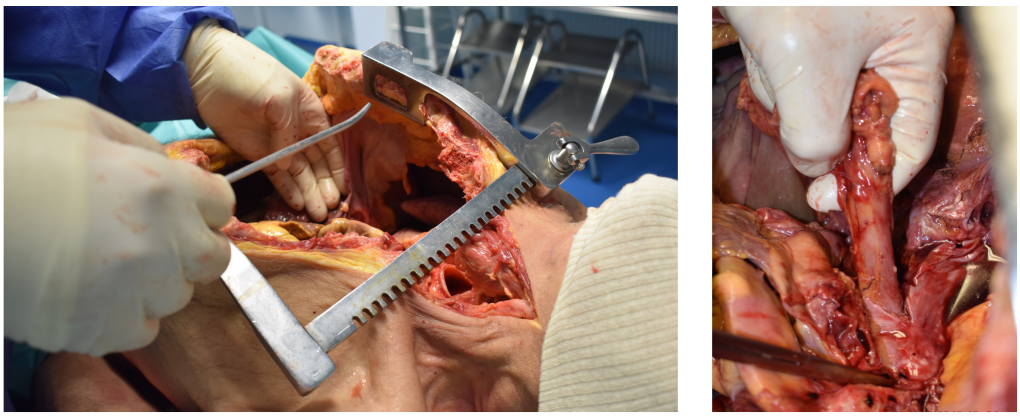

(a) (b)

Figure 24. During dissection of the human oesophagus, showing the chest cavity opened up (**a**) and the oesophagus *in situ* in the body before being sectioned below the pharynx (**b**).

For Cadaver 7, an extra step was carried out in order to consider the longitudinal prestretch of the human oesophagus. For this, three sections 5 cm apart were marked *in situ* on the organ's thoracic region using a dissolvable ink pen. After excision, the length of these sections were measured. The difference in length of the sections between the oesophagus' *in situ* and *ex vivo* state was then used to calculate the average (mean) longitudinal prestretch of the thoracic region of the organ.

Once removed from the cadavers, the oesophagi were taken immediately for sample preparation for the mechanical tests. The experiments were performed in compliance with French regulations on postmortem testing, and the protocol approved by a local scientific committee from Université

Grenoble Alpes.

3.3 Histology

Prior to mechanical testing, samples for histological analysis were obtained from the oesophagi of Cadavers 1 and 2 in the transversal and longitudinal planes along different sections of the organ. Samples were conserved in formaldehyde, fixed first in formalin 10% during 24 hrs at 4°C and then embedded in paraffin according to the usual protocol [342]. Sections of 3 µm were then realised with a microtome Leica RM 2245 (Wetzlar, Germany). The slides were stained with Haematoxylin Eosin Saffron (HES) to see the nucleic acids and connective tissue (amongst other collagen), with Orcein to highlight elastin fibres, or with Sirius Red to highlight all types of collagen and muscular fibres. Histological images were taken and assessed qualitatively. Then, the images were processed to approximate the percentage fibre content of each plane and layer. For this, collagen and elastin content were calculated due to their involvement in the mechanical behaviour of soft tissues.

Firstly, the images were manually segmented to allow the fibre content of the different layers to be determined. Next, ImageJ [343] was used to process the images and estimate the percentage collagen content from the Sirius Red and HES images, and the percentage elastin content from the Orecin images. For this, the non-tissue background was removed from the images, the contrast was increased, and the area of the whole tissue region was evaluated. Then, the area of colour specific to the fibre of interest was determined. Finally, the percentage fibre content was calculated by dividing the area of the fibre by the area of the whole tissue region and multiplying the answer by 100. This was repeated for each layer of the longitudinal and transversal histological images. The final fibre contents were calculated as a mean percentage taken from images from three sections along the thoracic region (top, middle and bottom) across the two oesophagi.

3.4 Uniaxial tensile testing

3.4.1 Sample preparation

Upon excision from the human cadavers, the oesophagi were first gently rinsed through the lumen using physiological saline solution (0.9% NaCl). They were then carefully cleaned of any excess connective tissue and separated into their three main regions (cervical, thoracic and abdominal), as seen in Figure 25a. At this point, samples were cut for zero-stress state analysis from the oe-

sophagus of Cadaver 7, the protocol of which is described in Section 3.5. As the region-dependent tensile properties were not being considered, only the thoracic region was used for uniaxial testing. This region was chosen for consistency as it comprises the vast majority of the organ and contains a mix of both striated and smooth muscle [340].

Next, the thoracic region of each oesophagus was fully separated into its two layers. For this, firstly a longitudinal incision was made along the length of the region, cutting through only the muscularis propria layer. This incision allowed access to the connective tissue between the layers, which was then very carefully cut to dissect the two main layers. An image taken during the layer separation process can be seen in Figure 25b, while the fully separated layers can be seen in Figure 25c. Once separated, the mucosa-submucosa layer was cut along its longitudinal length and unravelled. The layers were then examined visually to determine if any damage, i.e. cuts penetrating partially or fully into the tissue of the layers, had been incurred during separation, of which there had not. Prior to testing, samples approximately 22.00 mm $\times$ 4.10 mm (length $\times$ width) were cut in both the longitudinal and circumferential directions. In between tests, the tissue layers were stored in saline at 4°C, and were then brought to room temperature before testing. All testing was completed within 5 days of explantation.

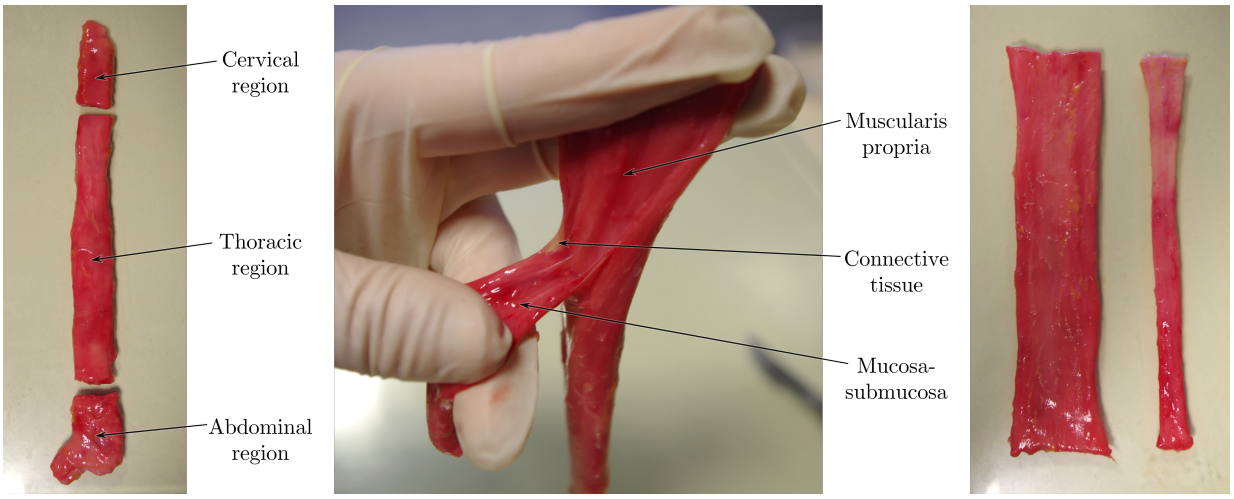

Figure 25. **a**) Separation of a fresh oesophagus into its three main regions (cervical, thoracic and abdominal). **b**) Dissection of the two main oesophageal layers. **c**) Fully separated layers of the human oesophagus showing the unravelled muscularis propria on the left and the tubular mucosa-submucosa on the right.

3.4.2 Experimental setup

Once cut, the rectangular samples were secured within the grips using the following procedure: first, the samples were laid on the base grips and back support of a special device designed to setup soft tissue samples within the grips, as seen in Figure 26. Next, the samples were flattened and aligned as centrally as possible upon the grips. This step often took some time due to the very soft and sticky nature of the tissue. Then, the upper grips were placed on the base grips and the screws tightened using a torque limiter set at 0.5 Nm, to prevent the samples slipping during testing and for consistency across the different samples. After this, the long screws situated either side of the grips, as shown in Figure 26, were tightened to create an assembly in which the soft sample could be moved and setup in the machine, an MTS Criterion model C41 (MTS Systems, Minnesota). The assembly was used to position the sample within the machine, as seen in Figure 27a, by attaching the lower portion of the assembly directly to it and then the upper portion to a highly sensitive 25 N load cell. Once secured within the machine, the long screws situated either side of the grips were loosened to release the assembly. The back support holding the tissue sample in place was then removed. The final setup of the sample within the machine prior to commencement of the tests can be seen in Figure 27b. At this point, the width and thickness of the sample was measured at three separate points along its length, and the average (mean) was used for the calculation of stress (Section 3.4.5). Tensile deformation was employed via upward traction of the upper grip attached to the crosshead and load cell while the lower grip remained fixed.

3.4.3 Cyclic tests

Cyclic tests were performed in the form of increasing stretch level tests with two cycles per level to explore the softening behaviour of the human oesophagus, the protocol of which can be seen in Figure 28a. This form of test was chosen over a single cycle test or a single deformation level cyclic test to be able to observe the most phenomena whilst testing the fewest samples. Deformation levels of 10-70% in increments of 10% (stretch levels of 1.1-1.7 with increments of 0.1) were chosen for all samples. The cyclic tests were conducted at two different strain rates, $1\%s^{-1}$ and $10\%s^{-1}$, to explore any rate-dependent behaviour of the tissue. An average of 9 tests for the embalmed tissue and 7 tests for the fresh tissue were conducted per oesophagus, layer, direction and strain rate. All tests were carried out at ambient temperature and conducted under a uniaxial tensile test condition. The samples were kept moist during the tests via routine spraying with physiological saline solution.

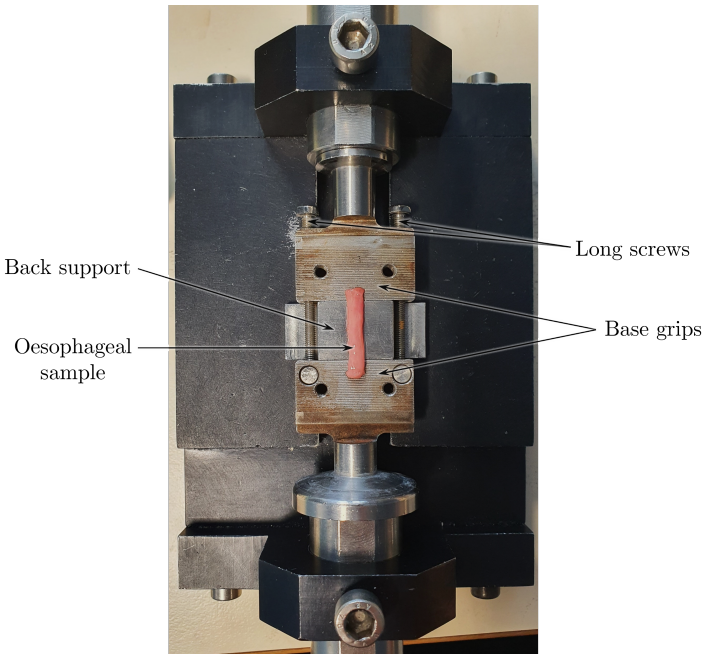

Figure 26. Sample positioned on the support ready to be secured within the grips.

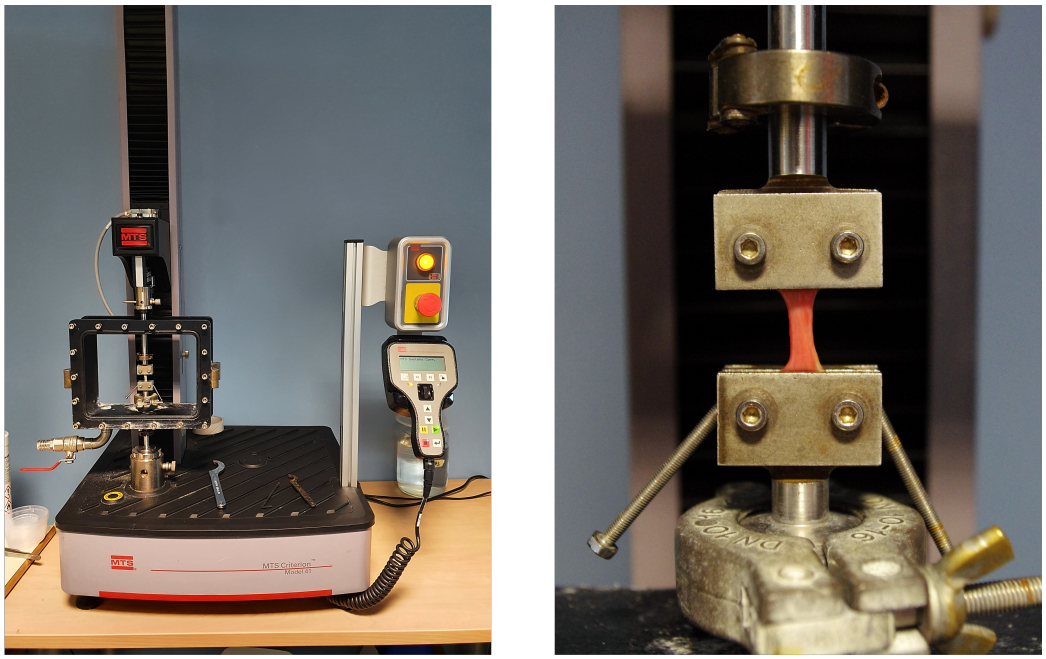

(a) (b)

Figure 27. Machine setup (**a**) and a sample loaded within the machine (**b**).

3.4.4 Stress-relaxation tests

To investigate the equilibrium stress of each layer of the oesophagus, stress-relaxation tests were conducted, where in which the samples were stretched at a rate of $100\%s^{-1}$ and held initially for

20 minutes for the first trial of all layers and directions. The remaining trials were then held for 15 minutes as the drop in stress between the 20 and 15 minute mark was only 2%. Due to the limited number of samples available from a single human oesophagus, the stress-relaxation tests were conducted in the form of multi-step tests to extract the most amount of information from a single sample. The longitudinal samples for both layers were stretched in increments of 5% deformation and the circumferential samples were stretched in 10% deformation increments to ensure at least four relaxation steps were completed in each direction before the sample ruptured, at which point the tests were stopped. A schematic of the test protocol for the longitudinal samples can be seen in Figure 28b. Again, all tests were carried out at ambient temperature and conducted under a uniaxial tensile test condition, and the samples were kept moist during testing via routine spraying with saline solution.

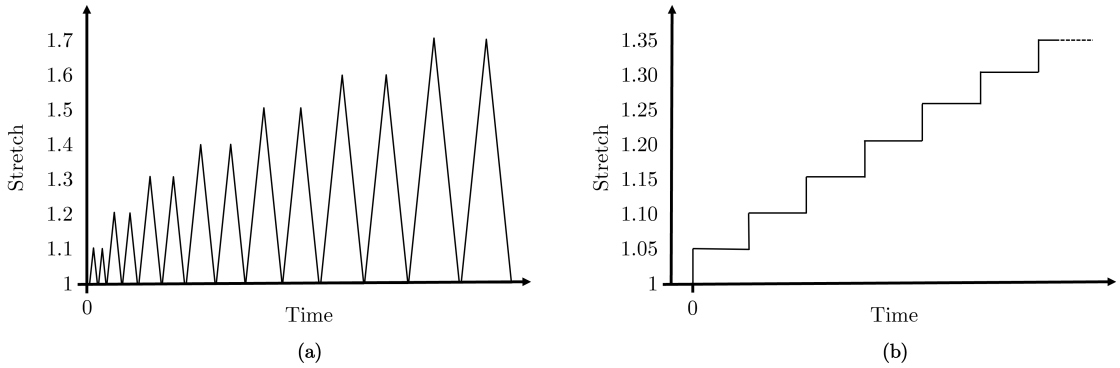

Figure 28. Stretch-time schematic of the mechanical test protocol for the cyclic tests for both the longitudinal and circumferential samples (**a**) and for the stress-relaxation tests for the longitudinal samples (**b**).

3.4.5 Mechanical characterisations

The experimental strain is expressed in terms of stretch, λ, which relates to nominal strain by $\varepsilon = \lambda - 1$. Stretch is defined as $\lambda = \frac{l}{l_0}$, where l and l_0 are the current and initial lengths of the sample, respectively. The strain rates are described in units of percentage deformation per second ($\%s^{-1}$). Similarly, the stress is expressed as the nominal stress (i.e., first Piola-Kirchhoff stress), which is defined as:

$$P = \frac{F}{A_0} \tag{1}$$

where F is the applied force and A_0 is the original, undeformed cross-sectional area.

3.5 Zero-stress state

3.5.1 Sample preparation

The longitudinal prestretch of the oesophagus from Cadaver 7 was measured as described in Section 3.2. To determine the oesophageal specimen's residual circumferential strains, ring-like segments were cut from four different locations along the length of the specimen, as seen in Figure 29. At each location, two samples approximately 2 mm in length were retrieved. The proximal segment at each location was used to investigate the opening angle and residual strains of the intact wall, while the more distal segment was used for layer-dependent analysis (Figure 29). To separate the layers of the rings, careful cutting was administered to the connective tissue binding the layers together, while keeping both the layers in their ring-like forms.

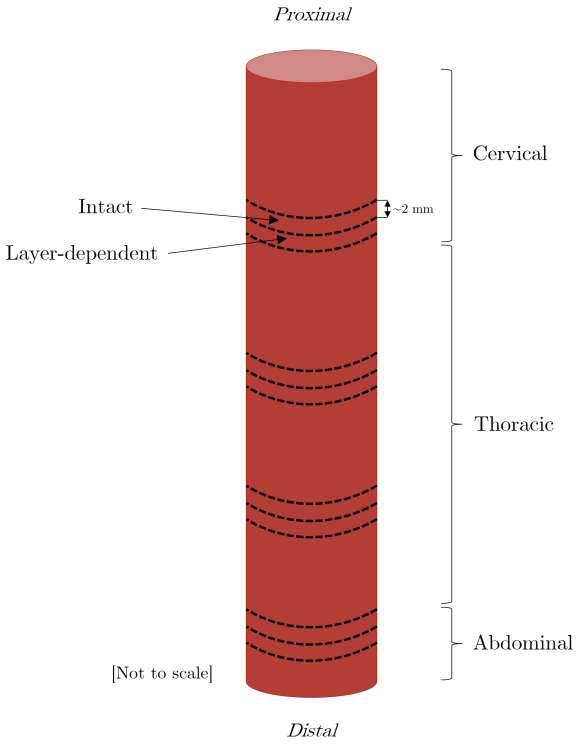

Figure 29. Drawing illustrating the location of the zero-stress state analysis samples.

3.5.2 Experimental setup and protocol

A zero-stress state analysis was conducted as per the protocol outlined in Liu and Fung [344]. The ring-like segments were all submerged in physiological saline solution at room temperature in individual containers. Photographs were taken at this point to be able to determine the dimensions of the samples in the no-load state, as illustrated in Figure 10a in Section 2.3.1.9. All images were taken using a Pentax K-5 camera with a 50 mm lens. The segments were then cut radially using surgical scissors while still submerged in the solution. Photographs were taken immediately after the samples were cut, then again at 0.5, 1, 2, 3, 4, 5 and 24 hrs to assess the time evolution of the opening of the sector. The testing was complete within 36 hrs of dissection. The opening angle, θ, as defined in Figure 10b (Section 2.3.1.9), was then measured for all the open segment images.

3.5.3 Measurement of circumferential residual strains

The residual circumferential strains were initially measured in terms of Green's strain using the change in wall dimensions between the no-load and the zero-stress state. The following equations were used to calculate the residual Green's strain at the inner and outer surfaces, respectively:

$$e_i = \frac{(c_{i,n}/c_{i,z})^2 - 1}{2} \tag{2}$$

$$e_o = \frac{(c_{o,n}/c_{o,z})^2 - 1}{2} \tag{3}$$

where, $c_{i,n}$ and $c_{i,z}$ are the circumference of the inner surface at the no-load and zero-stress state, respectively, and $c_{o,n}$ and $c_{o,z}$ are the circumference of the outer surface at the no-load and zero-stress state, respectively. The definitions of these quantities can be seen schematically in Figure 10 (Section 2.3.1.9). The stretch relates to Green's strain by $e = (\lambda^2 - 1)/2$.

3.6 Statistical analysis

Usually, a mean is used to describe the average result of a certain quantity. However, this should only be used if the dispersion of the quantity follows a normal distribution. Therefore, initially, tests were carried out to determine if the quantities of interest were normally distributed. For this, a Shapiro-Wilk test was conducted using IBM SPSS Statistics (Version 27.0) [345] with a significance level, α, of $\alpha = 0.05$. The distribution was considered normal if $p > 0.05$. If this was

the case, a mean value would be used to represent the quantity. If, however, the quantity was not normally distributed, tests would be carried out to see if its dispersion followed other distributions, later outlined in Section 4.3.2, using R statistical software [346]. For the comparison of differences between groups, an independent non-parametric test was used in the form of the Mann-Whitney U test. To determine if there was a correlation between variables, a Spearman rank-order correlation test was conducted. These tests, carried out in SPSS, were used due to the often non-normal distribution of the data.

3.7 Conclusion

In this chapter, the experimental methodology of the thesis was outlined. Oesophagi were retrieved from embalmed and fresh human cadavers, and samples from embalmed oesophagi were taken for histological analysis. The muscularis propria and mucosa-submucosa layers were dissected through careful cutting to the loose connective tissue binding them together. The mechanical tests used to explore the viscoelastic behaviour of the human oesophageal layers were increasing stretch level cyclic tests and multi-step stress-relaxation tests, both carried out under a uniaxial tensile test condition. The longitudinal prestretch and circumferential residual strains of the fresh oesophagus were also considered, the latter of which was carried out via opening angle experiments.

CHAPTER
FOUR

4 EXPERIMENTAL RESULTS

In this chapter, the experimental findings in regard to the mechanical behaviour of the human oesophagus will be presented. Firstly, the results of the histological analysis of the two main oesophageal layers are presented. Then, the demographics of the cadavers used for the study are outlined. Further to this, the statistical and experimental results of the cyclic and stress-relaxation tests of the layers are provided. Finally, the residual circumferential strains are displayed and compared for the layers of the oesophagus and its intact wall.

4.1 Histology of the human oesophagus

4.1.1 Qualitative analysis

In the transversal plane, the five layers of the oesophagus (outlined in Section 3.1) are clearly visible and can be seen in Figure 30a. These layers are also evident in the longitudinal plane, as shown in Figure 30b. For the qualitative analysis, the histological images were assessed by a practising clinician who marked on the images the orientation of the fibre bundles, and used this to build a picture of the fibre orientations and concentrations in the different planes.

The mucosa and the submucosa layers are richer in collagen and elastin fibres than the muscularis propria. Overall, there are more collagen fibres than elastin fibres in the fibrous composition of the muscularis propria (both circular and longitudinal layers). In the inner circular layer, the collagen fibres form a mesh orthogonal to the axis of the oesophagus. Fibres have a transversal orientation with some oriented along the muscle cells and others towards the lumen. Elastin fibres have a similar orientation in this layer. The fibres are mostly concentrated at the circular/longitudinal junction of the muscularis propria, organised mainly along the axis of the oesophagus. The outer longitudinal layer has its collagen fibres mainly oriented in the longitudinal direction, with few fibres oriented towards the lumen. The elastin fibres have a longitudinal orientation also, but with a very wavy appearance. The elastin fibres seem to be more abundant in the outer longitudinal layer than in the inner circular layer. The distribution of collagen and elastin fibres within the muscularis propria are summarised in Table 14.

The distribution of the collagen and elastin fibres within the mucosa-submucosa have been summarised in Table 15. The mucosa contains more collagen fibres than elastin, with the collagen fibres being mainly oriented longitudinally, which is also the case for the elastin fibres of the layer.

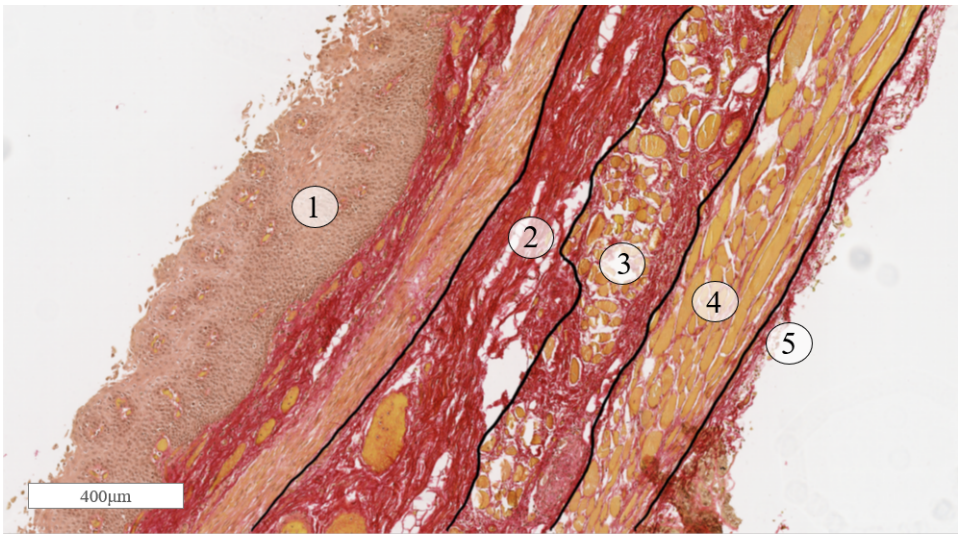

(a)

(b)

Figure 30. Sirius Red staining in the longitudinal plane (**a**) and Haematoxylin Eosin Saffron staining in the transversal plane (**b**) showing the mucosa (**1**), submucosa (**2**), the circular muscle fibres of the muscularis propria (**3**), the longitudinal muscle fibres of the muscularis propria (**4**) and the adventitia (**5**).

The muscle fibres of muscularis mucosae are longitudinally oriented as well. In the submucosa, there is more collagen than elastin. The collagen and elastin fibres do not have the same orientation throughout the thickness of this layer. In the inner part, the collagen and elastin fibres are oriented longitudinally in the direction of the oesophagus. In the outer part, close to the muscularis propria, the fibres are oriented transversely, following the muscle fibres of the adjacent inner circular muscular layer.

Table 14: Distribution of collagen and elastin in the muscularis propria; +, low density; +++++, high density.

Layer	Collagen	Elastin
Circular muscle	++	+
Circular/longitudinal junction	++++	+++
Longitudinal muscle	++	++

Table 15: Distribution of collagen and elastin in the mucosa-submucosa; +, low density; +++++, high density.

Layer	Collagen	Elastin
Mucosa	+++++	+
Submucosa	+++++	++

4.1.2 Quantitive analysis

The histological images were processed to approximate the amount of collagen and elastin in each layer and direction of the human oesophagus. As both the Sirius Red and HES stains display the collagen of the tissue, the Sirius Red images were analysed first to determine the percentage of collagen in each layer and direction. Then, the transverse sections of the HES images were analysed to validate the percentage of collagen estimated using the Sirius Red images. The validation was successful with only a 5% difference between the two percentages for the mucosa-submucosa, and a 12% difference between the two collagen content values for the muscularis propria. The results of the percentage collagen in each layer and plane can be found in Figure 31a. The results of the Orecin image analysis can be seen in Figure 31b. As there was only one stain that highlighted the elastin fibres of the tissue, there could be no validation of the elastin content calculation.

4.2 Demographics and specimen details

Oesophagi were retrieved from both embalmed and fresh cadavers, the demographics of which can been seen in Table 16. Table 16 also shows the length of the oesophagi extracted and details about which tests were performed on which layers. The time of embalming for Cadavers 1-4 was 29, 24, 71 and 40 days, respectively.

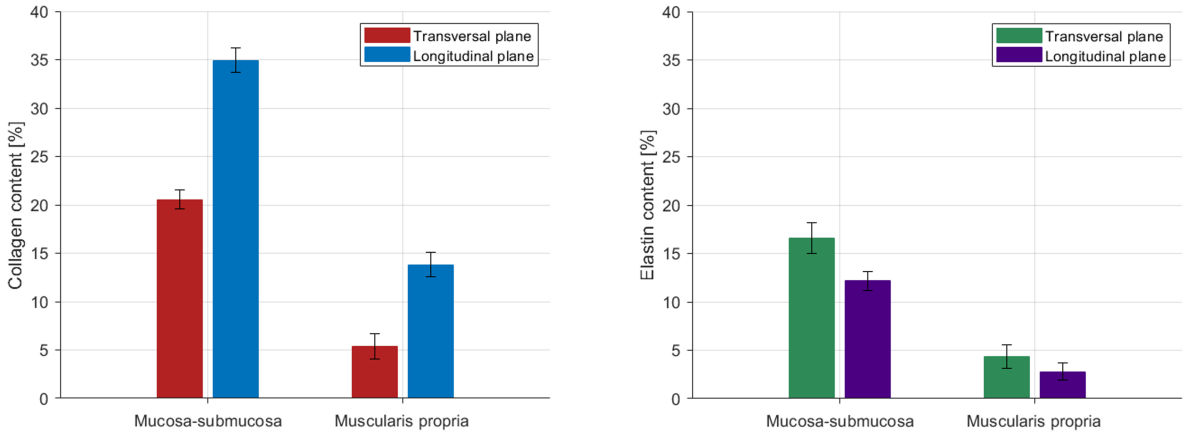

(a) (b)

Figure 31. Comparison of the collagen (**a**) and elastin (**b**) in the different layers and planes of the human oesophagus determined by histological image analysis.

Table 16: Patient demographics, length of oesophagus extracted, which layers were tested and the type of tests conducted for each cadaver.

	Cadaver	Sex	Height [cm]	Weight [kg]	Age [years]	Length [cm]	Layers tested	Type of tests performed
Embalmed	1	Male	180	73	90	27	Muscular only	Cyclic
	2	Female	165	75	88	25	Mucosal only	Cyclic
	3	Female	153	40	97	26	Both	Cyclic
	4	Female	140	40	101	22	Both	Cyclic
Fresh	5	Female	144	42	96	24	Both	Cyclic
	6	Male	185	78	89	28	Both	Cyclic, stress-relaxation
	7	Male	170	100	97	26	Both	Cyclic, stress-relaxation, zero-stress state

4.3 Cyclic results

4.3.1 Variations in experimental samples

The total number of cyclic experiments carried out per layer, direction, strain rate and cadaver can be found for the embalmed tissue in Table 17 and the fresh tissue in Table 18. Dimensions such as thickness can vary from sample to sample due to the variable nature of biological tissues. The mean and standard deviations of the sample dimensions for each preservation state, layer and direction can be seen in Table 19.

When comparing the stress-strain behaviour of the tests within a single test condition (preservation state, layer, direction and strain rate), there was a high amount of dispersion. This is demonstrated in Figure 32 which shows the point of complete rupture, in terms of stress and stretch, for each

test conducted at $10\%s^{-1}$ on emablmed tissue, highlighting the differences between cadavers and directions. Rupture of the sample was defined as irreversible macrostructural damage, visible on the stress-strain graph as a sudden reduction in stress. The samples, both fresh and embalmed, always ruptured during the first out of the two cycles for each stretch level, and in various locations, including in the middle of the sample, at the grip location, or a combination of both.

Table 17: Number of cyclic tests performed on embalmed tissue per layer, per direction, per strain rate, per cadaver.

Layer	Direction	Strain rate	Cadaver	Tests	Total
Muscularis propria	Longitudinal	1%/s	1	5	n=25
			3	10	
			4	10	
		10%/s	1	5	n=25
			3	10	
			4	10	
	Circumferential	1%/s	1	5	n=26
			3	10	
			4	11	
		10%/s	1	5	n=26
			3	10	
			4	11	
Mucosa-submucosa	Longitudinal	1%/s	2	5	n=24
			3	10	
			4	9	
		10%/s	2	5	n=24
			3	10	
			4	9	
	Circumferential	1%/s	2	5	n=23
			3	10	
			4	8	
		10%/s	2	5	n=21
			3	10	
			4	6	

Table 18: Number of cyclic tests performed on fresh tissue per layer, per direction, per strain rate, per cadaver.

Layer	Direction	Strain rate	Cadaver	Tests	Total
Muscularis propria	Longitudinal	1%/s	5	7	n=20
			6	10	
			7	3	
		10%/s	5	5	n=20
			6	10	
			7	5	
	Circumferential	1%/s	5	5	n=20
			6	10	
			7	5	
		10%/s	5	5	n=20
			6	10	
			7	5	
Mucosa-submucosa	Longitudinal	1%/s	5	5	n=20
			6	10	
			7	5	
		10%/s	5	6	n=20
			6	10	
			7	4	
	Circumferential	1%/s	5	5	n=20
			6	10	
			7	5	
		10%/s	5	3	n=20
			6	10	
			7	7	

Table 19: Mean $\pm$ population standard deviation of sample dimensions for the cyclic experiments across both strain rates.

		Muscularis propria		Mucosa-submucosa	
	Direction	Width [mm]	Thickness [mm]	Width [mm]	Thickness [mm]
Embalmed	Longitudinal	4.09 ± 0.28	1.15 ± 0.36	4.05 ± 0.36	0.74 ± 0.14
	Circumferential	4.08 ± 0.25	1.37 ± 0.44	4.19 ± 0.32	0.80 ± 0.15
Fresh	Longitudinal	4.11 ± 0.35	1.96 ± 0.40	4.15 ± 0.22	0.87 ± 0.17
	Circumferential	4.09 ± 0.36	2.44 ± 0.42	4.12 ± 0.29	0.69 ± 0.13

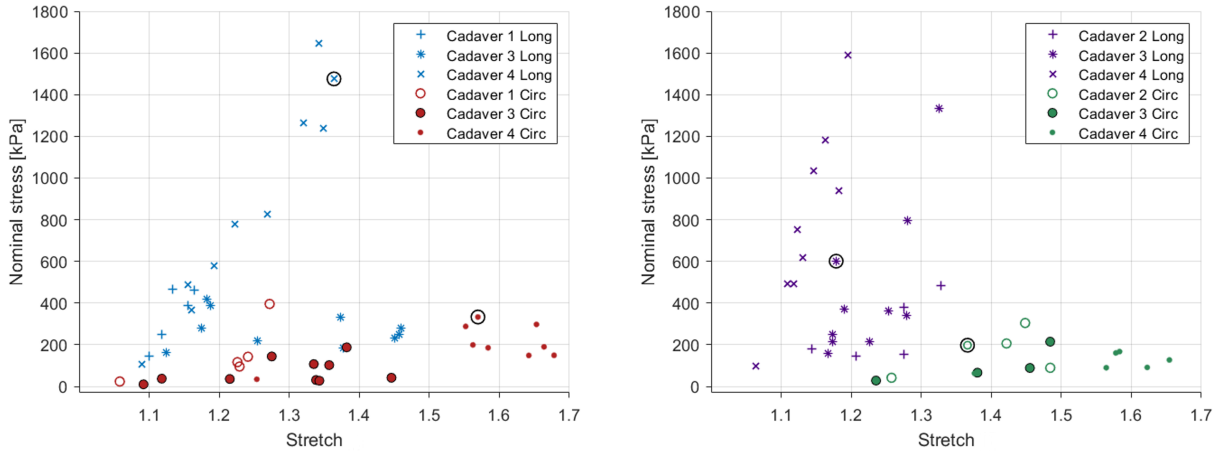

Figure 32. Rupture points of each test conducted at $10\%s^{-1}$ on embalmed tissue, highlighting the dispersion between cadavers and the longitudinal and circumferential directions for the muscular (**a**) and mucosa-submucosa layers (**b**). The circled points show the rupture stress-stretch of the curves selected for analysis via statistical means.

4.3.2 Statistical analysis

4.3.2.1 Embalmed tissue

Due to the dispersion of the data, a statistical approach was undertaken to retrieve the most representative behaviour of the embalmed layers of the human oesophagus (per direction and strain rate) to use for analysis and constitutive modelling. Firstly, the Young's modulus of each test was calculated by taking the gradient of the first loading curve of the first cycle from 1.00 to 1.01 stretch. The Young's modulus, E, is defined as:

$$E = \frac{P}{\varepsilon} \tag{4}$$

where, P is the nominal stress and ε is the nominal strain as described in Section 3.4.5. A histogram with 20 bins was then plotted for each layer and test condition with density on the y-axis and Young's modulus on the x-axis, as seen in Figure 33. The histogram for each layer and test condition presented a right skewed distribution of Young's moduli, therefore a number of non-normal distributions were chosen to test against a null hypothesis, including chi-squared distribution [347], gamma distribution [348] and Fréchet distribution [349]. The null hypotheses were,"The Young's modulus of the [specific] direction of the [muscular/mucosa-submucosa] layer of the embalmed human oesophagus tested at a strain rate of [specific]$\%s^{-1}$ is distributed according to the [specific] distribution.". These statistical tests were carried out using R statistical software with $\alpha = 0.05$,

meaning that the null hypothesis was rejected if $p < 0.05$.

The null hypotheses for all test conditions were retained for the gamma and Fréchet distributions. The Fréchet distribution, however, was chosen as it is the most suitable for the application of material properties [349], the p-values for which can be seen in Table 20. The mode of the Fréchet distribution gives the most likely value of Young's modulus for the population, and the range, in this circumstance, provides the range in which 70% of all Young's moduli of the population reside. An example of these measures can be seen in Figure 33, while their values for each test condition will be presented later in Section 6.1. To provide the most representative behaviour of embalmed tissue for the following analysis and constitutive modelling, the test with the Young's modulus closest to the mode of the Fréchet distribution for each condition was selected. The circled rupture points in Figure 32 correspond to the selected $10\%s^{-1}$ tests in each direction, the cyclic stress-strain data of which will be subsequently presented in Section 4.3.4.

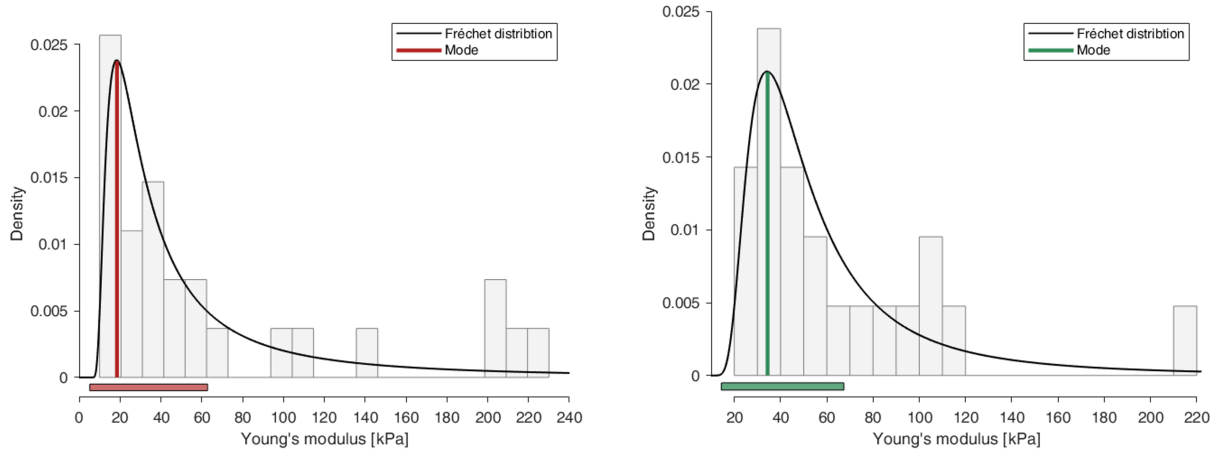

Figure 33. The combined histogram and probability distribution graph showing the dispersion of Young's modulus for the $10\%s^{-1}$ circumferential experimental results across three cadavers for the embalmed muscular layer (**a**) and the embalmed mucosa-submucosa layer (**b**), displaying a significant Fréchet distribution at $\alpha = 0.05$ with a mode (range) of 18.5 (5.2–62.9) for the muscularis propria (**a**) and 34.4 (14.4–67.4) for the mucosa-submucosa (**b**). The vertical red and green lines show the mode of the probability distribution for the muscular and mucosal layers, respectively, while the horizontal bars depict the range.

Table 20: p-values for the Young's moduli of the embalmed tissue cyclic results following a Fréchet distribution, where $p > 0.05$ indicates a significant distribution.

Layer	Direction	Strain rate	p-value
Muscularis propria	Longitudinal	1%/s	0.367
		10%/s	0.748
	Circumferential	1%/s	0.808
		10%/s	0.972
Mucosa-submucosa	Longitudinal	1%/s	0.247
		10%/s	0.899
	Circumferential	1%/s	0.783
		10%/s	0.975

4.3.2.2 Fresh tissue

For the embalmed tissue, the Young's modulus was used to quantify the variability of the data and to extract the most representative curve. This was sufficient for this preservation state as there was a distinct initial stiffness of the stress-strain response. However, for the fresh tissue results, the Young's modulus on its own did not provide a good representation of the variation of the results due to the low initial stiffnesses seen for all trials. Therefore, a different approach was employed to extract the most representative curve for the fresh tissue. For this, 11 features (characteristics) were extracted from $\lambda = 1.1$ of all the cyclic experimental data. This cycle was chosen as it allowed for comparison across all layers, directions and strain rates, as well as between the embalmed and fresh tissue. The characteristics include the Young's modulus of the first loading curve, the Young's modulus of the second loading curve, the hysteresis of the first cycle, the hysteresis of the second cycle, the difference between the two hystereses, the rupture stretch, the maximum stress, and the areas under the loading and unloading curves for both the first and second cycle of $\lambda = 1.1$; the definitions of which can be seen in Figure 34. The distributions of all these features were established by first testing if they were normally distributed using a Shapiro-Wilk test in SPSS. If the characteristic was normally distributed for a certain layer, direction and strain rate, the mean of the value would be taken as the most representative. Next, if the distribution was not normally distributed, the characteristic would be tested to see if it followed a Fréchet distribution [349]. It was found that all non-normally distributed characteristics followed this distribution. Therefore, the mode of the Fréchet distribution for these characteristics was taken as the most representative value, of which the values and range of E_1 will be presented later in Section 6.1. Then, the mean or mode of each characteristic was compared with the values of each individual test. The test with

the highest number of characteristics close to the mean or mode was chosen to represent the behaviour of the specific layer, direction and strain rate. These experimental curves were used for analysis of the cyclic behaviour of the fresh human oesophageal layers and will be presented in the subsequent graphs. Additionally, the differences between groups were measured regarding all the aforementioned characteristics of the $\lambda = 1.1$ cycles using a Mann-Whitney U test. The results of the statistically significant layer differences, strain rate differences and direction differences for both the fresh and embalmed tissue can be seen in Tables 21, 22 and 23, respectively. These tables indicate the variable for which the characteristic was higher than for the other variable, e.g. mucosa or muscle for the layer differences, by a statistically significant degree. They also include the p-value for the statistical difference.

Table 21 shows that, overall, the muscularis propria ruptures later than the mucosa-submucosa in the longitudinal direction; that, in general, the mucosa-submucosa dissipates more energy than the muscular layer across both directions; and that the mucosal layer tends to store more energy than the muscle layer, particularly at the higher strain rate. It can be seen from Table 22 that an increase in strain rate statistically increased energy storage and dissipation in the circumferential direction for both the mucosa-submucosa and the muscularis propria. Finally, Table 23 shows that at 10% deformation, stiffness, energy storage and energy dissipation were greater in the longitudinal direction compared to the circumferential direction for all layers, strain rates and preservation states.

To assess if the time between dissection and testing of the sample had an influence on the mechanical properties, a Spearman's correlation test was carried out for each layer, direction and strain rate for the fresh tissue results. Table 24 shows that apart from the longitudinal mucosal layer at $10\%s^{-1}$, there was no significant correlation between days since dissection and the maximum stress of the samples.

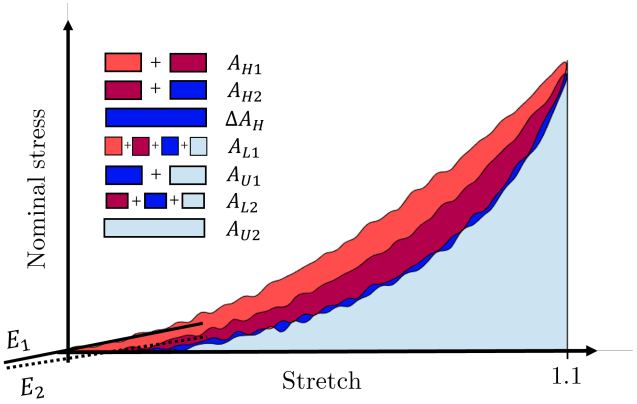

Figure 34. Schematic diagram showing the different characteristics extracted from the two 1.1 cycles, where E_1 = Young's modulus of the loading curve of the first cycle, E_2 = Young's modulus of the loading curve of the second cycle, A_{H1} = hysteresis area of the first cycle, A_{H2} = hysteresis area of the second cycle, ΔA_H = difference in hysteresis area between the two cycles, A_{L1} = area under loading curve of the first cycle, A_{U1} = area under unloading curve of the first cycle, A_{L2} = area under loading curve of the second cycle, and A_{U2} = area under unloading curve of the second cycle.

Table 21: Statistical differences in characteristics between the layers (muscularis propria and mucosa-submucosa) for both the fresh and embalmed tisssue. Blank cells indicate no statistical significance between the two groups, "–" mean that a statistical test is not relevant, and filled cells indicate the layer for which the characteristic is statistically higher than for the other layer, including the respective p-value.

Pres. state	**Test cond.**	**Characteristic**										
		E_1	E_2	A_{H1}	A_{H2}	ΔA_H	λ_{rup}	P_{max}	A_{L1}	A_{U1}	A_{L2}	A_{U2}
Fresh	1%/s Long						Muscle $p = 0.020$	Mucosa $p = 0.001$				
	10%/s Long	Mucosa $p = 0.037$		Mucosa $p = 0.001$	Mucosa $p < 0.000$	Mucosa $p = 0.001$	Muscle $p < 0.000$		Mucosa $p = 0.003$	Mucosa $p = 0.030$	Mucosa $p = 0.004$	
	1%/s Circ			Mucosa $p < 0.000$	Mucosa $p < 0.000$	Mucosa $p < 0.000$	–		Mucosa $p = 0.045$			
	10%/s Circ	Mucosa $p < 0.000$	Mucosa $p < 0.000$	Mucosa $p < 0.000$	Mucosa $p < 0.000$	Mucosa $p = 0.001$	–		Mucosa $p < 0.000$	Mucosa $p < 0.000$	Mucosa $p < 0.000$	Mucosa $p < 0.000$
Embalmed	1%/s Long		Mucosa $p = 0.001$				Muscle $p = 0.041$	Mucosa $p = 0.034$		Mucosa $p = 0.014$	Mucosa $p = 0.031$	Mucosa $p = 0.015$
	10%/s Long											
	1%/s Circ			Muscle $p = 0.039$	Muscle $p = 0.029$	Muscle $p = 0.041$						
	10%/s Circ			Muscle $p = 0.016$		Muscle $p = 0.006$	Mucosa $p = 0.039$					

Table 22: Statistical differences in characteristics between the strain rates ($1\%s^{-1}$ and $10\%s^{-1}$) for both the fresh and embalmed tisssue. Blank cells indicate no statistical significance between the two groups, "–" mean that a statistical test is not relevant, and filled cells indicate the strain rate for which the characteristic is statistically higher than for the other strain rate, including the respective p-value.

Pres. state	**Test cond.**	**Characteristic**										
		E_1	E_2	A_{H1}	A_{H2}	ΔA_H	λ_{rup}	P_{max}	A_{L1}	A_{U1}	A_{L2}	A_{U2}
Fresh	Long Muscle				10%/s $p = 0.018$		10%/s $p = 0.011$	10%/s $p = 0.037$				
	Circ Muscle	1%/s $p < 0.000$	1%/s $p < 0.000$	10%/s $p < 0.000$	10%/s $p < 0.000$	10%/s $p < 0.000$	–		10%/s $p < 0.000$	1%/s $p = 0.029$	10%/s $p < 0.000$	
	Long Mucosa											
	Circ Mucosa		1%/s $p = 0.041$	10%/s $p < 0.000$	10%/s $p < 0.000$	10%/s $p = 0.001$	–		10%/s $p < 0.000$	10%/s $p < 0.000$	10%/s $p < 0.000$	10%/s $p < 0.000$
Embalmed	Long Muscle		10%/s $p = 0.025$									
	Circ Muscle											
	Long Mucosa											
	Circ Mucosa		1%/s $p = 0.021$	10%/s $p = 0.009$	10%/s $p = 0.001$							

Table 23: Statistical differences in characteristics between the directions (longitudinal and circumferential) for both the fresh and embalmed tisssue. Blank cells indicate no statistical significance between the two groups , "–" mean that a statistical test is not relevant, and filled cells indicate the direction for which the characteristic is statistically higher than for the other direction, including the respective p-value.

Pres. state	**Test cond.**	**Characteristic**										
		E_1	E_2	A_{H1}	A_{H2}	ΔA_H	λ_{rup}	P_{max}	A_{L1}	A_{U1}	A_{L2}	A_{U2}
Fresh	Muscle 1%/s	Long $p < 0.000$	Long $p < 0.000$	Long $p < 0.000$	Long $p < 0.000$	Long $p < 0.000$	–	–	Long $p < 0.000$	Long $p < 0.000$	Long $p < 0.000$	Long $p < 0.000$
	Muscle 10%/s	Long $p < 0.000$	Long $p < 0.000$	Long $p < 0.000$	Long $p < 0.000$	Long $p < 0.000$	–	–	Long $p < 0.000$	Long $p < 0.000$	Long $p < 0.000$	Long $p < 0.000$
	Mucosa 1%/s	Long $p < 0.000$	Long $p < 0.000$	Long $p < 0.000$	Long $p < 0.000$	Long $p < 0.000$	–	–	Long $p < 0.000$	Long $p < 0.000$	Long $p < 0.000$	Long $p < 0.000$
	Mucosa 10%/s	Long $p < 0.000$	Long $p = 0.001$	Long $p < 0.000$	Long $p = 0.001$	Long $p < 0.000$	–	–	Long $p < 0.000$	Long $p = 0.012$	Long $p < 0.000$	
Embalmed	Muscle 1%/s	Long $p = 0.001$	Long $p = 0.009$	Long $p < 0.000$	Long $p < 0.000$	Long $p < 0.000$	Circ $p = 0.003$	Long $p < 0.000$	Long $p < 0.000$	Long $p < 0.000$	Long $p < 0.000$	Long $p < 0.000$
	Muscle 10%/s	Long $p < 0.000$	Long $p < 0.000$	Long $p < 0.000$	Long $p < 0.000$	Long $p < 0.000$	Circ $p = 0.001$	Long $p < 0.000$	Long $p < 0.000$	Long $p < 0.000$	Long $p < 0.000$	Long $p < 0.000$
	Mucosa 1%/s	Long $p < 0.000$	Long $p < 0.000$	Long $p < 0.000$	Long $p < 0.000$	Long $p < 0.000$	Circ $p < 0.000$	Long $p < 0.000$	Long $p < 0.000$	Long $p < 0.000$	Long $p < 0.000$	Long $p < 0.000$
	Mucosa 10%/s	Long $p < 0.000$	Long $p < 0.000$	Long $p < 0.000$	Long $p < 0.000$	Long $p < 0.000$	Circ $p < 0.000$	Long $p < 0.000$	Long $p < 0.000$	Long $p < 0.000$	Long $p < 0.000$	Long $p < 0.000$

Table 24: Spearman's correlation coefficient, r_s, and p-values between days since dissection that the sample was tested and the maximum stress of the sample, where $p < 0.05$ indicates a statistically significant correlation and $|r_s|$ close to 1 shows a strong correlation, for which a positive r_s is a positive correlation.

Layer	Direction	Strain rate	r_s	p-value
Muscularis propria	Longitudinal	1%/s	0.146	0.539
		10%/s	-0.365	0.181
	Circumferential	1%/s	-0.383	0.095
		10%/s	0.168	0.479
Mucosa-submucosa	Longitudinal	1%/s	0.286	0.235
		10%/s	0.585	0.014
	Circumferential	1%/s	-0.245	0.299
		10%/s	0.058	0.810

4.3.3 Presentation of cyclic results

The cyclic tests were performed with two cycles per stretch level, and both cycles have been presented here. As can be seen in Figure 32, rupture of the samples occurred at different stretches. With that in mind, only the full cycles of each result have been presented. For instance, the $10\%s^{-1}$ embalmed longitudinal muscular layer sample ruptured during the 1.4 stretch level cycle between 1.3 and 1.4 stretch (Figure 32a), therefore only the results up until the 1.3 stretch level are presented for this test. Furthermore, for analysis, the raw cyclic stress-stretch curves were smoothed using a moving average filter through the `smooth` function in MATLAB.

4.3.4 Cyclic stress-strain behaviour

4.3.4.1 Embalmed tissue

For the embalmed muscular layer, the results comparing the loading directions for the two strain rates are presented in Figures 35a and 35b. These figures show that the muscularis propria layer of the embalmed human oesophagus displayed anisotropic properties, for which the stiffness was higher in the longitudinal direction than the circumferential direction for the $1\%s^{-1}$ and $10\%s^{-1}$ tests, and the samples in the longitudinal direction ruptured earlier than those in the circumferential direction. Figures 35c and 35d compare the strain rates for the longitudinal and circumferential directions. The strain rate was found to affect the stiffness in the longitudinal and circumferential directions, with an increase in the strain rate resulting in an increase in the stiffness. At comparable stretches, the change in stiffness was greater in the longitudinal direction than in the circumferen-

tial direction. Hysteresis was also found to be greater for the $10\%s^{-1}$ results compared to the $1\%s^{-1}$ results in both directions.

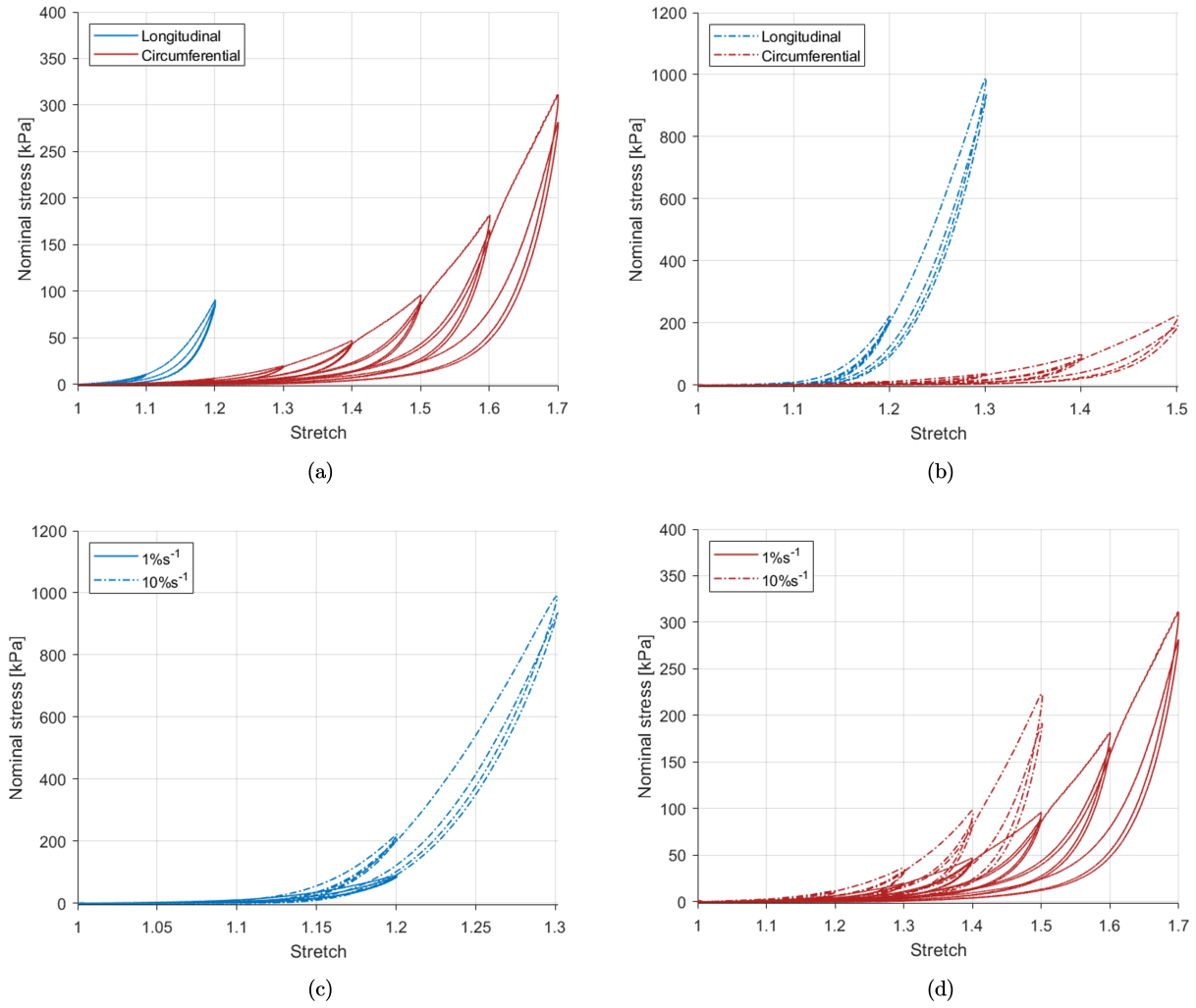

Figure 35. Effects of loading direction on the results at $1\%s^{-1}$ (**a**) and $10\%s^{-1}$ (**b**) and effects of loading rate on the results in the longitudinal direction (**c**) and the circumferential direction (**d**) of the embalmed muscularis propria layer.

The embalmed mucosa-submucosa of the human oesophagus also displayed anisotropic behaviour at both strain rates. The results of the $1\%s^{-1}$ tests for the mucosal layer can be seen in Figure 36a and the results of the $10\%s^{-1}$ tests are depicted in Figure 36b. The longitudinal direction was stiffer than the circumferential direction at both strain rates. Additionally, it can been seen that the longitudinal samples ruptured at a lower stretch level than the circumferential samples. Figures 36c and 36d compare the results of the two different strain rates in the longitudinal and circumferential

directions, respectively. A strain rate dependency was evident in both directions, with an increase in strain rate resulting in an increase in stiffness. A more pronounced dependency was observed for the longitudinal direction compared to the circumferential direction. While in the longitudinal direction the hysteresis does not seem to be significantly affected by the loading rate, the difference between the two loading curves for $\lambda = 1.1$ is greater at the higher strain rate. This implies that the stress-softening in this direction is greater with an increase in strain rate. Contrary to the longitudinal direction, hysteresis in the circumferential direction of the embalmed mucosa-submucosa layer was found to be greater at $10\%s^{-1}$ than $1\%s^{-1}$.

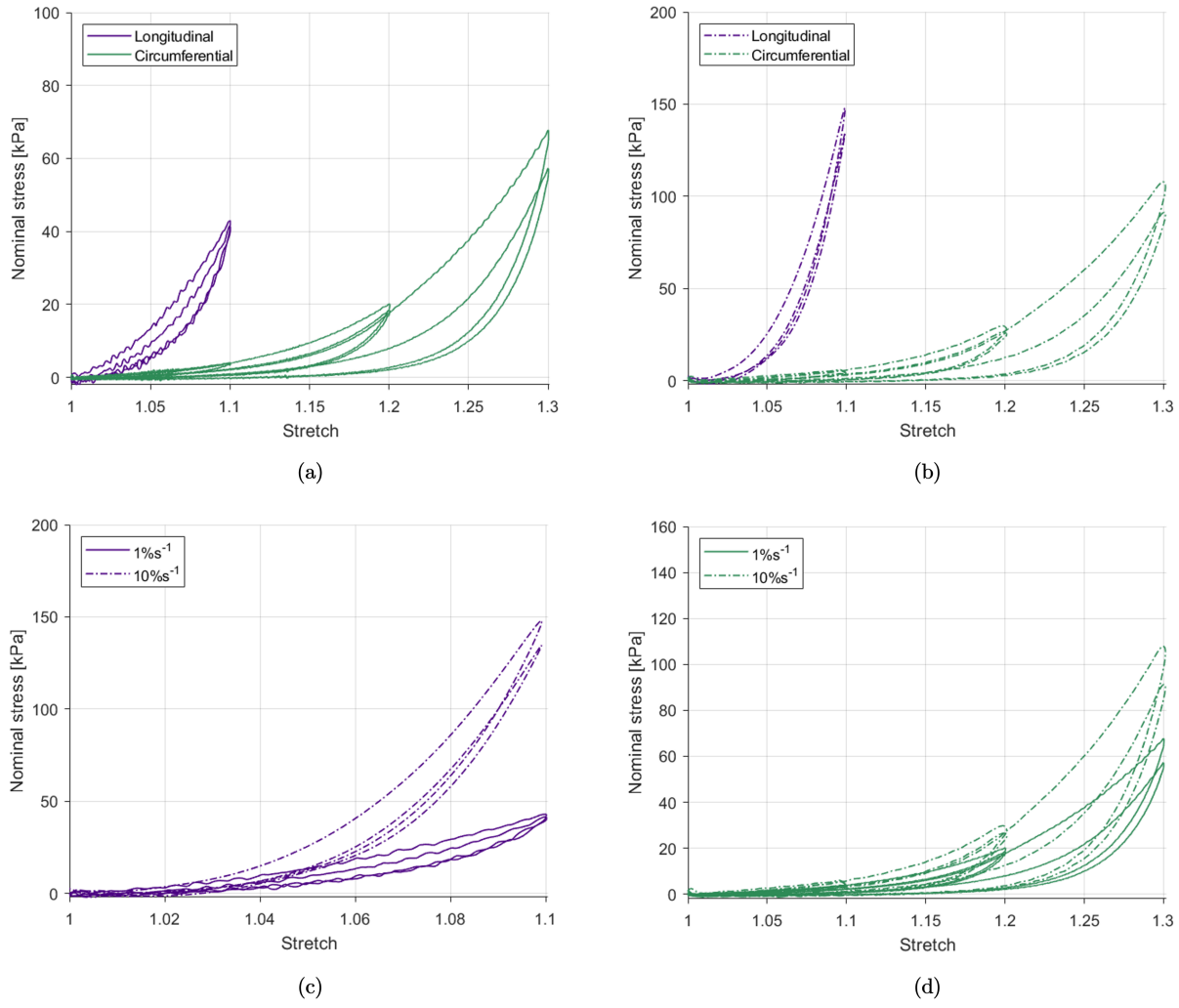

Figure 36. Effects of loading direction on the results at $1\%s^{-1}$ (**a**) and $10\%s^{-1}$ (**b**) and effects of loading rate on the results in the longitudinal direction (**c**) and the circumferential direction (**d**) of the embalmed mucosa-submucosa layer.

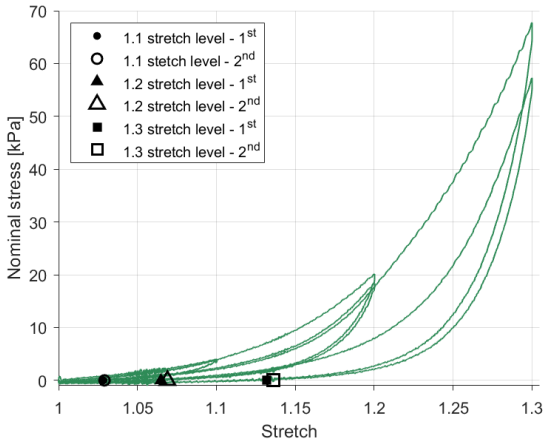

Figure 37. Markers showing the permanent set of the $1\%s^{-1}$ circumferential results for the embalmed mucosa-submucosa layer for each stretch level and cycle.

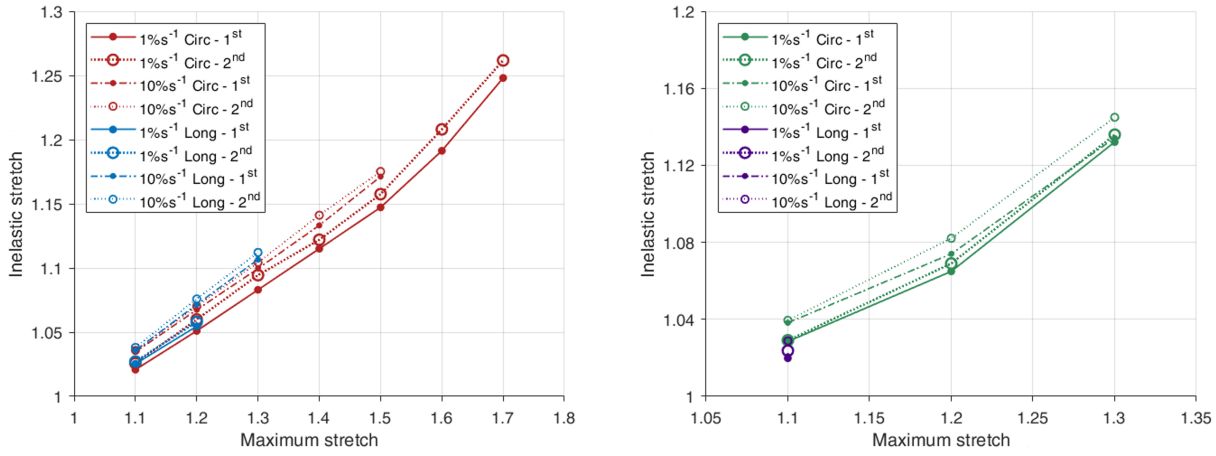

Figure 38. Permanent set in each loading direction with respect to the maximum stretch of the previous cycle for the embalmed muscular layer (**a**) and mucosa-submucosa layer (**b**) for both the first and second cycles at both strain rates ($1\%s^{-1}$ and $10\%s^{-1}$).

Permanent deformations, also known as permanent set, refer to the residual strains present in the tissue test sample when the experimental unloading path reaches zero force. Figure 37 shows the permanent stretch values for the $1\%s^{-1}$ circumferential mucosa-submucosa results, i.e. the stretch of the unloading curves when $P = 0$. Figure 38 presents this with respect to the previous maximum stretch of the sample for each layer, direction and strain rate, including a comparison between the permanent set of the first and second cycles for a single stretch level. Permanent set was found to increase with an increase in maximum stretch for all layers, directions, strain rates and cycles. For the muscular layer, the gradient of increase was similar for both the longitudinal

and circumferential directions. For the mucosal layer, the results suggest anisotropic behaviour, with slightly greater permanent set in the circumferential direction compared to the longitudinal direction. The inelastic strains were found to be greater for the second cycle compared to the first cycle for all layers, directions and strain rates. They were also found to be greater for the $10\%s^{-1}$ tests than the $1\%s^{-1}$ tests for both layers and directions, thus implying strain rate effects within the permanent set.

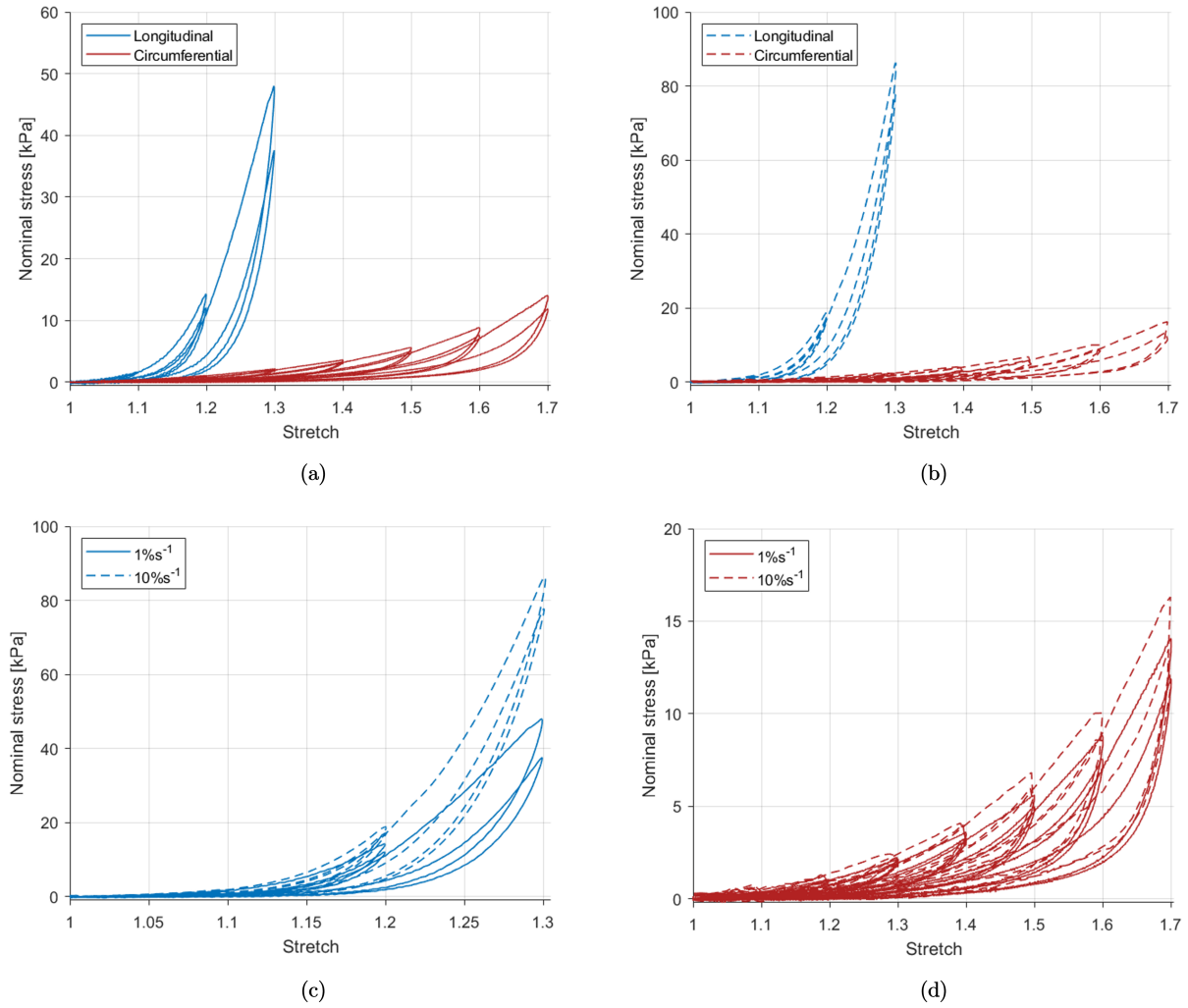

Figure 39. Effects of loading direction on the results at $1\%s^{-1}$ (**a**) and $10\%s^{-1}$ (**b**) and effects of loading rate on the results in the longitudinal direction (**c**) and the circumferential direction (**d**) of the fresh muscularis propria.

4.3.4.2 Fresh tissue

Figures 39 and 40 show the cyclic results of the fresh muscularis propria and mucosa-submucosa layer, respectively. Both layers present highly anisotropic behaviour, which greater stiffness and earlier rupture in the longitudinal directions compared to the circumferential directions. Strain rate-dependent behaviour is also apparent with an increase in strain rate resulting in an increase in the stiffness for both layers and directions. Furthermore, hysteresis seems to increase with an increase in strain rate for all layers and directions apart from the longitudinal muscular layer.

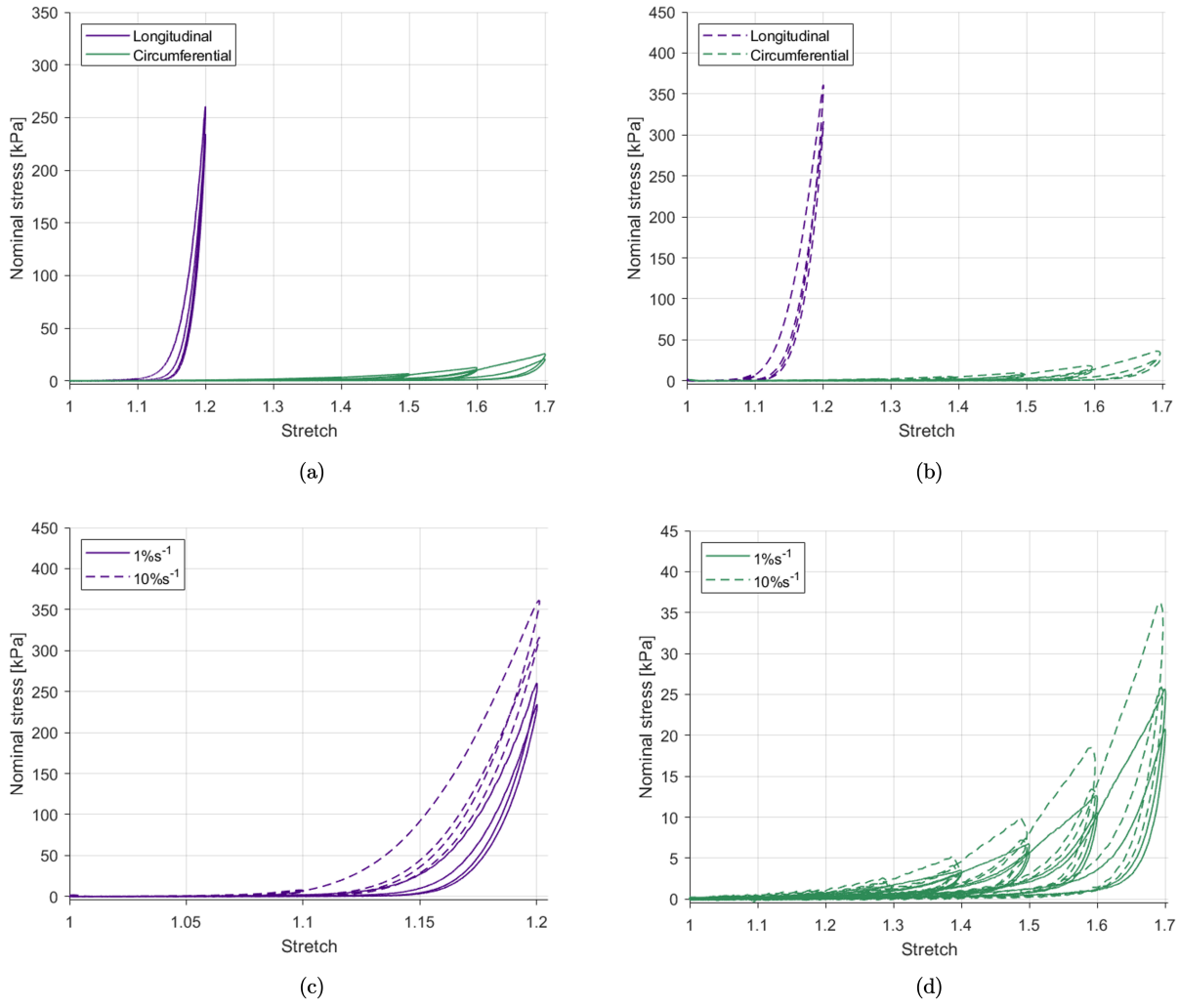

Figure 40. Effects of loading direction on the results at $1\%s^{-1}$ (**a**) and $10\%s^{-1}$ (**b**) and effects of loading rate on the results in the longitudinal direction (**c**) and the circumferential direction (**d**) of the fresh mucosa-submucosa layer.

Figures 41a and 41b show a layer comparison for the $1\%s^{-1}$ and $10\%s^{-1}$ results, respectively. In

the longitudinal direction, past 1.07 stretch, the stress of the mucosa-submucosa is much higher than that of the muscular layer. The mucosal layer also ruptures earlier than the muscularis propria in this direction across both strain rates. While the difference in the stiffness between the two layers is not as great for the circumferential direction compared to the longitudinal direction, it can be seen that after 1.4 stretch the stiffness of the mucosa-submucosa layer is greater than the muscularis propria. Permanent deformations of the cyclic results were also found to be layer-dependent in that there was greater permanent set in the mucosa-submucosa than the muscularis propria when comparing across each direction; the graphs of which will be presented later in Section 6.1.

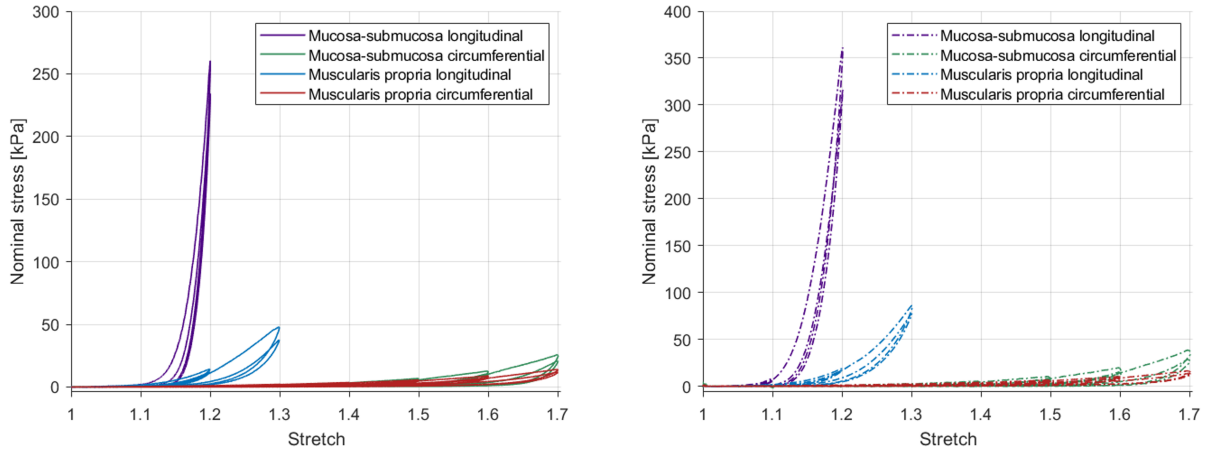

Figure 41. Fresh cyclic results showing the difference between the the two fresh layers at $1\%s^{-1}$ (**a**) and $10\%s^{-1}$ (**b**).

4.4 Stress-relaxation results

4.4.1 Variations in experimental samples and statistical analysis

The total number of stress-relaxation tests conducted per layer, per direction and per fresh cadaver can be found in Table 25. A number of factors can contribute to the dispersion seen amongst experimental data of soft biological tissues, including heterogeneity of the tissue, different levels of moisture, fluctuations in ambient temperature and variations in sample dimensions. These variations in dimensions of the stress-relaxation samples are displayed in Table 26.

To establish the time-independent behaviour of the oesophageal layers, the equilibrium stress-stretch points for each test were recorded. This was done by extracting the stress at the most

relaxed point, i.e. after 15 minutes hold time, for each stretch step, e.g. $\lambda = 1.05, 1.10, 1.15...$ for the longitudinal samples (Figure 28b). There was variability in these points between the different tests for each direction and layer. To obtain the average equilibrium stress-stretch points, outlying tests were removed (maximum 2 per layer, per direction) and the mean was calculated using the remaining values. These values were then used to plot the equilibrium stress-stretch curve to determine the time-independent response of each layer and direction of the human oesophagus under large deformation, i.e. its hyperelastic behaviour.

Table 25: Number of stress-relaxation tests performed on fresh tissue per layer, per direction, per cadaver.

Layer	**Direction**	**Step in strain [%]**	**Cadaver**	**Tests**	**Total**
Muscularis propria	Longitudinal	5	6 7	5 5	n=10
	Circumferential	10	6 7	5 4	n=9
Mucosa-submucosa	Longitudinal	5	6 7	5 5	n=10
	Circumferential	10	6 7	5 5	n=10

Table 26: Mean $\pm$ population standard deviation of sample dimensions for the stress-relaxation experiments performed on fresh tissue.

	Muscularis propria		**Mucosa-submucosa**	
	Width [mm]	Thickness [mm]	Width [mm]	Thickness [mm]
Longitudinal	4.22 ± 0.26	1.75 ± 0.45	4.01 ± 0.21	0.75 ± 0.16
Circumferential	4.14 ± 0.29	1.92 ± 0.35	3.90 ± 0.20	0.64 ± 0.29

4.4.2 Stress-relaxation behaviour

The multi-step stress-relaxation behaviour of fresh human oesophageal tissue was found to be different depending on the layer and direction. An example of a typical stress-time response can be seen for the longitudinal mucosa-submucosa layer in Figure 42. The mean equilibrium stress-stretch curve for each layer and direction can be found in Figure 43, including the standard deviation. The mucosa-submucosa reveals a greater equilibrium stress for a certain stretch compared to

the muscularis propria in the longitudinal direction. In the circumferential direction, the behaviour of the two layers is similar until 1.4 stretch, at which point the muscularis propria becomes slightly stiffer than the mucosa-submucosa. Then, after 1.6 stretch, the stress of the mucosa-submucosa increases exponentially compared to the muscularis propria. For both layers, the equilibrium stress is greater in the longitudinal direction than in the circumferential direction. The equilibrium stress-stretch results reveal that the time-independent behaviour of the human oesophagus is both layer and direction-dependent.

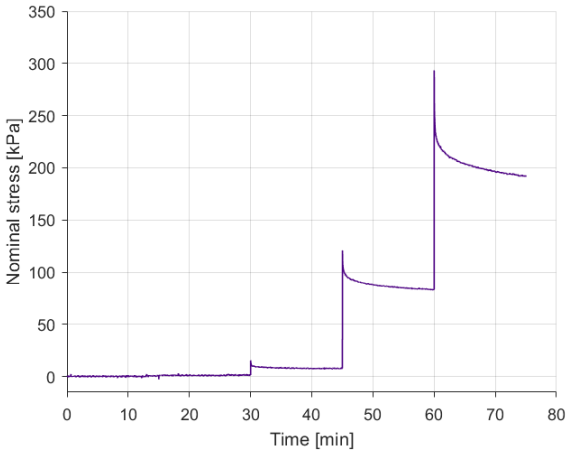

Figure 42. Stress-time example of the fresh mucosa-submucosa layer in the longitudinal direction from the multi-step stress-relaxation experiments.

4.5 Opening angle and residual strains

The average longitudinal prestretch of the oesophagus from Cadaver 7 from its *ex vivo* state to its *in situ* position was found to be 1.06, meaning that the human oesophagus *in vivo* is under a slight longitudinal tension compared to its zero-stress state. For the circumferential zero-stress state analysis, the time-dependent investigation showed that most of the creep of the samples occurred between 0 and 0.5 hrs, however that some slow creep occurred until 24 hrs. Therefore, the opening angle and residual strain measurements presented here are from the photographs taken at 24 hrs. The opening angle varies along the length of the oesophagus, and between the different layers, as can be seen in Figure 44a. The results reveal that there are greater residual strains in the mucosa-submucosa layer than the muscularis propria along the majority of the oesophagus apart from in the abdominal region. The circumferential residual strains, as displayed in Figure 44b, show that while the layers are intact, the mucosa-submucosa layer of the thoracic region is mainly

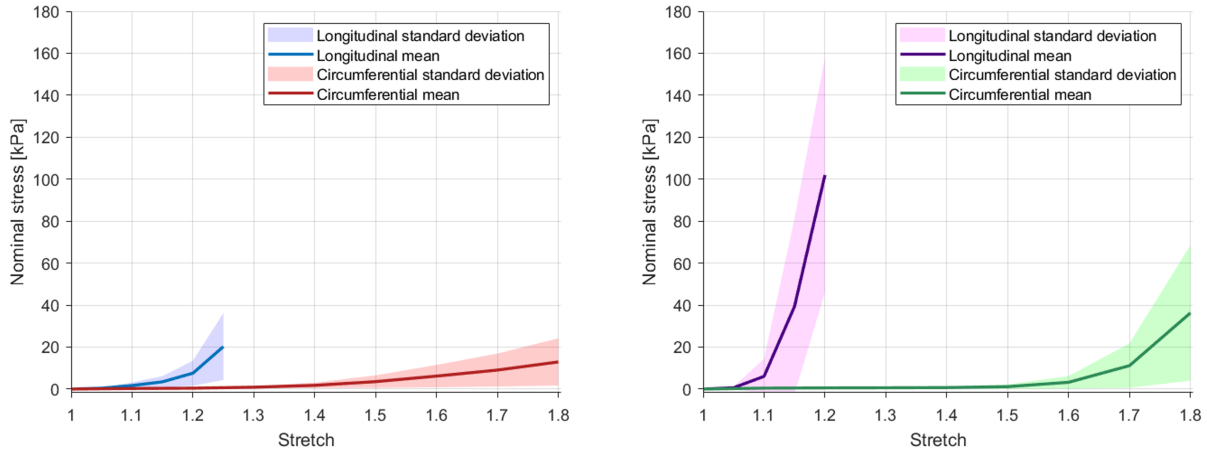

Figure 43. Mean equilibrium stress-stretch obtained from multi-step stress-relaxation tests for the fresh muscular layer (**a**) and the mucosa-submucosa layer (**b**) including shaded areas showing the sample standard deviations.

under compression (dashed green line), while the muscularis propria is fully in tension (dashed red line). The values in Figure 44b are the average of both thoracic locations investigated. The residual strains of the separated layers (solid coloured lines) show the typical inner surface under compression, outer surface in tension relationship seen for tubular soft tissues. The magnitude of these residual strains do not differ much between the separated layers, which is similar to the finding of Zhao et al. [13] for the pig oesophagus.

4.6 Conclusion

This chapter presented the experimental findings regarding the layered behaviour of the human oesophagus retrieved from both embalmed and fresh cadavers. Both the cyclic and stress-relaxation results showed the oesophageal layers to be highly anisotropic, with greater stiffness in the longitudinal direction compared to the circumferential direction, and greater resistance to rupture in the circumferential direction compared to the longitudinal direction. The behaviour of the fresh and embalmed human oesophagi were layer-dependent, with greater stiffness in the mucosal layer compared to the muscular layer when considering each direction individually. The tissue layers were found to be strain rate-dependent, with an increase in strain rate resulting in an increase in stiffness for each layer and direction. Notably, the hysteresis also increased for most layers and directions with an increase in strain rate. Permanent deformations were shown within the cyclic experimental results, and were layer, direction, strain rate and cycle-dependent. Finally, longitu-

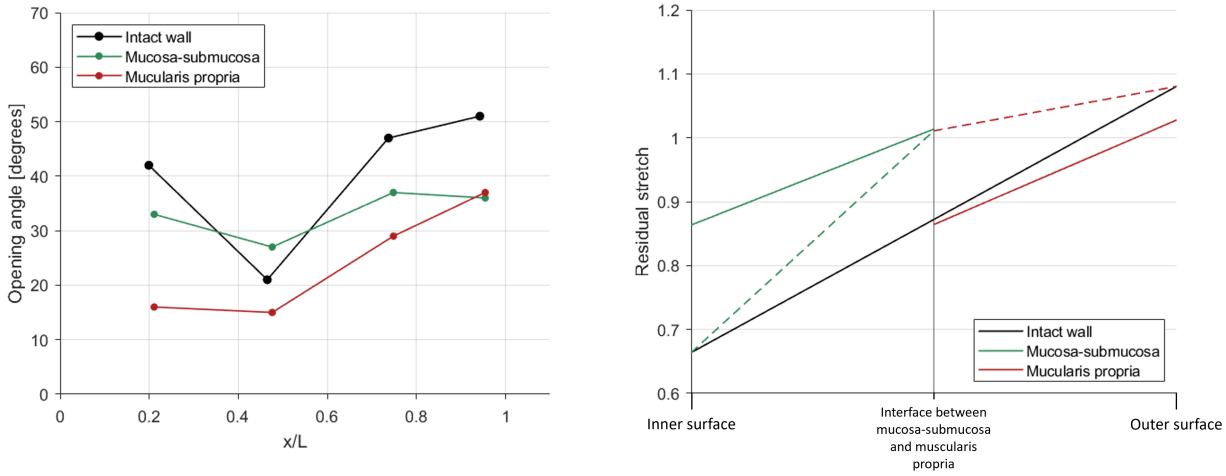

(a) (b)

Figure 44. **a**) Opening angle as a function of axial length along the oesophagus, where $x/L = 0$ is the proximal end and $x/L = 1$ is the distal end. **b**) Circumferential residual stretch of the thoracic region of the human oesophagus throughout the tissue wall, where the dashed $(- - -)$ green and red lines represent the residual strains of the mucosa-submucosa layer and muscularis propria, respectively, calculated by considering their inner and outer surfaces within the inact wall samples.

dinal prestretch and circumferential residual strains were found to be present within the human oesophagus in its *in situ* and no-load state, respectively.

CHAPTER

FIVE

5 CONSTITUTIVE MODELLING

In this chapter, the constitutive modelling of the oesophagus and other GI organs currently found in literature will firstly be discussed. Then, the model chosen for this thesis will be subsequently outlined, and the fitting procedure described. Finally, the model parameter identification and validation will be presented, along with a local sensitivity analysis of the parameter identification results.

5.1 Introduction

The experimental findings presented in Chapter 4 of this thesis show that both layers of the human oesophagus, across both preservation states, behave as non-linear, anisotropic materials with strain rate-dependent behaviour, hysteresis, stress-softening and permanent set. Due to the softness of the oesophageal layers, they are able to undergo large deformations. Therefore, models based on non-linear continuum theory can be used to capture their material behaviour [129, 350]. In this context, there have been a number of different constitutive models used to simulate the passive mechanical behaviour of oesophageal tissue. Currently, however, these have only captured its hyperelastic response and modelled its behaviour based on animal experimental data. The Fung model, originally developed for arterial tissue [351], was used to phenomenologically model the behaviour of the intact wall [53,66,68,74,214,219] and individual layers [63,66–68,214] of the oesophagus using experimental data from rat [53, 74, 214], rabbit [67, 68] and porcine tissue [63, 66]. The Fung model was able to capture well the non-linearity of oesophageal tissue, as well as its anisotropy [66–68, 219]. Structure-based models that include information on the microstructural components of the tissue have also been used to model the response of the intact wall [64, 69, 219] and individual layers [60, 62, 64, 69, 70, 209] of the oesophagus. Notably, models based on those developed by Holzapfel, Gasser, Ogden and their collaborators [352–354] have been used to model the oesophagus in this way [60,70,209,219]. These models, originally developed for arterial tissue, consist of an additive split of the strain energy function (SEF) into contributions from the isotropic matrix material and the anisotropic collagen fibres. Yang et al. [60] used a neo-Hookean model for the isotropic matrix and a classic Holzapfel model [352] to capture the anisotropic behaviour of the tissue layers. They implemented two families of collagen fibres oriented symmetrically at an angle to the circumferential direction, the fibre angle of which was determined by fitting it as an additional material parameter rather than from structural imaging. Yang et al. [60] found that by modifying the SEF of the fibres to be less non-linear, they were able to obtain a better fit with their experimental data on porcine oesophagi. They then went on to use their bilinear SEF, which

incorporates the actual strain of the fibres, in a following study on the inflation-extension behaviour of the oesophagus [209]. To model the response of ovine oesophageal tissue layers, Sommer et al. [70] used a neo-Hookean and a classic Holzapfel model [352] with one family of collagen fibres. They determined the fibre angle phenomenologically as an additional material parameter and concluded that, due to the angle being greater than 45°, the collagen fibres were preferentially aligned in the longitudinal direction for both the muscular and mucosal layers. Moreover, a new structure-based model developed by Natali and coworkers [62] was used to model the hyperelastic behaviour of layers of the oesophagus from porcine. This model involved an additive split of the SEF into isotropic and anisotropic parts, where, unlike other approaches in which the families of fibres represent collagen in both oesophageal layers, the fibres in the muscular layer of the model are the muscle fibres, and the fibres in the mucosa-submucosa layer are collagen fibres. For the muscular and mucosal layers, Natali et al. [62] included the stretch along the fibre directions and the influence of the fibres to the overall tissue response, while for the mucosal layer they also incorporated the contribution of the interaction between the two families of fibres. This resulted in an eight and ten parameter model being used to capture just the hyperelastic response of the muscular and mucosal layers of the oesophagus, respectively.

While phenomenological models can often provide a very good fit with experimental data, there is a risk that the model can become over-fitted to the loading mode used for identification and validation of the material parameters, which may not be transferable to other loading modes [131]. Furthermore, as they do not account for the tissue's structure, we cannot use the model to gain insight into the role of the material's components on its mechanical behaviour [160]. For this reason, a structure-based approach will be employed here to model the hyperelastic behaviour of the human oesophagus, with the microstructural information being obtained from histological image analysis. Additionally, Ngwangwa et al. [219], who studied the ability of phenomenological and structure-based models to simulate the behaviour of ovine oesophageal tissue, found that structure-based models were able to more accurately capture its mechanical behaviour.

As previously stated, there have been no studies attempting to model the viscoelastic behaviour of the oesophagus, despite there being a number of time-dependent investigations of the tissue (Table 13). However, there have been a small number who have modelled the viscoelastic response of the other GI tissues, including the stomach [226], small intestine [355], large intestine [355, 356] and rectum [355]. For instance, Higa et al. [356] modelled the compressive behaviour of the goat large intestine using a Mooney-Rivlin model [357] for its hyperelastic behaviour and a convolution

integral to model its time-dependent response. Their model provided a good fit with the experimental data, however they did not validate their parameters using another loading mode or strain rate. Panda and Buist [355] proposed a viscoelastic framework for modelling the time-dependent behaviour of the GI tissues specifically in regard to their distension response, and tested the efficacy of the model against experimental data from three different GI organs. This model involved an internal variable method based on the work of Huber and Tsakmakis [358] and used either neo-Hookean or Humphrey [359] SEFs for the elastic and overstress parts of the Cauchy stress. For the small intestine, they found that a neo-Hookean model with linear or non-linear viscosity was able to capture very well the distension experimental data of Carniel et al. [277], however that non-linear viscosity performed slightly better. Furthermore, they successfully simulated the creep distension behaviour of the large intestine using experimental findings also from Carniel and coworkers [360]. They found that, in this case, a Humphrey model with linear viscosity was best able to capture the experimental data. Carniel et al. [277,360] constitutively modelled their own experimental data using a physio-mechanical viscoelastic formulation, however their model was not thermodynamically consistent [355]. Moreover, for rectal tissue, Panda and Buist [355] modelled the radial stress-relaxation using a neo-Hookean viscoelastic model with linear viscosity, which captured well the tissue's time-dependent response. However, neither Higa et al. [356] or Panda and Buist [355] considered the direction-dependent response of the organ studied. Fontanella et al. [226] utilised viscous variables to capture the viscoelasticity of piglet stomachs and modelled the behaviour in both the circumferential and longitudinal directions. For the hyperelastic component of the tissue behaviour, they used a Natali structure-based model, and found good overall agreement between the model and experimental data. However, Fontanella et al. [226] only considered the time-dependent softening of the stomach and did not incorporate its history-dependent response.

Petiteau et al. [361] compared two viscoelastic frameworks in the context of the strain rate-dependent behaviour of materials in the large deformation domain. These frameworks included, what Petiteau et al. [361] named, the Convolution Integral Model (CIM) and the Internal Variable Model (IVM). They found that the IVM, based on the work of Huber and Tsakmakis [358], exhibited more dissipation at higher strain rates compared to the CIM. Thus, as we found that hysteresis of the human oesophageal was the one of the characteristics to significantly increase with strain rate (Table 22), an internal variable approach will be employed here. Using the IVM, Masri et al. [7] successfully modelled the layer, direction and time-dependent behaviour of the male human urethra, incorporating its history-dependent response through a stress-softening function developed by Rebouah et

al. [362,363]. For the tissue's hyperelastic behaviour, Masri et al. [7] used a Holzapfel model [352] with three fibre families in which the fibre angles were derived from histological analysis of the tissues layers. However, they did not consider the behaviour of the tissue over different strain rates or with more than one cycle per stretch level.

As of yet, there has been no modelling carried out on oesophageal mechanical data from human tissue, and the modelling that exists for the oesophagus using animal experimental data only looks at its time-independent response. There have been a number of different ways to model other GI tissues in terms of their time-dependent behaviour, however they either did not consider the anisotropic behaviour or the history-dependent softening of the tissues. Therefore, an invariant-based formulation from modelling the human male urethra [7] has been adapted here according to the microstructural composition and experimentally-observed behaviour of the human oesophageal layers. For this, an anisotropic matrix-fibre IVM with a history-dependent damage function was employed, in which the fibre angle was determined from histologically obtained images.

5.2 Anisotropic matrix-fibre model with damage

In this section, a constitutive formluation for describing the passive material properties of the human oesophageal layers will be outlined.

Consider a continuum in which the reference (undeformed) configuration $\kappa_0 \in \mathbb{R}^3$ undergoes a deformation according to the map $\boldsymbol{\varphi}$ as a function of time t. Every particle $\boldsymbol{X}$ in this continuum is mapped onto a corresponding point in the deformed configuration κ by $\boldsymbol{x} = \boldsymbol{\varphi}(\boldsymbol{X}, t)$ [364]. The deformation gradient tensor $\boldsymbol{F}$ describes the mapping of the undeformed line elements onto the deformed line elements and is defined as:

$$\boldsymbol{F}(\boldsymbol{X}, t) = \frac{\partial \boldsymbol{\varphi}(\boldsymbol{X}, t)}{\partial \boldsymbol{X}} \tag{5}$$

where $\boldsymbol{X}$ and $\boldsymbol{x}$ are the position vectors in the reference and deformed configurations, respectively. The non-linear behaviour of soft materials undergoing large deformations is best described by a Helmholtz free SEF, Ψ. This function can be used to relate the stress and the strain of the material either from the point of view of the undeformed configuration or the deformed configuration: both will be expressed here and either will be used depending on convenience. The second Piola-Kirchhoff (PK) stress tensor describes the stress in the reference configuration and is defined as:

$$\boldsymbol{S} = 2\frac{\partial \Psi}{\partial \boldsymbol{C}} \tag{6}$$

where $\boldsymbol{C} = \boldsymbol{F}^T \boldsymbol{F}$ is the right Cauchy-Green tensor. The stress expressed in the deformed configuration is described by the Cauchy stress tensor:

$$\boldsymbol{\sigma} = 2J^{-1}\frac{\partial \Psi}{\partial \boldsymbol{b}}\boldsymbol{b} \tag{7}$$

where $\boldsymbol{b} = \boldsymbol{F}\,\boldsymbol{F}^T$ is the left Cauchy-Green tensor and $J = \det(\boldsymbol{F})$ is the Jacobian of the deformation map, in which "det" refers to the determinant operator. The principal stretches, λ_i where $i = 1, 2, 3$, are the squareroots of the principal components of the right or left Cauchy-Green tensors, i.e. $\lambda_i^2 = \text{eigen}(\boldsymbol{C})$. Now, the Helmholtz free SEF can be decoupled into:

$$\Psi = U(J) + W \tag{8}$$

where U is a function of J and represents the strain energy due to the volumetric deformation, while W is the volume preserving (isochoric) contribution to the strain energy, i.e. the shape change. The oesophagus is considered as incompressible here as the high water content of soft tissues means they are often regarded as such [164, 365]. For incompressible materials, $J \equiv 1$ and the U term of Equation 10 disappears. For thermodynamic consistency, a new term appears for the stress of incompressible materials and is shown for the second PK stress tensor as follows:

$$\boldsymbol{S} = -pJ\boldsymbol{C}^{-1} + 2\frac{\partial W}{\partial \boldsymbol{C}} \tag{9}$$

where p is the used as a Lagrange multiplier to impose the material incompressibility constraint. It is referred to as the unknown hydrostatic pressure and can be determined through the equilibrium equations and boundary conditions.

Now, for anisotropic materials, the isochoric SEF can undergo an additive split into the contributions from the isotropic part and the anisotropic part. For structure-based models of soft tissues, usually the isotropic part is assumed to consist of the non-collagenous part of the material such as the matrix, elastin and muscle fibres, while the anisotropic part is associated with the response of the collagen fibres [131] as follows:

$$W = W_0 + W_{\text{fibres}} \tag{10}$$

This approach has been employed here where the matrix of the tissue has been considered as purely

elastic and isotropic, with the anisotropy coming from the collagen fibres and their predominant orientations. The viscoelasticity and damage have also been assumed to originate from the collagen fibres due to the strain rate effects of the oesophageal layers not being seen at initial stretches (Table 22), rather once the fibres have been activated (Figures 39c,d and 40c,d) [366], and the permanent set being commonly applied to the fibrous component of models for soft tissues [367–369]. For the mucosal layer, the fibres are the collagen within the mucosa and submucosa layers. For the muscular layer, the fibres are composed of the collagen networks surrounding and connecting the muscle fibres, as well as those concentrated at the circular/longitudinal junction. From the histological analysis, as outlined in Section 4.1, the collagen fibres of both layers were observed to sit predominantly in the longitudinal and circumferential directions. Therefore, an orthotropic model has been used to capture the anisotropy of the oesophageal layers, the collagen fibre orientations for which have been demonstrated in Figure 45. This is contrary to the animal studies who used a similar matrix-fibre approach, mentioned in Section 5.1, but modelled the collagen fibres orientated at an angle to the circumferential direction [69, 70], i.e. not parallel and perpendicular to the longtiduinal and circumferential directions as is adopted here.

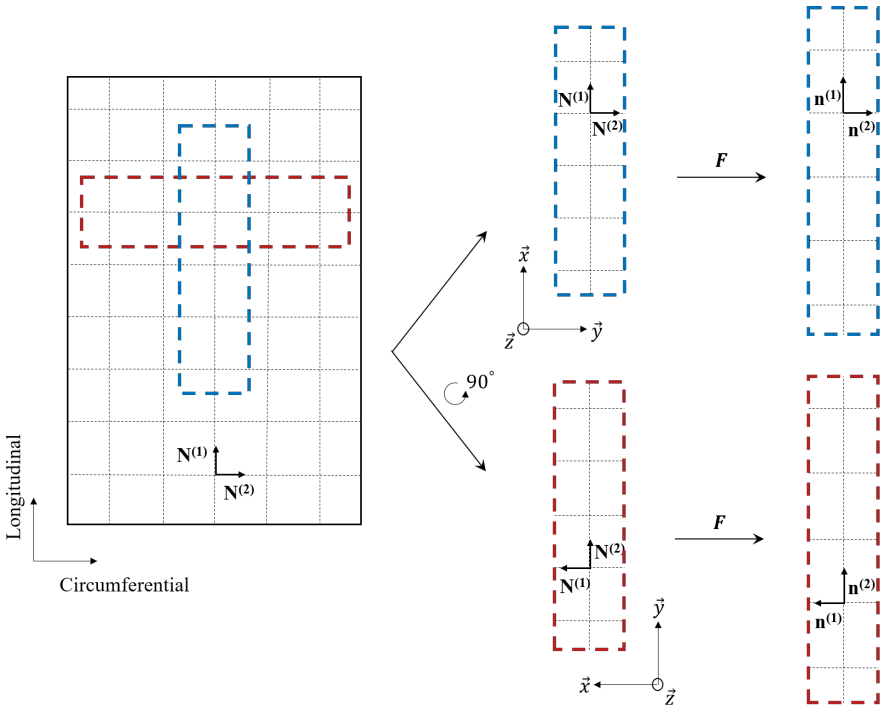

Figure 45. Drawing to illustrate the fibre orientations in the layers of the human oesophagus based on the histological observations outlined in Section 4.1.

The isotropic SEF can be described in terms of the first three invariants of the right and left Cauchy-

Green tensors, I_1, I_2 and I_3, where for incompressible materials $I_3 = 1$ [350]. Here, however, for simplicity, only I_1 will be used. For anisotropic materials, a fourth invariant, I_4, of the right or left Cauchy-Green tensors is introduced and describes the stretch of a single family of fibres along their specific direction. Two families of fibres will be used here and so the second PK stress tensor defined in terms of these invariants for incompressible, anisotropic materials is:

$$\boldsymbol{S} = -p\boldsymbol{C}^{-1} + 2\frac{\partial W_0}{\partial I_1}\boldsymbol{I} + 2\sum_{i=1,2} I_4^{(i)}\frac{\partial W_{\text{fibres}}^{(i)}}{\partial I_4^{(i)}}\left[\boldsymbol{N}^{(i)} \otimes \boldsymbol{N}^{(i)}\right] \tag{11}$$

where, $\boldsymbol{I}$ is the identity tensor, $\boldsymbol{N}^{(i)}$ is the direction of each set of fibres in the undeformed configuration, and W_0 and $W_{\text{fibres}}^{(i)}$ are the SEFs of the matrix and fibres, respectively, in which I_1 and $I_4^{(i)}$ are defined in terms of the right Cauchy-Green tensor as:

$$I_1 = \text{tr}(\boldsymbol{C}); \quad I_4^{(i)} = \boldsymbol{C} : \left[\boldsymbol{N}^{(i)} \otimes \boldsymbol{N}^{(i)}\right]. \tag{12}$$

The Cauchy stress tensor is defined for incompressible, anisotropic materials in terms of I_1 and $I_4^{(i)}$ by:

$$\boldsymbol{\sigma} = -p\boldsymbol{I} + 2\frac{\partial W_0}{\partial I_1}\boldsymbol{b} + 2\sum_{i=1,2} I_4^{(i)}\frac{\partial W_{\text{fibres}}^{(i)}}{\partial I_4^{(i)}}\left[\boldsymbol{n}^{(i)} \otimes \boldsymbol{n}^{(i)}\right] \tag{13}$$

where, $\boldsymbol{n}^{(i)}$ is the local direction of each set of fibres in the deformed configuration.

Next, the damage is modelled using a stress-softening evolution function developed by Rebouah et al. [362]. This function, χ, is also able to capture the permanent set of a material and is applied here to the fibre portion of the equation. Thus, the Cauchy stress tensor becomes:

$$\boldsymbol{\sigma} = -p\boldsymbol{I} + 2\frac{\partial W_0}{\partial I_1}\boldsymbol{b} + 2\sum_{i=1,2} \chi^{(i)}\left(I_4^{(i)}, I_4^{(i)max}\right) I_4^{(i)}\frac{\partial W_{\text{fibres}}^{(i)}}{\partial I_4^{(i)}}\left[\boldsymbol{n}^{(i)} \otimes \boldsymbol{n}^{(i)}\right]. \tag{14}$$

The stress-softening function considers the difference between the current stretch and the previous maximum stretch, therefore capturing the history-dependent behaviour of the material. The function was applied to soft tissues by Rebouah and Chagnon [363] and is described as:

$$\chi^{(i)}\left(I_4^{(i)}, I_4^{(i)max}\right) = 1 - \eta_m^{(i)}\left[\frac{I_4^{(i)max} - I_4^{(i)}}{I_4^{(i)max} - 1}\right]^{\beta^{(i)}} \tag{15}$$

where, η_m and β are non-dimensional parameters, and $I_4^{(i)max}$ is the maximum value of $I_4^{(i)}$ for each direction throughout the whole history of the material.

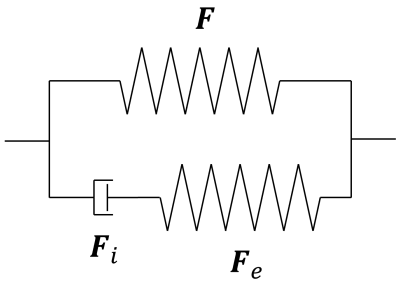

Figure 46. Rheological representation of the viscoelastic model.

Now the time-dependent behaviour is considered using a large strain version of the Standard Linear Solid model [358] and is also captured solely by the fibres. An internal variable-based model advocated by Petiteau et al. [361] is employed, and can be represented using a spring-dashpot analogy. A schematic of the generalised Maxwell model can be seen in Figure 46. The deformation gradient tensor of the lower, inelastic branch can be described by a multiplicative decomposition into an elastic part, $\boldsymbol{F}_e$, and an inelastic part, $\boldsymbol{F}_i$, in which $\boldsymbol{F} = \boldsymbol{F}_e\boldsymbol{F}_i$. Figure 47 shows a visual representation of this decomposition.

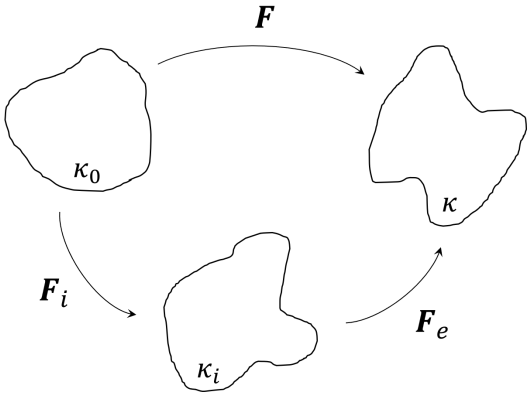

Figure 47. A decomposition of the deformation gradient tensor $\boldsymbol{F}$, where κ_0 is the undeformed configuration, κ_i is the intermediate configuration and κ is the final configuration.

We assume that the viscoelasticity has no volumetric contributions, so the SEF of the fibres can be written as:

$$W_{\text{fibres}}(\boldsymbol{F}, \boldsymbol{F}_e) = W_1(\boldsymbol{F}) + W_2(\boldsymbol{F}_e) \tag{16}$$

where, W_1 is associated with the deformation between κ_0 and κ, and W_2 is the SEF involved in the deformation between κ_i and κ [361]. Now, the Clausius–Duhem inequality, as detailed in Petiteau et al. [361], arises through the application of the Second Law of Thermodynamics on the fibres such that:

$$\mathcal{D}_{\text{int}} = \boldsymbol{\sigma}_{\text{fibres}} : \boldsymbol{D} - \dot{W}_{\text{fibres}} \geq 0 \tag{17}$$

where, $\mathcal{D}_{\text{int}}$ is the internal dissipation and $\boldsymbol{D}$ is the rate of deformation tensor. Taking into account Equation 16, the dissipation inequality can be written as:

$$\boldsymbol{\sigma}_{\text{fibres}} : \boldsymbol{D} - \frac{\partial W_1}{\partial \boldsymbol{b}} : \dot{\boldsymbol{b}} - \frac{\partial W_2}{\partial \boldsymbol{b}_e} : \dot{\boldsymbol{b}}_e \geq 0 \tag{18}$$

where, $\boldsymbol{b}_e = \boldsymbol{F}_e \, \boldsymbol{F}_e^T$ is the left Cauchy-Green tensor of the elastic deformation, and $\dot{\boldsymbol{b}}$ and $\dot{\boldsymbol{b}}_e$, through some algebraic manipulations, are:

$$\dot{\boldsymbol{b}} = \boldsymbol{L}\boldsymbol{b} + \boldsymbol{b}\boldsymbol{L}^T; \quad \dot{\boldsymbol{b}}_e = \boldsymbol{L}\boldsymbol{b}_e + \boldsymbol{b}_e\boldsymbol{L}^T - 2\boldsymbol{F}_e\boldsymbol{D}_i\boldsymbol{F}_e^T \tag{19}$$

where, $\boldsymbol{D}_i$ is the inelastic strain rate tensor defined as:

$$\boldsymbol{D}_i = \frac{1}{2}\left(\boldsymbol{L}_i + \boldsymbol{L}_i^T\right) \tag{20}$$

and $\boldsymbol{L} = \dot{\boldsymbol{F}}\boldsymbol{F}^{-1}$ and $\boldsymbol{L}_i = \dot{\boldsymbol{F}}_i\boldsymbol{F}_i^{-1}$ are the global and inelastic velocity gradient tensors, respectively. Equation 18 can then be written as:

$$\left(\boldsymbol{\sigma}_{\text{fibres}} - 2\frac{\partial W_1}{\partial \boldsymbol{b}}\boldsymbol{b} - 2\frac{\partial W_2}{\partial \boldsymbol{b}_e}\boldsymbol{b}_e\right) : \boldsymbol{D} + 2\boldsymbol{F}^T\frac{\partial W_2}{\partial \boldsymbol{b}_e}\boldsymbol{F}_e : \boldsymbol{D}_i \geq 0. \tag{21}$$

To satisfy Equation 21 according to the incompressibility constraints, the Cauchy stress of the fibres and the dissipation inequality are now defined, respectively, as:

$$\boldsymbol{\sigma}_{\text{fibres}} = -p\boldsymbol{I} + 2\frac{\partial W_1}{\partial \boldsymbol{b}}\boldsymbol{b} + 2\frac{\partial W_2}{\partial \boldsymbol{b}_e}\boldsymbol{b}_e \tag{22}$$

and

$$2\boldsymbol{F}_e^T \frac{\partial W_2}{\partial \boldsymbol{b}_e} \boldsymbol{F}_e : \boldsymbol{D}_i \geq 0. \tag{23}$$

The simplest condition which satisfies Equation 23 is:

$$\boldsymbol{D}_i = \frac{1}{\eta_0} \left(\boldsymbol{F}_e^T \frac{\partial W_2}{\partial \boldsymbol{b}_e} \boldsymbol{F}_e \right)^D \tag{24}$$

where, the dashpot of Figure 46 is expressed linearly with the viscosity parameter η_0, and $(\cdot)^D$ is the deviatoric operator. This gives rise to the evolution equation for the elastic strain as follows:

$$\dot{\boldsymbol{b}}_e = \boldsymbol{L}\boldsymbol{b}_e + \boldsymbol{b}_e\boldsymbol{L}^T - \frac{4}{\eta_0}\boldsymbol{b}_e \left(\frac{\partial W_2}{\partial \boldsymbol{b}_e}\boldsymbol{b}_e \right)^D. \tag{25}$$

Therefore, in this case, the evolution equation to describe the elastic deformation of the fibres can be written as:

$$\dot{\boldsymbol{b}}_e = \boldsymbol{L}\boldsymbol{b}_e + \boldsymbol{b}_e\boldsymbol{L}^T - \frac{4}{\eta_0}\frac{\partial W_2}{\partial I_{4,e}} I_{4,e}\boldsymbol{b}_e \left[[\boldsymbol{n}_e \otimes \boldsymbol{n}_e] - \frac{1}{3} I_{4,e}\boldsymbol{I} \right] \tag{26}$$

where, $\boldsymbol{n}_e^{(i)}$ is the orientation of the fibres in the elastically deformed state and $I_{4,e}$ is the fourth invariant of the elastic strain. The final Cauchy stress then becomes:

$$\boldsymbol{\sigma} = -p\boldsymbol{I} + 2\frac{\partial W_0}{\partial I_1}\boldsymbol{b} + 2\sum_{i=1,2} \chi^{(i)} \left[I_4^{(i)} \frac{\partial W_1^{(i)}}{\partial I_4^{(i)}} \left[\boldsymbol{n}^{(i)} \otimes \boldsymbol{n}^{(i)} \right] + I_{4,e}^{(i)} \frac{\partial W_2^{(i)}}{\partial I_{4,e}^{(i)}} \left[\boldsymbol{n}_e^{(i)} \otimes \boldsymbol{n}_e^{(i)} \right] \right] \tag{27}$$

where,

$$I_{4,e}^{(i)} = \boldsymbol{C}_e : \left[\boldsymbol{N}^{(i)} \otimes \boldsymbol{N}^{(i)} \right] \tag{28}$$

in which, $\boldsymbol{C}_e = \boldsymbol{F}_e^T \boldsymbol{F}_e$ is the right Cauchy-Green tensor associated with the elastic deformation.

5.3 One-dimensional formulation of the model

In this section, the one-dimensional constitutive law will be formulated following the uniaxial tensile test condition of this study. For the muscularis propria and mucosa-submucosa layers, it is assumed that the collagen fibres, residing mainly in the longitudinal and circumferential directions, can be captured by two families of fibres whose mean orientations in the undeformed configuration are denoted by $\boldsymbol{N}^{(1)}$ and $\boldsymbol{N}^{(2)}$, as seen in Figure 45. For the longitudinal samples, the direction vectors are simply:

$$\boldsymbol{N}^{(1)} = \begin{bmatrix} 1 & 0 & 0 \end{bmatrix}; \quad \boldsymbol{N}^{(2)} = \begin{bmatrix} 0 & 1 & 0 \end{bmatrix}. \tag{29}$$

For uniaxial tension, the samples are loaded in only one direction, while the other two directions are unhindered, hence $\lambda_1 = \lambda$ for the longitudinal samples. In this model, as is with Holzapfel et al. [352], it is assumed that the fibres are only active in tension, i.e., $I_4^{(i)} \geq 1$ and $I_{4,e}^{(i)} \geq 1$. It is also considered that the material is incompressible. Therefore, with the assumption of symmetry, the uniaxial tension deformation gradient tensor can be written as follows:

$$\begin{bmatrix} \boldsymbol{F} \end{bmatrix} = \begin{bmatrix} \lambda & 0 & 0 \\ 0 & \lambda^{-\frac{1}{2}} & 0 \\ 0 & 0 & \lambda^{-\frac{1}{2}} \end{bmatrix} \tag{30}$$

where, λ is the stretch as defined in Section 3.4.5. A neo-Hookean SEF is used to model the matrix of the oesophageal layers and is described as:

$$W_0 = c_1[I_1 - 3] \tag{31}$$

where, c_1 is a stress-like material parameter. For the time-independent response of the fibres, a classic Holzapfel [352] SEF is used:

$$W_1^{(i)} = \frac{k_1^{(i)}}{2k_2^{(i)}}[e^{k_2^{(i)}[I_4^{(i)}-1]^2} - 1] \tag{32}$$

where, $k_1 > 0$ is a stress-like material parameter and $k_2 > 0$ is a dimensionless parameter. For the elastic deformation of the fibres, a Kaliske [15] SEF, as used by Rebouah and Chagnon [370], is employed (with $n = 3$) and is described as:

$$W_2^{(i)} = C_2^{(i)}[I_{4,e}^{(i)} - 1]^2 + C_3^{(i)}[I_{4,e}^{(i)} - 1]^3 + C_4^{(i)}[I_{4,e}^{(i)} - 1]^4 \tag{33}$$

where, C_2, C_3 and C_4 are stress-like material parameters. Using the definitions of Eqns. (12) and (28) with (30), the strain invariants can be written in terms of global stretch, λ, and the elastic stretch component, λ_e, for uniaxial tension as:

$$I_1 = \lambda^2 + 2\lambda^{-1}; \quad I_4^{(1)} = \lambda^2; \quad I_4^{(2)} = \lambda^{-1}; \quad I_{4,e}^{(1)} = \lambda_e^2; \quad I_{4,e}^{(2)} = \lambda_e^{-1}. \tag{34}$$

The first PK stress tensor is then calculated from the Cauchy stress using $\boldsymbol{P} = J\boldsymbol{\sigma}\,\boldsymbol{F}^{-T}$. The unknown hydrostatic pressure is solved using the knowledge that $P_3 = 0$ for this test condition. Therefore, by inserting this and the definitions from (34), the one-dimensional first PK stress for the longitudinal samples becomes:

$$P_1 = 2\frac{\partial W_0}{\partial I_1}[\lambda - \lambda^{-2}] + 2\chi^{(1)}\lambda^{-1}\left[\frac{\partial W_1^{(1)}}{\partial I_4^{(1)}}\lambda^4 + \frac{\partial W_2^{(1)}}{\partial I_{4,e}^{(1)}}\lambda_e^4\right], \tag{35}$$

where, the partial derivatives of the SEFs for the fibres and the matrix with respect to their invariants are as follows:

$$\frac{\partial W_0}{\partial I_1} = c_1; \quad \frac{\partial W_1^{(1)}}{\partial I_4^{(1)}} = \left[\lambda^2 - 1\right] k_1^{(1)} e^{k_2[\lambda^2-1]^2}; \tag{36}$$

$$\frac{\partial W_2^{(1)}}{\partial I_{4,e}^{(1)}} = 2C_2^{(1)}[\lambda_e^2 - 1] + 3C_3^{(1)}[\lambda_e^2 - 1]^2 + 4C_4^{(1)}[\lambda_e^2 - 1]^3. \tag{37}$$

The first PK stress is now expressed in terms of λ and can be compared to the experimentally obtained data. The same procedure is used to derive the one-dimensional equation for the circumferential direction, i.e. when $\boldsymbol{N}^{(2)}$ is parallel to the axis of loading. The evolution equation of Eqn. (26) is used to attain the elastic deformation during loading and is written in its one-dimensional form in terms of λ_e for uniaxial tension as:

$$\dot{\lambda}_e = \lambda_e\frac{\dot{\lambda}}{\lambda} - \frac{4}{3\eta_0}\frac{\partial W_2}{\partial I_{4,e}}\lambda_e^5 \tag{38}$$

5.4 Parameter identification and model validation

5.4.1 Embalmed tissue

The first step in parameter identification for the embalmed tissue was to isolate the approximate hyperelastic portion of the experimental results. For this, the loading path closest to that of a preconditioned sample from the $1\%s^{-1}$ tests was selected. Therefore, the loading path of the second cycle of the highest stretch level reached by each sample was extracted and used to identify only the hyperelastic parameters. For each layer, the hyperelastic portion of the first PK stress equations, i.e. *sans* stress-softening and viscoelasticity, for the longitudinal and circumferential directions were compared to the linear region of the experimental data to simultaneously fit the c_1 parameter using a manual slider. The $k_1^{(i)}$ and $k_2^{(i)}$ parameters were then obtained independently for each direction also by using a manual slider. The results of these fittings can be seen in Figure 48, revealing a good fitting of the experimental data for both layers and directions. The hyperelastic parameters were then kept frozen during the identification of the damage and viscous parameters.

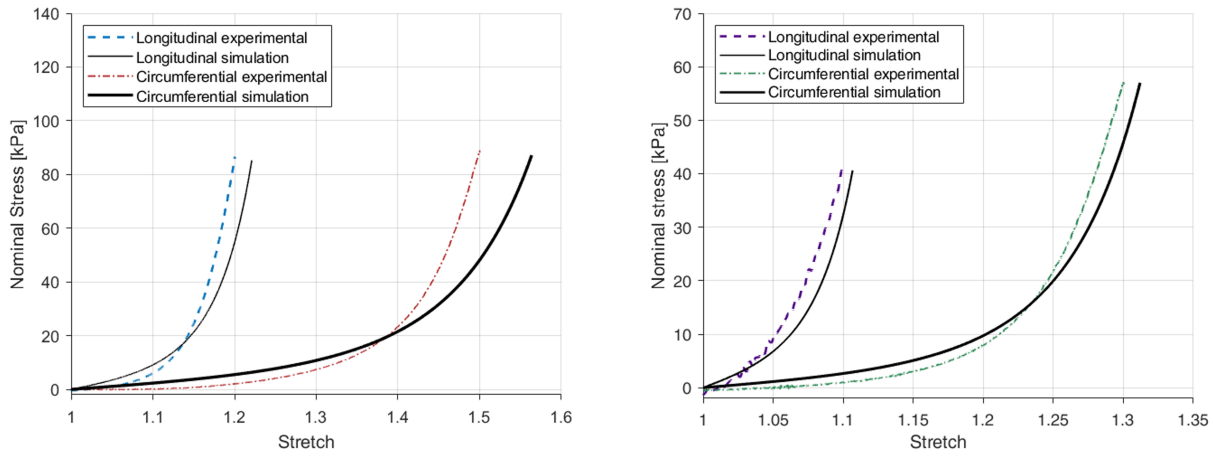

Figure 48. Identification of the hyperelastic parameters in the longitudinal and circumferential directions for the embalmed muscularis propria (**a**) and mucosa-submucosa (**b**) layers from the $1\%\text{s}^{-1}$ cyclic experimental results using the loading path of the second cycle of the final full stretch level.

The cyclic data for the $1\%\text{s}^{-1}$ results in each direction and layer were used to identify the viscous and damage parameters. For this, a non-linear least squares approach was employed, where the `lsqcurvefit` function from the Optimization Toolbox in MATLAB was utilised to obtain the parameters separately for the longitudinal and circumferential directions of each layer.

The `lsqcurvefit` function employs the non-linear least squares optimisation technique. This technique is sensitive to the initial starting point given, therefore the initial estimates of the parameters were varied over a range ($1e^{-1} - 1e^{5}$) to attain the correct fit: the set of parameters retained most frequently over the range of initial estimates were regarded as the global minimum.

The evolution equation was solved implicitly for each time step using the backward Euler method. For this, the evolution equation was discretised as follows:

$$\frac{\lambda_e^{m+1} - \lambda_e^m}{\Delta t} = \lambda_e^{m+1} \frac{\lambda^{m+1} - \lambda^m}{\lambda^{m+1} \Delta t} - \frac{4}{3\eta_0} \left(\frac{\partial W_2}{\partial I_{4,e}} \right)^{m+1} (\lambda_e^5)^{m+1} \tag{39}$$

where, m identifies the current time step and Δt is the time step. Then, the equation was rearranged so that it equalled zero and the solution for the unknown λ_e could be found using the `fzero` function in MATLAB, which finds the root of a non-linear function.

The results for the $1\%\text{s}^{-1}$ cyclic data fittings can be found in Figure 49. The model provides a good fit for both layers and directions, capturing well the non-linearity and hysteresis of the experimental results. All the parameter values for the embalmed tissue can be found in Table 27. The next step was to validate the model using experimental data that had not been used in the identification process. For this, the $10\%\text{s}^{-1}$ results for each layer and direction were predicted. The results of this validation can be seen in Figure 50.

Table 27: A complete set of material parameter values for the visco-anisotropic damage model identified in a modularised way for the layers of the embalmed human oesophagus.

		c_1[kPa]	k_1[kPa]	$k_2[-]$	$\eta_m[-]$	$\beta[-]$	η_0	C_2[kPa]	C_3[kPa]	C_4[kPa]
Muscular	$N^{(1)}$	1.32	13.4	6.85	2.16	1.20	2280	0.02	0.01	82.3
	$N^{(2)}$		3.36	0.82	1.29	0.42	3309	0.02	1.14	3.00
Mucosal	$N^{(1)}$	0.86	23.5	24.4	0.09	0.66	824	5.50	0.01	1846
	$N^{(2)}$		3.98	3.85	0.89	0.31	371	12.8	0.01	65.4

For the muscular layer, the model validation in the longitudinal direction, the results of which are depicted in Figure 50a, simulates the general increase in the stiffness seen, but does not ideally predict the non-linearity, steep gradient and hysteresis seen at the higher strain rate. The prediction of the $10\%\text{s}^{-1}$ circumferential results simulates very well the behaviour up until the 1.4 stretch level (Figure 50b), however past this point underestimates the maximum stress for this direction.

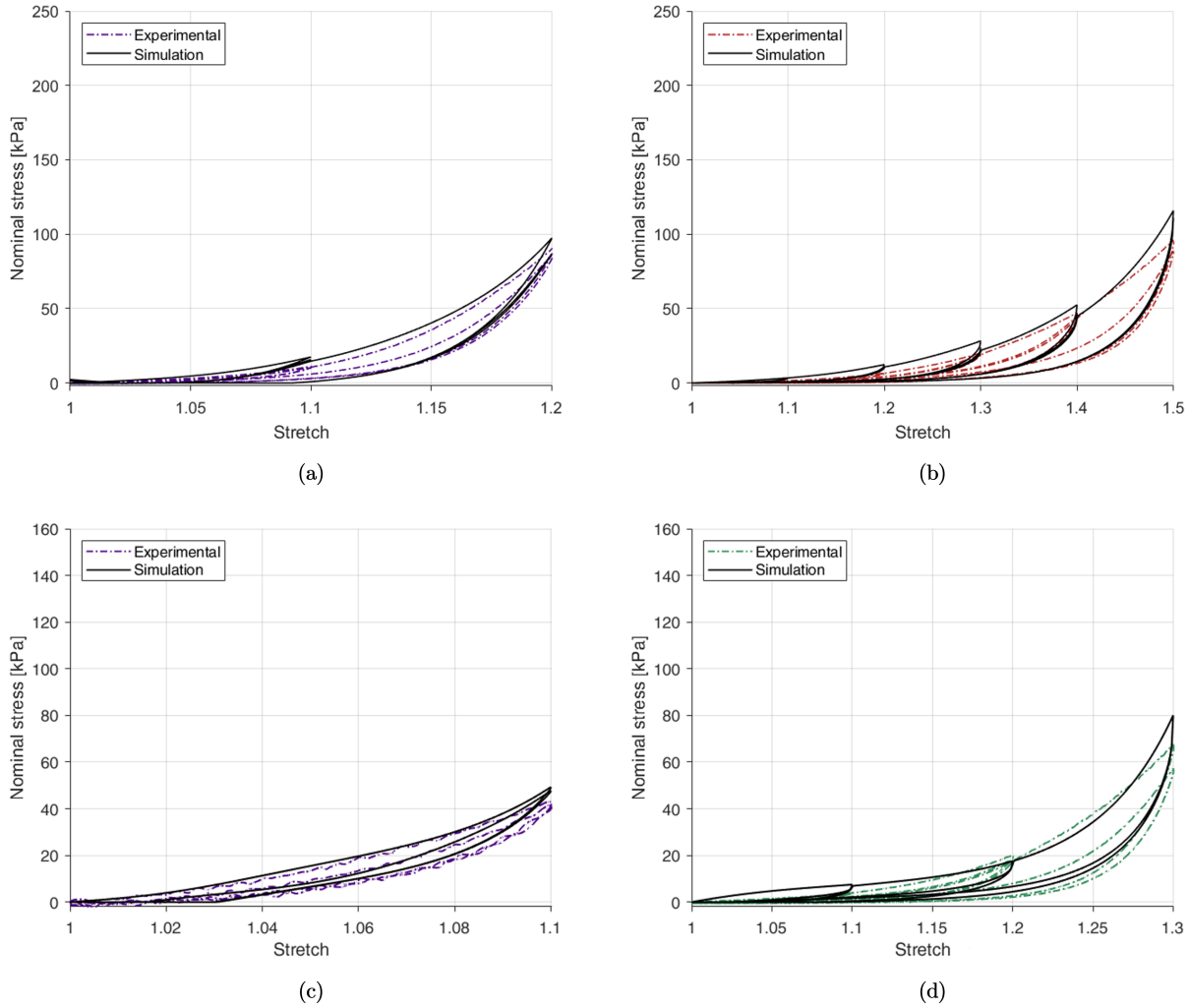

Figure 49. Parameter identification and modelling of the $1\%s^{-1}$ cyclic behaviour of the embalmed muscularis propria layer in the longitudinal (**a**) and circumferential (**b**) directions, and the embalmed mucosa-submucosa layer in the longitudinal (**c**) and circumferential (**d**) directions.

All the model results do not adequately simulate the second cycle of each stretch level. The results overall, however, do well in modelling a good number of features of the stress-stretch response of the embalmed muscularis propria, including permanent deformations, hysteresis, non-linearity, and predict well the effect of the increase in strain rate on the tissue's behaviour, particularly in the circumferential direction.

For the mucosa-submucosa layer, the longitudinal direction results, shown in Figure 50c, predict very well the behaviour of this direction up until approximately 1.045 stretch. However, past this point it can be seen that the model underestimates the change in stiffness experienced at the higher

strain rate, while the hysteresis and difference between the two loading-unloading paths are overestimated compared to the experimental data. Overall, the model performs fairly well in capturing the behaviour of the longitudinal direction, particularly the increased stress-softening between the two cycles seen at the higher strain rate. The circumferential direction validation results, as seen in Figure 50d, are found to overestimate the stiffness and hysteresis seen in the first two stretch levels of the stress-stretch response, but provide a very good prediction of the strain rate dependency at higher stretches, resembling well the non-linearity and hysteresis of the experimental results at these points. The simulations for the circumferential direction, however, underrepresent the hysteresis of the second cycle for each stretch level. That is to say, the model does not ideally capture the estimated preconditioned behaviour of the layer in the circumferential direction.

5.4.2 Fresh tissue

The same identification process was employed for the fresh tissue as for the embalmed tissue, however for the fresh oesophageal layers, the equilibrium stress-stretch results were used to identify the hyperelastic parameters. As outlined in Section 4.4.1, the equilibrium stress-stretch curve was obtained from the stress-relaxation experiments by recording the stress after 15 minutes relaxation and plotting this against the stretch the sample was held at. Figure 51 shows the parameter identification results for the hyperelastic response of the muscularis propria (Figure 51a) and mucosa-submucosa (Figure 51b) layers, which provide a very good fit with the stress-stretch relations in both directions. These hyperelastic parameters were then kept frozen during the identification of the viscous and damage parameters using the cyclic experimental results.

Figure 52 shows the identification of the viscous and damage parameters using the $1\%s^{-1}$ cyclic results, the values of which will be presented later in Section 5.5. The identification of these parameters for the fresh longitudinal muscular layer (Figure 52a) provides a good fit with the experimentally observed response in terms of hysteresis of the first cycle for each stretch level and overall non-linearity, however at around $\lambda = 1.25 - 1.3$, the stress of the model becomes higher than the experimental data. This is thought to be mainly caused by the frozen strain-hardening parameter obtained from the hyperelastic behaviour. The fitting for the circumferential muscularis propria (Figure 52b) presents very well the overall form of the experimental data, particularly at lower strains, however, the identification does not capture the hysteresis of the second cycle, where at higher strains the unloading path of both cycles is in between the loading and unloading path of the second cycle. For the fresh mucosa-submucosa in the longitudinal direction (Figure 52c),

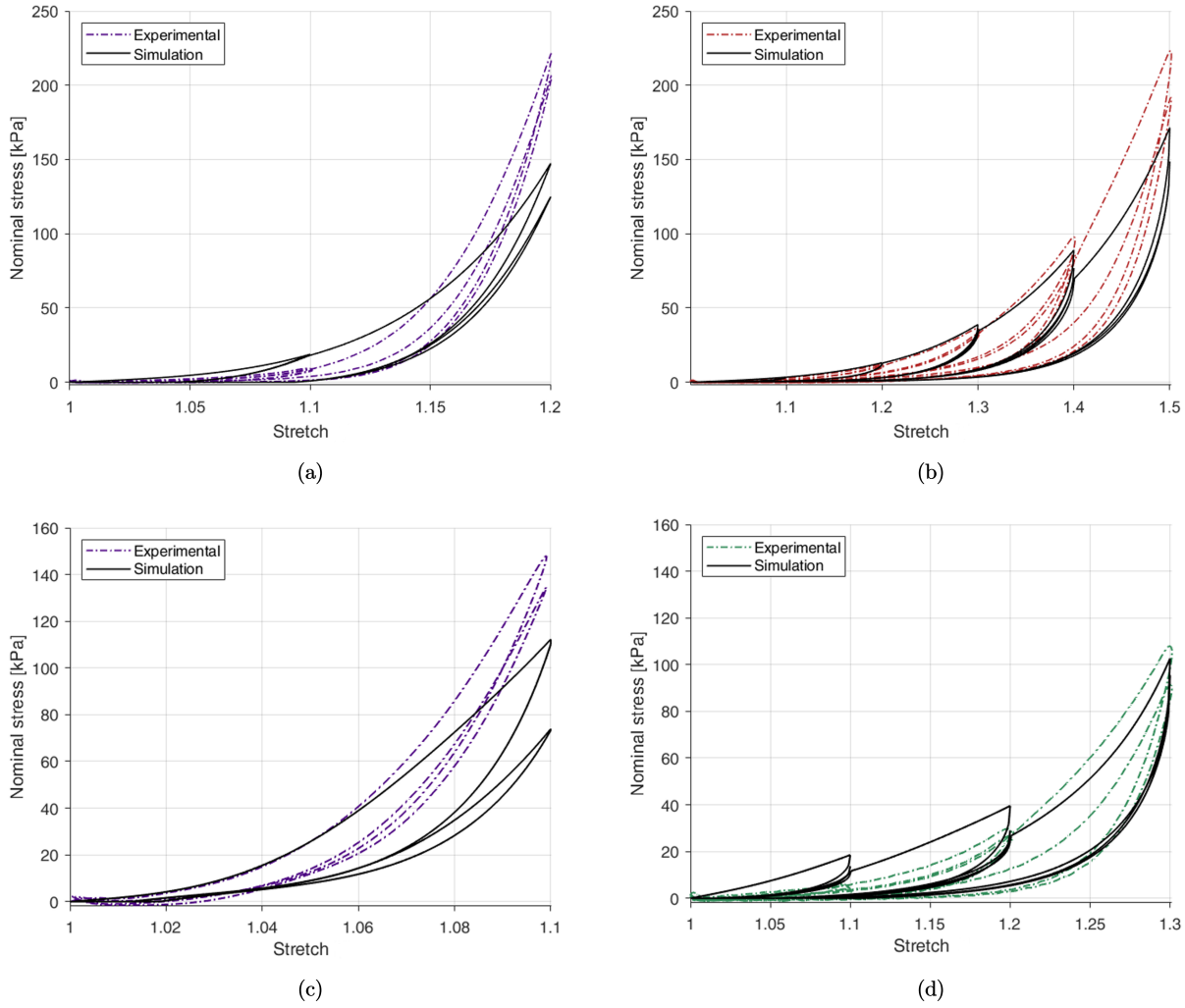

Figure 50. Parameter validation and modelling of the $10\%s^{-1}$ cyclic behaviour of the embalmed muscularis propria layer in the longitudinal (**a**) and circumferential (**b**) directions, and the embalmed mucosa-submucosa layer in the longitudinal (**c**) and circumferential (**d**) directions.

the fitting models well the sharp strain hardening seen in the experimental data and imitates the observed hysteresis of this direction and layer, but slightly overrepresents the stress seen at lower stretches. Similarly to the circumferential muscular layer, the parameter identification for the fresh circumferential mucosal layer (Figure 52d) resembles well the shape of the experimentally observed response, particularly at lower strains, but does not capture the second cycle hysteresis.

Figure 53 shows the model validation for the fresh tissue using the $10\%s^{-1}$ cyclic results. It can be seen that for the predication of the $10\%s^{-1}$ cyclic behaviour of the longitudinal muscularis propria (Figure 53a), the model captures well the response for the 1.3 stretch level cycles, but overesti-

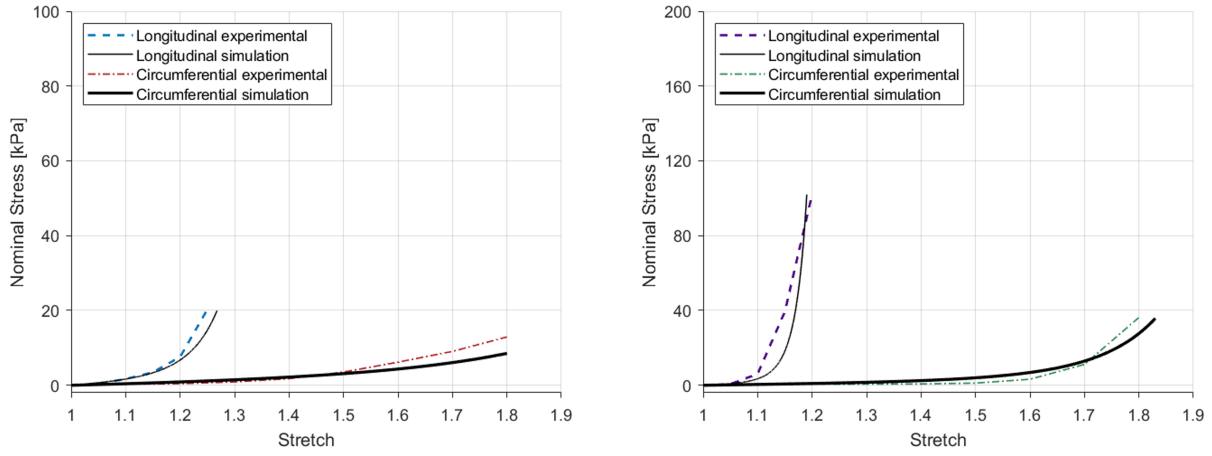

Figure 51. Parameter identification for the hyperelastic behaviour of the fresh muscularis propria layer (**a**) and mucosa-submucosa layer (**b**) in the longitudinal and circumferential directions using the equilibrium stress-stretch response as determined by stress-relaxation experiments.

mates the stress for the 1.1 and 1.2 cycles. The hysteresis of the first 1.2 and 1.3 cycles are also overestimated for this layer and direction. For the circumferential muscular layer (Figure 53b), the model is shown to provide an almost perfect resemblance of the loading and unloading paths of the first cycle of each stretch level, but still fails to capture the hysteresis of the second cycle. The same can be said for the circumferential mucosa-submucosa (Figure 53d). The model predicts well the behaviour of the mucosa-submucosa at $10\%s^{-1}$ in the longitudinal direction up until $\lambda = 1.1$, after this point, however, the stress is slightly underestimated, along with the hysteresis of the first cycle. Overall, the behaviour of the second cycle for each stretch level was not ideally captured by the model.

5.5 Local sensitivity analysis

In this section, a local sensitivity analysis is carried out on the parameters using the fresh tissue model identification results, i.e. the fresh $1\%\text{s}^{-1}$ cyclic results for each layer and direction [355]. For this, each parameter was changed one at a time to firstly 90% of its baseline value and then 110% of its baseline value. The coefficient of determination, R^2, provides a measure of the quality of fit of a model compared to the experimental data. The R^2 value was calculated for the change of each parameter $\pm$ 10% from its baseline, and compared with the original R^2 for the identified parameters. It can be seen in Figure 54 that for all directions and layers, the k_1 and k_2 parame-

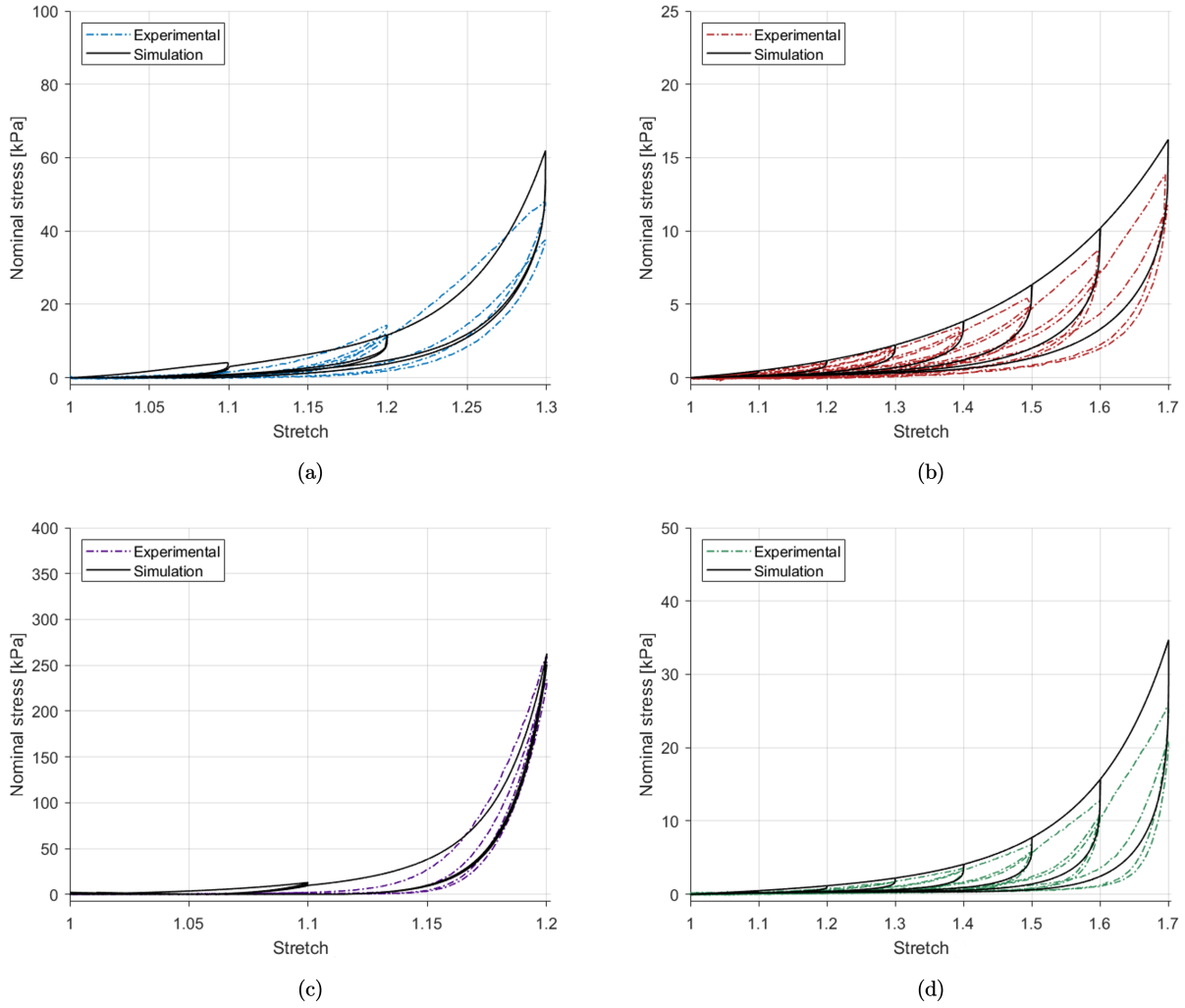

Figure 52. Parameter identification and modelling of the $1\%s^{-1}$ cyclic behaviour of the fresh muscularis propria layer in the longitudinal (**a**) and circumferential (**b**) directions, and the mucosa-submucosa in the longitudinal (**c**) and circumferential (**d**) directions.

ters are the most sensitive as a $\pm 10\%$ change in their value caused the greatest difference in R^2 value. The effect of the changes of these parameters in the most sensitive directions, i.e -10% or +10%, have been shown in Figure 58 in the Appendix. For some parameters, e.g. k_1 and k_2 for the circumferential directions (Figures 54b and 54d), the decrease of its value by 10% increased its R^2. This is due to these parameters being fixed from the hyperelastic identification process and not being the most ideal for modelling the $1\%\text{s}^{-1}$ cyclic results.

Figure 54 highlights how the C_2, C_3 and C_4 parameters were not so influential to the overall quality of fit. It is possible for the Kaliske model just to be based on the C_2 parameter, i.e. $n = 1$ (Section

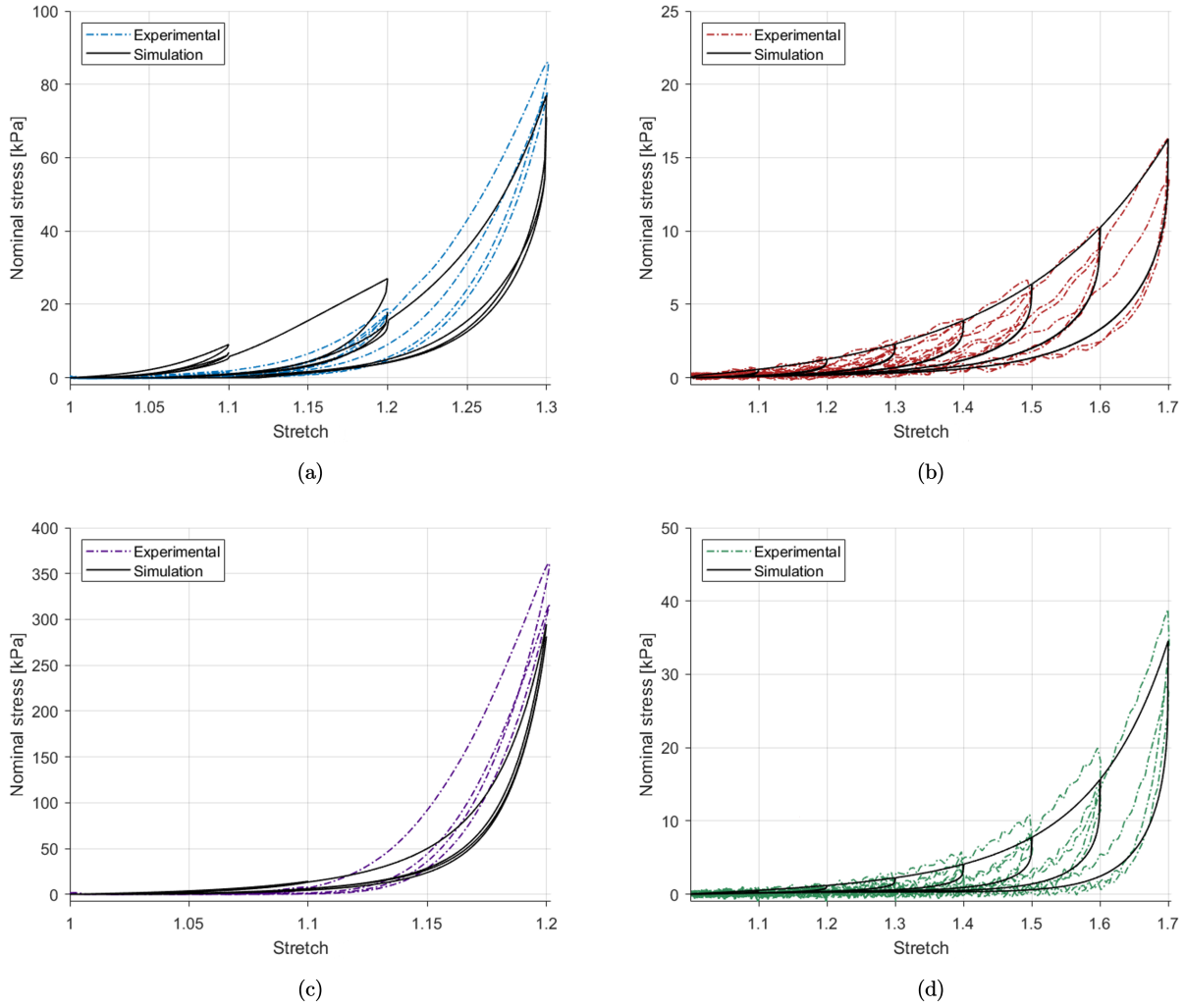

Figure 53. Parameter validation and modelling of the $10\%s^{-1}$ cyclic behaviour of the fresh muscularis propria layer in the longitudinal (**a**) and circumferential (**b**) directions, and the mucosa-submucosa in the longitudinal (**c**) and circumferential (**d**) directions.

5.3). Therefore, the R^2 values were considered for each direction and layer when both $C_3 = 0$ and $C_4 = 0$. The results of the change in R^2 value between the originally identified parameters (baseline) and when only a one parameter Kaliske model is used is shown in Table 28. It can be seen that for the circumferential direction, the C_3 and C_4 parameters make almost no difference to the overall fit of the model, while in the longitudinal direction they do. Therefore, for the fresh tissue, a 9 parameter model will be appointed for the longitudinal direction and a 7 parameter model for circumferential direction. The final set of parameters for the layers of the human oesophagus based on fresh, *ex vivo* experimental results can be found in Table 29.

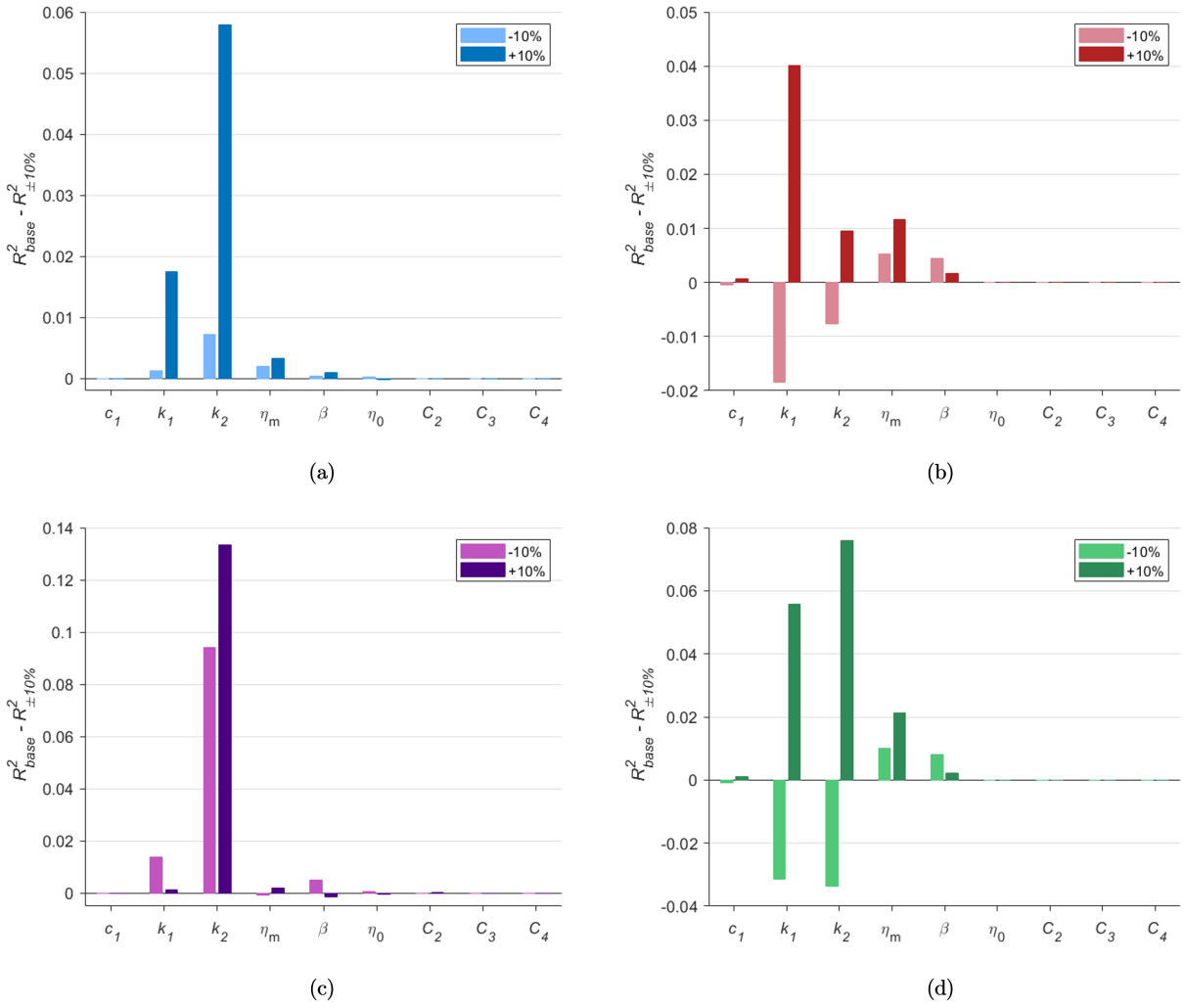

Figure 54. Local sensitivity analysis results for each parameter for the fresh muscularis propria layer in the longitudinal (**a**) and circumferential (**b**) directions, and the mucosa-submucosa in the longitudinal (**c**) and circumferential (**d**) directions.

Table 28: Effect of a one parameter Kaliske [15] SEF on the coefficient of determination, R^2, when modelling the fresh $1\%s^{-1}$ cyclic results for each layer and direction.

		R^2_{base}	$R^2_{C_3=0,C_4=0}$	Difference
Muscularis propria	Longitudinal	0.964204	0.961140	0.003064
	Circumferential	0.919693	0.919693	1.07E-07
Mucosa-submucosa	Longitudinal	0.983976	0.978410	0.005566
	Circumferential	0.899059	0.899058	4.50E-07

Table 29: A complete set of material parameter values for the visco-anisotropic damage model identified in a modularised way for the layers of the fresh human oesophagus.

		c_1[kPa]	k_1[kPa]	$k_2[-]$	$\eta_m[-]$	$\beta[-]$	η_0	C_2[kPa]	C_3[kPa]	C_4[kPa]
Muscular	$N^{(1)}$	0.25	2.74	4.17	0.73	0.19	212	1.54	0.01	76.2
	$N^{(2)}$		0.59	0.10	1.15	0.27	0.87	3.23	–	–
Mucosal	$N^{(1)}$	0.45	2.78	20.8	1.93	0.79	3239	4.69	0.65	48.5
	$N^{(2)}$		0.43	0.40	1.33	0.22	0.43	9.97	–	–

5.6 Conclusion

This chapter outlined the matrix-fibre IVM adapted from Masri et al. [7] used to model the visco-hyperelastic behaviour of the human oesophageal muscular and mucosal layers. The results of the parameter identification and validation show the model to be capable of capturing the non-linearity, stress-softening, permanent set and strain-rate dependency seen in the experimental results. However, across all directions, layers and preservation states, the model struggled to simulate the hysteresis behaviour of the second cycle for each stretch level. Through a local sensitivity analysis, it was found that the hyperelastic parameters k_1 and k_2 had the greatest influence on the overall quality of fit of the model to the experimental data.

Formalin embalming was found to affect the mechanical behaviour of the oesophagus in a number of ways. Experimentally, a greater magnitude of Young's modulus, hysteresis and stress-softening was found for the embalmed tissue compared to the fresh tissue, for which the increase in Young's modulus was greater for the mucosa-submucosa than the muscularis propria. The rupture stretch, however, was higher for the fresh tissue. By considering the hyperelastic parameters of the constitutive model, it can be seen that these agree with the experimental results in that the stiffness parameters increased for the embalmed modelling compared to the fresh, with a greater increase for the mucosal layer than the muscular layer. Interestingly, the strain hardening parameter was also found to increase for the embalmed modelling compared to the fresh modelling, the effect of which was much greater in the circumferential direction than in the longitudinal direction across both layers.

CHAPTER

SIX

6 COMPARISON OF FRESH AND EMBALMED TISSUE

Performing the same cyclic tests on both the fresh and embalmed tissue has allowed for a direct comparison to be made between the two preservation states. In this chapter, the differences and similarities in experimental results and constitutive modelling between the fresh and embalmed oesophageal tissue will be presented.

6.1 Experimental findings

The characteristics as outlined in Section 4.3.2.2 were compared between the embalmed and fresh results for each layer, direction and strain rate using the Mann-Whitney U test. It was found that for almost all of the characteristics considered, their value was statistically higher for the embalmed tissue compared to the fresh tissue, the results of which can be seen in Table 30. The rupture stretch, however, was found to be higher for the fresh tissue compared to embalmed tissue, particularly in regard to the muscularis propria. Table 31 presents the average Young's modulus for the $1\%s^{-1}$ cyclic results for both fresh and embalmed tissue, revealing a greater increase in stiffness caused by embalming for the mucosa-submucosa compared to the muscularis propria.

Table 30: Statistical differences in characteristics between the preservation states (fresh and embalmed) for both the muscularis propria and the mucosa-submucosa. Blank cells indicate no statistical significance between the two groups, and filled cells indicate the preservation state for which the characteristic is statistically higher than for the other preservation state, including the respective p-value.

Layer	**Test cond.**	**Characteristic**										
		E_1	E_2	A_{H1}	A_{H2}	ΔA_H	λ_{rup}	P_{max}	A_{L1}	A_{U1}	A_{L2}	A_{U2}
Muscle	1%/s Long	Embalm $p < 0.000$	Embalm $p < 0.000$	Embalm $p < 0.000$	Embalm $p < 0.000$	Embalm $p < 0.000$		Embalm $p < 0.000$	Embalm $p < 0.000$	Embalm $p < 0.000$	Embalm $p < 0.000$	Embalm $p < 0.000$
	10%/s Long	Embalm $p < 0.000$	Embalm $p < 0.000$	Embalm $p < 0.000$	Embalm $p < 0.000$	Embalm $p < 0.000$	Fresh $p = 0.021$	Embalm $p = 0.006$	Embalm $p < 0.000$	Embalm $p < 0.000$	Embalm $p < 0.000$	Embalm $p < 0.000$
	1%/s Circ	Embalm $p < 0.000$	Embalm $p < 0.000$	Embalm $p < 0.000$	Embalm $p < 0.000$	Embalm $p < 0.000$	Fresh $p < 0.000$	Embalm $p < 0.000$	Embalm $p < 0.000$	Embalm $p < 0.000$	Embalm $p < 0.000$	Embalm $p < 0.000$
	10%/s Circ	Embalm $p < 0.000$	Embalm $p < 0.000$	Embalm $p < 0.000$	Embalm $p < 0.000$	Embalm $p < 0.000$	Fresh $p < 0.000$	Embalm $p < 0.000$	Embalm $p < 0.000$	Embalm $p < 0.000$	Embalm $p < 0.000$	Embalm $p < 0.000$
Mucosa	1%/s Long	Embalm $p < 0.000$	Embalm $p < 0.000$	Embalm $p < 0.000$	Embalm $p < 0.000$	Embalm $p = 0.001$			Embalm $p < 0.000$	Embalm $p < 0.000$	Embalm $p < 0.000$	Embalm $p < 0.000$
	10%/s Long	Embalm $p < 0.000$	Embalm $p < 0.000$	Embalm $p < 0.000$	Embalm $p < 0.000$	Embalm $p = 0.001$			Embalm $p < 0.000$	Embalm $p < 0.000$	Embalm $p < 0.000$	Embalm $p < 0.000$
	1%/s Circ	Embalm $p < 0.000$	Embalm $p < 0.000$	Embalm $p < 0.000$	Embalm $p < 0.000$	Embalm $p < 0.000$	Fresh $p = 0.007$		Embalm $p < 0.000$	Embalm $p < 0.000$	Embalm $p < 0.000$	Embalm $p < 0.000$
	10%/s Circ	Embalm $p < 0.000$	Embalm $p < 0.000$					Embalm $p = 0.001$	Embalm $p < 0.000$	Embalm $p = 0.008$	Embalm $p < 0.000$	

Table 31: Fresh and embalmed tissue's mode and range of Young's modulus, E_1, for each layer and direction from the first loading path of the $1\%s^{-1}$ cyclic results, and p-values for testing if the distribution of Young's moduli followed a Fréchet distribution. The circumferential muscularis propria for the fresh tissue did not follow a Fréchet distribution and was normally distributed, therefore, for this layer, direction and preservation state, the mean, standard deviation and p-value for the Shapiro-Wilk test are presented.

Layer	**Direction**	**Pres. state**	**Mode** [kPa]	**Range** [kPa]	p**-value**
Muscularis propria	Longitudinal	Fresh	7.94	2.67 - 20.7	0.722
		Embalmed	32.2	6.0 - 266	0.367
	Circumferential	Fresh	*Mean:*	*Standard deviation:*	*Normally distributed:*
			3.45	$\pm$ 0.99	0.141
		Embalmed	16.1	3.7 - 81.5	0.808
Mucosa-submucosa	Longitudinal	Fresh	8.36	2.57 - 24.8	0.926
		Embalmed	93.5	25.8 - 331	0.247
	Circumferential	Fresh	1.89	0.83 - 3.52	0.858
		Embalmed	38.4	21.2 - 47.5	0.783

Figure 55 shows that when the axis are scaled accordingly, the anisotropic properties within the two preservation states are similar. The anisotropy of stiffness and non-linearity of each direction, as well as the degree of hysteresis and stress-softening, remain relatively consistent despite the change in magnitude of these phenomena between the embalmed and fresh tissue, suggesting that, apart from rupture stretch, embalming proportionally increases the mechanical properties of oesophageal tissue. It should be noted that due to the limit of the sensor and the softness of the preservation state, there was more noise at lower stretches of the fresh tissue compared to the embalmed tissue, particularly for the mucosa-submucosa layer in the circumferential direction (Figure 55c).

The differences in permanent set were also analysed between the fresh and the embalmed tissue results. Figure 56 shows a comparison of the permanent deformation at $1\%s^{-1}$ between the two preservation states. It can be seen that the degree of damage of the fresh circumferential muscular layer was almost identical to that of the embalmed, while the fresh longitudinal muscle, longitudinal mucosa and circumferential mucosa all had greater permanent set than their embalmed equivalents.

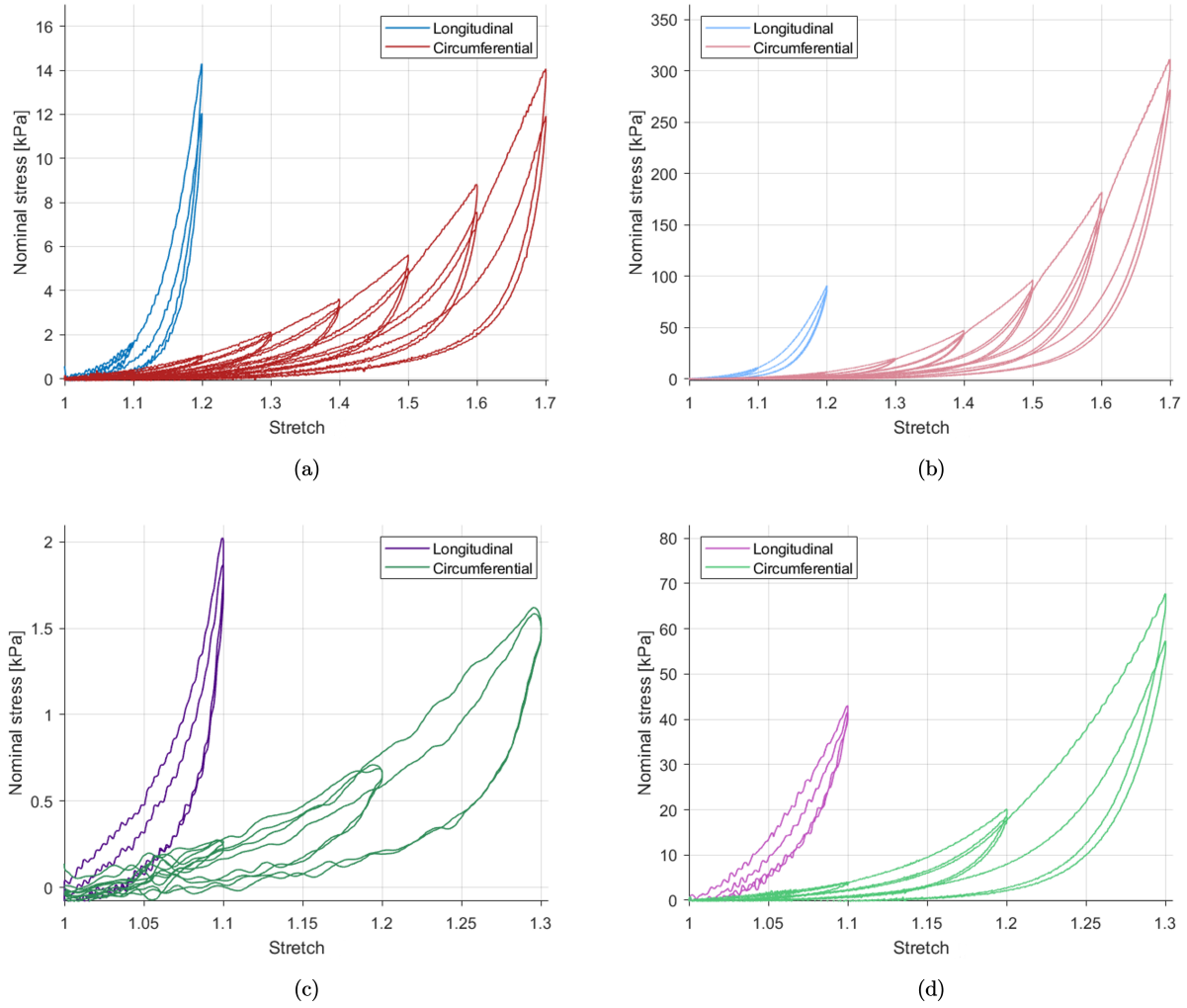

Figure 55. Comparing the fresh (**a**) and embalmed (**b**) $1\%s^{-1}$ cyclic results of the muscular layer, and the fresh (**c**) and embalmed (**d**) $1\%s^{-1}$ cyclic results of the mucosa-submucosa layer.

6.2 Constitutive modelling

Figure 57 shows the magnitude change of the fibre stiffness parameter, k_1, and the fibre strain hardening parameter, k_2, from the fresh to embalmed state. This reveals that the fibre stiffness parameter increased for both the muscular and mucosal layers, however that the increase was greater for the mucosa-submucosa than the muscularis propria across both directions. In terms of the strain hardening parameter, this increased from the fresh to embalmed tissue, however the increase was much greater for the circumferential direction of both layers compared to the longitudinal direction.

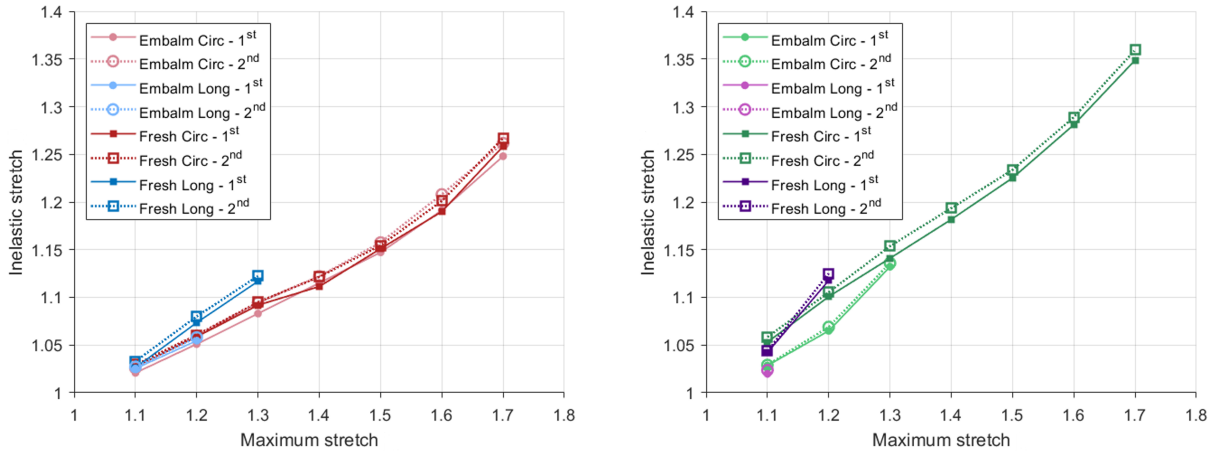

Figure 56. Permanent set of the fresh and embalmed muscularis propria (**a**) and mucosa-submucosa (**b**) at $1\%s^{-1}$, including the differences between the first and second cycles.

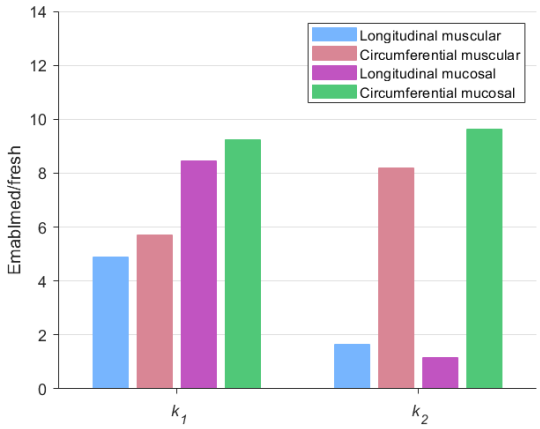

Figure 57. Change in k_1 and k_2 material parameters from the fresh to embalmed tissue for each direction and layer.

6.3 Conclusion

Formalin embalming was found to affect the mechanical behaviour of the oesophagus in a number of ways. Experimentally, a greater magnitude of Young's modulus, hysteresis and stress-softening was found for the embalmed tissue compared to the fresh tissue, for which the increase in Young's modulus was greater for the mucosa-submucosa than the muscularis propria. The rupture stretch, however, was higher for the fresh tissue. By considering the hyperelastic parameters of the constitutive model, it can be seen that these agree with the experimental results in that the stiffness parameters increased for the embalmed modelling compared to the fresh, with a greater increase

for the mucosal layer than the muscular layer. Interestingly, the strain hardening parameter was also found to increase for the embalmed modelling compared to the fresh modelling, the effect of which was much greater in the circumferential direction than in the longitudinal direction across both layers.

CHAPTER

SEVEN

7 DISCUSSION

In this chapter, the experimental methods and findings of this thesis will be discussed, as well as the constitutive modelling of the human oesophageal layers. Furthermore, the differences between the mechanical behaviour of the fresh and embalmed oesophagi will be considered.

7.1 Experimentation

7.1.1 Oesophageal mechanical behaviour and physiological perspectives

The equilibrium stress-stretch behaviour and the cyclic results revealed the longitudinal direction to be stiffer than the circumferential direction for both layers of the oesophagus. The circumferential direction also ruptured at a much higher strain than the longitudinal direction for both layers. These may be related to the oesophagus' physiological function where more compliance is required in the circumferential direction due to distension caused by varying sizes of fluid bolus, while the stiffness in the longitudinal direction supports the function of the longitudinal muscle fibres in carrying out longitudinal shortening during peristalsis, which reduces the work needed by the circular muscle fibres to move the bolus [334]. Microstructurally, there was greater collagen in the longitudinal direction compared to the circumferential direction and greater elastin in the circumferential direction than in the longitudinal direction for both the mucosal and muscular layers. This histological distribution may explain the anisotropic behaviour of the tissue, as collagen is associated with withstanding tensile loads [371] and elastin allows soft tissues to undergo repetitive loading [372]. The layer-dependent differences also correlate with the histological findings and the role that collagen plays in the mechanical behaviour of soft tissues [373]. Furthermore, the non-linear response of the tissue layers is associated with the function of the oesophagus in that compliance is required at low stretches to allow for the passage of the bolus, while stiffening occurs at higher stretches to impede over-dilatation. It is thought that the muscularis propria supports the majority of the load at low intraluminal pressures, while the mucosa-submucosa stiffens quickly when the diameter of the oesophagus is approximately double its undeformed size [45,51]. This is inline with the fresh cyclic results here in that in the circumferential direction, the mucosa-submucosa strain hardens at a higher stretch than the muscular layer, as well as, at high stretches, is stiffer than the muscular layer. *In vivo*, the mucosa-submucosa layer is folded and so would only undergo the circumferential loads experienced in the tension experiments carried out here once the layer was distended so far that it unfolded. At this point, the higher stiffness of the mucosa-submucosa would take the load and prevent over-dilatation of the organ. Future testing of the intact

layers of the human oesophagus would help to understand the contribution of the individual layers on the overall behaviour of the tissue wall.

It was once assumed that the no-load state of human tissues was also its stress-free state. However, it was determined that since unloaded, ring-like cross-sectional segments of the arterial wall sprung open upon a radial cut, there must exist residual stresses and strains within arteries [183,374–376]. Since then, residual strains and stresses have been found in different tissues of the human body, including aortic valve leaflets [185] and the ureter [377]. Outside of this work, however, only the residual strains present in rabbit [67, 68, 212], rat [52, 53, 214], porcine [13, 66] and guinea pig [57, 58, 216] oesophagi have been determined. Gregersen et al. [216] found that the inclusion of residual strains within the guinea pig oesophagus provided more accurate strain measures at its luminal surface, while Holzapfel et al. [352] found that residual stresses in arteries gave way to a more homogenised stress distribution throughout the arterial wall. The zero-stress state analysis in this work showed there to be circumferential residual strains and longitudinal prestretch in the oesophagus' no-load state [212], therefore, these should be considered when conducting FE modelling of the human oesophagus [143]. In this study, however, only the residual strains of the oesophagus from Cadaver 7 were considered. Therefore, for a more robust quantification of the human oesophageal residual strains, more specimens should be taken into account.

7.1.2 Comparison with other experimental studies

The main *ex vivo* tensile studies of the human oesophagus were conducted on the intact tissue wall [47, 48], for which Egorov et al. [47] only considered the behaviour in the longitudinal direction. Vanags et al. [48], who studied the direction-dependent behaviour of the organ, found the mechanical properties of the human oesophagus to be anisotropic, following the same relationship as the findings of this study: the stress and Young's modulus were greater in the longitudinal direction, while the strain the tissue could be subjected to before rupture was higher in the circumferential direction. As mentioned in Section 1, Vanags and coworkers [48] also studied the effect of age on the mechanical properties of the human oesophagus [48]. From their findings, it could be expected that the Young's moduli for the oesophagus determined in this thesis might be greater than for younger oesophageal tissue due to the high ages of the cadaveric tissue tested (Table 16).

Through the use of vibrational OCE together with OCT, Wang et al. [97] found the lamina muscularis mucosae, a thin muscle layer in the mucosa (60.28 kPa), to be less stiff than the submucosa

(205.25 kPa) or lamina propria (115.64 kPa), which agrees with the findings of this work where the more muscular and less collagenous layer, the lower the stiffness. They attributed the greater stiffness of the submucosa and lamina propria to be due to the greater collagen content of these sublayers. However, despite the human oesophagi being retrieved from Thiel-embalmed cadavers [124], the Young's moduli established by Wang et al. [97] are substantially higher than those derived from both the formalin-embalmed and fresh mucosa-submucosa layer in this work. This could be due to differences in the scales in which the mechanical behaviour of the oesophagus was investigated [378]: the approach of Wang and coworkers [97] that measures elasticity at a micrometre scale (strains of less than 0.067%) has the potential to be very useful for clinical diagnosis and staging of oesophageal cancer, but does not seem to represent the material response of the oesophagus at larger length scales which is necessary for applications such as FE models for medical device design [44].

Sommer et al. [70] studied the mechanical behaviour of ovine oesophagi and carried out tests with a variety of loading modes. They found the inflation-extension behaviour of ovine oesophagi with their layers intact to be direction-dependent, with the longitudinal direction being stiffer than the circumferential direction. This finding agrees with the other inflation-extension tests conducted on intact oesophagi from rats [75] and rabbits [68], as well as the anisotropic results of this study. Comparing the layer-dependent uniaxial results of ovine oesophagi from Sommer et al. [70] to those presented here, there was similar maximum stress in the longitudinal direction across both layers, and a similar strain hardening for the muscular layer. However, for the mucosal layer in the longitudinal direction, strain hardening occurred at 1.4 stretch compared to around 1.1 stretch in this work. The circumferential direction of both layers proved to be stiffer for ovine tissue compared to human tissue despite conducting their tests at a slower strain rate: the maximum stress found for ovine oesophagus in this direction was in the range of 200 – 350 kPa, while for the fresh tissue in this study it was around 10 – 40 kPa. Similar layer-dependent, uniaxial tensile tests were carried out by Yang et al. [60] on porcine oesophagi, for which the stress in both directions was substantially higher than in the current study. While they found the longitudinal direction to be stiffer than the circumferential direction, strain hardening across both layers occurred later in the longitudinal direction and earlier in circumferential direction compared to the results here, suggesting porcine oesophageal tissue to be less direction-dependent than human tissue. These differences could be due to differences in the species' digestive systems [87], as well as slight variations in the experimental technique and setup [379].

Layer-dependent distension tests of animal oesophagi performed *ex vivo* were found to agree with the results of this thesis in that, particularly at higher strains, the mucosa-submucosa was stiffer than the muscularis propria [52,55,66,67,75,214]. This, however, differs to the findings of Frøkjær et al. [44] who performed *in vivo* distension tests on healthy humans. They found the stiffness of the oesophagus to be lowest at the inner, mucosal surface across all strains. This discrepancy is thought to be due to the fact that mucosal layer is folded *in vivo* and so most of the stiffness during the tests would be provided by the muscular layer [44]. Therefore, the results of the current study can be used to develop material models of the oesophagus which include the discrete behaviour of the layers, while the findings of Frøkjær and coworkers [44] would be ideal for contributing towards the validation of FE models of the human organ [131]. While it may be expected that, due to the high ages of cadavers tested in this study [48] and the *ex vivo* test condition [305], the stiffness of the fresh oesophageal tissue tested here would be a lot greater than that found by Frøkjær et al. [44], this was not the case, with the Young's moduli being well within the same order of magnitude (1.9 – 3.5 vs. 2.5 – 5 kPa, respectively). Despite the similarities in Young's moduli between *in vivo* oesophageal findings and the uniaxial tensile results presented here, the distension behaviour of the human oesophagus is of great interest due to it being a tubular organ undergoing distensions *in vivo*. Therefore, future experiments of inflation-extension tests of the separated layers of the human oesophagus, as well as the intact wall, should be performed in order to study, quantify and model its material behaviour in more a physiological-like way. Furthermore, an increase in individual oesophagi tested and the testing of younger tissue would provide a more thorough understanding of the mechanical response of the human oesophagus across the wider population.

A variety of viscoelastic and history-dependent behaviours were observed within the cyclic experimental results. Stress-softening was seen for all trials, wherein the stiffness of the second cycle for a single stretch level was much lower than that of the first cycle. Hysteresis was also found to decrease for the second cycle compared to the first, with the second cycle representing approximately the behaviour of the tissue if the sample had been preconditioned. As outlined in the Section 1, Liao et al. [58] established that the majority of softening of guinea pig oesophagi was due to irreversible structural changes dependent on the previous maximum stretch, and only partly due to the time-dependent softening wherein the viscoelasticity of the tissue causes reversible softening dependent on the strain rate. This may not be the case with the human oesophagus, for which the dissipated energy of the first and second cycles were found to statistically increase with an increase in strain rate for several test conditions (Table 22), suggesting that time-dependent soften-

ing may have a greater impact on oesophagi from humans compared to guinea pig. This is further supported by the permanent set also increasing as strain rate increased. However, the influence of strain rate on the permanent set may imply: 1) that the strain rate affects the degree to which the tissue is permanently damaged, or 2) that the "permanent deformations" are not so permanent and are mainly dependent on the rate at which the sample is loaded. Future work looking into the recovery response of the human oesophagus after loading at various strain rates should be carried out to clarify this mechanism.

The quantitative histological results for collagen content presented in Figure 31a agree mostly with those established by Stavropoulou et al. [67] for the rabbit oesophagus, in which collagen was greater in the longitudinal direction than the circumferential direction across both layers, and there was more collagen overall in the mucosa-submucosa compared to the muscularis propria. Similar percentage contents were also determined in each direction and layer apart from in the longitudinal direction of the mucosa-submucosa layer for which there was found to be more collagen for the human oesophagus (35%) compared to rabbit (20%). However, in terms of elastin content, Stavropoulou and co-workers [67] determined there to be more in the longitudinal directions than in the circumferential directions across both layers, contrary to the quantitative results established here (Figure 31b). The findings here agree more with the mechanical behaviour of the oesophagus in that stressibility was greater in the circumferential direction than the longitudinal direction. Overall, Stavropoulou et al. [67] found the elastin content to be greater in the mucosal layer compared to the muscular layer, which agrees with the findings of this thesis.

7.1.3 Variation in experimental results and statistical analysis

Variation when testing human soft tissues is prevalent, with many variables potentially affecting their mechanical properties and therefore the mechanical data collected. These include, but are not exclusive to, age, sex, and health of the patient, as well as experimental variables such as time since explantation, sample thickness due to variation in biological composition throughout the tissue, temperature and moisture of the samples, and storage technique. In the current study, variability in terms of rupture stretch, rupture stress and stiffness were observed between different tests of the same direction and strain rate. Some of these differences may be attributed to the variations seen in sample dimensions. Natural variations in thickness and composition were present throughout both tissue layers, leading to the range of sample thicknesses seen in Tables 19 and 26. The differences amongst the width of the samples are attributed to the human error associated with cutting samples

by hand. Human error was also potentially present in the measuring of the width and thickness of the samples. To reduce the risk of this, measurements were taken by a single person, and to reduce any effect, three separate measurements were taken per dimension along the sample and an average was used. As a significant correlation was found for only one test condition ($10\%s^{-1}$ longitudinal mucosa-submucosa), for which there was a medium strength correlation, time since dissection has not been considered as a major factor affecting the dispersion of the results (Table 24). The variability is thought to be most influenced by the intra and inter-cadaver heterogeneity. However, due to the low number of samples per test condition from a statistical point of view, the sample size might not be large enough to properly establish a correlation between mechanical properties and time since dissection. This may also be the case for the comparison of characteristics between the different strain rates, layers, directions and preservation states. Therefore, a greater sample size in terms of oesophageal specimens as well as individual samples would increase the overall robustness of the statistical analysis.

7.2 Modelling

Inspired by Masri et al. [7], the constitutive formulation here was adapted to the oesophagus with two families of fibres and the viscoelasticity in terms of I_4 to model its experimentally-observed strain rate-dependent behaviour. This was represented fairly well by the model, where in which an increase in strain rate resulted in an increase in hysteresis and stiffness. However, these components were not perfectly captured with the stress for the $10\%s^{-1}$ prediction being either overestimated at lower stretches (Figures 50d and 53a) or underestimated at higher stretches (Figures 50b, 50c and 53c) or both of these (Figure 50a). Additionally. in general, the hysteresis of the second cycle was less for the model compared to the experimental data, and in some cases the hysteresis of the second cycle was non-existent (Figures 53b and 53d). Panda and Buist [380] proposed a new model to capture the visco-hyperelastic behaviour of soft tissues also based on the work of Huber and Tsakmakis [358]. They compared three different forms of the IVM model, including with constant (linear) viscosity, Haupt viscosity [381] and their own non-linear viscosity. For modelling cyclic experimental data of porcine stomach tissue [229], Panda and Buist's [380] own non-linear viscosity function was best able to capture the behaviour of the second loading cycle; something that was not ideally captured in the model of this thesis. Therefore, to improve the accuracy of the model to be able to simulate the second cycle response of the human oesophagus, as well as to potentially improve the modelling of its strain rate-dependent behaviour, non-linear viscosity should be considered in the future. As non-linear viscosity will require additional parameters, to

keep the parameters to a minimum, the use of a one parameter Kaliske model could be investigated to see if, along with the non-linear viscosity, it provided a sufficient simulation, especially as the C_3 and C_4 parameters were shown to be almost redundant in the circumferential direction (Table 28).

The function used here to capture the history-dependent behaviour of the oesophagus was that developed by Rebouah et al [362, 363]. Originally proposed for polymers [362] but later adapted to soft tissues [363], the evolution function in terms of I_4 considers a macromolecular network of fibres and tracks the previous maximum strain of them, capturing both stress-softening and permanent set. Other notable models able to capture the stress-softening of soft biological tissues are those by Pena and Doblaré [382] who employed a pseudoelastic approach and Elías-Zúñiga and Rodríguez [383] who proposed a non-monotonous phenomenological continuum damage model. However, these either did not consider permanent set [382] or were not suitable for anisotropic materials [383]. Mayer et al. [384] developed a constitutive model able to capture both stress-softening and permanent set for anisotropic arterial tissue by applying a continuum damage mechanics approach to the former and internal variables to account for the latter. They considered inelastic phenomena in both the isotropic matrix and anisotropic fibres, which could be attempted here to establish if softening of the matrix as well as the fibres would provide a better fit with the experimental data. However, as the model of Rebouah and Chagnon [363] captured well the softening between the loading and unloading curves and the permanent set of the tissue without the inclusion of matrix inelastic behaviour, it is posited that the implementation of non-linear viscosity would have more of an impact on the improving the fit of the model to the cyclic data.

The non-linearity of the oesophageal layers was captured very well by the hyperelastic model, for which a physically-driven classic Holzapfel model was used [352]. Yang et al. [60], however, required a modified version of this Holzapfel SEF to model the results of uniaxial tensile tests on porcine oesophageal layers, as previously mentioned in Section 5.1. This could be due to the layers of porcine oesophagi being less non-linear than human tissue, especially in the longitudinal direction. An extension to the classic Holzapfel model developed by Gasser et al. [353] takes into account the dispersion of the fibres within a material. This method, however, was not adopted here due to 1) the histological findings showing that the collagen fibres predominantly reside in the longitudinal and circumferential directions and 2) the lack of means to establish the fibre dispersion experimentally. Although some degree of fibre dispersion is inherent to biological tissues, the classic Holzapfel model is more suited to the type of histological data collected in this study.

In addition, if a dispersion model were to be implemented without any experimentally determined fibre dispersion data, a phenomenological fitting of the dispersion parameter would be required, which would result only in increasing the number of parameters of the model without providing any insight into the physical composition of the layer [160]. Overall, the parameters of the classic Holzapfel model correlated well with the histological findings of the study in that the fibre stiffness parameter was higher for the longitudinal direction than the circumferential direction across both preservation states and layers. However, as the ratio between fibre stiffness parameter in the two directions is greater than the ratio of collagen fibre contents, this could suggest that the collagen fibres in the circumferential direction are wavier than the longitudinal direction so that, while still present in the histological findings, they require a greater stretch compared to the longitudinal direction to activate [366]. This is further supported by the later strain-hardening in the circumferential direction.

The $10\%s^{-1}$ cyclic results were used to validate the model which produced a reasonable prediction of the behaviour of the oesophagus at the higher strain rate. However, uniaxial experiments conducted at an angle and not just along the principal directions would allow for further validation of the model. Additionally, to determine the ability of the layer-dependent model to predict the overall response of the oesophageal wall, a FE model of the layers of the intact oesophageal wall, including the mucosal folds, could be validated against uniaxial tensile tests of the intact wall [385]. Moreover, to evaluate the strain rate-dependent aspect of the model, it could be validated against experiments carried out at another strain rate, for instance $0.1\%s^{-1}$. Furthermore, only the uniaxial tension loading mode was used for parameter identification here. To increase the ability of the model to predict *in vivo* stress-strain relations, parameter identification and validation using data from experiments carried out in loading modes closer to that which the oesophagus undergoes *in vivo*, such as biaxial tension and inflation-extension, could be conducted. These aspects should be consider for future work on modelling the passive mechanical behaviour of the layers of the human oesophagus.

The model assumed homogeneity within each of the oesophageal layers, while in reality these layers are made of their own sublayers (Section 3.1). However, due to how difficult it would be to separate these without significant damage, it is unlikely that one would be able to model the discrete behaviour of these sublayers based on *ex vivo* experimental data. Furthermore, discretisation of the oesophageal wall into its two main layers may be adequate for the majority of macroscale applications. Moreover, a statistical approach prior to modelling was employed to extract the most

representative curve for each test condition. This is sufficient to provide an average response of the main oesophageal layers, however soft biological tissues possess a certain variability, and therefore it would be of value to incorporate this into the model by considering a stochastic approach in the future [386].

7.3 Comparison of fresh and embalmed tissue

7.3.1 Experimentation

The results presented here regarding the effects of embalming on the human oesophagus may be used by medical students to adjust their expectations when performing practise surgery on cadavers fixed in formalin. It can be seen from the results that the type of non-linear behaviour is comparable, particularly in regard to the oesophageal layers' anisotropic relationship and point of strain-hardening, however that the degree of stiffness is different. When cutting into embalmed tissue, for instance, the initial stiffness would be approximately 3–5 times higher for the muscular layer compared to fresh tissue and 9–11 times higher for the mucosa-submucosa layer. Furthermore, the embalmed tissue may rupture at a lower strain as well, particularly the muscular layer. This increase in stiffness caused by embalming agrees with the finding of Hohmann et al. [126], implying that the cross-links formed by formalin may be more predominant in affecting the mechanical properties of human soft tissues than the partial denaturing of collagen [127]. The fact that the stiffness increase between the fresh and embalmed tissue is greater for the more collagen-rich layer, the mucosa-submucosa, further supports the theory that the formation of collagen cross-links causes the difference in stiffness observed between the two preservation states. It should be noted that the histological results of this work were obtained from embalmed oesophagi rather than fresh tissue. However, as it is believed that formalin embalming mainly affects the cross-links of the tissue, we do not expect there to be much of a difference in collagen or elastin content estimates caused by the preservation state, but this could be investigated in the future.

When comparing the same stretch levels for each layer and preservation state at $1\%s^{-1}$ (Figure 55), it can be seen that the behaviour of the oesophageal layers in terms of stiffness, hysteresis and stress-softening of the longitudinal and circumferential directions is very similar between the two states, with the main difference being the vast change in magnitude of these mechanical properties (Table 30). Now, the investigation of the influence of collagen cross-links is becoming increasingly popular within biomechanical literature [387–391], with models being developed recently that include collagen cross-link density and orientation [155, 392]. It is known that an

increase in cross-links leads to an increase in tensile strength [393–395], however, does the relationship between embalmed and fresh tissue seen in this study suggest that the density of collagen cross-links has a much greater influence on the mechanical behaviour of soft tissues than was once thought, including its viscoelastic and stress-softening properties? If the behaviour between the two directions is the same, with just the magnitude of properties increasing with increasing cross-links caused by embalming, could the properties that are seen, even in the fresh tissue, be mainly influenced by the orientation and density of the cross-links? Furthermore, the degree by which the permanent set decreased from the fresh tissue to the embalmed tissue was correlated with the amount of collagen in each layer and direction. The more collagen in a specific layer and direction, the greater the decrease in permanent deformations of the embalmed tissue compared to the fresh tissue. Could this mean that an increase in collagen cross-links causes a resistance to permanent set? Mass spectrometry should be conducted to contrast the collagen cross-link density between fresh and embalmed tissue to determine more concretely if this is the main reason for the difference in properties seen [389].

7.3.2 Modelling

The constitutive model, defined in Section 5.2, was able to capture the behaviour of both the embalmed and fresh oesophageal tissue results. This, along with the fact that the ratio between the fibre stiffness parameter (k_1) of the fresh and embalmed preservation states remains relatively consistent across each direction for a single layer, 1:5–6 for the muscular layer and 1:9 for the mucosal layer, shows that, while the magnitude of the mechanical properties are different, formalin-embalmed oesophageal tissue presents the "signature" stress-strain response of fresh tissue. Therefore, as embalmed human tissue is often more readily available than fresh tissue, experimental data from embalmed tissue can be used to develop constitutive models for a specific human organ. The formulation of which can then be applied to fresh human experimental findings once data becomes available to provide more physiologically-relevant material parameters.

The ratio of parameters between embalmed and fresh tissue presented in Figure 57 shows that the mucosa-submucosa was more influenced in regard to increase in stiffness than the muscularis propria across both directions. This could be due to the mucosal layer having a greater increase in collagen cross-links caused by embalming compared to the muscular layer as the former has a greater collagen content overall. To further investigate this theory, a cross-link model could be used to model the difference between the two preservation states [155]. Furthermore, the strain-hardening

in the circumferential direction was much more influenced by embalming than the longitudinal direction across both layers. This could be due to the cross-links forming between the more wavy collagen fibres in the circumferential direction, as hypothesised in Section 7.2, and thus causing an earlier strain-hardening in embalmed tissue than is usually the case with fresh tissue.

CHAPTER

EIGHT

8 SUMMARY AND OUTLOOK

In this thesis, the passive mechanical behaviour of the human oesophagus was investigated in regard to its layer, direction and time-dependent response. The findings show the oesophagus possesses discrete properties in each of its layers, and displays highly anisotropic, non-linear behaviour. The tissue layers are also viscoelastic with an increase in strain rate resulting in an increase in stiffness and hysteresis. The complex behaviour of the human oeosphageal layers was modelled using a transversely isotropic, visco-hyperelastic matrix-fibre model that was also able to capture the history-dependent behaviour of the materials.

The unforseen restrictions on the anatomy laboratory caused by the COVID-19 pandemic meant that embalmed human oesophageal tissue was studied as well as fresh tissue. Due to the similarities seen between the fresh and embalmed results, the consistent increase in stiffness of the muscular and mucosal layers across both directions, and the fact that embalmed human tissue is often more readily available and has fewer constraints than fresh tissue, embalmed tissue is proposed as a preservation state in which the "signature" stress-strain curve of a human soft tissue can be established and, as such, an organ-specific model be developed. Fresh tissue results are then recommended to be used to determine physiologically-relevant parameters, with *in vivo* experimental findings used for model validation.

There are many diseases which affect the mechanical properties of the GI organs and, thus, their functions. There are also numerous medical devices that interact with the GI tract and surgical techniques whose efficacy are dependent on the tissues' biomechanical characteristics. To be able to study these characteristics, without wastage of animal or human biological test specimens, accurate computational models are needed. Firstly, however, to create these models, experimental data, ideally from human tissue, is essential. The results of this thesis present a novel understanding of the layer-dependent mechanical behaviour of the human oesophagus. The findings presented here are key in comprehending the relationship between the organ's material properties and physiological function, while also providing experimental data that can be used for a multitude of biomedical engineering applications, such as validating the mechanical properties of tissue engineered oesophagi, and FE modelling the behaviour of the tissue layers to help improve the design of oesophageal stents.

In light of the findings of the research presented in this thesis, the suggestions for future work include:

- Consider non-linear viscosity in the model to better capture the hysteresis of the experimental data.
- More strain rates to fully characterise and model oesophageal tissue's strain-rate dependency, including investigation of the recovery response of the tissue as a function of strain rate.
- Finite element modelling of the intact wall using layered model and compare to experimental behaviour of the intact wall to validate.
- Biaxial tensile and inflation-extension testing of human oesophagus to determine parameters under more physiologically-relevant loading regimes and use to increase robustness of parameter identification.
- Quantify and compare the collagen cross-links of embalmed and fresh tissue to determine if they are repsonsible for the changes in the mechanical behaviour seen.
- Model both embalmed and fresh tissue results simultaneously using a cross-link model where only the cross-link parameters change.
- Zero-stress state analysis of more human oesophageal specimens to increase robustness of residual strain quantification.

8.1 Contributions to the field

A number of scientific journal publications regarding the research of this thesis have been formed and are either published or in progress; a summary of which can be found in Table 32.

Table 32: Publications from the research outlined in this thesis.

Authors	Title	Publication	Date online
Ciara Durcan, Mokarram Hossain, Grégory Chagnon, Djordje Perić, Lara Bsiesy, Georges Karam, Edouard Girard	Experimental investigations of the human oesophagus: anisotropic properties of the embalmed muscular layer under large deformation	Biomechanics and Modeling in Mechanobiology, 21:1169–1186 [137]	27/04/2022
Ciara Durcan, Mokarram Hossain, Grégory Chagnon, Djordje Perić, Georges Karam, Lara Bsiesy, Edouard Girard	Experimental investigations of the human oesophagus: anisotropic properties of the embalmed mucosa–submucosa layer under large deformation	Biomechanics and Modeling in Mechanobiology, 21:1685–1702 [174]	28/08/2022
Ciara Durcan, Mokarram Hossain, Grégory Chagnon, Djordje Perić, Edouard Girard	Mechanical experimentation of the gastrointestinal tract: a systematic review	Biomechanics and Modeling in Mechanobiology [396]	Accepted [in print]
Ciara Durcan, Mokarram Hossain, Grégory Chagnon, Djordje Perić, Edouard Girard	Characterisation of the layer, direction and time-dependent mechanical behaviour of the human oesophagus and the effects of formalin preservation	Journal of the Royal Society Interface	Under review
Ciara Durcan, Mokarram Hossain, Grégory Chagnon, Djordje Perić, Edouard Girard	Constitutive modelling of the layer-dependent, anisotropic, visco-hyperelastic behaviour of the human oeosphagus with stress-softening	Journal of the Mechanical Behavior of Biomedical Materials	In progress

References

[1] Cleveland Clinic, "Stomach: What is the stomach?," 2021.

[2] Y. Goto and M. Kakizaki, "The spontaneous-diabetes rat: a model of noninsulin dependent diabetes mellitus," *Proceedings of the Japan Academy, Series B*, vol. 57, no. 10, pp. 381–384, 1981.

[3] J. Zhao and H. Gregersen, "Diabetes-induced mechanophysiological changes in the esophagus," *Annals of the New York Academy of Sciences*, vol. 1380, no. 1, pp. 139–154, 2016.

[4] J. Zhao, D. Liao, and H. Gregersen, "Biomechanical and histomorphometric esophageal remodeling in type 2 diabetic gk rats," *Journal of Diabetes and its Complications*, vol. 21, no. 1, pp. 34–40, 2007.

[5] S. Nagaraja, K. Leichsenring, M. Ambati, L. De Lorenzis, and M. Böl, "On a phase-field approach to model fracture of small intestine walls," *Acta Biomaterialia*, vol. 130, pp. 317–331, 2021.

[6] C. Bellini, P. Glass, M. Sitti, and E. S. Di Martino, "Biaxial mechanical modeling of the small intestine," *Journal of the Mechanical Behavior of Biomedical Materials*, vol. 4, no. 8, pp. 1727–1740, 2011.

[7] C. Masri, G. Chagnon, D. Favier, H. Sartelet, and E. Girard, "Experimental characterization and constitutive modeling of the biomechanical behavior of male human urethral tissues validated by histological observations," *Biomechanics and Modeling in Mechanobiology*, vol. 17, no. 4, pp. 939–950, 2018.

[8] Y. Qiao, E. Pan, S. Chakravarthula, F. Han, J. Liang, and S. Gudlavalleti, "Measurement of mechanical properties of rectal wall," *Journal of Materials Science: Materials in Medicine*, vol. 16, no. 2, pp. 183–188, 2005.

[9] D. C. Stewart, A. Rubiano, M. M. Santisteban, V. Shenoy, Y. Qi, C. J. Pepine, M. K. Raizada, and C. S. Simmons, "Hypertension-linked mechanical changes of rat gut," *Acta Biomaterialia*, vol. 45, pp. 296–302, 2016.

[10] X. Lu, Z. Zhang, J. Choy, and G. Kassab, "Role of distension on duodenal and colonic contractility in mice: a novel myograph for intestines," *Neurogastroenterology & Motility*, vol. 24, no. 5, pp. 487–493, 2012.

[11] D. Liao, J. Zhao, and H. Gregersen, "Three-dimensional geometry analysis of the stomach in type ii diabetic gk rats," *Diabetes Research and Clinical Practice*, vol. 71, no. 1, pp. 1–13, 2006.

[12] D. P. Sokolis, I. K. Orfanidis, and M. Peroulis, "Biomechanical testing and material characterization for the rat large intestine: regional dependence of material parameters," *Physiological Measurement*, vol. 32, no. 12, p. 1969, 2011.

[13] J. Zhao, X. Chen, J. Yang, D. Liao, and H. Gregersen, "Opening angle and residual strain in a three-layered model of pig oesophagus," *Journal of Biomechanics*, vol. 40, no. 14, pp. 3187–3192, 2007.

[14] O. Remesz, "Wiki-pl: Orem, commons: Orem, CC BY-SA 2.5," *Wikimedia Commons*.

[15] M. Kaliske, "A formulation of elasticity and viscoelasticity for fibre reinforced material at small and finite strains," *Computer Methods in Applied Mechanics and Engineering*, vol. 185, no. 2-4, pp. 225–243, 2000.

[16] N. Kuijsters, W. Methorst, M. Kortenhorst, C. Rabotti, M. Mischi, and B. Schoot, "Uterine peristalsis and fertility: current knowledge and future perspectives: a review and meta-analysis," *Reproductive Biomedicine Online*, vol. 35, no. 1, pp. 50–71, 2017.

[17] J. Misra and S. Maiti, "Peristaltic pumping of blood through small vessels of varying cross-section," *Journal of Applied Mechanics*, vol. 79, no. 6, 2012.

[18] M. R. Carvalho, J. P. Ferreira, D. A. Oliveira, M. P. Parente, and R. M. Natal Jorge, "Biomechanical characterization of the small intestine to simulate gastrointestinal tract chyme propulsion," *International Journal for Numerical Methods in Biomedical Engineering*, vol. 38, no. 5, p. e3588, 2022.

[19] A.-C. Kinn and H. Lykkeskov-Andersen, "Impact on ureteral peristalsis in a stented ureter. an experimental study in the pig," *Urological Research*, vol. 30, no. 4, pp. 213–218, 2002.

[20] E. McLafferty, C. Johnstone, C. Hendry, and A. Farley, "Male and female reproductive systems and associated conditions," *Nursing Standard*, vol. 28, no. 36, 2014.

[21] Y. Dou, S. Gregersen, J. Zhao, F. Zhuang, and H. Gregersen, "Morphometric and biomechanical intestinal remodeling induced by fasting in rats," *Digestive Diseases and Sciences*, vol. 47, pp. 1158–1168, 2002.

[22] C. Y. Scovil and J. L. Ronsky, "Sensitivity of a hill-based muscle model to perturbations in model parameters," *Journal of Biomechanics*, vol. 39, no. 11, pp. 2055–2063, 2006.

[23] M. Mir, M. N. Ali, U. Ansari, and J. Sami, "Structure and motility of the esophagus from a mechanical perspective," *Esophagus*, vol. 13, pp. 8–16, 2016.

[24] K. B. Orvar, H. Gregersen, and J. Christensen, "Biomechanical characteristics of the human esophagus," *Digestive Diseases and Sciences*, vol. 38, no. 2, pp. 197–205, 1993.

[25] G. E. Villadsen, J. H. Storkholm, L. Hendel, H. Vilstrup, and H. Gregersen, "Impedance planimetric characterization of esophagus in systemic sclerosis patients with severe involvement of esophagus," *Digestive Diseases and Sciences*, vol. 42, no. 11, pp. 2317–2326, 1997.

[26] R. S. Patel and S. S. Rao, "Biomechanical and sensory parameters of the human esophagus at four levels," *American Journal of Physiology-Gastrointestinal and Liver Physiology*, vol. 275, no. 2, pp. G187–G191, 1998.

[27] V. R. Mujica, R. S. Mudipalli, and S. S. Rao, "Pathophysiology of chest pain in patients with nutcracker esophagus," *The American Journal of Gastroenterology*, vol. 96, no. 5, pp. 1371–1377, 2001.

[28] S. Rao, B. Hayek, and R. Summers, "Functional chest pain of esophageal origin: hyperalgesia or motor dysfunction," *The American Journal of Gastroenterology*, vol. 96, no. 9, pp. 2584–2589, 2001.

[29] G. Villadsen, J. Storkholm, H. Zachariae, L. Hendel, F. Bendtsen, and H. Gregersen, "Oesophageal pressure–cross-sectional area distributions and secondary peristalsis in relation to subclassification of systemic sclerosis," *Neurogastroenterology & Motility*, vol. 13, no. 3, pp. 199–210, 2001.

[30] T. Takeda, G. Kassab, J. Liu, J. L. Puckett, R. R. Mittal, and R. K. Mittal, "A novel ultrasound technique to study the biomechanics of the human esophagus in vivo," *American Journal of Physiology-Gastrointestinal and Liver Physiology*, vol. 282, no. 5, pp. G785–G793, 2002.

[31] A. M. Drewes, K.-P. Schipper, G. Dimcevski, P. Petersen, O. K. Andersen, H. Gregersen, and L. Arendt-Nielsen, "Multimodal assessment of pain in the esophagus: a new experimental model," *American Journal of Physiology-Gastrointestinal and Liver Physiology*, vol. 283, no. 1, pp. G95–G103, 2002.

[32] S. S. C. Rao, B. Hayek, R. Mudipalli, and H. Gregersen, "Does esophageal function vary at the striated and smooth muscle segments in functional chest pain?," *The American Journal of Gastroenterology*, vol. 97, no. 9, pp. 2201–2207, 2002.

[33] A. Drewes, J. Pedersen, W. Liu, L. Arendt-Nielsen, and H. Gregersen, "Controlled mechanical distension of the human oesophagus: sensory and biomechanical findings," *Scandinavian Journal of Gastroenterology*, vol. 38, no. 1, pp. 27–35, 2003.

[34] A. M. Drewes, H. Reddy, C. Staahl, J. Pedersen, P. Funch-Jensen, L. Arendt-Nielsen, and H. Gregersen, "Sensory-motor responses to mechanical stimulation of the esophagus after sensitization with acid," *World Journal of Gastroenterology: WJG*, vol. 11, no. 28, p. 4367, 2005.

[35] A. Drewes, J. Pedersen, H. Reddy, K. Rasmussen, P. Funch-Jensen, L. Arendt-Nielsen, and H. Gregersen, "Central sensitization in patients with non-cardiac chest pain: a clinical experimental study," *Scandinavian Journal of Gastroenterology*, vol. 41, no. 6, pp. 640–649, 2006.

[36] I. Nasr, A. Attaluri, S. Hashmi, H. Gregersen, and S. S. Rao, "Investigation of esophageal sensation and biomechanical properties in functional chest pain," *Neurogastroenterology & Motility*, vol. 22, no. 5, pp. 520–e116, 2010.

[37] H. Gregersen, G. E. Villadsen, and D. Liao, "Mechanical characteristics of distension-evoked peristaltic contractions in the esophagus of systemic sclerosis patients," *Digestive Diseases and Sciences*, vol. 56, no. 12, p. 3559, 2011.

[38] J. M. Remes-Troche, A. Attaluri, P. Chahal, and S. S. C. Rao, "Barostat or dynamic balloon distention test: which technique is best suited for esophageal sensory testing?," *Diseases of the Esophagus*, vol. 25, no. 7, pp. 584–589, 2012.

[39] D. Liao, G. Villadsen, and H. Gregersen, "Distension-evoked motility analysis in human esophagus," *Neurogastroenterology & Motility*, vol. 25, no. 5, pp. 407–e297, 2013.

[40] F. Mojoli, G. A. Iotti, F. Torriglia, M. Pozzi, C. A. Volta, S. Bianzina, A. Braschi, and L. Brochard, "In vivo calibration of esophageal pressure in the mechanically ventilated patient makes measurements reliable," *Critical Care*, vol. 20, no. 1, p. 98, 2016.

[41] T. Takeda, G. Kassab, J. Liu, T. Nabae, and R. K. Mittal, "Effect of atropine on the biomechanical properties of the oesophageal wall in humans," *The Journal of Physiology*, vol. 547, no. 2, pp. 621–628, 2003.

[42] J. D. Barlow, H. Gregersen, and D. G. Thompson, "Identification of the biomechanical factors associated with the perception of distension in the human esophagus," *American Journal of Physiology-Gastrointestinal and Liver Physiology*, vol. 282, no. 4, pp. G683–G689, 2002.

[43] J. B. Frøkjær, S. D. Andersen, N. Ejskjær, P. Funch-Jensen, A. M. Drewes, and H. Gregersen, "Impaired contractility and remodeling of the upper gastrointestinal tract in diabetes mellitus type-1," *World Journal of Gastroenterology: WJG*, vol. 13, no. 36, p. 4881, 2007.

[44] J. Frøkjaer, S. Andersen, S. Lundbye-christensen, P. Funch-Jensen, A. M. Drewes, and H. Gregersen, "Sensation and distribution of stress and deformation in the human oesophagus," *Neurogastroenterology & Motility*, vol. 18, no. 2, pp. 104–114, 2006.

[45] H. Gregersen, *Biomechanics of the gastrointestinal tract: new perspectives in motility research and diagnostics*. Springer Science & Business Media, 2003.

[46] Y. Payan and J. Ohayon, *Biomechanics of living organs: hyperelastic constitutive laws for finite element modeling*. Academic Press, 2017.

[47] V. I. Egorov, I. V. Schastlivtsev, E. V. Prut, A. O. Baranov, and R. A. Turusov, "Mechanical properties of the human gastrointestinal tract," *Journal of Biomechanics*, vol. 35, no. 10, pp. 1417–1425, 2002.

[48] I. Vanags, A. Petersons, V. Ose, I. Ozolanta, V. Kasyanov, J. Laizans, E. Vjaters, J. Gardovskis, and A. Vanags, "Biomechanical properties of oesophagus wall under loading," *Journal of Biomechanics*, vol. 36, no. 9, pp. 1387–1390, 2003.

[49] D. Sánchez-Molina, *A constitutive model of human esophagus tissue with application for the treatment of stenosis*. PhD thesis, Universitat Politècnica de Catalunya, 2013.

[50] A. Tøttrup, A. Forman, N. Uldbjerg, P. Funch-Jensen, and K. Andersson, "Mechanical properties of isolated human esophageal smooth muscle.," *The American Journal of Physiology*, vol. 258, no. 3 Pt 1, pp. G338–43, 1990.

[51] R. Goyal, P. Biancani, A. Phillips, and H. Spiro, "Mechanical properties of the esophageal wall.," *The Journal of Clinical Investigation*, vol. 50, no. 7, pp. 1456–1465, 1971.

[52] Y. Fan, H. Gregersen, and G. S. Kassab, "A two-layered mechanical model of the rat esophagus. experiment and theory," *BioMedical Engineering OnLine*, vol. 3, p. 40, 2004.

[53] J. Yang, D. Liao, J. Zhao, and H. Gregersen, "Shear modulus of elasticity of the esophagus," *Annals of Biomedical Engineering*, vol. 32, no. 9, pp. 1223–1230, 2004.

[54] H. Jiang, D. Liao, J. Zhao, G. Wang, and H. Gregersen, "Contractions reverse stress softening in rat esophagus," *Annals of Biomedical Engineering*, vol. 8, no. 42, pp. 1717–1728, 2014.

[55] H. Jiang, D. Liao, J. Zhao, G. Wang, and H. Gregersen, "Reversible stress softening in layered rat esophagus in vitro after potassium chloride activation," *Biomechanics and Modeling in Mechanobiology*, vol. 16, no. 3, pp. 1065–1075, 2017.

[56] J. Assentoft, H. Gregersen, and W. O'brien, "Determination of biomechanical properties in guinea pig esophagus by means of high frequency ultrasound and impedance planimetry," *Digestive Diseases and Sciences*, vol. 45, no. 7, pp. 1260–1266, 2000.

[57] H. Gregersen, D. Liao, and Y. Fung, "Determination of homeostatic elastic moduli in two layers of the esophagus.," *Journal of Biomechanical Engineering*, vol. 130, no. 1, pp. 011005–011005, 2008.

[58] D. Liao, J. Zhao, P. Kunwald, and H. Gregersen, "Tissue softening of guinea pig oesophagus tested by the tri-axial test machine," *Journal of Biomechanics*, vol. 42, no. 7, pp. 804–810, 2009.

[59] W. Yang, T. Fung, K. Chian, and C. Chong, "Investigations of the viscoelasticity of esophageal tissue using incremental stress-relaxation test and cyclic extension test," *Journal of Mechanics in Medicine and Biology*, vol. 6, no. 03, pp. 261–272, 2006.

[60] W. Yang, T. Fung, K. Chian, and C. Chong, "Directional, regional, and layer variations of mechanical properties of esophageal tissue and its interpretation using a structure-based constitutive model.," *Journal of Biomechanical Engineering*, vol. 128, no. 3, pp. 409–418, 2006.

[61] J. Zhao, C. S. Jørgensen, D. Liao, and H. Gregersen, "Dimensions and circumferential stress-strain relation in the porcine esophagus in vitro determined by combined impedance planimetry and high-frequency ultrasound," *Digestive Diseases and Sciences*, vol. 52, no. 5, pp. 1338–1344, 2007.

[62] A. N. Natali, E. L. Carniel, and H. Gregersen, "Biomechanical behaviour of oesophageal tissues: material and structural configuration, experimental data and constitutive analysis," *Medical Engineering & Physics*, vol. 31, no. 9, pp. 1056–1062, 2009.

[63] E. A. Stavropoulou, Y. F. Dafalias, and D. P. Sokolis, "Biomechanical behavior and histological organization of the three-layered passive esophagus as a function of topography," *Proceedings of the Institution of Mechanical Engineers, Part H: Journal of Engineering in Medicine*, vol. 226, no. 6, pp. 477–490, 2012.

[64] D. Sanchez-Molina, J. Velazquez-Ameijide, C. Arregui-Dalmases, D. Rodríguez, V. Quintana, M. Shafieian, and J. Crandall, "A microcontinuum model for mechanical properties of esophageal tissue: experimental methodology and constitutive analysis," *Annals of Biomedical Engineering*, vol. 42, no. 1, pp. 62–72, 2014.

[65] J. M. Aho, B. Qiang, D. A. Wigle, D. J. Tschumperlin, and M. W. Urban, "Nondestructive measurement of esophageal biaxial mechanical properties utilizing sonometry," *Physics in Medicine & Biology*, vol. 61, no. 13, p. 4781, 2016.

[66] P. Ren, X. Deng, K. Li, G. Li, and W. Li, "3d biomechanical properties of the layered esophagus: fung-type sef and new constitutive model," *Biomechanics and Modeling in Mechanobiology*, vol. 20, no. 5, pp. 1775–1788, 2021.

[67] E. A. Stavropoulou, Y. F. Dafalias, and D. P. Sokolis, "Biomechanical and histological characteristics of passive esophagus: Experimental investigation and comparative constitutive modeling," *Journal of Biomechanics*, vol. 16, no. 42, pp. 2654–2663, 2009.

[68] D. Sokolis, "Strain-energy function and three-dimensional stress distribution in esophageal biomechanics.," *Journal of Biomechanics*, vol. 43, no. 14, pp. 2753–2764, 2010.

[69] D. P. Sokolis, "Structurally-motivated characterization of the passive pseudo-elastic response of esophagus and its layers," *Computers in Biology and Medicine*, vol. 9, no. 43, pp. 1273–1285, 2013.

[70] G. Sommer, A. J. Schriefl, G. Zeindlinger, A. Katzensteiner, H. Ainödhofer, A. Saxena, and G. Holzapfel, "Multiaxial mechanical response and constitutive modeling of esophageal tissues: Impact on esophageal tissue engineering.," *Acta Biomaterialia*, vol. 9, no. 12, pp. 9379–9391, 2013.

[71] A. K. Saxena, E. Biro, G. Sommer, and G. A. Holzapfel, "Esophagus stretch tests: Biomechanics for tissue engineering and possible implications on the outcome of esophageal atresia repairs performed under excessive tension," *Esophagus*, vol. 18, no. 2, pp. 346–352, 2021.

[72] J. Yang, J. Zhao, Y. Zeng, and H. Gregersen, "Biomechanical properties of the rat oesophagus in experimental type-1 diabetes," *Neurogastroenterology & Motility*, vol. 16, no. 2, pp. 195–203, 2004.

[73] Y.-J. Zeng, J. Yang, J.-B. Zhao, D.-H. Liao, E.-P. Zhang, H. Gregersen, X.-H. Xu, H. Xu, and C.-Q. Xu, "Morphologic and biomechanical changes of rat oesophagus in experimental diabetes," *World Journal of Gastroenterology: WJG*, vol. 10, no. 17, p. 2519, 2004.

[74] Y. Zeng, Y. Qiao, J. Yang, H. Gregersen, E. Zhang, X. Xu, and H. Xu, "Torque properties of a rat oesophagus for physiological and diabetic conditions," *Physiological Measurement*, vol. 25, no. 5, p. 1211, 2004.

[75] J. Yang, J. Zhao, D. Liao, and H. Gregersen, "Biomechanical properties of the layered oesophagus and its remodelling in experimental type-1 diabetes," *Journal of Biomechanics*, vol. 39, no. 5, pp. 894–904, 2006.

[76] G.-F. Liu, J.-B. Zhao, Z. Zhen, H. Sha, P.-M. Chen, M. Li, J.-C. Zhang, M.-Z. Yuan, W. Gao, H. Gregersen, *et al.*, "Effect of tangweian jianji on upper gastrointestinal remodeling in streptozotocin-induced diabetic rats," *World Journal of Gastroenterology: WJG*, vol. 18, no. 35, p. 4875, 2012.

[77] H. Jiang, J. Zhao, D. Liao, G. Wang, and H. Gregersen, "Esophageal stress softening recovery is altered in stz-induced diabetic rats," *Journal of Biomechanics*, vol. 92, pp. 126–136, 2019.

[78] L. Jensen, S. Laurberg, C. Juhl, and T. Andreassen, "Esophageal collagen content and mechanical strength after endoscopic sclerotherapy of esophageal varices: an experimental study in rabbits," *Scandinavian Journal of Gastroenterology*, vol. 22, no. 6, pp. 743–749, 1987.

[79] H. Gregersen, L. Knudsen, B. Eika, L. S. Nerstrøm, L. Rasmussen, and L. Jensen, "A time-dependent study of passive esophageal wall properties and collagen content in rabbits with esophageal varices," *Digestive Diseases and Sciences*, vol. 36, no. 8, pp. 1050–1056, 1991.

[80] H. Gregersen, L. Jensen, and J. Djurhuus, "Changes in oesophageal wall biomechanics after portal vein banding and variceal sclerotherapy measured by a new technique. an experimental study in rabbits.," *Gut*, vol. 29, no. 12, pp. 1699–1704, 1988.

[81] J. Zhao, D. Liao, and H. Gregersen, "Mechanical analysis of intestinal contractility in a neonatal maternal deprivation irritable bowel syndrome rat model," *Journal of Biomechanics*, vol. 93, pp. 42–51, 2019.

[82] A. Ouyang, K. Zimmerman, K.-L. Wong, D. Sharp, and J. C. Reynolds, "Effect of celiac ganglionectomy on tachykinin innervation, receptor distribution and intestinal responses in the rat," *Journal of the Autonomic Nervous System*, vol. 61, no. 3, pp. 292–300, 1996.

[83] Y. Dou, X. Lu, J. Zhao, and H. Gregersen, "Morphometric and biomechanical remodelling in the intestine after small bowel resection in the rat," *Neurogastroenterology & Motility*, vol. 14, no. 1, pp. 43–53, 2002.

[84] L. Marie, C. Masson, B. Gaborit, S. V. Berdah, and T. Bège, "An experimental study of intraluminal hyperpressure reproducing a gastric leak following a sleeve gastrectomy," *Obesity Surgery*, vol. 29, no. 9, pp. 2773–2780, 2019.

[85] L. Vinter-Jensen, C. O. Juhl, B. Eika, H. Gregersen, and E. Dajani, "Epidermal growth factor attenuates the sclerotherapy-induced biomechanical properties of the oesophagus: an experimental study in minipigs," *Scandinavian Journal of Gastroenterology*, vol. 30, no. 7, pp. 614–619, 1995.

[86] H. Sha, J.-B. Zhao, Z.-Y. Zhang, S.-P. Zhou, X.-L. Tong, F.-Y. Zhuang, and H. Gregersen, "Effect of Kaiyu Qingwei Jianji on the morphometry and residual strain distribution of small intestine in experimental diabetic rats," *World Journal of Gastroenterology*, vol. 12, no. 44, pp. 7149–7154, 2006.

[87] M. B. Christensen, K. Oberg, and J. C. Wolchok, "Tensile properties of the rectal and sigmoid colon: a comparative analysis of human and porcine tissue," *SpringerPlus*, vol. 4, no. 1, pp. 1–10, 2015.

[88] D. B. MacManus, A. Menichetti, B. Depreitere, N. Famaey, J. Vander Sloten, and M. Gilchrist, "Towards animal surrogates for characterising large strain dynamic mechanical properties of human brain tissue," *Brain Multiphysics*, vol. 1, p. 100018, 2020.

[89] M. Prange, D. Meaney, and S. Margulies, "Defining brain mechanical properties: effects of region, direction, and species," *Stapp Car Crash Journal*, vol. 44, p. 205—213, November 2000.

[90] J. Yekrang, D. Semnani, and A. Z. Seyghlani, "Simulation and characterization of the mechanical properties of knitted esophageal stents using finite element and mathematical models," *Journal of Industrial Textiles*, vol. 51, no. 5_suppl, pp. 7835S–7859S, 2022.

[91] M. Peirlinck, N. Debusschere, F. Iannaccone, P. D. Siersema, B. Verhegghe, P. Segers, and M. De Beule, "An in silico biomechanical analysis of the stent–esophagus interaction," *Biomechanics and Modeling in Mechanobiology*, vol. 17, no. 1, pp. 111–131, 2018.

[92] C. Lin, P. Ren, W. Li, H. Deng, and Z. Zhou, "Finite-element modelling of frictional behaviour between oesophagus and endoscope," *Biosurface and Biotribology*, vol. 6, no. 3, pp. 75–81, 2020.

[93] E. Lee, A. Milan, L. Urbani, P. De Coppi, and M. W. Lowdell, "Decellularized material as scaffolds for tissue engineering studies in long gap esophageal atresia," *Expert Opinion on Biological Therapy*, vol. 17, no. 5, pp. 573–584, 2017.

[94] E. Biro, G. Sommer, G. Leitinger, H. Abraham, D. J. Kardos, Z. Oberritter, and A. K. Saxena, "Ultrastructural changes in esophageal tissue undergoing stretch tests with possible impact on tissue engineering and long gap esophageal repairs performed under tension," *Scientific Reports*, vol. 13, no. 1, p. 1750, 2023.

[95] Z. A. Taylor, O. Comas, M. Cheng, J. Passenger, D. J. Hawkes, D. Atkinson, and S. Ourselin, "On modelling of anisotropic viscoelasticity for soft tissue simulation: Numerical solution and gpu execution," *Medical Image Analysis*, vol. 13, no. 2, pp. 234–244, 2009.

[96] C. Choi, J. Kim, H. Han, B. Ahn, and J. Kim, "Graphic and haptic modelling of the oesophagus for vr-based medical simulation," *The International Journal of Medical Robotics and Computer Assisted Surgery*, vol. 5, no. 3, pp. 257–266, 2009.

[97] M. Wang, J. Li, M. Boga, L. Reid, C. Li, and Z. Huang, "Quantitative tissue elasticity measurement of human cadaver oesophagus by using vibrational optical coherence elastography," *Applied Sciences*, vol. 13, no. 6, p. 3844, 2023.

[98] J. Emery, J. Omens, and A. McCulloch, "Strain softening in rat left ventricular myocardium.," *Journal of Biomechanical Engineering*, vol. 119, no. 1, pp. 6–12, 1997.

[99] H. Gregersen, J. Emery, and A. McCulloch, "History-dependent mechanical behavior of guinea-pig small intestine," *Annals of Biomedical Engineering*, vol. 26, no. 5, pp. 850–858, 1998.

[100] J. M. Giles, A. E. Black, and J. E. Bischoff, "Anomalous rate dependence of the preconditioned response of soft tissue during load controlled deformation," *Journal of Biomechanics*, vol. 40, no. 4, pp. 777–785, 2007.

[101] M. Van Loocke, C. Simms, and C. Lyons, "Viscoelastic properties of passive skeletal muscle in compression—cyclic behaviour," *Journal of Biomechanics*, vol. 42, no. 8, pp. 1038–1048, 2009.

[102] C. Jayyosi, N. Lee, A. Willcockson, S. Nallasamy, M. Mahendroo, and K. Myers, "The mechanical response of the mouse cervix to tensile cyclic loading in term and preterm pregnancy," *Acta Biomaterialia*, vol. 78, pp. 308–319, 2018.

[103] D. Remache, M. Caliez, M. Gratton, and S. Dos Santos, "The effects of cyclic tensile and stress-relaxation tests on porcine skin," *Journal of the Mechanical Behavior of Biomedical Materials*, vol. 77, pp. 242–249, 2018.

[104] W. Yang, T. Fung, K. Chian, and C. Chong, "Viscoelasticity of esophageal tissue and application of a QLV model," *Journal of Biomechanical Engineering*, vol. 128, no. 6, pp. 909–916, 2006.

[105] E. Peña, P. Martins, T. Mascarenhas, R. N. Jorge, A. Ferreira, M. Doblaré, and B. Calvo, "Mechanical characterization of the softening behavior of human vaginal tissue," *Journal of the Mechanical Behavior of Biomedical Materials*, vol. 4, no. 3, pp. 275–283, 2011.

[106] C. Rubod, M. Brieu, M. Cosson, G. Rivaux, J.-C. Clay, L. de Landsheere, and B. Gabriel, "Biomechanical properties of human pelvic organs," *Urology*, vol. 79, no. 4, pp. 968–e17, 2012.

[107] H. Weisbecker, D. M. Pierce, P. Regitnig, and G. A. Holzapfel, "Layer-specific damage experiments and modeling of human thoracic and abdominal aortas with non-atherosclerotic intimal thickening," *Journal of the Mechanical Behavior of Biomedical Materials*, vol. 12, pp. 93–106, 2012.

[108] B. Fereidoonnezhad, R. Naghdabadi, and G. A. Holzapfel, "Stress softening and permanent deformation in human aortas: continuum and computational modeling with application to arterial clamping," *Journal of the Mechanical Behavior of Biomedical Materials*, vol. 61, pp. 600–616, 2016.

[109] S. Budday, G. Sommer, C. Birkl, C. Langkammer, J. Haybaeck, J. Kohnert, M. Bauer, F. Paulsen, P. Steinmann, E. Kuhl, *et al.*, "Mechanical characterization of human brain tissue," *Acta Biomaterialia*, vol. 48, pp. 319–340, 2017.

[110] E. Anttila, D. Balzani, A. Desyatova, P. Deegan, J. MacTaggart, and A. Kamenskiy, "Mechanical damage characterization in human femoropopliteal arteries of different ages," *Acta Biomaterialia*, vol. 90, pp. 225–240, 2019.

[111] W. G. Paterson, "Esophageal peristalsis," *GI Motility Online*, 2006.

[112] M. Boettcher, M. Hauck, M. Fuerboeter, J. Elrod, D. Vincent, J. Boettcher, and K. Reinshagen, "Clinical outcome, quality of life, and mental health in long-gap esophageal atresia: comparison of gastric sleeve pull-up and delayed primary anastomosis," *Pediatric Surgery International*, vol. 39, no. 1, p. 166, 2023.

[113] A. B. Penikis, P. S. Salvi, S. R. Sferra, A. J. Engwall-Gill, D. S. Rhee, D. G. Solomon, and S. M. Kunisaki, "Delayed primary repair in 100 infants with isolated long-gap esophageal atresia: A nationwide analysis of children's hospitals," *Surgery*, 2023.

[114] S. Sundaram, T. Jensen, T. Roffidal, K. Paquin, H. Wanczyk, M. D. Cockman, S. Shadman, C. Finck, and W. Fodor, "Esophageal regeneration following surgical implantation of a tissue engineered esophageal implant in a pediatric model," *NPJ Regenerative Medicine*, vol. 7, no. 1, p. 1, 2022.

[115] S. Hayashi, M. Naito, S. Kawata, N. Qu, N. Hatayama, S. Hirai, and M. Itoh, "History and future of human cadaver preservation for surgical training: from formalin to saturated salt solution method," *Anatomical Science International*, vol. 91, pp. 1–7, 2016.

[116] V. N. Palter and T. P. Grantcharov, "Simulation in surgical education," *CMAJ: Canadian Medical Association Journal*, vol. 182, no. 11, pp. 1191–1196, 2010.

[117] I. Badash, K. Burtt, C. A. Solorzano, and J. N. Carey, "Innovations in surgery simulation: a review of past, current and future techniques," *Annals of Translational Medicine*, vol. 4, no. 23, 2016.

[118] W. Thiel, "The preservation of the whole corpse with natural color," *Annals of anatomy= Anatomischer Anzeiger: Official Organ of the Anatomische Gesellschaft*, vol. 174, no. 3, pp. 185–195, 1992.

[119] W. Thiel, "An arterial substance for subsequent injection during the preservation of the whole corpse," *Annals of Anatomy= Anatomischer Anzeiger: Official Organ of the Anatomische Gesellschaft*, vol. 174, no. 3, pp. 197–200, 1992.

[120] W. Thiel, "Supplement to the conservation of an entire cadaver according to w. thiel," *Annals of anatomy= Anatomischer Anzeiger: official organ of the Anatomische Gesellschaft*, vol. 184, no. 3, pp. 267–269, 2002.

[121] P. Liao and Z. Wang, "Thiel-embalming technique: investigation of possible modification in embalming tissue as evaluation model for radiofrequency ablation," *Journal of Biomedical Research*, vol. 33, no. 4, p. 280, 2019.

[122] L. Kennel, D. M. Martin, H. Shaw, and T. Wilkinson, "Learning anatomy through thiel- vs. formalin-embalmed cadavers: Student perceptions of embalming methods and effect on functional anatomy knowledge," *Anatomical Sciences Education*, vol. 11, no. 2, pp. 166–174, 2018.

[123] G. Fessel, K. Frey, A. Schweizer, M. Calcagni, O. Ullrich, and J. G. Snedeker, "Suitability of thiel embalmed tendons for biomechanical investigation," *Annals of Anatomy-Anatomischer Anzeiger*, vol. 193, no. 3, pp. 237–241, 2011.

[124] S.-J. Estermann, S. Förster-Streffleur, L. Hirtler, J. Streicher, D. H. Pahr, and A. Reisinger, "Comparison of thiel preserved, fresh human, and animal liver tissue in terms of mechanical properties," *Annals of Anatomy-Anatomischer Anzeiger*, vol. 236, p. 151717, 2021.

[125] F. Sanchez-Ferrer, M. D. Grima-Murcia, F. Sánchez-del Campo, M. L. Sánchez-Ferrer, and E. Fernández-Jover, "Thiel embalming in neonates: methodology and benefits in medical training," *Anatomical Science International*, vol. 97, no. 3, pp. 290–296, 2022.

[126] E. Hohmann, N. Keough, V. Glatt, K. Tetsworth, R. Putz, and A. Imhoff, "The mechanical properties of fresh versus fresh/frozen and preserved (thiel and formalin) long head of biceps tendons: a cadaveric investigation," *Annals of Anatomy-Anatomischer Anzeiger*, vol. 221, pp. 186–191, 2019.

[127] E. Girard, G. Chagnon, E. Gremen, M. Calvez, C. Masri, J. Boutonnat, B. Trilling, and B. Nottelet, "Biomechanical behaviour of human bile duct wall and impact of cadaveric preservation processes," *Journal of the Mechanical Behavior of Biomedical Materials*, vol. 98, pp. 291–300, 2019.

[128] S. Chatelin, A. Constantinesco, and R. Willinger, "Fifty years of brain tissue mechanical testing: from in vitro to in vivo investigations," *Biorheology*, vol. 47, no. 5-6, pp. 255–276, 2010.

[129] S. Budday, T. C. Ovaert, G. A. Holzapfel, P. Steinmann, and E. Kuhl, "Fifty shades of brain: a review on the mechanical testing and modeling of brain tissue," *Archives of Computational Methods in Engineering*, vol. 27, pp. 1187–1230, 2020.

[130] J. D. Humphrey, *Cardiovascular solid mechanics: cells, tissues, and organs*. Springer Science & Business Media, 2013.

[131] B. Patel, A. Gizzi, J. Hashemi, Y. Awakeem, H. Gregersen, and G. Kassab, "Biomechanical constitutive modeling of the gastrointestinal tissues: a systematic review," *Materials & Design*, p. 110576, 2022.

[132] I. Ogobuiro, J. Gonzales, and F. Tuma, "Physiology, gastrointestinal," in *StatPearls [Internet]*, StatPearls Publishing, 2021.

[133] H. F. Helander and L. Fändriks, "Surface area of the digestive tract–revisited," *Scandinavian Journal of Gastroenterology*, vol. 49, no. 6, pp. 681–689, 2014.

[134] R. Wanamaker and I. Grimm, "Encyclopedia of gastroenterology," *Gastroenterology*, vol. 127, no. 4, pp. 1274–1275, 2004.

[135] K. Van de Graaff, "Anatomy and physiology of the gastrointestinal tract.," *Pediatric Infectious Disease*, vol. 5, no. 1 Suppl, pp. S11–6, 1986.

[136] N. Baidoo, E. Crawley, C. H. Knowles, G. J. Sanger, and A. Belai, "Total collagen content and distribution is increased in human colon during advancing age," *PloS One*, vol. 17, no. 6, p. e0269689, 2022.

[137] C. Durcan, M. Hossain, G. Chagnon, D. Perić, L. Bsiesy, G. Karam, and E. Girard, "Experimental investigations of the human oesophagus: anisotropic properties of the embalmed muscular layer under large deformation," *Biomechanics and Modeling in Mechanobiology*, vol. 21, pp. 1169–1186, 2022.

[138] M. Horowitz and M. Samsom, *Gastrointestinal function in diabetes mellitus*, vol. 5. John Wiley & Sons, 2004.

[139] C. S. Jørgensen, J. M. Ahrensberg, H. Gregersen, and A. Flyvberg, "Tension–strain relations and morphometry of rat small intestine in experimental diabetes," *Digestive Diseases and Sciences*, vol. 46, no. 5, pp. 960–967, 2001.

[140] J. Zhao, J. Yang, and H. Gregersen, "Biomechanical and morphometric intestinal remodelling during experimental diabetes in rats," *Diabetologia*, vol. 46, no. 12, pp. 1688–1697, 2003.

[141] J. Zhao, T. Nakaguchi, and H. Gregersen, "Biomechanical and histomorphometric colon remodelling in stz-induced diabetic rats," *Digestive Diseases and Sciences*, vol. 54, no. 8, pp. 1636–1642, 2009.

[142] I. Toniolo, C. G. Fontanella, M. Foletto, and E. L. Carniel, "Coupled experimental and computational approach to stomach biomechanics: Towards a validated characterization of gastric tissues mechanical properties," *Journal of the Mechanical Behavior of Biomedical Materials*, vol. 125, p. 104914, 2022.

[143] W. Yang, T. Fung, K. Chian, and C. Chong, "Three-dimensional finite element model of the two-layered oesophagus, including the effects of residual strains and buckling of mucosa," *Proceedings of the Institution of Mechanical Engineers, Part H: Journal of Engineering in Medicine*, vol. 221, no. 4, pp. 417–426, 2007.

[144] W. Yang, T. C. Fung, K. S. Chian, and C. K. Chong, "Finite element simulation of food transport through the esophageal body," *World Journal of Gastroenterology: WJG*, vol. 13, no. 9, p. 1352, 2007.

[145] C. Skamniotis, C. H. Edwards, S. Bakalis, G. Frost, and M. Charalambides, "Eulerian-lagrangian finite element modelling of food flow-fracture in the stomach to engineer digestion," *Innovative Food Science & Emerging Technologies*, vol. 66, p. 102510, 2020.

[146] S. Panda and M. Buist, "A finite element approach for gastrointestinal tissue mechanics.," *International Journal for Numerical Methods in Biomedical Engineering*, vol. 35, no. 12, p. e3269, 2019.

[147] C. Shanahan, S. A. Tofail, and P. Tiernan, "Viscoelastic braided stent: Finite element modelling and validation of crimping behaviour," *Materials & Design*, vol. 121, pp. 143–153, 2017.

[148] J. Kim, I. Sung, Y. Kim, D. Kim, and Y. Jang, "Analytical model development for the prediction of the frictional resistance of a capsule endoscope inside an intestine," *Proceedings of the Institution of Mechanical Engineers, Part H: Journal of Engineering in Medicine*, vol. 221, no. 8, pp. 837–845, 2007.

[149] M. Gao, C. Hu, Z. Chen, H. Zhang, and S. Liu, "Design and fabrication of a magnetic propulsion system for self-propelled capsule endoscope," *IEEE Transactions on Biomedical Engineering*, vol. 57, no. 12, pp. 2891–2902, 2010.

[150] D. Ye, F. Zhang, S. Yuan, S. Song, and M. Q.-H. Meng, "Magnetically driven wireless capsule robot with targeting biopsy function," in *2019 IEEE International Conference on Robotics and Biomimetics (ROBIO)*, pp. 1222–1227, IEEE, 2019.

[151] V. Nováček, T. Trân, U. Klinge, R. Tolba, M. Staat, D. Bronson, A. Miesse, J. Whiffen, and F. Turquier, "Finite element modelling of stapled colorectal end-to-end anastomosis: advantages of variable height stapler design," *Journal of Biomechanics*, vol. 45, no. 15, pp. 2693–2697, 2012.

[152] H. Guo, J. Hu, Z. Shen, D. Du, Y. Zheng, and J. Peng, "In vitro and in vivo studies of biodegradable zn-li-mn alloy staples designed for gastrointestinal anastomosis," *Acta Biomaterialia*, vol. 121, pp. 713–723, 2021.

[153] I. Toniolo, A. Berardo, M. Foletto, C. Fiorillo, G. Quero, S. Perretta, and E. L. Carniel, "Patient-specific stomach biomechanics before and after laparoscopic sleeve gastrectomy," *Surgical Endoscopy*, pp. 1–14, 2022.

[154] S. Chakravarthy, A. Rao, and G. Ananthasuresh, "A haptic simulator for upper gastrointestinal endoscopy," in *The Hamlyn Symposium on Medical Robotics*, p. 16, 2014.

[155] G. A. Holzapfel and R. W. Ogden, "An arterial constitutive model accounting for collagen content and cross-linking," *Journal of the Mechanics and Physics of Solids*, vol. 136, p. 103682, 2020.

[156] S. Dargar, R. Rahul, U. Kruger, and S. De, "In vivo layer-specific mechanical characterization of porcine stomach tissue using a customized ultrasound elastography system," *Journal of Biomechanical Engineering*, vol. 141, no. 10, pp. 1010041–10100410, 2019.

[157] J. Rosen, J. Brown, S. De, M. Sinanan, and B. Hannaford, "Biomechanical properties of abdominal organs in vivo and postmortem under compression loads.," *Journal of Biomechanical Engineering*, vol. 130, no. 2, pp. 021020–021020, 2008.

[158] M. Borsdorf, M. Böl, and T. Siebert, "Influence of layer separation on the determination of stomach smooth muscle properties," *Pflügers Archiv-European Journal of Physiology*, vol. 473, no. 6, pp. 911–920, 2021.

[159] G. A. Holzapfel and R. W. Ogden, eds., *Mechanics of Biological Tissue*. Springer Science & Business Media, 2006.

[160] G. Chagnon, M. Rebouah, and D. Favier, "Hyperelastic energy densities for soft biological tissues: a review," *Journal of Elasticity*, vol. 120, no. 2, pp. 129–160, 2015.

[161] S. Siri, Y. Zhao, F. Maier, D. M. Pierce, and B. Feng, "The macro-and micro-mechanics of the colon and rectum I: Experimental evidence," *Bioengineering*, vol. 7, no. 4, p. 130, 2020.

[162] A. Weizel, T. Distler, R. Detsch, A. Boccaccini, L. Bräuer, F. Paulsen, H. Seitz, and S. Budday, "Hyperelastic parameter identification of human articular cartilage and substitute materials," *Journal of the Mechanical Behavior of Biomedical Materials*, vol. 133, p. 105292, 2022.

[163] D. Nolan and J. McGarry, "On the compressibility of arterial tissue," *Annals of biomedical engineering*, vol. 44, no. 4, pp. 993–1007, 2016.

[164] M. Gilchrist, J. G. Murphy, W. Parnell, and B. Pierrat, "Modelling the slight compressibility of anisotropic soft tissue," *International Journal of Solids and Structures*, vol. 51, no. 23-24, pp. 3857–3865, 2014.

[165] Y. Liu, J. Zhao, D. Liao, G. Wang, and H. Gregersen, "Intestinal mechanomorphological remodeling induced by long-term low-fiber diet in rabbits," *Annals of Biomedical Engineering*, vol. 45, no. 12, pp. 2867–2878, 2017.

[166] A. International, *E8/E8M-16a: Standard Test Methods for Tension Testing of Metallic Materials*. ASTM International, 2016.

[167] J. Zhao, D. Liao, and H. Gregersen, "Tension and stress in the rat and rabbit stomach are location-and direction-dependent," *Neurogastroenterology & Motility*, vol. 17, no. 3, pp. 388–398, 2005.

[168] F. Gao, D. Liao, J. Zhao, A. M. Drewes, and H. Gregersen, "Numerical analysis of pouch filling and emptying after laparoscopic gastric banding surgery," *Obesity Surgery*, vol. 18, no. 3, pp. 243–250, 2008.

[169] E. Carniel, V. Gramigna, C. Fontanella, A. Frigo, C. Stefanini, A. Rubini, and A. Natali, "Characterization of the anisotropic mechanical behaviour of colonic tissues: experimental activity and constitutive formulation," *Experimental Physiology*, vol. 99, no. 5, pp. 759–771, 2014.

[170] G. Ivakhov, A. Kolygin, S. Titkova, M. Anurov, and A. Sazhin, "Development and evaluation of a novel simulation model for transabdominal preperitoneal (tapp) inguinal hernia repair," *Hernia*, vol. 24, no. 1, pp. 159–166, 2020.

[171] A. S. Khan and H. Liu, "Strain rate and temperature dependent fracture criteria for isotropic and anisotropic metals," *International Journal of Plasticity*, vol. 37, pp. 1–15, 2012.

[172] M. Mehnert and P. Steinmann, "On the influence of the compliant electrodes on the mechanical behavior of vhb 4905," *Computational Materials Science*, vol. 160, pp. 287–294, 2019.

[173] N. F. Davis, J. J. Mulvihill, S. Mulay, E. M. Cunnane, D. M. Bolton, and M. T. Walsh, "Urinary bladder vs gastrointestinal tissue: a comparative study of their biomechanical properties for urinary tract reconstruction," *Urology*, vol. 113, pp. 235–240, 2018.

[174] C. Durcan, M. Hossain, G. Chagnon, D. Perić, G. Karam, L. Bsiesy, and E. Girard, "Experimental investigations of the human oesophagus: anisotropic properties of the embalmed mucosa-submucosa layer under large deformation," *Biomechanics and Modeling in Mechanobiology*, vol. 21, pp. 1685–1702, 2022.

[175] E. L. Carniel, A. Albanese, C. G. Fontanella, P. G. Pavan, L. Prevedello, C. Salmaso, S. Todros, I. Toniolo, and M. Foletto, "Biomechanics of stomach tissues and structure in patients with obesity," *Journal of the Mechanical Behavior of Biomedical Materials*, vol. 110, p. 103883, 2020.

[176] J. Zhao, D. Liao, J. Yang, and H. Gregersen, "Viscoelastic behavior of small intestine in streptozotocin-induced diabetic rats," *Digestive Diseases and Sciences*, vol. 48, no. 12, pp. 2271–2277, 2003.

[177] Z. Jia, W. Li, and Z. Zhou, "Mechanical characterization of stomach tissue under uniaxial tensile action," *Journal of Biomechanics*, vol. 48, no. 4, pp. 651–658, 2015.

[178] M. Hossain, D. K. Vu, and P. Steinmann, "Experimental study and numerical modelling of vhb 4910 polymer," *Computational Materials Science*, vol. 59, pp. 65–74, 2012.

[179] A. Tomalka, M. Borsdorf, M. Böl, and T. Siebert, "Porcine stomach smooth muscle force depends on history-effects," *Frontiers in Physiology*, vol. 8, p. 802, 2017.

[180] J. J. Mulvihill and M. T. Walsh, "On the mechanical behaviour of carotid artery plaques: the influence of curve-fitting experimental data on numerical model results," *Biomechanics and Modeling in Mechanobiology*, vol. 12, no. 5, pp. 975–985, 2013.

[181] D. Moreira and L. Nunes, "Comparison of simple and pure shear for an incompressible isotropic hyperelastic material under large deformation," *Polymer Testing*, vol. 32, no. 2, pp. 240–248, 2013.

[182] M. Mishra and A. R. Rao, "Peristaltic transport in a channel with a porous peripheral layer: model of a flow in gastrointestinal tract," *Journal of Biomechanics*, vol. 38, no. 4, pp. 779–789, 2005.

[183] R. N. Vaishnav and J. Vossoughi, "Estimation of residual strains in aortic segments," in *Biomedical engineering II*, pp. 330–333, Elsevier, 1983.

[184] Y. Fung, "What principle governs the stress distribution in living organs?," *Biomechanics in China, Japan and USA*, pp. 1–13, 1984.

[185] A. Aggarwal, A. M. Pouch, E. Lai, J. Lesicko, P. A. Yushkevich, J. H. Gorman III, R. C. Gorman, and M. S. Sacks, "In-vivo heterogeneous functional and residual strains in human aortic valve leaflets," *Journal of Biomechanics*, vol. 49, no. 12, pp. 2481–2490, 2016.

[186] H. Gregersen, G. Kassab, and Y. Fung, "The zero-stress state of the gastrointestinal tract," *Digestive Diseases and Sciences*, vol. 45, no. 12, pp. 2271–2281, 2000.

[187] Y. Fung and S. Liu, "Change of residual strains in arteries due to hypertrophy caused by aortic constriction.," *Circulation research*, vol. 65, no. 5, pp. 1340–1349, 1989.

[188] T. Sigaeva, M. Destrade, and E. S. Di Martino, "Multi-sector approximation method for arteries: the residual stresses of circumferential rings with non-trivial openings," *Journal of the Royal Society Interface*, vol. 16, no. 156, p. 20190023, 2019.

[189] S. Lefloch, P. Cañadas, D. Ambard, and G. Dusfour, "Residual strains estimation in the annulus fibrosus through digital image correlation," *Journal of Theoretical, Computational and Applied Mechanics*, p. jtcam:6971, 2021.

[190] Y. Dou, Y. Fan, J. Zhao, and H. Gregersen, "Longitudinal residual strain and stress-strain relationship in rat small intestine," *BioMedical Engineering OnLine*, vol. 5, no. 1, pp. 1–9, 2006.

[191] S. Dargar, A. C. Akyildiz, and S. De, "In situ mechanical characterization of multilayer soft tissue using ultrasound imaging," *IEEE Transactions on Biomedical Engineering*, vol. 64, no. 11, pp. 2595–2606, 2016.

[192] A. M. Drewes, P. Petersen, P. Rössel, C. Gao, J. Hansen, and L. Arendt-Nielsen, "Sensitivity and distensibility of the rectum and sigmoid colon in patients with irritable bowel syndrome," *Scandinavian Journal of Gastroenterology*, vol. 36, no. 8, pp. 827–832, 2001.

[193] P. Petersen, C. Gao, L. Arendt-Nielsen, H. Gregersen, and A. M. Drewes, "Pain intensity and biomechanical responses during ramp-controlled distension of the human rectum," *Digestive Diseases and Sciences*, vol. 48, no. 7, pp. 1310–1316, 2003.

[194] G.-Y. Li and Y. Cao, "Mechanics of ultrasound elastography," *Proceedings of the Royal Society A: Mathematical, Physical and Engineering Sciences*, vol. 473, no. 2199, p. 20160841, 2017.

[195] A. Evans, P. Whelehan, K. Thomson, D. McLean, K. Brauer, C. Purdie, L. Jordan, L. Baker, and A. Thompson, "Quantitative shear wave ultrasound elastography: initial experience in solid breast masses," *Breast cancer research*, vol. 12, no. 6, pp. 1–11, 2010.

[196] S. K. Venkatesh, M. Yin, and R. L. Ehman, "Magnetic resonance elastography of liver: technique, analysis, and clinical applications," *Journal of magnetic resonance imaging*, vol. 37, no. 3, pp. 544–555, 2013.

[197] B. F. Kennedy, P. Wijesinghe, and D. D. Sampson, "The emergence of optical elastography in biomedicine," *Nature Photonics*, vol. 11, no. 4, pp. 215–221, 2017.

[198] B. F. Kennedy, K. M. Kennedy, and D. D. Sampson, "A review of optical coherence elastography: fundamentals, techniques and prospects," *IEEE Journal of Selected Topics in Quantum Electronics*, vol. 20, no. 2, pp. 272–288, 2013.

[199] G. Low, S. A. Kruse, and D. J. Lomas, "General review of magnetic resonance elastography.," *World journal of radiology*, vol. 8, no. 1, pp. 59–72, 2016.

[200] H. Gregersen, S. Weis, and A. McCulloch, "Oesophageal morphometry and residual strain in a mouse model of osteogenesis imperfecta," *Neurogastroenterology & Motility*, vol. 13, no. 5, pp. 457–464, 2001.

[201] J. M. Aho, I. Z. Nenadic, S. Aristizabal, D. A. Wigle, D. J. Tschumperlin, and M. W. Urban, "Use of shear wave ultrasound vibrometry for detection of simulated esophageal malignancy in ex vivo porcine esophagi," *Biomedical Physics & Engineering Express*, vol. 2, no. 6, p. 065002, 2016.

[202] H. Gregersen, X. Lu, and J. Zhao, "Physiological growth is associated with esophageal morphometric and biomechanical changes in rats," *Neurogastroenterology & Motility*, vol. 16, no. 4, pp. 403–412, 2004.

[203] J. Zhao and H. Gregersen, "Esophageal morphometric and biomechanical changes during aging in rats," *Neurogastroenterology & Motility*, vol. 27, no. 11, pp. 1638–1647, 2015.

[204] A. Wareham and I. Whitmore, "A comparison of the mechanical properties of oesophageal striated muscle with skeletal muscles of the guinea pig.," *Pflugers Archiv: European Journal of Physiology*, vol. 395, no. 4, pp. 312–317, 1982.

[205] H. Gregersen, I. M. Giversen, L. M. Rasmussen, and A. Tøttrup, "Biomechanical wall properties and collagen content in the partially obstructed opossum esophagus," *Gastroenterology*, vol. 103, no. 5, pp. 1547–1551, 1992.

[206] C. O. Juhl, L. Vinter-Jensen, J. Djurhuus, H. Gregersen, and E. Z. Dajani, "Biomechanical properties of the oesophagus damaged by endoscopic sclerotherapy: An impedance planimetric study in minipigs," *Scandinavian Journal of Gastroenterology*, vol. 29, no. 10, pp. 867–873, 1994.

[207] B. K. Tay, J. Kim, and M. A. Srinivasan, "In vivo mechanical behavior of intra-abdominal organs," *IEEE Transactions on Biomedical Engineering*, vol. 53, no. 11, pp. 2129–2138, 2006.

[208] C. Lin, Q. Yu, J. Wang, W. Ji, W. Li, and Z. Zhou, "Friction behavior between endoscopy and esophageal internal surface," *Wear*, vol. 376, pp. 272–280, 2017.

[209] W. Yang, T. Fung, K. Chian, and C. Chong, "3d mechanical properties of the layered esophagus: experiment and constitutive model.," *Journal of Biomechanical Engineering*, vol. 128, no. 6, pp. 899–908, 2006.

[210] Y. Taira, K. Kamiya, Y. Shiraishi, H. Miura, T. Shiga, M. Hashem, A. Yamada, Y. Tsuboko, K. Sano, D. Homma, *et al.*, "Examination of natural esophageal mechanical properties for the design of an artificial esophagus," *Transactions of Japanese Society for Medical and Biological Engineering*, vol. 52, no. Supplement, pp. O–557–O–558, 2014.

[211] S. F. Badylak, D. A. Vorp, A. R. Spievack, A. Simmons-Byrd, J. Hanke, D. O. Freytes, A. Thapa, T. W. Gilbert, and A. Nieponice, "Esophageal reconstruction with ecm and muscle tissue in a dog model," *Journal of Surgical Research*, vol. 128, no. 1, pp. 87–97, 2005.

[212] X. Lu and H. Gregersen, "Regional distribution of axial strain and circumferential residual strain in the layered rabbit oesophagus," *Journal of Biomechanics*, vol. 34, no. 2, pp. 225–233, 2001.

[213] D. Liao, J. Cassin, J. Zhao, and H. Gregersen, "The geometric configuration and morphometry of the rabbit oesophagus during luminal pressure loading," *Physiological Measurement*, vol. 27, no. 8, p. 703, 2006.

[214] D. Liao, Y. Fan, Y. Zeng, and H. Gregersen, "Stress distribution in the layered wall of the rat oesophagus," *Medical Engineering & Physics*, vol. 25, no. 9, pp. 731–738, 2003.

[215] J. Assentoft, H. Gregersen, and W. O'Brien Jr, "Propagation speed of sound assessment in the layers of the guinea-pig esophagus in vitro by means of acoustic microscopy," *Ultrasonics*, vol. 39, no. 4, pp. 263–268, 2001.

[216] H. Gregersen, C. Lee, S. Chien, R. Skalak, and Y. Fung, "Strain distribution in the layered wall of the esophagus," *Journal of Biomechanical Engineering*, vol. 121, pp. 442–448, 1999.

[217] Y. Fan, J. Zhao, D. Liao, and H. Gregersen, "The effect of digestion of collagen and elastin on histomorphometry and the zero-stress state in rat esophagus," *Digestive Diseases and Sciences*, vol. 50, no. 8, pp. 1497–1505, 2005.

[218] C. Lin, W. Li, H. Deng, K. Li, and Z. Zhou, "Friction behavior of esophageal mucosa under axial and circumferential extension," *Tribology Letters*, vol. 67, no. 1, pp. 1–14, 2019.

[219] H. Ngwangwa, T. Pandelani, M. Msibi, I. Mabuda, L. Semakane, and F. Nemavhola, "Biomechanical analysis of sheep oesophagus subjected to biaxial testing including hyperelastic constitutive model fitting," *Heliyon*, vol. 8, no. 5, p. e09312, 2022.

[220] H. Gregersen, L. Vinter-Jensen, C. O. Juhl, and E. Z. Dajani, "Impedance planimetric characterization of the distal oesophagus in the goettingen minipig," *Journal of Biomechanics*, vol. 29, no. 1, pp. 63–68, 1996.

[221] A. Merlo and S. Cohen, "Mechanics and neuropeptide responses of feline pylorus and gastric muscle in vitro," *American Journal of Physiology-Gastrointestinal and Liver Physiology*, vol. 256, no. 5, pp. G862–G867, 1989.

[222] L. Klemm, R. Seydewitz, M. Borsdorf, T. Siebert, and M. Böl, "On a coupled electrochemomechanical model of gastric smooth muscle contraction," *Acta Biomaterialia*, vol. 109, pp. 163–181, 2020.

[223] C. Salmaso, I. Toniolo, C. Fontanella, P. Da Roit, A. Albanese, L. Polese, C. Stefanini, M. Foletto, and E. Carniel, "Computational tools for the reliability assessment and the engineering design of procedures and devices in bariatric surgery," *Annals of Biomedical Engineering*, vol. 48, no. 10, pp. 2466–2483, 2020.

[224] H. Saraf, K. Ramesh, A. Lennon, A. Merkle, and J. Roberts, "Mechanical properties of soft human tissues under dynamic loading," *Journal of Biomechanics*, vol. 40, no. 9, pp. 1960–1967, 2007.

[225] Y.-J. Lim, D. Deo, T. P. Singh, D. B. Jones, and S. De, "In situ measurement and modeling of biomechanical response of human cadaveric soft tissues for physics-based surgical simulation," *Surgical Endoscopy*, vol. 6, no. 23, pp. 1298–1307, 2009.

[226] C. G. Fontanella, C. Salmaso, I. Toniolo, N. de Cesare, A. Rubini, G. M. De Benedictis, and E. L. Carniel, "Computational models for the mechanical investigation of stomach tissues and structure," *Annals of Biomedical Engineering*, vol. 47, no. 5, pp. 1237–1249, 2019.

[227] M. Kunkel, A. Moral, R. Westphal, D. Rode, M. Rilk, and F. Wahl, "Using robotic systems in order to determine biomechanical properties of soft tissues.," *Studies in Health Technology and Informatics*, vol. 133, pp. 156–165, 2008.

[228] D. Liao, J. Zhao, and H. Gregersen, "Regional surface geometry of the rat stomach based on three-dimensional curvature analysis," *Physics in Medicine & Biology*, vol. 50, no. 2, p. 231, 2004.

[229] J. Zhao, D. Liao, P. Chen, P. Kunwald, and H. Gregersen, "Stomach stress and strain depend on location, direction and the layered structure," *Journal of Biomechanics*, vol. 41, pp. 3441–7, 2008.

[230] F. S. Julie, H. T. Strøm, P. Mette, G. Hans, and N. J. Vinge, "Dynamic viscoelastic properties of porcine gastric tissue: Effects of loading frequency, region and direction," *Journal of Biomechanics*, vol. 143, p. 111302, 2022.

[231] R. Aydin, S. Brandstaeter, F. Braeu, M. Steigenberger, R. Marcus, K. Nikolaou, M. Notohamiprodjo, and C. Cyron, "Experimental characterization of the biaxial mechanical properties of porcine gastric tissue," *Journal of the Mechanical Behavior of Biomedical Materials*, vol. 74, pp. 499–506, 2017.

[232] M. Bauer, E. Morales-Orcajo, L. Klemm, R. Seydewitz, V. Fiebach, T. Siebert, and M. Böl, "Biomechanical and microstructural characterisation of the porcine stomach wall: location- and layer-dependent investigations," *Acta Biomaterialia*, vol. 102, pp. 83–99, 2020.

[233] A. Shafik, "Effect of duodenal distension on the pyloric sphincter and antrum and the gastric corpus: Duodenopyloric reflex," *World Journal of Surgery*, vol. 22, no. 10, pp. 1061–1064, 1998.

[234] J. Zhao, H. Sha, S. Zhou, X. Tong, F. Zhuang, and H. Gregersen, "Remodelling of zero-stress state of small intestine in streptozotocin-induced diabetic rats. Effect of gliclazide," *Digestive and Liver Disease*, vol. 34, no. 10, pp. 707–716, 2002.

[235] J. Zhao, P. Chen, and H. Gregersen, "Morpho-mechanical intestinal remodeling in type 2 diabetic gk rats–is it related to advanced glycation end product formation?," *Journal of Biomechanics*, vol. 46, no. 6, pp. 1128–34, 2013.

[236] J. Zhao, J. Yang, D. Liao, and H. Gregersen, "Interdependency between mechanical parameters and afferent nerve discharge in remodeled diabetic goto-kakizaki rat intestine," *Clinical and Experimental Gastroenterology*, vol. 10, pp. 303–314, 2017.

[237] R. S. Radhakrishnan, H. Xue, N. Weisbrodt, F. A. Moore, S. J. Allen, G. A. Laine, and C. S. Cox Jr, "Resuscitation-induced intestinal edema decreases the stiffness and residual stress of the intestine," *Shock*, vol. 24, no. 2, pp. 165–170, 2005.

[238] R. S. Radhakrishnan, H. Xue, S. D. Moore-Olufemi, N. W. Weisbrodt, F. A. Moore, S. J. Allen, G. A. Laine, and C. S. Cox Jr, "Hypertonic saline resuscitation prevents hydrostatically induced intestinal edema and ileus," *Critical Care Medicine*, vol. 34, no. 6, pp. 1713–1718, 2006.

[239] J.-B. Zhao, P.-M. Chen, and H. Gregersen, "Changes of phasic and tonic smooth muscle function of jejunum in type 2 diabetic goto-kakizaki rats," *World Journal of Diabetes*, vol. 4, no. 6, p. 339, 2013.

[240] J. W. Peck and F. A. Gibbs Jr, "Assay of premorbid murine jejunal fibrosis based on mechanical changes after x irradiation and hyperthermia," *Radiation Research*, vol. 112, no. 3, pp. 525–543, 1987.

[241] H. S. Hosseini and J. C. Dunn, "Biomechanical force prediction for lengthening of small intestine during distraction enterogenesis," *Bioengineering*, vol. 7, no. 4, p. 140, 2020.

[242] X. Lu, J. Zhao, and H. Gregersen, "Small intestinal morphometric and biomechanical changes during physiological growth in rats," *Journal of Biomechanics*, vol. 38, no. 3, pp. 417–426, 2005.

[243] L. Vinter-Jensen, B. U. Duch, J. A. K. Petersen, A. Ryslev, and H. Gregersen, "Systemic treatment with epidermal growth factor in the rat. Biomechanical properties of the growing small intestine," *Regulatory Peptides*, vol. 61, no. 2, pp. 135–142, 1996.

[244] J. Zhao, J. Yang, L. Vinter-Jensen, F. Zhuang, and H. Gregersen, "The morphometry and biomechanical properties of the rat small intestine after systemic treatment with epidermal growth factor," *Biorheology*, vol. 39, no. 6, pp. 719–733, 2002.

[245] D. Liao, J. Yang, J. Zhao, Y. Zeng, L. Vinter-Jensen, and H. Gregersen, "The effect of epidermal growth factor on the incremental young's moduli in the rat small intestine," *Medical Engineering & Physics*, vol. 25, no. 5, pp. 413–418, 2003.

[246] J. Yang, J.-B. Zhao, Y.-J. Zeng, and H. Gregersen, "Biomechanical properties of ileum after systemic treatment with epithelial growth factor," *World Journal of Gastroenterology*, vol. 9, no. 10, p. 2278, 2003.

[247] D. Liao, J. Zhao, and H. Gregersen, "3d mechanical properties of the partially obstructed guinea pig small intestine," *Journal of Biomechanics*, vol. 43, no. 11, pp. 2079–2086, 2010.

[248] D. Sun, J. Zhao, D. Liao, P. Chen, and H. Gregersen, "Shear modulus of the partially obstructed rat small intestine," *Annals of Biomedical Engineering*, vol. 45, no. 4, pp. 1069–1082, 2017.

[249] J. Zhao, D. Liao, J. Yang, and H. Gregersen, "Biomechanical remodelling of obstructed guinea pig jejunum," *Journal of Biomechanics*, vol. 43, no. 7, pp. 1322–1329, 2010.

[250] D. Sun, J. Zhao, D. Liao, Z. Huang, and H. Gregersen, "The turning point for morphomechanical remodeling during complete intestinal obstruction in rats occurs after 12–24 h," *Annals of Biomedical Engineering*, vol. 46, no. 5, pp. 705–716, 2018.

[251] J. Zhao, D. Liao, J. Yang, and H. Gregersen, "Phasic and tonic smooth muscle function of the partially obstructed guinea pig intestine," *Journal of Biomedicine and Biotechnology*, vol. 2011, no. 3, p. 489720, 2011.

[252] J. Zhao, D. Liao, J. Yang, and H. Gregersen, "Stress and strain analysis of contractions during ramp distension in partially obstructed guinea pig jejunal segments," *Journal of Biomechanics*, vol. 44, no. 11, pp. 2077–2082, 2011.

[253] J. Zhao and H. Gregersen, "Morphometric and biomechanical remodeling of the small intestine during aging in rats," *Journal of Biomechanics*, vol. 48, no. 16, pp. 4271–4278, 2015.

[254] Y. Dou, S. Gregersen, J. Zhao, F. Zhuang, and H. Gregersen, "Morphometric and biomechanical intestinal remodeling induced by fasting in rats," *Digestive Diseases and Sciences*, vol. 47, no. 5, pp. 1158–1168, 2002.

[255] Y. Dou, S. Gregersen, J. Zhao, F. Zhuang, and H. Gregersen, "Effect of re-feeding after starvation on biomechanical properties in rat small intestine," *Medical Engineering & Physics*, vol. 23, no. 8, pp. 557–566, 2001.

[256] P. Chen, J. Zhao, V. H. Nielsen, T. Clausen, and H. Gregersen, "Intestinal remodelling in mink fed with reduced protein content," *Journal of Biomechanics*, vol. 42, no. 4, pp. 443–448, 2009.

[257] Y. Liu, J. Zhao, D. Liao, L. Bao, and H. Gregersen, "Low-residue diet fed to rabbits induces histomorphological and biomechanical remodeling of small intestine," *Neurogastroenterology & Motility*, vol. 29, no. 4, p. e12983, 2017.

[258] Y. Liu, J. Zhao, D. Liao, G. Wang, and H. Gregersen, "Stress–strain analysis of duodenal contractility in response to flow and ramp distension in rabbits fed low-fiber diet," *Neurogastroenterology & Motility*, vol. 31, no. 1, p. e13476, 2019.

[259] H. Elbrønd, A. Tøttrup, and A. Forman, "Mechanical properties of isolated smooth muscle from rabbit sphincter of oddi and duodenum," *Scandinavian Journal of Gastroenterology*, vol. 26, no. 3, pp. 289–294, 1991.

[260] J. Zhao, D. Liao, and H. Gregersen, "Phasic and tonic stress-strain data obtained in intact intestinal segment in vitro," *Digestive Diseases and Sciences*, vol. 53, no. 12, pp. 3145–3151, 2008.

[261] B. S. Terry, A. B. Lyle, J. A. Schoen, and M. E. Rentschler, "Preliminary mechanical characterization of the small bowel for in vivo robotic mobility," *Journal of Biomechanical Engineering*, vol. 133, no. 9, p. 091010, 2011.

[262] J. Pedersen, C. Gao, H. Egekvist, P. Bjerring, L. Arendt-Nielsen, H. Gregersen, and A. M. Drewes, "Pain and biomechanical responses to distention of the duodenum in patients with systemic sclerosis," *Gastroenterology*, vol. 124, no. 5, pp. 1230–1239, 2003.

[263] H. Gregersen, D. Liao, J. Pedersen, and A. Drewes, "A new method for evaluation of intestinal muscle contraction properties: studies in normal subjects and in patients with systemic sclerosis," *Neurogastroenterology & Motility*, vol. 19, no. 1, pp. 11–19, 2007.

[264] F. Gao, D. Liao, A. M. Drewes, and H. Gregersen, "Modelling the elastin, collagen and smooth muscle contribution to the duodenal mechanical behaviour in patients with systemic sclerosis," *Neurogastroenterology & Motility*, vol. 21, no. 9, pp. 914–e68, 2009.

[265] C. Gao, L. Arendt-Nielsen, W. Liu, P. Petersen, A. M. Drewes, and H. Gregersen, "Sensory and biomechanical responses to ramp-controlled distension of the human duodenum," *American Journal of Physiology-Gastrointestinal and Liver Physiology*, vol. 284, no. 3, pp. G461–G471, 2003.

[266] B. Johnson, S. Campbell, and N. Campbell-Kyureghyan, "Biomechanical properties of abdominal organs under tension with special reference to increasing strain rate," *Journal of Biomechanics*, vol. 109, p. 109914, 2020.

[267] S. Bourgouin, T. Bège, C. Masson, P. Arnoux, J. Mancini, S. Garcia, C. Brunet, and S. Berdah, "Biomechanical characterisation of fresh and cadaverous human small intestine: applications for abdominal trauma.," *Medical & Biological Engineering & Computing*, vol. 50, no. 12, pp. 1279–1288, 2012.

[268] B. S. Terry, X. Wang, J. A. Schoen, and M. E. Rentschler, "A preconditioning protocol and biaxial mechanical measurement of the small intestine," *International Journal of Experimental and Computational Biomechanics*, vol. 2, no. 4, pp. 293–309, 2014.

[269] H. Zhou, G. Alici, T. D. Than, and W. Li, "Experimental investigation into biomechanical and biotribological properties of a real intestine and their significance for design of a spiral-type robotic capsule," *Proceedings of the Institution of Mechanical Engineers, Part H: Journal of Engineering in Medicine*, vol. 228, no. 3, pp. 280–286, 2014.

[270] C. Zhang, H. Liu, R. Tan, and H. Li, "Interaction model between capsule robot and intestine based on nonlinear viscoelasticity," *Proceedings of the Institution of Mechanical Engineers, Part H: Journal of Engineering in Medicine*, vol. 228, no. 3, pp. 287–296, 2014.

[271] C. Jørgensen, F. Dall, J. Storkholm, S. Jensen, and H. Gregersen, "Elastic properties of the isolated perfused porcine duodenum," *Digestive Diseases*, vol. 9, no. 6, pp. 401–407, 1991.

[272] M. Lyons, D. Winter, and C. Simms, "Extrusion properties of porcine intestines and surrogate materials for ventral hernia modelling.," *Journal of the Mechanical Behavior of Biomedical Materials*, vol. 18, pp. 57–66, 2012.

[273] C. Gao, J. Zhao, and H. Gregersen, "Histomorphometry and strain distribution in pig duodenum with reference to zero-stress state," *Digestive Diseases and Sciences*, vol. 45, no. 8, pp. 1500–1508, 2000.

[274] X. Chen, J. Zhao, and H. Gregersen, "The villi contribute to the mechanics in the guinea pig small intestine," *Journal of Biomechanics*, vol. 41, no. 4, pp. 806–812, 2008.

[275] J. Yang, J. Zhao, W. Jiang, T. Nakaguchi, P. Kunwald, D. Grundy, and H. Gregersen, "Neurogenic adaptation contributes to the afferent response to mechanical stimulation," *American Journal of Physiology-Gastrointestinal and Liver Physiology*, vol. 302, no. 9, pp. G1025–G1034, 2012.

[276] J. Storkholm, G. Villadsen, S. Jensen, and H. Gregersen, "Passive elastic wall properties in isolated guinea pig small intestine," *Digestive Diseases and Sciences*, vol. 40, no. 5, pp. 976–982, 1995.

[277] E. L. Carniel, A. Rubini, A. Frigo, and A. N. Natali, "Analysis of the biomechanical behaviour of gastrointestinal regions adopting an experimental and computational approach," *Computer methods and programs in biomedicine*, vol. 113, no. 1, pp. 338–345, 2014.

[278] H. Gregersen, G. Kassab, E. Pallencaoe, C. Lee, S. Chien, R. Skalak, and Y. Fung, "Morphometry and strain distribution in guinea pig duodenum with reference to the zero-stress

state," *American Journal of Physiology-Gastrointestinal and Liver Physiology*, vol. 273, no. 4, pp. G865–G874, 1997.

[279] J.-B. Zhao, H. Sha, F.-Y. Zhuang, and H. Gregersen, "Morphological properties and residual strain along the small intestine in rats," *World Journal of Gastroenterology*, vol. 8, no. 2, pp. 312–317, 2002.

[280] Y. Dou, J. Zhao, and H. Gregersen, "Morphology and stress-strain properties along the small intestine in the rat," *Journal of Biomechanical Engineering*, vol. 125, no. 2, pp. 266–273, 2003.

[281] J. B. Smith, J.-B. Zhao, Y.-L. Dou, and H. Gregersen, "Time-dependent viscoelastic properties along rat small intestine," *World Journal of Gastroenterology*, vol. 11, no. 32, pp. 4974–4978, 2005.

[282] J. Li, J. Zhao, D. Liao, and H. Gregersen, "Effect of smooth muscle tone on morphometry and residual strain in rat duodenum, jejunum and ileum," *Journal of Biomechanics*, vol. 41, no. 12, pp. 2667–2672, 2008.

[283] D. Sokolis, "Experimental study and biomechanical characterization for the passive small intestine: Identification of regional differences.," *Journal of the Mechanical Behavior of Biomedical Materials*, vol. 74, pp. 93–105, 2017.

[284] C. Jørgensen, F. Dall, S. Jensen, and H. Gregersen, "A new combined high-frequency ultrasound-impedance planimetry measuring system for the quantification of organ wall biomechanics in vivo," *Journal of Biomechanics*, vol. 28, no. 7, pp. 863–867, 1995.

[285] C. Hillemeier and P. Biancani, "Mechanical properties of obstructed colon in a hirschsprung's model," *Gastroenterology*, vol. 99, no. 4, pp. 995–1000, 1990.

[286] R. W. Stidham, J. Xu, L. A. Johnson, K. Kim, D. S. Moons, B. J. McKenna, J. M. Rubin, and P. D. Higgins, "Ultrasound elasticity imaging for detecting intestinal fibrosis and inflammation in rats and humans with Crohn's disease," *Gastroenterology*, vol. 141, no. 3, pp. 819–826, 2011.

[287] X. Gong, X. Xu, S. Lin, Y. Cheng, J. Tong, and Y. Li, "Alterations in biomechanical properties and microstructure of colon wall in early-stage experimental colitis," *Experimental and Therapeutic Medicine*, vol. 14, no. 2, pp. 995–1000, 2017.

[288] A. Nair, C. H. Liu, S. Das, T. Ho, Y. Du, S. Soomro, C. Mohan, and K. V. Larin, "Detecting murine inflammatory bowel disease using optical coherence elastography," in *2018 40th Annual International Conference of the IEEE Engineering in Medicine and Biology Society (EMBC)*, pp. 830–833, IEEE, 2018.

[289] A. Nair, C. H. Liu, M. Singh, S. Das, T. Le, Y. Du, S. Soomro, S. Aglyamov, C. Mohan, and K. V. Larin, "Assessing colitis ex vivo using optical coherence elastography in a murine model," *Quantitative Imaging in Medicine and Surgery*, vol. 9, no. 8, p. 1429, 2019.

[290] H. Christensen, A. Flyvbjerg, H. Ørskov, and S. Laurberg, "Effect of growth hormone on the inflammatory activity of experimental colitis in rats," *Scandinavian Journal of Gastroenterology*, vol. 28, no. 6, pp. 503–511, 1993.

[291] J. Yang, J. Zhao, T. Nakaguchi, and H. Gregersen, "Biomechanical changes in oxazolone-induced colitis in balb/c mice," *Journal of Biomechanics*, vol. 42, no. 7, pp. 811–817, 2009.

[292] P. Deptuła, D. Łysik, K. Pogoda, M. Cieśluk, A. Namiot, J. Mystkowska, G. Król, S. Głuszek, P. A. Janmey, and R. Bucki, "Tissue rheology as a possible complementary procedure to advance histological diagnosis of colon cancer," *ACS Biomaterials Science & Engineering*, vol. 6, no. 10, pp. 5620–5631, 2020.

[293] W. Percy, M. Burton, F. Fallick, and R. Burakoff, "A comparison in vitro of human and rabbit distal colonic muscle responses to inflammatory mediators," *Gastroenterology*, vol. 99, no. 5, pp. 1324–1332, 1990.

[294] J. Yang, J. Zhao, Y. Zeng, L. Vinter-Jensen, and H. Gregersen, "Morphological properties of zero-stress state in rat large intestine during systemic egf treatment," *Digestive Diseases and Sciences*, vol. 48, no. 3, pp. 442–448, 2003.

[295] D. Watters, A. Smith, M. Eastwood, K. Anderson, and R. Elton, "Mechanical properties of the rat colon: the effect of age, sex and different conditions of storage," *Quarterly Journal of Experimental Physiology: Translation and Integration*, vol. 70, no. 1, pp. 151–162, 1985.

[296] D. Massalou, C. Masson, S. Afquir, P. Baque, P.-J. Arnoux, and T. Bège, "Influence of gender, age, shelf-life, and conservation method on the biomechanical behavior of colon tissue under dynamic solicitation," *Clinical Biomechanics*, vol. 65, pp. 34–40, 2019.

[297] D. Watters, A. Smith, M. Eastwood, K. Anderson, R. Elton, and J. Mugerwa, "Mechanical properties of the colon: comparison of the features of the african and european colon in vitro.," *Gut*, vol. 26, no. 4, pp. 384–392, 1985.

[298] P. Petersen, C. Gao, P. Rössel, P. Qvist, L. Arendt-Nielsen, H. Gregersen, and A. M. Drewes, "Sensory and biomechanical responses to distension of the normal human rectum and sigmoid colon," *Digestion*, vol. 64, no. 3, pp. 191–199, 2001.

[299] M. Pescatori, F. Grassetti, G. Ronzoni, R. Mancinelli, A. Bertuzzi, and S. Salinari, "Peristalsis in distal colon of the rabbit: an analysis of mechanical events.," *American Journal of Physiology-Endocrinology and Metabolism*, vol. 236, no. 4, p. E464, 1979.

[300] R. Gill, K. Cote, K. Bowes, and Y. Kingma, "Human colonic smooth muscle: spontaneous contractile activity and response to stretch.," *Gut*, vol. 27, no. 9, pp. 1006–1013, 1986.

[301] A. Merlo and S. Cohen, "Neuropeptide responses and mechanics of the proximal and distal feline colon in vitro," *American Journal of Physiology-Gastrointestinal and Liver Physiology*, vol. 255, no. 6, pp. G787–G793, 1988.

[302] A. E. Bharucha, R. D. Hubmayr, I. J. Ferber, and A. R. Zinsmeister, "Viscoelastic properties of the human colon," *American Journal of Physiology-Gastrointestinal and Liver Physiology*, vol. 281, no. 2, pp. G459–G466, 2001.

[303] A. Bhattarai, A. J. Horbach, M. Staat, W. Kowalczyk, and T. N. Tran, "Virgin passive colon biomechanics and a literature review of active contraction constitutive models," *Biomechanics*, vol. 2, no. 2, pp. 138–157, 2022.

[304] B. Patel, H. Chen, A. Ahuja, J. F. Krieger, J. Noblet, S. Chambers, and G. S. Kassab, "Constitutive modeling of the passive inflation-extension behavior of the swine colon," *Journal of the Mechanical Behavior of Biomedical Materials*, vol. 77, pp. 176–186, 2018.

[305] M. Higa, Y. Luo, T. Okuyama, T. Takagi, Y. Shiraishi, and T. Yambe, "Passive mechanical properties of large intestine under in vivo and in vitro compression.," *Medical Engineering & Physics*, vol. 29, no. 8, pp. 840–844, 2006.

[306] S. Itasaka, K. Shiratori, T. Takahashi, M. Ishikawa, K. Kaneko, and Y. Suzuki, "Stimulation of intramural secretory reflex by luminal distension pressure in rat distal colon," *American Journal of Physiology-Gastrointestinal and Liver Physiology*, vol. 263, no. 1, pp. G108–G114, 1992.

[307] C. Gao and H. Gregersen, "Biomechanical and morphological properties in rat large intestine," *Journal of Biomechanics*, vol. 33, no. 9, pp. 1089–1097, 2000.

[308] S. Siri, F. Maier, L. Chen, S. Santos, D. M. Pierce, and B. Feng, "Differential biomechanical properties of mouse distal colon and rectum innervated by the splanchnic and pelvic afferents," *American Journal of Physiology-Gastrointestinal and Liver Physiology*, vol. 316, no. 4, pp. G473–G481, 2019.

[309] D. Massalou, C. Masson, P. Foti, S. Afquir, P. Baqué, S.-V. Berdah, and T. Bège, "Dynamic biomechanical characterization of colon tissue according to anatomical factors," *Journal of Biomechanics*, vol. 49, no. 16, pp. 3861–3867, 2016.

[310] D. Massalou, C. Masson, S. Afquir, P. Baqué, P.-J. Arnoux, and T. Bège, "Mechanical effects of load speed on the human colon," *Journal of Biomechanics*, vol. 91, pp. 102–108, 2019.

[311] P. Ciarletta, P. Dario, F. Tendick, and S. Micera, "Hyperelastic model of anisotropic fiber reinforcements within intestinal walls for applications in medical robotics," *The International Journal of Robotics Research*, vol. 28, no. 10, pp. 1279–1288, 2009.

[312] E. L. Carniel, V. Gramigna, C. G. Fontanella, C. Stefanini, and A. N. Natali, "Constitutive formulations for the mechanical investigation of colonic tissues," *Journal of Biomedical Materials Research Part A*, vol. 102, no. 5, pp. 1243–1254, 2014.

[313] S. Puértolas, E. Peña, A. Herrera, E. Ibarz, and L. Gracia, "A comparative study of hyperelastic constitutive models for colonic tissue fitted to multiaxial experimental testing," *Journal of the Mechanical Behavior of Biomedical Materials*, vol. 102, p. 103507, 2020.

[314] A. Bhattarai, C. A. May, M. Staat, W. Kowalczyk, and T. N. Tran, "Layer-specific damage modeling of porcine large intestine under biaxial tension," *Bioengineering*, vol. 9, no. 10, p. 528, 2022.

[315] D. P. Sokolis and S. G. Sassani, "Microstructure-based constitutive modeling for the large intestine validated by histological observations," *Journal of the Mechanical Behavior of Biomedical Materials*, vol. 21, pp. 149–166, 2013.

[316] S. Siri, F. Maier, S. Santos, D. M. Pierce, and B. Feng, "Load-bearing function of the colorectal submucosa and its relevance to visceral nociception elicited by mechanical stretch," *American Journal of Physiology-Gastrointestinal and Liver Physiology*, vol. 317, no. 3, pp. G349–G358, 2019.

[317] M. Higa, Y. Luo, T. Okuyama, T. Takagi, Y. Shiraishi, and T. Yambe, "Passive mechanical properties of large intestine under in vivo and in vitro compression," *Medical Engineering & Physics*, vol. 29, no. 8, pp. 840–844, 2007.

[318] E. Glavind, A. Forman, G. Madsen, D. Svane, K. Andersson, and A. Tottrup, "Mechanical properties of isolated smooth muscle from human rectum and internal anal sphincter," *American Journal of Physiology-Gastrointestinal and Liver Physiology*, vol. 265, no. 4, pp. G792–G798, 1993.

[319] H. Gregersen, L. Lundby, and J. Overgaard, "Early and late effects of irradiation on morphometry and residual strain of mouse rectum," *Digestive Diseases and Sciences*, vol. 47, no. 7, pp. 1472–1479, 2002.

[320] I. Brunenieks, K. Pekarska, V. Kasyanov, and V. Groma, "Biomechanical and morphological peculiarities of the rectum in patients with obstructed defecation syndrome.," *Romanian Journal of Morphology and Embryology= Revue Roumaine de Morphologie et Embryologie*, vol. 58, no. 4, pp. 1193–1200, 2017.

[321] P. Arhan, G. Devroede, K. Danis, C. Dornic, C. Faverdin, B. Persoz, D. Pellerin, *et al.*, "Viscoelastic properties of the rectal wall in Hirschsprung's disease," *The Journal of clinical investigation*, vol. 62, no. 1, pp. 82–87, 1978.

[322] L. Lundby, F. Dall, H. Gregersen, J. Overgaard, and S. Laurberg, "Distensibility of the mouse rectum: application of impedance planimetry for studying age-related changes," *Colorectal Disease*, vol. 1, pp. 34–41, 1999.

[323] A. M. Drewes, J. B. Frφkjær, E. Larsen, H. Reddy, L. Arendt-Nielsen, and H. Gregersen, "Pain and mechanical properties of the rectum in patients with active ulcerative colitis," *Inflammatory Bowel Diseases*, vol. 12, no. 4, pp. 294–303, 2006.

[324] S.-D. Pedro, C. Moreno-Sanz, A. Morandeira-Rivas, J. M. Tenías-Burillo, C. Alhambra-Rodríguez De Guzmán, *et al.*, "Colorectal anastomosis facilitated by the use of the ligasure® sealing device: comparative study in an animal model," *Surgical Endoscopy*, vol. 28, no. 2, pp. 508–514, 2014.

[325] F. Dall, C. Jørgensen, D. Houe, H. Gregersen, and J. Djurhuus, "Biomechanical wall properties of the human rectum. a study with impedance planimetry.," *Gut*, vol. 34, no. 11, pp. 1581–1586, 1993.

[326] F. Dall, C. Jørgensen, J. Djurhuus, and H. Gregersen, "Biomechanical wall properties of the porcine rectum: a study using impedance planimetry," *Digestive Diseases*, vol. 9, no. 6, pp. 347–353, 1991.

[327] J. B. Frøkjær, D. Liao, A. Bergmann, B. McMahon, E. Steffensen, A. M. Drewes, and H. Gregersen, "Three-dimensional biomechanical properties of the human rectum evaluated with magnetic resonance imaging," *Neurogastroenterology & Motility*, vol. 17, no. 4, pp. 531–540, 2005.

[328] M. Righi and V. Balbi, "Foundations of viscoelasticity and application to soft tissue mechanics," in *Modeling Biomaterials*, pp. 71–103, Springer, 2021.

[329] D. Liao, X. Lu, A. J. Kirkup, W. Jiang, D. Grundy, and H. Gregersen, "Interdependency of stress relaxation and afferent nerve discharge in rat small intestine," *Journal of Biomechanics*, vol. 45, no. 9, pp. 1574–1579, 2012.

[330] A. Dorfmann and R. W. Ogden, "A constitutive model for the mullins effect with permanent set in particle-reinforced rubber," *International Journal of Solids and Structures*, vol. 41, no. 7, pp. 1855–1878, 2004.

[331] S. Nicolle and J.-F. Palierne, "Dehydration effect on the mechanical behaviour of biological soft tissues: observations on kidney tissues," *Journal of the Mechanical Behavior of Biomedical Materials*, vol. 3, no. 8, pp. 630–635, 2010.

[332] W. Goth, J. Lesicko, M. S. Sacks, and J. W. Tunnell, "Optical-based analysis of soft tissue structures," *Annual Review of Biomedical Engineering*, vol. 18, pp. 357–385, 2016.

[333] S. Donmazov, S. Piskin, and K. Pekkan, "Noninvasive in vivo determination of residual strains and stresses," *Journal of Biomechanical Engineering*, vol. 137, no. 6, p. 061011, 2015.

[334] J. Brasseur, M. Nicosia, A. Pal, and L. Miller, "Function of longitudinal vs circular muscle fibers in esophageal peristalsis, deduced with mathematical modeling.," *World Journal of Gastroenterology*, vol. 13, no. 9, pp. 1335–1346, 2007.

[335] "Chapter 7 - Esophagus," in *Biomechanics of Living Organs* (Y. Payan and J. Ohayon, eds.), vol. 1 of *Translational Epigenetics*, pp. 147–167, Oxford: Academic Press, 2017.

[336] J. Ruan, R. El-Jawahri, L. Chai, S. Barbat, and P. Prasad, "Prediction and analysis of human thoracic impact responses and injuries in cadaver impacts using a full human body finite element model," *Stapp Car Crash Journal*, vol. 47, pp. 299–321, 2003.

[337] S.-W. Khoo, S. Karuppanan, and C.-S. Tan, "A review of surface deformation and strain measurement using two-dimensional digital image correlation," *Metrology and Measurement Systems*, vol. 23, no. 3, pp. 461–480, 2016.

[338] L. Huang, R. K. Korhonen, M. J. Turunen, and M. A. Finnilä, "Experimental mechanical strain measurement of tissues," *PeerJ*, vol. 7, p. e6545, 2019.

[339] M. F. Ferhatoglu and T. Kıvılcım, "Anatomy of esophagus," in *Esophageal Abnormalities*, IntechOpen, 2017.

[340] R. Mittal, "Motor function of the pharynx, esophagus, and its sphincters," in *Colloquium Series on Integrated Systems Physiology: From Molecule to Function*, vol. 3, pp. 1–84, Morgan & Claypool Life Sciences, 2011.

[341] B. Kuo and D. Urma, "Esophagus-anatomy and development," *GI Motility Online*, 2006.

[342] K. Canene-Adams, "Preparation of formalin-fixed paraffin-embedded tissue for immunohistochemistry," *Methods in Enzymology*, vol. 533, pp. 225–233, 2013.

[343] C. A. Schneider, W. S. Rasband, and K. W. Eliceiri, "NIH Image to ImageJ: 25 years of image analysis," *Nature Methods*, vol. 9, no. 7, pp. 671–675, 2012.

[344] S. Liu and Y. Fung, "Relationship between hypertension, hypertrophy, and opening angle of zero-stress state of arteries following aortic constriction," *Journal of Biomechanical Engineering*, vol. 111, no. 4, pp. 325–335, 1989.

[345] IBM Corp., "IBM SPSS Statistics for Windows, Version 27.0," *Armonk, NY: IBM Corp*, 2020.

[346] R Core Team, "R: A language and environment for statistical computing," *R Foundation for Statistical Computing*, 2018.

[347] R. L. Kissell and J. Poserina, *Optimal sports math, statistics, and fantasy*. Academic Press, 2017.

[348] H. C. Thom, "A note on the gamma distribution," *Monthly Weather Review*, vol. 86, no. 4, pp. 117–122, 1958.

[349] D. G. Harlow, "Applications of the fréchet distribution function," *International Journal of Materials and Product Technology*, vol. 17, no. 5-6, pp. 482–495, 2002.

[350] G. Chagnon, J. Ohayon, J.-L. Martiel, and D. Favier, "Chapter 1 - hyperelasticity modeling for incompressible passive biological tissues," in *Biomechanics of Living Organs* (Y. Payan and J. Ohayon, eds.), vol. 1 of *Translational Epigenetics*, pp. 3–30, Oxford: Academic Press, 2017.

[351] Y. Fung, K. Fronek, and P. Patitucci, "Pseudoelasticity of arteries and the choice of its mathematical expression," *American Journal of Physiology - Heart and Circulatory Physiology*, vol. 6, no. 5, p. H620–H631, 1979.

[352] G. A. Holzapfel, T. C. Gasser, and R. W. Ogden, "A new constitutive framework for arterial wall mechanics and a comparative study of material models," *Journal of Elasticity and the Physical Science of Solids*, vol. 61, pp. 1–48, 2000.

[353] T. C. Gasser, R. W. Ogden, and G. A. Holzapfel, "Hyperelastic modelling of arterial layers with distributed collagen fibre orientations," *Journal of the Royal Society, Interface*, vol. 3, no. 6, pp. 15–35, 2006.

[354] G. A. Holzapfel and R. W. Ogden, "Constitutive modelling of arteries," *Proceedings of the Royal Society A: Mathematical, Physical and Engineering Sciences*, vol. 466, no. 2118, pp. 1551–1597, 2010.

[355] S. K. Panda and M. L. Buist, "A viscoelastic framework for inflation testing of gastrointestinal tissue," *Journal of the Mechanical Behavior of Biomedical Materials*, vol. 103, p. 103569, 2020.

[356] M. Higa, Y. Luo, T. Okuyama, Y. Shiraishi, H. Liu, T. Yambe, and T. Takagi, "In vivo measurements and constitutive modeling of colon tissue," in *World Congress on Medical Physics and Biomedical Engineering 2006*.

[357] M. Mooney, "A theory of large elastic deformation," *Journal of Applied Physics*, vol. 11, no. 9, pp. 582–592, 1940.

[358] N. Huber and C. Tsakmakis, "Finite deformation viscoelasticity laws," *Mechanics of Materials*, vol. 32, no. 1, pp. 1–18, 2000.

[359] J. Humphrey and F. Yin, "A new constitutive formulation for characterizing the mechanical behavior of soft tissues," *Biophysical Journal*, vol. 52, no. 4, pp. 563–570, 1987.

[360] E. L. Carniel, M. Mencattelli, G. Bonsignori, C. G. Fontanella, A. Frigo, A. Rubini, C. Stefanini, and A. N. Natali, "Analysis of the structural behaviour of colonic segments by inflation tests: Experimental activity and physio-mechanical model," *Proceedings of the Institution of Mechanical Engineers, Part H: Journal of Engineering in Medicine*, vol. 229, no. 11, pp. 794–803, 2015.

[361] J.-C. Petiteau, E. Verron, R. Othman, H. Le Sourne, J.-F. Sigrist, and G. Barras, "Large strain rate-dependent response of elastomers at different strain rates: convolution integral vs. internal variable formulations," *Mechanics of Time-Dependent Materials*, vol. 17, pp. 349–367, 2013.

[362] M. Rebouah, G. Machado, G. Chagnon, and D. Favier, "Anisotropic mullins stress softening of a deformed silicone holey plate," *Mechanics Research Communications*, vol. 49, pp. 36–43, 2013.

[363] M. Rebouah and G. Chagnon, "Permanent set and stress-softening constitutive equation applied to rubber-like materials and soft tissues," *Acta Mechanica*, vol. 225, no. 6, pp. 1685–1698, 2014.

[364] G. Holzapfel, *Nonlinear solid mechanics: a continuum approach for engineering science*. John Wiley & Sons, second print ed., 2001.

[365] N. Briot, *Caractérisation ex vivo et in vivo des tissus mous humains pour la modélisation biomécanique du sein*. PhD thesis, Université Grenoble Alpes, 2022.

[366] A. Pukaluk, H. Wolinski, C. Viertler, P. Regitnig, G. A. Holzapfel, and G. Sommer, "Changes in the microstructure of the human aortic adventitia under biaxial loading investigated by multi-photon microscopy," *Acta Biomaterialia*, vol. 161, pp. 154–169, 2023.

[367] T. C. Gasser and G. A. Holzapfel, "A rate-independent elastoplastic constitutive model for biological fiber-reinforced composites at finite strains: continuum basis, algorithmic formulation and finite element implementation," *Computational Mechanics*, vol. 29, no. 4, pp. 340–360, 2002.

[368] T. C. Gasser, "An irreversible constitutive model for fibrous soft biological tissue: a 3-d microfiber approach with demonstrative application to abdominal aortic aneurysms," *Acta Biomaterialia*, vol. 7, no. 6, pp. 2457–2466, 2011.

[369] E. Peña, "Prediction of the softening and damage effects with permanent set in fibrous biological materials," *Journal of the Mechanics and Physics of Solids*, vol. 59, no. 9, pp. 1808–1822, 2011.

[370] M. Rebouah and G. Chagnon, "Extension of classical viscoelastic models in large deformation to anisotropy and stress softening," *International Journal of Non-Linear Mechanics*, vol. 61, pp. 54–64, 2014.

[371] S. V. Eleswarapu, D. J. Responte, and K. A. Athanasiou, "Tensile properties, collagen content, and crosslinks in connective tissues of the immature knee joint," *PloS One*, vol. 6, no. 10, p. e26178, 2011.

[372] L. D. Muiznieks and F. W. Keeley, "Molecular assembly and mechanical properties of the extracellular matrix: A fibrous protein perspective," *Biochimica et Biophysica Acta (BBA)-Molecular Basis of Disease*, vol. 1832, no. 7, pp. 866–875, 2013.

[373] H. Trebacz and A. Barzycka, "Mechanical properties and functions of elastin: An overview," *Biomolecules*, vol. 13, no. 3, p. 574, 2023.

[374] Y.-C. Fung, *Biomechanics: circulation*. Springer Science & Business Media, 2013.

[375] C.-J. Chuong and Y.-C. Fung, "Residual stress in arteries," *Frontiers in Biomechanics*, pp. 117–129, 1986.

[376] X. Li and K. Hayashi, "Alternate method for the analysis of residual strain in the arterial wall," *Biorheology*, vol. 33, no. 6, pp. 439–449, 1996.

[377] D. C. Petsepe, S. K. Kourkoulis, S. A. Papadodima, and D. P. Sokolis, "Regional and age-dependent residual strains, curvature, and dimensions of the human ureter," *Proceedings of the Institution of Mechanical Engineers, Part H: Journal of Engineering in Medicine*, vol. 232, no. 2, pp. 149–162, 2018.

[378] C. T. McKee, J. A. Last, P. Russell, and C. J. Murphy, "Indentation versus tensile measurements of young's modulus for soft biological tissues," *Tissue Engineering Part B: Reviews*, vol. 17, no. 3, pp. 155–164, 2011.

[379] W. F. Larrabee Jr, "A finite element model of skin deformation. i. biomechanics of skin and soft tissue: a review," *The Laryngoscope*, vol. 96, no. 4, pp. 399–405, 1986.

[380] S. K. Panda and M. L. Buist, "A finite nonlinear hyper-viscoelastic model for soft biological tissues," *Journal of Biomechanics*, vol. 69, pp. 121–128, 2018.

[381] P. Haupt and K. Sedlan, "Viscoplasticity of elastomeric materials: experimental facts and constitutive modelling," *Archive of Applied Mechanics*, vol. 71, pp. 89–109, 2001.

[382] E. Peña and M. Doblaré, "An anisotropic pseudo-elastic approach for modelling mullins effect in fibrous biological materials," *Mechanics Research Communications*, vol. 36, no. 7, pp. 784–790, 2009.

[383] A. Elías-Zúñiga and C. Rodríguez, "A non-monotonous damage function to characterize stress-softening effects with permanent set during inflation and deflation of rubber balloons," *International Journal of Engineering Science*, vol. 48, no. 12, pp. 1937–1943, 2010.

[384] E. Maher, A. Creane, C. Lally, and D. J. Kelly, "An anisotropic inelastic constitutive model to describe stress softening and permanent deformation in arterial tissue," *Journal of the Mechanical Behavior of Biomedical Materials*, vol. 12, pp. 9–19, 2012.

[385] Y. Zhao, S. Siri, B. Feng, and D. Pierce, "Computational modeling of mouse colorectum capturing longitudinal and through-thickness biomechanical heterogeneity," *Journal of the Mechanical Behavior of Biomedical Materials*, vol. 113, p. 104127, 2021.

[386] B. Staber and J. Guilleminot, "Stochastic hyperelastic constitutive laws and identification procedure for soft biological tissues with intrinsic variability," *Journal of the Mechanical Behavior of Biomedical Materials*, vol. 65, pp. 743–752, 2017.

[387] M. J. Buehler, "Nanomechanics of collagen fibrils under varying cross-link densities: atomistic and continuum studies," *Journal of the Mechanical Behavior of Biomedical Materials*, vol. 1, no. 1, pp. 59–67, 2008.

[388] R. B. Svensson, H. Mulder, V. Kovanen, and S. P. Magnusson, "Fracture mechanics of collagen fibrils: influence of natural cross-links," *Biophysical Journal*, vol. 104, no. 11, pp. 2476–2484, 2013.

[389] K. Yoshida, H. Jiang, M. Kim, J. Vink, S. Cremers, D. Paik, R. Wapner, M. Mahendroo, and K. Myers, "Quantitative evaluation of collagen crosslinks and corresponding tensile mechanical properties in mouse cervical tissue during normal pregnancy," *PloS One*, vol. 9, no. 11, p. e112391, 2014.

[390] Y.-C. Chen, M. Chen, E. A. Gaffney, and C. P. Brown, "Effect of crosslinking in cartilage-like collagen microstructures," *Journal of the Mechanical Behavior of Biomedical Materials*, vol. 66, pp. 138–143, 2017.

[391] J. D. Eekhoff, F. Fang, and S. P. Lake, "Multiscale mechanical effects of native collagen cross-linking in tendon," *Connective Tissue Research*, vol. 59, no. 5, pp. 410–422, 2018.

[392] G. A. Holzapfel and R. W. Ogden, "A damage model for collagen fibres with an application to collagenous soft tissues," *Proceedings of the Royal Society A*, vol. 476, no. 2236, p. 20190821, 2020.

[393] A. Bailey, "Intermediate labile intermolecular crosslinks in collagen fibres," *Biochimica et Biophysica Acta (BBA)-Protein Structure*, vol. 160, no. 3, pp. 447–453, 1968.

[394] W. Opsahl, H. Zeronian, M. Ellison, D. Lewis, R. B. Rucker, and R. S. Riggins, "Role of copper in collagen cross-linking and its influence on selected mechanical properties of chick bone and tendon," *The Journal of Nutrition*, vol. 112, no. 4, pp. 708–716, 1982.

[395] S. P. Veres and J. M. Lee, "Designed to fail: a novel mode of collagen fibril disruption and its relevance to tissue toughness," *Biophysical Journal*, vol. 102, no. 12, pp. 2876–2884, 2012.

[396] C. Durcan, M. Hossain, G. Chagnon, D. Perić, and E. Girard, "Mechanical experimentation of the gastrointestinal tract: a systematic review," *Biomechanics and Modeling in Mechanobiology*, Nov. 2023.

Appendix

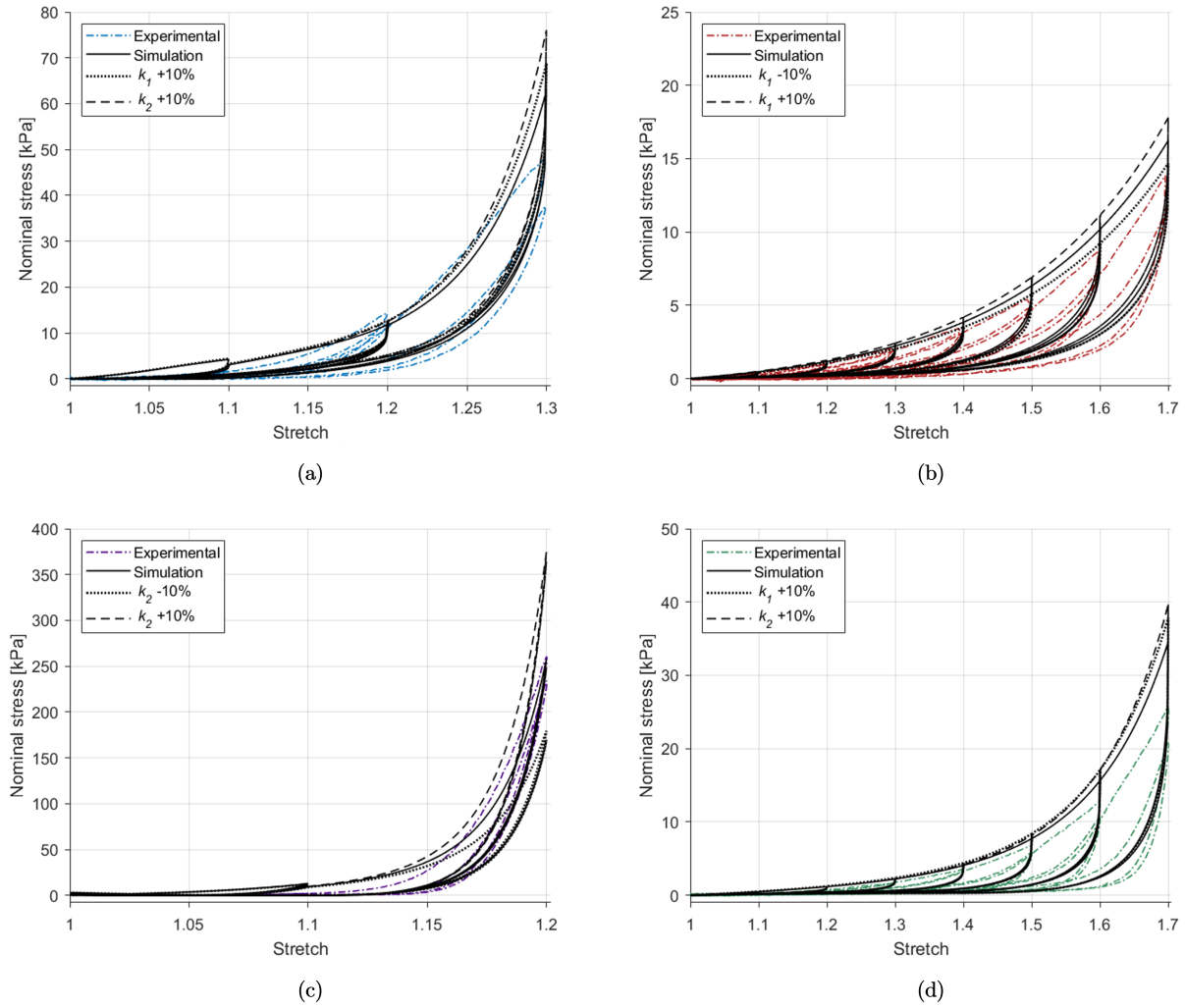

Figure 58. Effects of the two most sensitive parameters on the model for the $1\%s^{-1}$ cyclic behaviour of the fresh muscularis propria layer in the longitudinal (**a**) and circumferential (**b**) directions, and the mucosa-submucosa in the longitudinal (**c**) and circumferential (**d**) directions.